Control of intestinal progenitor cell fate by the microenvironment

Sujata Biswas

Hertford College

University of Oxford

Thesis submitted for the degree of *Doctor of Philosophy*

Supervisor: Simon Leedham

Trinity term 2018



Abstract

The conventional model of intestinal epithelial architecture describes a unidirectional tissue organisational hierarchy with stem cells situated at the crypt base and daughter cells proliferating and terminally differentiating as they progress along the vertical (crypt-luminal) axis. In this model, the fate of a cell that has left the niche is determined and its lifespan limited. I look at evidence to suggest that stem cell control and daughter cell fate determination is not solely an intrinsic, cell autonomous property but is heavily influenced by the microenvironment. Selective pressures that disrupt the homeostatic balance, such as intestinal inflammation or morphogen dysregulation, can cause committed progenitor cells and even some differentiated cells to regain stem cell properties. Disruption of cell fate determination can lead to somatic mutation and neoplastic transformation of cells situated outside the crypt base stem cell niche. The Wnt, BMP and Hedgehog pathways are explored in terms of epithelial and mesenchymal compartmentalisation and cross-talk, both in homeostasis and inflammation. Interactions between BMP and Hedgehog pathways are studied in vivo and in vitro. The BMP antagonist GREM1 is discussed, and the effect of a compartmental switch in its expression in humans (Hereditary Mixed Polyposis Syndrome) and in mouse models. This leads to ectopic crypts with supposed stem cell activity, and evidence for stem cell activity is interrogated using lineage tracing models and organoid cultures. The functionality of Sox9, a marker of ectopic crypts, is explored. An epithelial Sox9 knockout model is studied in terms of its effect on ectopic crypt formation. The role of Sox9 in intestinal restitution is also examined by using a chemical colitis model and a biopsy wounding model.

Acknowledgements

First and foremost I would like to thank my supervisor Simon Leedham. You are a shining example of Academic Clinician and have taught me the fundamentals of basic science, the importance of perseverance, but mostly how to think as an academic – to always be a step ahead of your next experiment and to reason every result robustly. I am immensely grateful for the opportunity to work in your lab and for everything I have learnt.

Next to Hayley Davis, without whom I would not have got to this stage. Beginning in a lab without a basic science background was so much harder than I had imagined, both technically and psychologically. You have taught me every procedure I know in the lab with unending patience. Your positive attitude and daily support, as a mentor and friend, has been invaluable.

To the other members of the lab and collaborators who have provided help and advice. Thanks to Martijn Koppens who has been a superb help with co-staining and immunofluorescence, and for keeping a cool head and a good sense of humour at all times. Thanks to Abby D'Cruz, Annie Lewis and Lennard Lee for being great colleagues and sounding boards for discussion, and to Helen Lockstone for training and help with bioinformatic work. I appreciate the help of all the animal technicians in the Functional Genomics Facility. Many thanks to clinical collaborators Lai Mun Wang, James East, and the Transitional Gastroenterology Unit staff and patients. In particular I would like to thank Kate Williams and the research nurses for help in collecting patient specimens. Thanks to Marnix Jansen, George Elia and Darren Treanor for your enormous help in collaborating on 3D histology. Many thanks also to Ian Tomlinson for access to your whole lab

and resources and for your guidance in this project. I am grateful to the Medical Research Council for funding this project so generously.

I would like to thank my husband Odysseas for being a pillar of support throughout this process. To my sister, Didi, who has steadfastly believed that there is no end to what I can achieve, and has backed me through every stage of life. And finally to my parents, for giving me everything, and for teaching by example that there is no substitute in life for hard work and principle.

Preface

This thesis is a collection of the research work carried out by the author in the Wellcome Trust Centre for Human Genetics, Nuffield Department of Medicine, University of Oxford, between September 2014 and September 2017, under the supervision of Professor Simon Leedham. I state that the research described herein is original, although the work of others is cited with appropriate references within the text. No part of this research has previously been submitted for a degree at this or any other University.

Some of the work described in this thesis has been published in the following papers:

Huels DJ, Ridgway RA, Radulescu S, Leushacke M, Campbell AD, **Biswas S**, Leedham S, Serra S, Chetty R, Moreaux G, Parry L, Matthews J, Song F, Hedley A, Kalna G, Ceteci F, Reed KR, Meniel VS, Maguire A, Doyle B, Sderberg O, Barker N, Watson A, Larue L, Clarke AR, Sansom OJ. E-cadherin can limit the transforming properties of activating -catenin mutations. *EMBO J*. 2015 Sep 14;34(18):2321-33.

Biswas S, Davis H, Irshad S, Sandberg T, Worthley D, Leedham S. Microenvironmental control of stem cell fate in intestinal homeostasis and disease. *J Pathol*. 2015 Oct;237(2):135-45.

Biswas S, Holyoake D, Maughan TS. Molecular Taxonomy and Tumourigenesis of Colorectal Cancer. *Clin Oncol*. 2016 Feb;28(2):73-82.

Irshad S, Bansal M, Guarnieri P, Davis H, Al Haj Zen A, Baran B, Pinna CMA, Rahman H, **Biswas S**, Bardella C, Jeffery R, Wang LM, East JE, Tomlinson I,

Lewis A, Leedham SJ. Bone morphogenetic protein and Notch signalling crosstalk in poor-prognosis, mesenchymal-subtype colorectal cancer. *J Pathol*. 2017 Jun;242(2):178-192.

Biswas S, Quante M, Leedham S, Jansen M. The metaplastic mosaic of Barrett's oesophagus. *Virchows Arch*. 2018 Jan;472(1):43-54.

Lee LYW, Woolley C, Starkey T, **Biswas S**, Mirshahi T, Bardella C, Segditsas S, Irshad S, Tomlinson I. Serum- and Glucocorticoid-induced Kinase Sgk1 Directly Promotes the Differentiation of Colorectal Cancer Cells and Restrains Metastasis. *Clin Cancer Res*. 2019 Jan;25(2):629-640.

Contents

1 Introduction **29**

1.1 Intestinal architecture 29

1.2 Stem cells 32

1.2.1 Description and function 32

1.2.2 The intestinal stem cell niche 33

1.2.3 Identification of stem cells 34

1.2.3.1 Crypt base columnar cells expressing *Lgr5* . . . 34

1.2.3.2 Facultative stem cell populations 36

1.2.3.3 Techniques to study stem cells 37

1.3 Control of cell fate determination: Morphogen signalling pathways 39

1.3.1 Morphogen pathways in intestinal development 41

1.3.2 Morphogen pathways in adult intestinal homeostasis . . . 43

1.3.2.1 Wnt 43

1.3.2.2 Bone Morphogenetic Protein (BMP) 45

1.3.2.3 Hedgehog 48

1.3.2.4 Notch 48

1.3.3 Signalling pathways in disrupted homeostasis 50

1.3.3.1 Cell-extrinsic repair: Mesenchymal control over epithelial cell fate 51

1.3.3.2 Cell-intrinsic repair: Stem cell plasticity 55

1.3.3.3 Restoration of homeostasis after temporary disruption 58

1.3.3.4 Disrupted homeostasis in human and mouse models 59

1.4 Carcinogenesis 62

1.4.1 Stem cell dynamics 62

1.4.1.1 Neutral drift 62

1.4.1.2 A spectrum of stem cells 62

1.4.2 The cell of origin debate 63

1.4.2.1 The “top-down versus bottom-up” debate 64

1.4.3 Non-stem cells as a potential cell of origin 65

1.4.3.1 Inflammation 65

1.4.3.2 Morphogen disruption 65

1.4.4 Colorectal cancer as a clinical problem 67

1.4.5 A hierarchy of cells within cancer: The cancer stem cell theory 68

1.4.6 Subtyping of colorectal cancer 69

1.4.7 Environmental factors in CRC 71

1.4.7.1 The inflammatory drive 71

1.4.7.2 Myofibroblasts in cancer 73

1.4.7.3 Genetic and environmental interaction 74

1.4.8 Signalling pathways in carcinogesis 74

1.4.8.1 Wnt pathway in carcinogenesis 74

1.4.8.1.1 Wnt in inherited colorectal cancer syndromes 76

1.4.8.1.2 Wnt disuption in transgenic mouse models 76

1.4.8.1.3 Wnt in sporadic colorectal cancer . . . 77

1.4.8.2 BMP pathway in carcinogenesis 77

1.4.8.2.1 BMP in inherited colorectal cancer syndromes 78

1.4.8.2.2 BMP in sporadic colorectal cancer . . 78

1.4.8.2.3 BMP disuption in transgenic mouse models 79

1.4.8.3 Hedgehog pathway in carcinogenesis 80

1.4.8.3.1 HH in sporadic colorectal cancer . . . 80

1.4.8.3.2 Hh disuption in transgenic mouse models 80

1.4.9 The role of *SOX9* in carcinogenesis 82

1.4.9.1 *Sox9* as a marker of stem cells 82

1.4.9.2 *Sox9* as an oncogene or tumour suppressor gene 83

1.4.10 Targets for therapy in CRC 85

1.5 Outline of thesis 86

2 Materials and Methods **89**

2.1 Human sample collection 89

2.1.1 Consent and ethics for human samples 89

2.1.2 Microdissection of fresh endoscopic biopsies 90

2.1.3 Human surgical specimens 90

2.2 Mouse procedures 91

2.2.1 Generation of *Sox9Cre*^{ERT2} *; Rosa26*^{YFP} mice 91

2.2.2 Generation of *Sox9*$^{fl/fl}$*/Vill-Cre* mice 92

2.2.3 APC^{Min} mice 93

2.2.4 Breeding 93

2.2.5 Ear snips 93

2.2.6 Gut preparation 93

2.2.7 Individual crypt isolation 94

2.2.8 Mouse endoscopy 94

2.2.9 Dextran Sodium Sulphate (DSS) colitis 95

2.3 Histology 96

2.3.1 Adenoma scoring 96

2.3.2 Processing 96

2.3.3 Embedding 97

2.3.4 Sectioning and staining 97

2.3.4.1 Sectioning 97

2.3.4.2 Serial sectioning for 3D processing 97

2.3.4.3 Laser capture microdissection and cresyl violet staining 98

2.3.4.4 Haematoxylin and Eosin (H and E) staining . . 98

2.3.4.5 Alcian Blue stain for goblet cells 99

2.4 DNA 99

2.4.1 DNA extraction 99

2.4.1.1 Isolation of DNA from mouse earsnips for genotyping 99

2.4.1.2 Polymerase Chain Reaction (PCR) 100

2.5 RNA / cDNA 101

2.5.1 RNA extraction 101

2.5.2 Determination of nucleic acid concentration and quality . 101

2.5.2.1 Nanodrop spectrophotometer 101

2.5.2.2 Qubit fluorometer 102

2.5.3 Reverse transcription of RNA into cDNA 102

2.5.4 Pre-amplification of cDNA 102

2.5.5 Quantitative Real Time-PCR (qPCR): TaqMan 103

2.5.5.1 Fluidigm Biomark HD system 104

2.5.6 *In situ* hybridisation 104

2.5.7 Microarrays of human biopsies 106

2.5.8 RNA sequencing 107

2.6 Protein 107

2.6.1 Immunohistochemistry 107

2.6.1.1 Co-staining protocol 108

2.6.1.2 Immunohistochemistry quantification 108

2.7 Cell culture 109

2.7.1 Counting cells 109

2.7.2 CRC cell line culture 109

2.7.3 Lentiviral knockdown of Sox9 110

2.7.4 Mouse organoid culture 111

2.7.4.1 Crypt organoids 111

2.7.4.2 Villus organoids 112

2.7.4.3 R-spondin1 conditioned media (CM) 112

2.7.5 Fibroblast culture 113

2.7.5.1 Purchased human colon fibroblasts 113

2.7.5.2 Human colon fibroblasts 113

2.7.5.3 Mouse colon fibroblasts 114

3 Epithelial-mesenchymal signalling pathways in homeostasis and inflammation 115

3.1 Aims 115

3.2 Introduction 116

3.2.1 The polarised epithelial axis 116

3.2.2 Changes in tissue regeneration 117

3.2.3 The polarised mesenchymal axis 118

3.3 Methods 118

3.4 Results 119

3.4.1 Microdissection of human intestinal biopsies in homeostasis 119

3.4.1.1 Colonic samples 119

3.4.1.2 Small bowel samples 120

3.4.1.3 Microarray results 120

3.4.1.3.1 Morphogen pathways across compartments in homeostasis 122

3.4.2 Human colonic biopsies in inflammation 127

3.4.2.1 Morphogen pathways across compartments in inflammation 131

3.4.3 Mouse intestinal compartments 132

3.4.4 Downstream verification of signalling pathways in homeostasis and inflammation 135

3.4.5 Stromal heterogeneity in homeostasis 138

3.4.5.1 Downstream verification of stromal markers . . 141

3.5 Discussion 141

3.5.1 Morphogen gradients 143

3.5.2 Fibroblast heterogeneity 143

3.5.3 Organoid cultures 144

3.5.4 Morphogens in wound repair 146

3.5.5 Implications for therapy 147

3.5.6 Limitations 148

4 *In vitro* and *in vivo* assessment of the role of *Grem1* in intestinal regeneration 149

4.1 Aims 149

4.2 Introduction 150

4.2.1 Grem1 as a paracrine BMP antagonist 150

4.2.2 Hedgehog may play a part in Grem1 regulation 151

4.2.3 Techniques to study wound regeneration 153

4.3 Methods 154

4.4 Results 155

4.4.1 Grem1 as a paracrine morphogen and proliferative mediator 155

4.4.2 BMP as an inhibitor of Grem1-induced regeneration . . . 157

4.4.3 *In vitro* interaction between Grem1 and HH 158

4.4.4 Grem1 in human IBD and mouse colitis 164

4.4.5 Grem1 in murine endoscopic biopsy injury 166

4.4.6 Grem1 in a model of Hedgehog knockdown 170

4.5 Discussion 172

4.5.1 The paracrine proliferative effects of Grem1 172

4.5.2 Grem1 and HH in homeostasis 173

4.5.3 Grem1 in inflammation 174

4.5.4 Limitations 175

5 *Grem1* in cancer initiation: Form and function of ectopic crypts in the *Vil1-Grem1* mouse model 177

5.1 Aims 177

5.2 Introduction 178

5.2.1 A model of compartmental disruption of *Grem1* 178

5.2.2 Ectopic epithelial expression of *Grem1*; the *Vil1-Grem1* mouse model 180

5.2.3 Hedgehog and Grem1 in colorectal cancer 181

5.2.4 "Top-down" cancer initiation 183

5.2.5 Stem cell potential in cells away from the crypt base . . . 185

5.3 Methods 186

5.4 Results 187

5.4.1 Contrasting crypt base and ectopic crypt progenitor cell populations 187

5.4.2 Evidence for ectopic crypts as progenitor cells 191

5.4.2.1 Lineage tracing in the *Vil1-Grem1; Sox9CreERT2; Rosa26YFP* model 191

5.4.2.2 Multipotentiality of ectopic lineage tracing ribbons 194

5.4.3 Proliferative capacity within ectopic crypts 196

5.4.4 Contrasting the microenvironment of the crypt base and ectopic crypts 197

5.4.4.1 Fibroblast markers 199

5.5 Discussion 202

5.5.1 Ectopic crypts differ from crypt bases 202

5.5.2 Stem cell potential in ectopic crypts 203

5.5.3 The microenvironmental difference between ECF and crypt base stem cells 204

5.5.4 The development of ectopic crypts 204

5.5.4.1 Theory 1: The crypt shape 205

5.5.4.2 Theory 2: In-folding due to stoichiometric pressure 205

5.5.4.3 Theory 3: Control by aberrant mesenchyme . . 206

5.5.4.4 Theory 4: Ectopic Paneth cells 207

5.5.5 Clinical implications 207

5.5.6 Limitations 210

6 The functional effect of *Sox9* in inflammation and carcinogenesis 211

6.1 Aims 211

6.2 Introduction 212

6.2.1 *Sox9* in inflammation 212

6.2.2 *Sox9* in carcinogenesis 213

6.3 Methods 218

6.4 Results 219

6.4.1 Sox9 in tissue restitution 219

6.4.1.1 Presence of Sox9 expressing cells in wounds . . 219

6.4.1.2 Functional requirement of Sox9 in healing: the Vill-Cre; Sox9fl/fl model 221

6.4.2 Sox9 in carcinogenesis 228

6.4.2.1 Sox9 in CRC cell lines 228

6.4.2.2 The functional effect of *Sox9* in mediating the ECF phenotype: the *Vil1-Grem1; Vill-Cre; Sox9fl/fl* mouse model 229

6.4.2.3 *Sox9* in the Apc^{Min} mouse model 232

6.5 Discussion 233

6.5.1 Sox9 in inflammation 233

6.5.2 Sox9 in carcinogenesis 235

6.5.3 Limitations 237

7 Discussion **238**

7.1 Summary of results 238

7.2 Morphogen gradients in homeostasis and inflammation 239

7.3 The *Vil1-Grem1* mouse model and formation of ectopic crypts . . 241

7.4 New therapeutic targets in inflammation and colorectal cancer . . 242

7.5 Further work 243

7.6 Closing summary 245

Bibliography **247**

List of Tables

2.1 Genotyping primers. 100

2.2 Human Taqman probe list. 104

2.3 Mouse Taqman probe list. 105

2.4 Antibodies for mouse Immunohistochemistry. 108

6.1 Number of offspring with genotype *Vil1-Grem1+;VillCre+;Sox9-/-* born to different breeding pairs 230

List of Figures

1.1 Crypt architecture and cell types. 31

1.2 Key morphogen signalling pathway gradients in intestinal homeostasis 44

1.3 The canonical Wnt pathway. 45

1.4 Schematic representation of the canonical BMP signalling cascade. 47

1.5 The Hedgehog pathway. 49

1.6 Fibroblast morphology 52

1.7 H&E stain and Sox9 staining in HMPS human polyps and in *Vil1-Grem1* mouse polyps 66

1.8 The CRC subtypes 70

1.9 Genetic and environmental influences variably contribute to cancer phenotype in different colorectal cancer subtypes 75

2.1 Immunohistochemistry for YFP in Sox9Cre^{ERT2} ; Rosa26^{YFP} mouse 92

3.1 Microdissection of intestinal crypts. 120

3.2 PCA plot showing clustering by tissue compartment 122

3.3 Differential gene expression across compartments in homeostasis . 123

3.4 Comparison of signalling pathways by compartment within small bowel and colon. 125

3.5 qPCR for BMP and HH pathways in intestinal homeostasis 126

3.6 Light microscope photos of non-budding and budding cryts 128

3.7 PCA plot showing clustering by tissue compartment 129

3.8 Comparison of inflamed and normal compartments. 130

3.9 GSEA across compartments in inflammation 131

3.10 Comparison of signalling pathways by compartment in healthy colon and colitis 133

3.11 qPCR for BMP and HH pathways in colitis 134

3.12 qPCR HH pathway in mouse 136

3.13 IHC and ISH stains in wild type mouse small bowel 137

3.14 Mouse small bowel before and after laser capture extraction of the upper mesenchyme 139

3.15 PCA plot showing clustering of mesenchyme compartments in mouse 140

3.16 Genes differentially expressed in mouse small bowel mesenchyme layers 142

4.1 Focal Wnt5a-induced clefts in colonic epithelial organoids 151

4.2 Crypts in wild type and *Ah-Cre; IHH*$^{fl/fl}$ mice 152

4.3 Gremlin-soaked microbeads in culture with mouse intestinal organoids 157

4.4 Microbeads soaked in varying concentrations of BMP4, in culture with mouse intestinal organoids with Gremlin in the media 159

4.5 Varying concentrations of recombinant BMP4 in media with Gremlin 160

4.6 Varying concentrations of recombinant BMP2 in media with Gremlin 161

4.7 Effect of cyclopamine on GLI1 and GREM1 expression in CCD-112 cells and human colon fibroblast primary culture 163

4.8 GREM1 ISH in human normal colon and IBD 165

4.9 Grem1 ISH in mouse colon and in DSS colitis 166

4.10 Mouse under general anaesthetic with endoscope in situ and view of monitor during endoscopy 168

4.11 Mouse colonic biopsy at specific timepoints: H&E stain 169

4.12 Mouse colonic biopsy after 24 hours: H&E stain and Grem1 ISH . 170

4.13 Grem1 ISH in wild-type mouse and *Ah-Cre; IHH*$^{fl/fl}$ mouse . . . 171

4.14 Interaction between BMP and HH in homeostasis and inflammation 175

5.1 Model summarising the proposed mechanistic consequences of disrupted *GREM1* morphogen gradients. 179

5.2 Methylene blue staining of *Vil1-Grem1* intestine 181

5.3 Histology of *Vil1-Grem1* animals 182

5.4 GREM1 in CRC disease-free survival and CRC subtypes 184

5.5 Vil1Grem1 mouse small intestine before and after laser dissection of ectopic and basal crypts 188

5.6 Genes differentially expressed in crypt base and ectopic crypts . . 189

5.7 Lysozyme, Bag1 and Caspase3 IHC in wild-type and *Vil1-Grem1* mice 190

5.8 Serial sections from 8-week old *Vil1-Grem; Sox9CreERT2 ; Rosa26YFP* mouse intestinal polyp 32 days after tamoxifen induction, with immunohistochemical staining for YFP. 192

5.9 Schematic of tracing ribbon annotation for 3D software and computerised image of polyp outline with tracing ribbons 195

5.10 Co-staining for YFP and enteric cell types 196

5.11 Co-stain for YFP and Ki67 in *Vil1-Grem; Sox9CreERT2 ; Rosa26YFP* mouse 198

5.12 qPCR for Hedgehog and Wnt pathway genes in wild-type and *Vil1-Grem1* intestinal mesenchyme 200

5.13 SMA, desmin and vimentin IHC in wild-type and *Vil1-Grem1* mouse small intestine 201

5.14 Schematic of signalling within an ectopic crypt 208

5.15 In situ hybridization for GREM1 in human TSA samples 209

6.1 Migration of clonal cell populations from labelled crypts after wounding. 214

6.2 The dose-dependent effect of *SOX9* on cell proliferation in healthy intestine and cancer 215

6.3 Ki67 IHC in wild-type and Sox9 floxed mice 216

6.4 Lysozyme IHC for Paneth cells in wild-type and Sox9 floxed mice 217

6.5 Sox9 IHC post DSS colitis 220

6.6 Mouse colonic biopsy after 5 hours, 24 hours, 3 days and 6 days: Sox9 IHC stain 220

6.7 Sox9 qPCR in wild-type and Sox9 fl/fl mice. Sox9 and EphB2 qPCR in wild-type and Sox9 floxed mouse organoids. 222

6.8 H+E, Sox9 IHC, Ki67 IHC, Lysozyme IHC and Grem1 ISH in wild-type and Sox9 floxed mice 223

6.9 Small intestinal crypt organoids from wild-type and Sox9 floxed mice 225

6.10 DSS in wild-type and Sox9 floxed mice: H+E stain and Sox9 IHC. Graph showing proportion of ulcerated colon in each group. . . . 226

6.11 H+E stain at different timepoints after biopsy injury in wild-type and Sox9 floxed mice. Sox9 IHC at 24 hours. 227

6.12 Sox9 expression in CRC cell lines 229

6.13 Phenotype of the small intestine in *Vil1-Grem1 and Vil1-Grem1; Vill-Cre; Sox9fl/fl mice* 231

6.14 Sox9 IHC in wild-type and Apc^{Min} mouse small intestine 233

6.15 Acute phase post epithelial wounding. 234

7.1 Levelling out of morphogen gradients in inflammation 240

List of Abbreviations

ACF	aberrant crypt foci
APC	adenomatous polyposis coli
BMP	Bone Morphogenetic Protein
BrdU	bromodeoxyuridine
BSA	bovine serum albumin
CCS	Colon Cancer Subtype
cDNA	complementary DNA
CMS	Consensus Molecular Subtype
CRC	colorectal carcinoma
Cre	cyclization recombination enzyme
CSC	cancer stem cell
DAB	3,3'-diaminobenzidine
DAPI	4',6-diamidino-2-phenylindole dihydrochloride
dH20	distilled water
DMSO	dimethyl sulfoxide
DMEM	Dulbecco's Modified Eagles Medium
DNA	deoxyribonucleic acid
DTT	dithiothreitol
E	embryonic age in days
ECF	ectopic crypt focus
EGF	Epidermal Growth Factor
EDTA	ethylenediamine tetra-acetic acid
EMT	epithelial-mesenchymal transition
FAP	familial adenomatous polyposis
FBS	foetal bovine serum

GAPDH	glyceraldehyde 3-phosphate dehydrogenase
GFP	green fluorescent protein
GSEA	Gene Set Enrichment Analysis
H&E	Haematoxylin and Eosin stain
HMPS	Hereditary Mixed Polyposis Syndrome
HOTSHOT	hot sodium hydroxide and tris
IBD	Inflammatory Bowel Disease
IHC	immunohistochemistry
ISC	intestinal stem cell
ISEMF	intestinal subepithelial myofibroblast
ISH	*in situ* hybridisation
Min	multiple intestinal neoplasia
mRNA	messenger RNA
MSI	microsatellite instability
NICD	Notch intracellular domain
PBS	phosphate buffered saline
PCR	polymerase chain reaction
PFA	paraformaldehyde
qPCR	quantitative PCR
RNA	ribonucleic acid
rpm	revolutions per minute
SB	small bowel
SEM	standard error of the mean
shRNA	short hairpin RNA
Sox9	Sex determining region Y box 9 gene
SMA	Smooth Muscle Actin
TBE	tris-borate-EDTA
TGF-β	transforming growth factor beta
TSA	Traditional Serrated Adenoma
TSG	tumour suppressor gene
Vil1	Villin gene
UC	Ulcerative Colitis
WAE	wound associated epithelium
WT	wild type
YFP	yellow fluorescent protein

Chapter 1

Introduction

This chapter outlines the current understanding of stem cell hierarchy within the intestinal niche and how microenvironmental aberration can occur and lead to inflammation and carcinogenesis. It explores evidence on how selective pressures that disrupt homeostatic balance can cause committed progenitor cells and even some differentiated cells to regain stem cell properties. I will discuss the role of *Sox9* in colorectal cancer and conclude with the research questions raised.

1.1 Intestinal architecture

In humans the small bowel is roughly 6 metres in length and the colon is 1.5 metres. Given the density of crypts this means there are around 10 million crypts in the colon. With this many proliferating cells it is clear that cell turnover needs to be tightly regulated. Stem cells constantly divide to give rise to immediate progeny, the transit-amplifying (TA) cells, which divide 4-5 times producing 300

cells in a crypt per day, before emerging as fully differentiated cells [1]. Transit amplifying cells are vigorously proliferating progenitor cells; cells which give rise to multiple cell types, but with limited potential in comparison to stem cells. A progenitor cell's capacity to self-renew is limited and it is oligopotent. It is already more specific than a stem cell and is pushed to differentiate into its target cells.

The differentiated cells arising from the TA cells finally apoptose and are shed into the lumen. The stereotypical architecture of the intestinal wall is a strict organisational hierarchy with stem cells residing at the crypt base, progenitor cells just above in the transit amplifying compartment, and differentiated cells at the luminal surface [2]. This creates a crypt-villus escalator, with cells differentiating as they pass along its axis as if on a conveyor belt. The process of self-renewal from bottom to top takes 5-7 days. In the small bowel several crypts give rise to a protruding villus; in the colon there are no villi.

There are five specialised epithelial cell lineages arising from post-mitotic, terminal differentiation. Enterocytes absorb nutrients and make up the majority (90%) of epithelial cells. Goblet cells produce mucus to provide a protective barrier and comprise 10% of intestinal epithelial cells. Enteroendocrine cells secrete gastrointestinal hormones. Despite being the largest endocrine system in the body, these cells make up less than 1% of the epithelium. Paneth cells, although differentiated, reside at the crypt base and secrete antimicrobial peptides as well as growth factors to maintain the stem cell niche. These are present in the small intestine but not in the colon in the healthy state. Tuft or brush cells are a secretory cell lineage, so-named by the brush of microvilli on their apical surface. They secrete prostaglandin precursors, are thought to mediate the interaction with the enteric

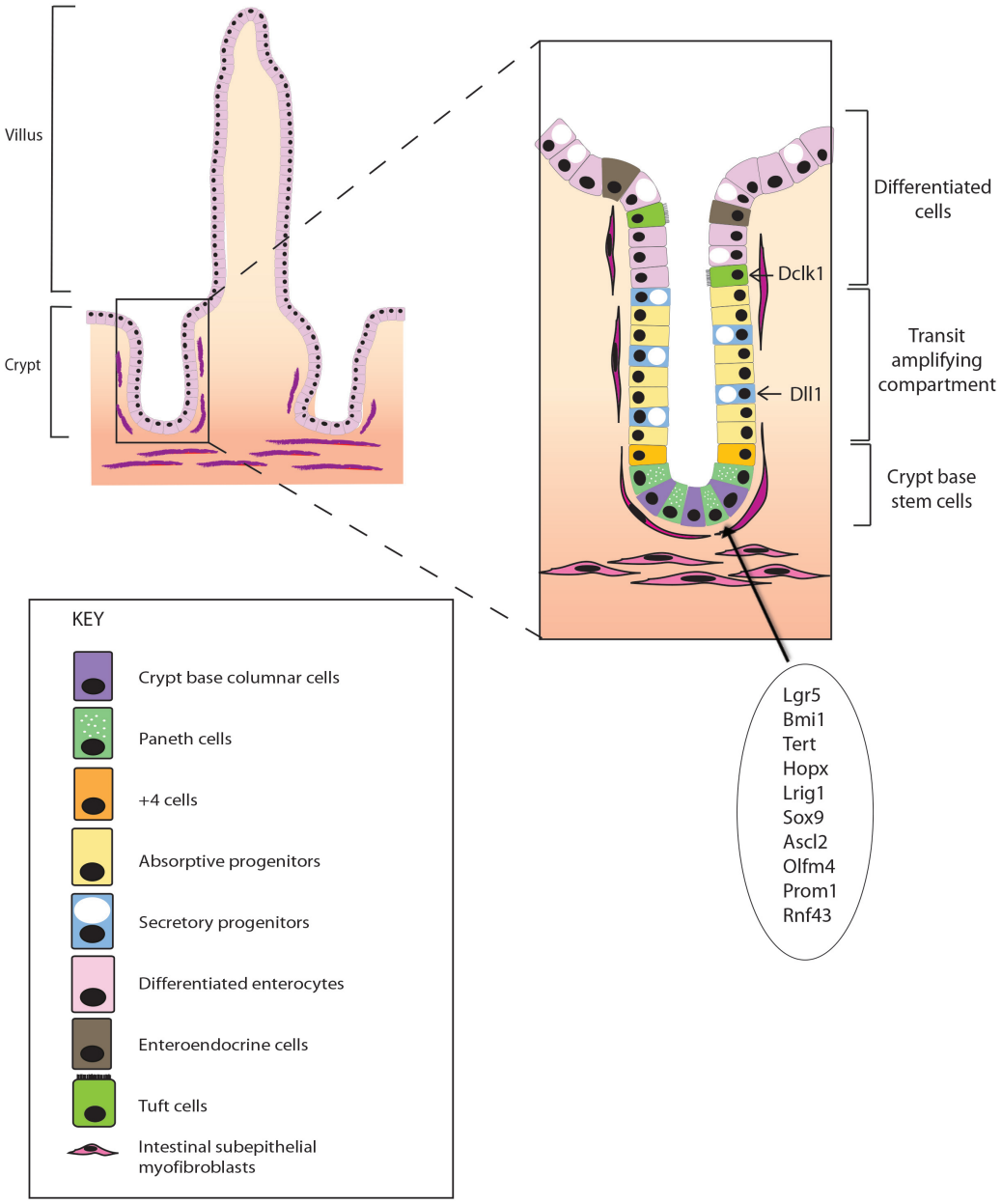

Figure 1.1: Crypt architecture and cell types. Model showing an amplified small intestinal crypt consisting of crypt base stem cells, the transit amplifying compartment with proliferating cells, and differentiated cells at the luminal surface. Markers defining cells are highlighted.

nervous system and are identified by expression of *DCLK1* (doublecortin-like kinase 1). These cell types and defining markers are shown in Figure 1.1.

The mesenchyme is the support structure and is critical in maintaining the stem cell niche (see section 1.2.2). The structural support cells are myofibroblasts, fibroblasts, pericytes, bone marrow-derived stromal stem cells, muscularis mucosae and smooth muscle associated with the lymphatic lacteals. These share similar marker molecules and some components express α-SMA (smooth muscle actin), a differentiation marker of smooth muscle cells. In addition to their role as structural elements, mesenchymal cells play a part in both the innate and adaptive immune response. Upon activation they produce chemokines and initiate the recruitment of leucocytes to the site of tissue injury and inflammation. The subepithelial myofibroblasts can become activated for the purpose of wound healing and activated fibroblasts in disrupted homoeostasis play an important role in carcinogenesis. Pericytes are similar to myofibroblasts but contribute proteins to the vascular basement membrane. In the distal small intestine, as well as being interspersed amongst mesenchymal cells, immune cells are organised into lymphoid follicles called Peyer's patches.

1.2 Stem cells

1.2.1 Description and function

A stem cell is defined as "An undifferentiated cell of a multicellular organism which is capable of giving rise indefinitely to more cells of the same type, and

from which certain other kinds of cell arise by differentiation." Embryonic stem cells arise from the blastocyst which develops shortly after fertilisation and they are pluripotent, giving rise to all germ layers. Adult or somatic stem cells are organ-specific and multipotential. Their function is to yield specialised cell types within an organ and to maintain and repair tissue. Both embryonic and adult stem cells have potential therapeutic uses.

The intestinal epithelium is one of the most rapidly proliferating adult tissue, making it an ideal model to study stem cells and cell fate determination. Intestinal stem cells give rise to the specialised lineages of the intestinal epithelium and are situated in small pits (the crypts of Lieberkühn) lining the intestinal tract, away from the shear stresses and toxic agents passing through the lumen of the intestinal tract.

In adult intestine stem cells undergo asymmetric cell division in which they give rise to one stem cell/progenitor and one committed daughter cell, to both self-replenish and differentiate.

1.2.2 The intestinal stem cell niche

Stem cells in animal tissues are often located in and controlled by bespoke tissue microenvironments known as niches. The niche is defined functionally rather than anatomically and constitutes a unique collection of cells which support the microenvironment for the maintenance and self-renewal of stem cells [3]. In the intestine this consists of epithelial cells, basement membrane, mesenchymal cells, neurons and endothelial cells. These components secrete ligands, growth factors

and cytokines important in maintaining the niche and regulating stem cells. Paneth cells, interspersed amongst stem cells, secrete antimicrobial peptides and constitute a vital part of the niche by supplying Wnt signals. The mesenchyme also provides Wnt signals [4] as epidermal growth factor (EGF) and BMP antagonists [5], and epithelial-mesenchymal crosstalk is required to maintain the stem cell niche. Other components of the mesenchyme include fibroblasts, myofibroblasts, immune cells, endothelial cells and neural cells. Maintaining a balance of stem cell quiescence and activity is the hallmark of an effective niche. This is vital to allow a robust adaptive response to microenvironmental pressures, as when the microenvironment is disrupted cell fate determination can be altered.

1.2.3 Identification of stem cells

Stem cells are defined functionally by their potential for self-renewal and multipotency; in the gut this effectively means the capacity to differentiate into all of the intestinal epithelial cell types listed above [3].

1.2.3.1 Crypt base columnar cells expressing *Lgr5*

The crypt base columnar cells are small cycling cells between Paneth cells which Cheng and Leblond considered to be true stem cells. This was at the time defined by the ability to label-retain. Transgenic activation of heritable fluorescent labels in cells expressing candidate stem cell markers allows accurate cell fate mapping and progeny lineage tracing over time, to satisfy the defining stem cell characteristics of self-renewal and multipotency.

Recent advances in biotechnology have led to a surge of studies that characterise the properties and interactions of putative intestinal stem cell populations *in vivo* [6] [7]. However this technique requires prior knowledge of the marker to be tested and cannot assess the stem cell capacity of cells not expressing the candidate gene. Furthermore stem cell markers generally identify a population of cells enriched for stem cell properties, and marker expression alone does not substitute for functional stem cell definition. Lineage tracing became the gold standard for assessing stem cell function and has resulted in significant advances in the characterisation of the crypt base columnar (CBC) cells [8] and the label retaining cells in the +4 crypt position [9].

To establish markers for supposed stem cells situated at the crypt base, it was first established which morphogens are active at the crypt base (section 1.3). By focusing on Wnt signalling as the main pathway controlling stem cell function (1.3.2.1), the Clevers group established a panel of Wnt target genes and used *in situ* hybridisation to identify those genes with restricted crypt base expression [10] [11]. Transgenic mice were generated to lineage trace cells expressing the Wnt target gene *Lgr5 (leucine-rich-repeat-containing G-protein-coupled receptor 5)* which is restricted to the crypt base columnar cells [12]. Over a 60-day period all epithelial cell types were produced from the *Lgr5*-positive transgenically labelled crypt base columnar cell. *Lgr5* has subsequently been validated as a bona fide stem cell marker in the small intestine, colon [13], stomach pylorus [14] and other organs such as the hair follicle [15].

Lineage tracing studies using different stem cell markers have defined a number of cell populations enriched for stem cell potential/activity within the base of the

crypt and dynamic studies using the most established markers have shown considerable variability in stem cell competence even during intestinal homeostasis. Recent work using both specific killing of a single marker defined cell population or more widespread damage has helped to assess stem and daughter cell dynamic changes when homeostasis is disrupted.

1.2.3.2 Facultative stem cell populations

In contrast to the *Lgr5*-positive cells which divide about once a day, the cells in the +4 position of the crypt, also defined by the property of label retention, are quiescent and slow-cycling. Several cell markers with expression patterns that overlie this position have been described, such as *Bmi1, mTert and Hopx* [16] [17] [18]. Using a tamoxifen inducible *Bmi1* Cre recombinase mouse, Sangiorgi et al demonstrated lineage tracing from cells at the +4 position [16]. Further work showed that Bmi1 is in fact expressed broadly throughout the crypt, diminishing this as a specific stem cell marker [19] [20] [21].

Numerous markers have now been used to identify populations that are enriched for cells capable of lineage tracing in the intestine including *Tert, Hopx, Lrig1, Sox9, Ascl2, Olfm4, Prom1, Rnf43* [19] [22] [23] [24] [25].

Within the stem cell niche, genetic ablation of a specific stem cell causes a reserve pool to step up to prevent an overall phenotypic change. Thus ablation of *Lgr5+* cells in mice, by knocking in a *diphtheria toxin receptor (DTR)* gene to the *Lgr5* locus, caused no change to the epithelium because of the compensatory effects of an expansion in the *Bmi1+* cell population [26]. This indicates the bidirectional

interconversion between +4 cells and the crypt base columnar cells. Induction of chemical colitis and radiation damage provokes a more indiscriminate intestinal injury, associated with a mucosal inflammatory response.

To characterise the cells in the +4 position capable of variable competence and plasticity, label retention was used. Rather than relying on putative marker expression, Buczacki et al focused on cells with functional label retention properties, and in a series of elegant experiments demonstrated that these cells are committed secretory cell precursors which retain the potential to return to stem cell function in the event of intestinal damage and regeneration [27]. These precursors are now known to be progenitor cells, situated above the crypt base having exited the stem cell niche. They are more differentiated than stem cells with a time-limited capacity to divide.

1.2.3.3 Techniques to study stem cells

Mouse models

Mouse models of disrupted morphogen signalling include inducible and non-inducible gene knockout within the intestinal epithelium. Techniques such as lineage tracing allow interrogation of stem cell properties. Environmental disruption is induced by radiation injury or by using chemical models of colitis.

The radiosensitivity of the small intestine is primarily a function of rapidly dividing progenitor cells. Although crypt epithelial cells are extremely sensitive to radiation-induced apoptosis, there is little to no apoptosis in the villi. After severe

irradiation, epithelial cell loss at the villus tips creates an imbalance between epithelial production and turnover, resulting in villus shortening and disruption of the mucosal barrier if all or most of the crypt stem cells die. However, if a single stem cell survives in the crypt region, regenerative crypts appear within 3 to 4 days, and crypt-villus architecture will be restored within 6 to 8 days. The balance between the rate and extent of crypt-villus regeneration, which depends on stem cells, is a major determinant of survival in the early period after acute radiation exposure.

Organoid cultures

Another technique to demonstrate stem cell potential is the use of *ex vivo* culture systems. They can maintain the long-term regenerative capacity of purified stem cells following their extraction from endogenous niches and have allowed us to exploit the clinical potential of adult stem cells. Major advances have been made in establishing culture systems that support the long-term growth and expansion of near-physiological intestinal epithelium from purified stem cells [28] [29].

The generation of *Lgr5-GFP* mice has allowed purification of *Lgr5+* stem cells from the small intestine by fluorescence activated cell sorting (FACS). Isolated cells can be grown in a 3D culture system using Matrigel, EGF, Noggin and R spondin 1 (Rspo1). There is an obligatory requirement to supplement niche-derived signals. Cultured cells multiply indefinitely and form spheres with a central lumen and protruding buds, called organoids. The central lumen of these organoids corresponds to the intestinal lumen with the surrounding epithelial cells

tightly packed, polarised and fully differentiated. The protruding buds constitute crypt-like domains with *Lgr5*+ stem cells at the bottom interspersed with lysozyme-positive Paneth cells. Rapidly dividing TA cells fill the remainder of these buds. Complete organoids with a gut-like architecture and containing all epithelial cell types can be grown from a single *Lgr5*+ stem cell.

Organoids defy the Hayflick limit, which indicates that somatic cells have a limited proliferative potential. There appears to be no inherent restriction in the replicative potential of adult stem cells *ex vivo* [30]. In contrast to adult epithelial organoids, which demonstrate budding morphology, foetal epithelial organoids frequently formed spherical organoids or spheroids. Unlike organoids, spheroids are composed primarily of stem cells and lack budding and branching structures enriched for differentiated cells. Cancer cells in 3D culture similarly grow as spheres.

1.3 Control of cell fate determination: Morphogen signalling pathways

Intestinal homeostasis relies on continuous rapid replacement of differentiated cells. Adult stem cell and daughter cell fate determination is controlled by the same signalling pathways that regulate embryonic stem cell function during development. A complex system of multifactorial, intercompartmental control by morphogens has evolved in both development and adulthood. Traditionally, the term morphogen (from the Greek “morphe” for shape and “genesis” for creation)

has been used in the context of embryonic patterning, where morphogen gradients effect patterning in a concentration-dependent manner. Morphogens are soluble molecules produced by a restricted region of a tissue that form an activity gradient away from its source. Morphogens specify cell fate and control mitogenesis. The concentration gradient of the diffusing morphogen subdivides fields of cells by controlling the expression of target genes at distinct concentration thresholds. As a result cells close to the morphogen source receive high levels of morphogen and express both low- and high-threshold target genes. Cells further from the source of the morphogen receive low levels of morphogen and express only low-threshold target genes. Consequently distinct cell types emerge. Morphogens have different effects at different stages of development. Within early stages of limb formation, although morphogens form concentration gradients, they drive proliferation uniformly. At later stages the rate of mitosis is specified by exposure to morphogens.

The stem cell niche provides an optimal microenvironment for production of differentiated progeny by the paracrine secretion of growth factors, cytokines and morphogens. Mesenchymal and epithelial derived cell signalling pathways result in polarised gradients that regulate stemness, cell proliferation, differentiation and apoptosis as cells progress along the crypt-villus axis. The phenotypic response of a cell is determined by its position within these concentration gradients. Important pathways include Wnt, BMP, Hedgehog and Notch.

1.3.1 Morphogen pathways in intestinal development

At the onset of gastrulation in the mouse at Embryonic day (E) 6, epiblast cells form endoderm which will go on to form the gastrointestinal tract. Between E7.5 and E9.5 invaginations form in the endodermal lining and the gut tube develops. At this stage, the primitive gut is composed of a uniform layer of cuboidal endodermal cells surrounded by splanchnic mesoderm. The intestine only becomes morphologically evident during a patterning phase at E9.5 to E14.5 in which the primordial gut is subdivided and reshaped along the anterior-posterior axis. At E14.5, after thickening of the epithelium, a major remodelling process occurs, resulting in the rapid conversion of the flat luminal surface into multiple villi. The regenerative capacity of the adult epithelium is established between E16.5 and postnatal day (P) 7, when mature crypts harbouring adult stem cells and progenitor cells develop from shallow pockets of proliferative cells that are restricted to the base of the embryonic villi. Crypt numbers rapidly increase during postnatal development by crypt fission. This is not well understood and may be triggered by a rapid increase in crypt size owing to increased stem and/or progenitor cell activity, which peaks approximately 2 weeks after birth in mice.

As in adult intestinal cells, the Wnt, BMP, Hedgehog (Hh) and Notch pathways control intestinal development. The Wnt pathway is complex developmentally. Wnt activity is found exclusively within the villus epithelium from E16 to P2, after which it is seen within the intervillus region [31]. This suggests that Wnt signalling and proliferation may be uncoupled during early development and that Wnt-independent mechanisms may drive early epithelial proliferation. Bmp4 is required for mesoderm development thus is critical for gastrulation. The underly-

ing smooth muscle of the embryonic gut is dependent on BMP signalling, especially Bmp2, for development [32].

The Hedgehog (Hh) pathway in Drosophila and vertebrates is conserved and known to play an important role in gut development. Sonic hedgehog (Shh) is expressed early in the endoderm. As the gut tube forms and undergoes morphogenesis, Shh expression expands and is maintained in the gut endoderm. Another member of the Hh family, Indian hedgehog (Ihh), is expressed later in the gut endoderm in a partially overlapping pattern [33]. Shh acts via its mesodermally expressed receptor Patched (Ptch) to induce mesodermal expression of Bmp4. Hh proteins are highly expressed in the murine embryonic gut and decrease after birth.

In most tissues, the Hh pathway is highly connected to the primary cilium (PC), an organelle that recruits functional components and regulates the Hh pathway [34]. However, normal epithelial cells of the intestine lack primary cilia. PC appear in the epiblast from E6. Hh ligands act at greater distances from their source in vertebrates and this long-range signalling may explain why a sensitive signal transduction system such as the primary cilium is required. Intraflagellar transport (IFT) proteins are important in Hh trafficking and are present in the endoderm from day E8.5. They are crucial for assembly and maintenance of the cilia. The central effectors of Hh signalling, Gli proteins, are regulated in a tiny compartment at the tip of the primary cilium, where components are concentrated to allow efficient responses to low levels of ligand. Mouse mutations have been identified that disrupt cilia in a variety of ways and have complex effects on Hedgehog signalling.

Notch signalling is required in the regulation of embryonic polarity and during left-right asymmetry determination in vertebrates [35].

1.3.2 Morphogen pathways in adult intestinal homeostasis

Important pathways include Wnt, BMP, Hedgehog and Notch (figure 1.2).

1.3.2.1 Wnt

This highly conserved signalling pathway is involved in cell fate specification and β-catenin is the key link in the pathway. Usually anchored to the basement membrane, intracellular β-catenin is minimised by phosphorylation and ubiquitin-proteasome degradation of its complex with Adenomatous Polyposis Coli (APC). Binding of Wnt ligands to Frizzled receptors inhibits β-catenin degradation and increases its cytosolic level, resulting in transcription of target genes driving proliferation.

Canonical Wnt/β-catenin signalling can be potentiated in the intestine by R-spondin ligands. R-spondin-1,2,3 ligands bind to receptors Lgr4,5,6 and co-receptors Rnf43 and Znrf3 [36]. A recent paper showed that there is a functionally non-equivalent but mutual interaction between Wnt and R-spondin ligands [37]. Canonical Wnt alone cannot induce *Lgr5*+ stem cell renewal and their fate is to differentiate, but the presence of R-spondin ligands can drive and specify the extent of stem cell expansion. Figure 1.3 shows this process.

The non-canonical Wnt pathways, which do not involve β-catenin, are also essential for epithelial proliferation. Non-canonical ligands such as Wnt5a stimulate diverse downstream pathways, including those involving calcium- and Rho/Rac-signalling and the c-jun N-terminal kinase (JNK) pathways [38].

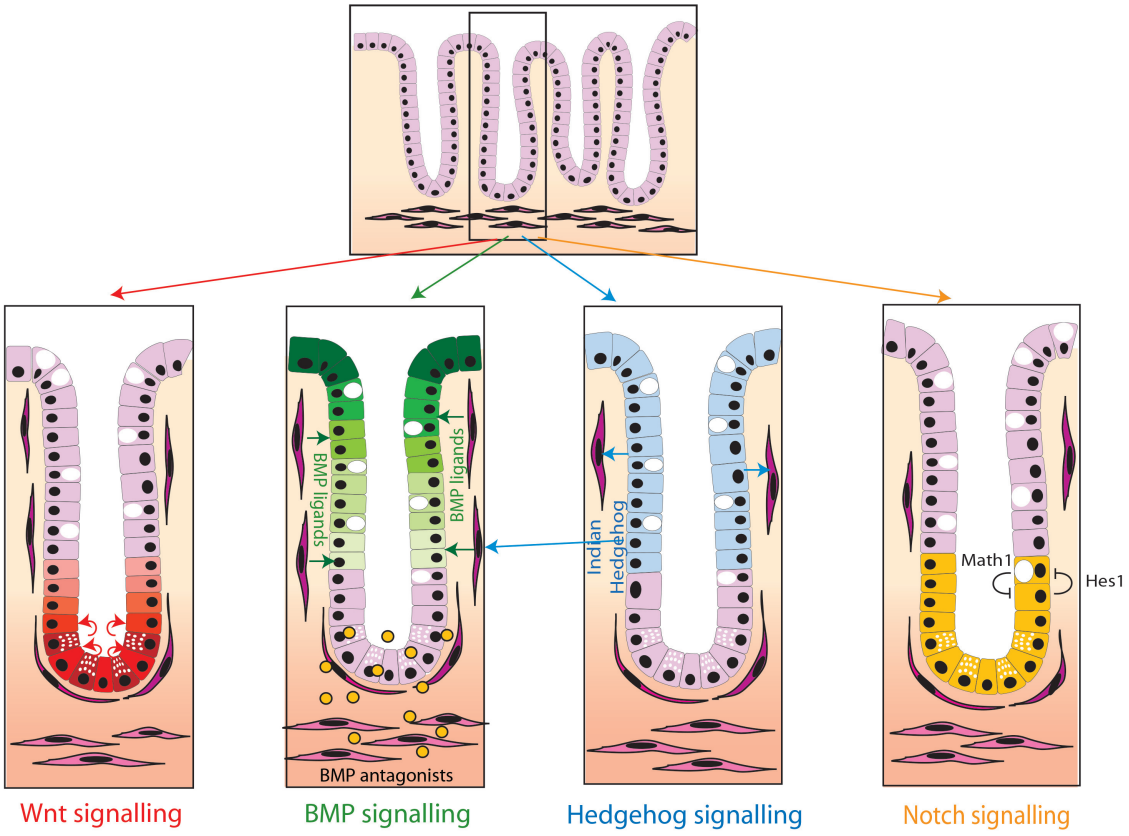

Figure 1.2: Key morphogen signalling pathway gradients in intestinal homeostasis include: A) **Wnt signalling**. Wnt ligands, secreted from the intestinal subepithelial myofibrobasts and Paneth cells act predominantly at the base of the crypt (red cells) to maintain stem cell function and TA cell proliferation. B) **BMP signalling**. BMP ligands are produced predominantly by the mesenchymal cells although Bmp2 is also expressed by epithelial cells. BMP represses Wnt signalling and promotes cell differentiation and apoptosis, acting predominantly in the upper part of the crypt and villus (green cells). There is reduced BMP activity at the crypt base, through diffusion gradients of the ligands and due to restricted expression of ligand-sequestering BMP antagonists from the sub-crypt myofibroblasts. C) **Hedgehog signalling**. Indian Hedgehog (Ihh) is the main ligand and is expressed by epithelial cells in the upper part of the crypt (blue cells). Ihh acts upon and maintains the myofibroblasts, and also promotes BMP ligand expression. D) **Notch signalling**. Notch regulates cell fate through cell-to-cell contact in the stem cell and transit amplifying zone at the base of the crypt (yellow cells). Notch activation via *Hes1* transcription factor and lateral inhibition via *Math1* transcription factor regulates enterocyte or secretory cell fate respectively.

In the intestine Wnt signalling is mainly restricted to the stem and proliferative zones in the bottom third of the crypt where it is involved in maintenance of stem cell function and driving transit amplifying cell proliferation [11].

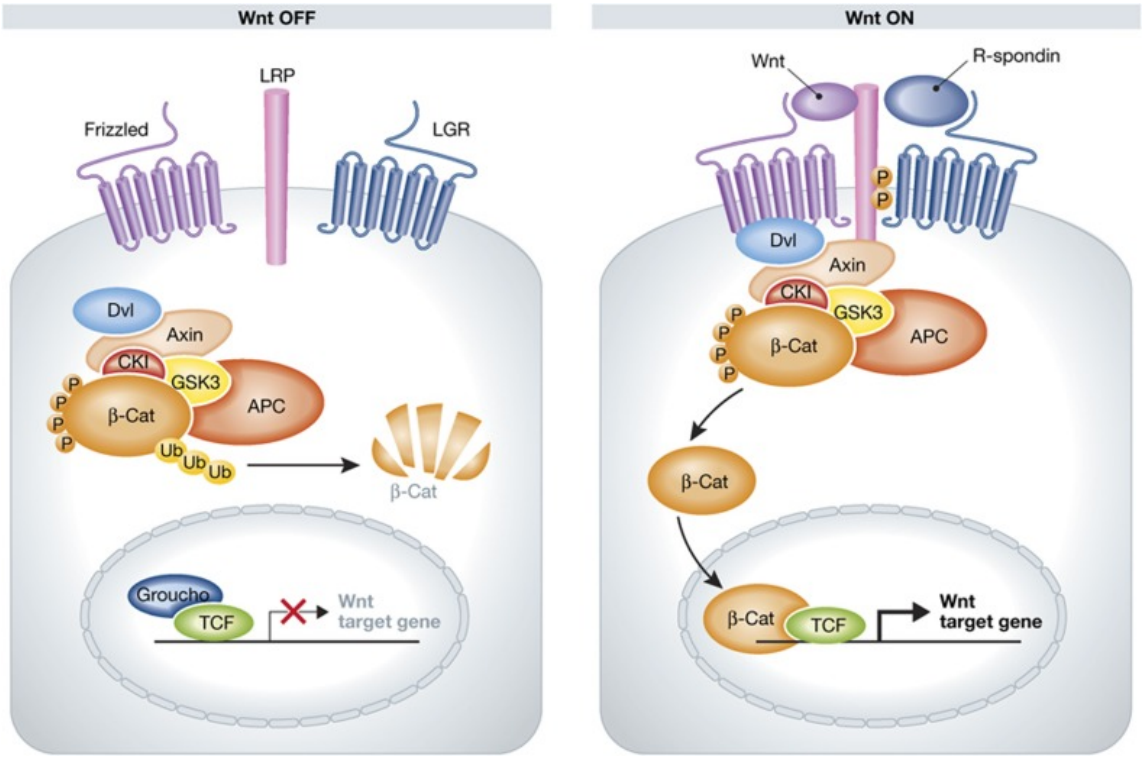

Figure 1.3: The canonical Wnt pathway. (Left) In the absence of Wnt stimulation, β-catenin levels are kept at a minimum through the destruction complex composed of APC, Axin, GSK3β, and CKI. In the nucleus, Tcf factors associate with transcriptional repressors to block target gene activation. (Right) In the presence of Wnt stimulation, the destruction complex is destabilised, and β-catenin accumulates in the nucleus to activate transcription of Tcf target genes. Lgrs are in direct contact with Lrp5/6 and Frizzleds. Adapted from [39].

1.3.2.2 Bone Morphogenetic Protein (BMP)

BMP is part of the TGF- β (transforming growth factor- β) superfamily and phosphorylates Smad proteins for signal transduction. It is required for control of

stem cell replication and terminal differentiation of mature intestinal cells [40]. The BMP ligands are secreted from both epithelial and mesenchymal cells but act mainly on the epithelial compartment through epithelial cell expression of BMP receptors [41]. These are transmembrane serine threonine kinase receptors type 1 and 2 (Bmpr1 and 2), and ligand binding triggers the phosphorylation and activation of the type 1 receptor by the type 2 receptor. The activated type 1 receptor phosphorylates a receptor-associated Smad (1/5/8) that subsequently complexes with Smad4 and translocates to the nucleus. Here it activates downstream target genes *Id1,2,3* as shown in figure 1.4. BMP may repress Wnt signalling so opposing gradients exist, with BMP signalling highest in the cells at the luminal surface [42]. PTEN, through phosphatidylinosital-3 kinase-Akt, may mediate the convergence of the BMP and Wnt pathways. BMP signalling enhances PTEN activity, in turn inhibiting the AKT pathway and destabilising β-catenin [43].

BMP signalling at the crypt base stem cell niche is carefully regulated by the expression of restricted gradients of exclusively mesenchymally expressed ligand-sequestering BMP antagonists such as Gremlin1 and 2 and Noggin. Gremlin1 is a cysteine knot secreted protein and member of the DAN (differential screening selected gene abberative in neuroblastoma) family. It is a soluble antagonist of BMP ligands and also exerts an inhibitory effect by blocking BMP secretion and increasing extracellular BMP endocytosis. Grem1 has differing affinities for BMP ligands; it has greater affinity for Bmp2 than Bmp4, than in turn for Bmp7 [44].

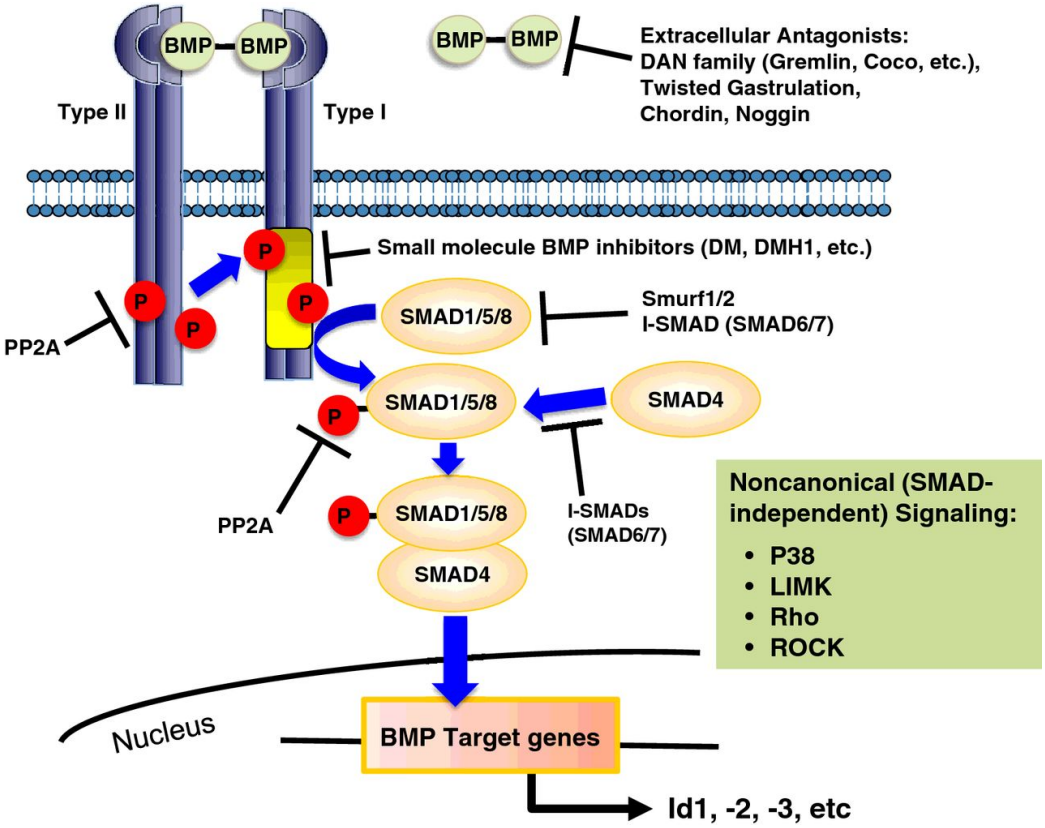

Figure 1.4: BMP ligands bind to receptors BMPR1 and BMPR2 to form the BMP transmembrane signalling complex. BMPR2 then phosphorylates and activates BMPR1. Phosphorylated BMPR1 subsequently phosphorylates SMAD1, SMAD5 and SMAD8 (SMAD1,5,8), which associate with SMAD4 and enter the nucleus. Here they activate the expression of BMP target genes such as Id1, -2 and -3. Extracellular antagonists such as Gremlin can complex with BMP ligand to prevent binding to its receptor. Smurf1/2 and SMAD6/7 can prevent phosphorylation of SMAD1/5/8 and binding to its co-factor SMAD4. Small molecule BMP inhibitors, such as dorsomorphin (DM) and DMH1, are competitive kinase inhibitors of BMP type I receptor. Inside the green insert are the non-canonical (SMAD-independent) signalling pathways, p38, LIMK, Rho and ROCK. Adapted from [45]

.

1.3.2.3 Hedgehog

Hedgehog controls tissue polarity. Three Hedgehog homologs, sonic hedgehog (Shh), indian hedgehog (Ihh), and desert hedgehog (Dhh) are known to be highly conserved in mammals. Of these, only Shh and Ihh are expressed in epithelium during development, and are redistributed after villus formation to be localised to the intervillus region. Ihh and Shh are secreted in a paracrine manner by differentiated epithelial cells to act on mesenchymal cells. They maintain homeostasis of mesenchymal cells and regulate epithelial cell proliferation through negative feedback to proliferating crypt base columnar cells by increasing BMP signalling [46]. Ligands Indian Hedgehog (Ihh) and Sonic Hedgehog (Shh) bind to patched homolog receptor 1 (Ptch1). In the absence of ligands, Ptch1 inhibits the activity of smoothened (Smo). On ligand binding this repression is relieved and allows nuclear translocation of Gli1,2,3. This leads to transciption of target genes Gli1, Ptch1 and Hhip. This is shown in figure 1.5. Primary cilia have not been observed in healthy adult intestine in relation to HH signalling 1.3.1.

1.3.2.4 Notch

Notch regulates cell fate decision between absorptive and secretory progenitor cell types [47]. Notch signalling is also involved in the control of stem cells and transit amplifying cell division [48] [49]. Notch interacts with Delta and Jagged ligands and signals through cell-cell contact to regulate post-mitotic differentiation into the different cell lineages. Four isoforms of the Notch receptor have been identified (Notch 1-4). Notch-ligand binding initiates proteolytic cleavage

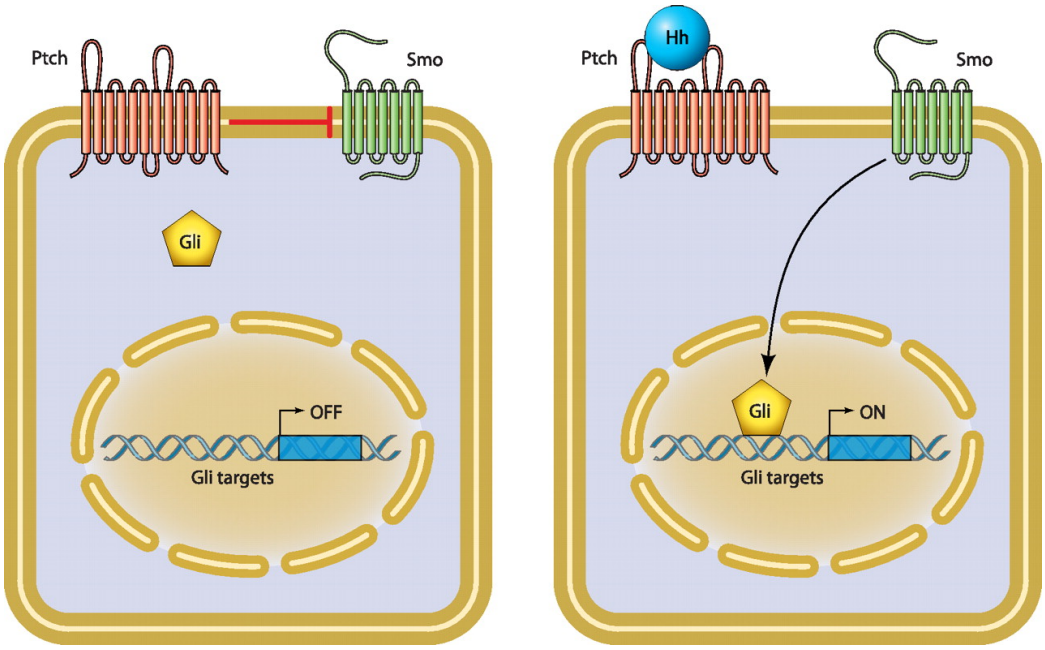

Figure 1.5: A model of interaction between receptors Smo and Ptch. A: in the absence of Hedgehog, Ptch functions to inhibit the signalling receptor Smo. B: binding of Hedgehog to Ptch alleviates the suppression of Smo and results in activation of the pathway. Adapted from [46].

at both the extracellular and intracellular regions of the Notch receptor, leading to the release of Notch intracellular domain (NICD). Nuclear localisation signals within the NICD direct its translocation, where it binds to and displaces a transcriptional co-repressor complex. High levels of Notch inhibit transcription of Math1 gene via the transcriptional repressor Hes1. Lateral inhibition in this cell-to-cell signalling pathway means that adjacent cells are driven towards different fates resulting in a "salt and pepper" distribution of progenitor cells committed to enterocyte and secretory lineages [47].

1.3.3 Signalling pathways in disrupted homeostasis

The intestinal epithelium is the first line of defence in a hostile environment and is subject to frequent chemical, microbiological and immunological mediated mucosal damage. Restoration of normal epithelial architecture and function after injury is a multistep process that involves tight regulatory control of epithelial stem cell dynamics. First, migration of adjacent epithelial cells over the wound re-establishes continuity of the epithelium. Stem cells divide to increase their numbers and to give rise to the more rapidly proliferating TA cells. The TA cell population then expands rapidly to form a regenerative crypt. A single surviving crypt stem cell is sufficient to facilitate crypt regeneration. If the injury has completely destroyed some crypts, the surviving crypt stem cells can divide to increase their numbers and subsequently restore sufficient numbers of crypts by crypt fission to maintain epithelial homeostasis [50]. As the epithelial stem cells within a crypt segregate to daughter crypts when crypt fission occurs, an expansion of stem cell number must accompany this repair response.

Epithelial restitution following injury involves mesenchymal control over epithelial cell fate, adaptive cell reprogramming and finally restoration of homeostasis.

1.3.3.1 Cell-extrinsic repair: Mesenchymal control over epithelial cell fate

Intestinal stromal cells, distinct from myofibroblasts, play a critical role in tissue regeneration and wound repair, and communicate both with the overlying epithelium and immune cells. The reciprocal interactions between the mesenchyme and epithelium are essential for epithelial cell fate.

Quiescent fibroblasts are inert spindle-shaped single cells in the interstitial space embedded in physiological extracellular matrix (ECM). In response to tissue injury and the associated stimuli, they are reversibly activated to facilitate repair and regeneration. The normal activated fibroblasts (NAFs) gain expression of smooth muscle actin (SMA) and vimentin and become stellate in shape (see figure 1.6). Together with enhanced ECM production, remodelling and cytoskeletal rearrangements, they gain contractile properties. The acquired synthetic functions are associated with secretory and migratory functions that amplify their activation, recruitment and proliferation. The reversibility of such activation may be mediated by reprogramming or apoptosis of the wound healing-associated activated fibroblasts when the repair process is complete.

The role of Wnt in tissue repair

Although the precise mediators of these epithelial-mesenchymal interactions are

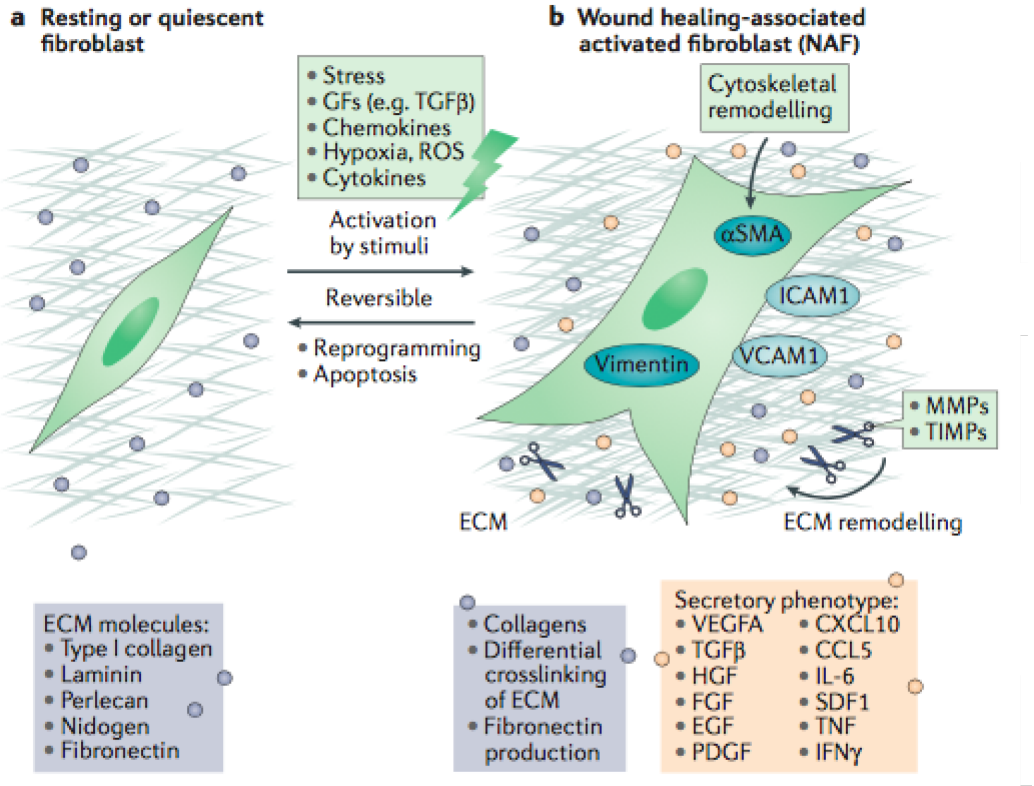

Figure 1.6: Fibroblast morphology. a) Quiescent fibroblasts are spindle-shaped single cells in the interstitial space embedded in physiological extracellular matrix (ECM). b) In response to tissue injury, quiescent fibroblasts are reversibly activated to facilitate repair and regeneration. The normal activated fibroblasts (NAFs) gain expression of smooth muscle actin (SMA) and vimentin and become stellate in shape. Adapted from [51].

not well defined, secreted Wnt ligands may be one of the first signals involved in this communication. In colitis the mesenchyme changes and provides optimal signalling required for regeneration. As evidence for this, infusion of human bone-marrow derived mesenchymal stem cells into irradiated mice accelerate recovery from radiation-induced intestinal damage [52]. Stromal mesenchymal cells contribute to the resolution of acute inflammation by normalising the proinflammatory mediator gradients. They also control the balance between resolution of acute inflammation and progression to chronic inflammation.

Wnt5a, a non-canonical Wnt ligand, is one factor required for restoration of homeostasis after injury in mice [53]. Miyoshi et al reported that after mucosal injury, a flattened layer of non-proliferative epithelial cells (wound-associated epithelium) emanated from crypts adjacent to the wound and migrated over the wound bed. Next crypts adjacent to the wound formed lateral, open extensions like channels towards the centre of the wound bed. These resembled crypts but had a proliferative, undifferentiated cell population, suggesting areas of new crypt formation. Wnt5a-positive stromal cells were found near these wound channels in the area of mucosal injury. In addition, Wnt5a-positive cells were located adjacent to non-proliferative wound channel epithelial cells. In uninjured areas, Wnt5a-positive mesenchymal cells were not associated with crypt bases that contain canonical Wnt-active epithelial cells. Wnt5a-positive mesenchymal cells may therefore induce new crypt formation by potentiating TGF-β signalling and locally inhibiting proliferation of the stem/progenitor cell population within the wound channel.

Multiple populations of stromal cells

In an animal model of intestinal inflammation, an increase in activated α-SMA+ stromal cells is noted in colonic mucosa. It has been demonstrated that bone marrow-derived cells contribute to this increase in inflamed regions when compared with non-inflamed regions of mucosa [52]. Both increases and decreases in intestinal subepithelial myofibroblasts (ISEMFs) have been reported in human IBD tissue. There also appears to be an increased sensitivity to apoptosis by ISEMFs isolated from IBD tissue. During the normal healing process, α-SMA+ myofibroblasts may increase and then decrease, thus explaining the difference in observed numbers as different stages of tissue repair may have been analysed. There also exists more than one population of α-SMA+ activated mesenchymal stromal cells. There are myofibroblasts derived from locally activated fibroblasts that contribute to tissue repair and then undergo apoptosis to resolve the inflammatory process. There are also myofibroblasts acutely derived from bone marrow precursors, which arrive at the site of ongoing inflammation and differentiate into myofibroblasts in the presence of inflammatory signals. The imbalance between these two cell types may contribute to a persistent proinflammatory phenotype of the intestinal stromal cells which perpetuates chronic inflammation.

Horiguchi et al [54] describe a novel mechanism by which ISEMFs control the Wnt/BMP gradient and the stem cell niche via secreted protein ANGPTL2. Secretion of ANGPTL2 is increased after chemical colitis or radiation in mice and is expressed by ISEMFs. It induces an autocrine positive feedback loop via integrins and the NF-KB pathway, ultimately leading to downregulation of BMP2

and BMP7. This regulates stem cell balance and contributes to wound healing.

Mesenchymal cells have distinct cell lineages and can respond to cellular damage differently. This has been shown in skin [55] in which two fibroblast lineages were identified, one of which acts first after injury to regenerate the epithelium and bring about the collagenous matrix seen in fibrosis. The other acts later in re-epithelialisation. The first cell type is not capable of inducing hair follicles hence explains the lack of hair follicles in newly closed wounds. With Wnt activation the latter lineage expands, so different fibroblasts may have different Wnt responsiveness. It is clear that mesenchymal control in inflammation is crucial for repair and to prevent ongoing inflammatory insult.

1.3.3.2 Cell-intrinsic repair: Stem cell plasticity

Adaptive plasticity in response to transient changes of environmental conditions has been reported in several organs including nerve and skin [56]. We have evolved to find ways to meet novel needs that arise during adverse conditions. Adaptive cellular reprogramming proceeds either by reprogramming a differentiated cell to pluripotency followed by directed differentiation to the desired cell type, or by direct reprogramming of one somatic cell type to another. The term transdifferentiation has been used for this latter type of direct cellular reprogramming. Both mechanisms combine loss of some differentiated features with re-differentiation along an alternative pathway, allowing one cell type, or differentiation state, to change into another.

In the intestine crypt budding and stem cell expansion occur after injury. It is

increasingly recognised that stem cell function is not an intrinsic, cell autonomous property and that stem cell fate is not fixed, even within the confines of the stem cell niche. Recent evidence has made us question the inflexible doctrine of a unidirectional hierarchy where cell fate is determined once a cell has left the crypt base niche. Disruption of the crypt microenvironment can provoke a return to stem cell function of progenitor cells. Dedifferentiation of both progenitors and fully differentiated cells has been reported.

Evidence against a unidirectional hierarchy

Within the stem cell niche, genetic ablation of a specific stem cell causes a reserve pool to step up to prevent an overall phenotypic change. Thus, diphtheria toxin receptor (DTR)-mediated ablation of *Lgr5*+ cells in mice caused no phenotypic change because of the compensatory effects of an expansion in the *Bmi1*+ cell population. This indicates the bidirectional interconversion between +4 cells and the crypt base columnar cells. Induction of chemical colitis and radiation damage provokes a more indiscriminate intestinal injury, associated with a mucosal inflammatory response. This disruption of the crypt microenvironment can provoke a return to stem cell function from progenitor cells that have ostensibly exited the stem cell niche [27].

Intestinal architecture can regenerate if either the stem cell or the progenitor zone remains intact following injury; however, if both cell populations are damaged/ ablated simultaneously, the intestinal architecture is irreversibly perturbed [57]. *Dll1 (Delta like 1)* is a marker of a progenitor cell with potential stem cell func-

tion. After intestinal radiation, lineage tracing from *Lgr5*-negative, Notch ligand *Dll1* expressing secretory progenitors resulted in full crypt-villus lineage tracing [58]. Both disease models and mouse models allow us to simulate the effects of morphogen pathway dysregulation.

Next to question whether enterocyte progenitors that express the Alkaline phosphate intestinal (*Alpi*) gene also have this capacity, lineage tracing was used in an *Alpi-IRES-CreERT2 model* [59]. Marked clones consisted entirely of enterocytes and were all lost from villus tips within days. After targeted ablation of *Lgr5*-expressing stem cells, *Alpi*+ cells generated long-lived ribbons, giving rise to Paneth-like cells and proliferative stem cells. Therefore these short-lived enterocyte precursors serve as a large reservoir of potential stem cells during crypt regeneration.

These findings oppose our dogmatic understanding of a strict unidirectional tissue organisational hierarchy in the intestine and raise questions over the limits of intestinal cell plasticity. Progenitor cells are capable of dedifferentiation and return to stem cell function following injury, but so too are fully differentiated cells. Post-mitotic Paneth cells have been reported to acquire a stem cell-like transcriptome after irradiation. They could give rise to differentiated epithelial cell types and form organoids [60]. This was shown to be through enhanced Notch signalling.

Westphalen et al used a doublecortinlike kinase1 (*Dclk1*) transgenic mouse to label and trace the fate of mature tuft cells in the murine colon. Deregulation of Wnt signalling by loss of *Apc* in *Dclk1*+ tuft cells was not able to induce tumourigenesis. However, when these *APC*-deficient tuft cells were challenged with DSS to induce colitis, these quiescent, post-mitotic, differentiated cells survived out-

side of the crypt base for many months, resisting the stream of enterocytes and goblet cells passing along the crypt-villus escalator [61]. Even 3 months after induction, they formed colonic tumours. Rare lineage tracing events in the stomach and intestine were seen from transgenically labelled tuft cells and genetic ablation of these cells impaired the ability of the intestine to respond to radiation- or colitis-induced damage.

Epithelial-mesenchymal transition

It could be argued that epithelial-mesenchymal transition (EMT) is another example of adaptive cell reprogramming. This is an important part of of wound healing and is a process by which epithelial cells lose their cell polarity and cell-cell adhesion, and gain migratory and invasive properties to detach from the basement membrane and become mesenchymal stem cells; these are multipotent stromal cells that can differentiate into a variety of cell types. This happens in response to environmental cues such as morphogen dysregulation, which can be a trigger to cell changes required in carcinogenesis.

1.3.3.3 Restoration of homeostasis after temporary disruption

Well controlled homeostatic morphogen balance is temporarily disrupted by inflammatory signalling cascades. Transient stem cell plasticity promotes crypt budding to effect epithelial regeneration. Resolution of inflammation restores normal morphogen balance. Re-establishing homeostasis after tissue damage depends on the proper organisation of stem cells and their progeny. Genetic and epigenetic

mechanisms (such as gene silencing from chromatin modification) provide an essential level of regulation for inflammatory responses.

Thus it appears that regulated, temporary disruption of morphogen gradients in damaged mucosa is essential to alter stem cell dynamics, de-differentiate progenitor and even some differentiated cells and promote epithelial cell migration and proliferation to effect epithelial restitution. However the same characteristics are key attributes of malignant cells, thus failure of restoration of tight homeostatic control in intestinal inflammation or pathological disruption of morphogen gradients can result in initiation of neoplasia.

Many of the evolutionarily conserved pathways that control cell fate determination in the intestine are also involved in the physiological response to damage and intestinal regeneration. Regulated disruption of these epithelial, stromal and immunological morphogen gradients with consequential change in epithelial stem cell function is a key feature of the response to damage and underpins the regenerative and reparative capacity of the intestinal epithelium. In inflammation/regeneration there is a transient dysregulation of signalling to promote epithelial restitution. IBD will be discussed as a model of intestinal disrupted homeostasis, encompassing Ulcerative Colitis (UC) and Crohn's disease.

1.3.3.4 Disrupted homeostasis in human and mouse models

In IBD (Inflammatory Bowel Disease), characterised by cycles of mucosal injury and ulceration, elevated crypt fission has been observed [62]. In homeostasis an adult crypt divides every 30-40 years [63], whereas in IBD up to 60% of crypts

have been reported to be in fission. There also appears to be an increased rate at which a single stem cell populates the niche within IBD crypts. Both mechanisms enable epithelial restitution to heal ulcers. Crypt fusion has been more recently reported in mice, an almost exact reverse phenomenon of crypt fission, in which 2 crypts fuse into 1 daughter crypt [64]. As counteracting processes, crypt fission and fusion can regulate crypt numbers and the balance becomes crucial in disrupted homeostasis.

Mouse models of chemical colitis are a useful technique to study the disease. These include trinitrobenzene sulfonic acid (TNBS)-induced colitis, oxazolone induced-colitis and dextran sulphate sodium (DSS)-induced colitis models are most widely used. TNBS elicits Th-1 driven immune response, whereas oxazolone predominantly exhibits immune response of Th-2 phenotype. DSS-induced colitis model also induces changes in the Th-1/Th-2 cytokine profile [65]. DSS is a long chain (5-140 kDa), negatively charged polysaccharide derived from the esterification of dextran and chlorosulfonic acid. The location of colitis is highly dependent on the DSS molecular weight, with low weight DSS (5 kDa) inducing lesions in the caecum and proximal colon, mid weight (40 kDa) DSS provoking lesions in the mid and distal colon and high weight DSS (500 kDa) failing to induce colitis in mice. The addition of a single injection of Azoxymethane (AOM) shortens the latency time for induction of CRC and acts as a model for colitis-associated cancer (CAC) [66].

It is not clear whether the Wnt pathway is upregulated in IBD, although mucosal repair in mice is enhanced by activation of the Wnt pathway [67]. Wnt ligands and *Fzd 3* and *4* receptors have been reported to be increased in IBD biopsies, but

there was no increase in a panel of Wnt target genes in that study [68]. In another paper Wnt target gene *C-myc* was increased in human and animal models of IBD [69] but there was no change in expression of β-catenin, APC or E-cadherin.

There is no conclusive evidence for the role of BMP in colitis. Analysis of *SMAD5* gene expression in human IBD patient samples revealed a significant downregulation of the gene transcript in Crohn's disease and ulcerative colitis samples. *Smad5* knockout mice exposed to DSS colitis were significantly more susceptible to disease and had impaired wound healing during the recovery phase [70]. BMP signalling is therefore required for intestinal regeneration, but may be downregulated in comparison to homeostasis.

In mouse models of colitis, genetic and pharmacological manipulations that decrease Hh pathway signalling in the colon worsen colitis [71]. *GLI1* activity is associated with IBD, predominantly UC [72]. Mice with reduced *Gli1* activity exposed to DSS developed severe intestinal inflammation, with considerable morbidity and mortality compared to wild-type. Early-stage blocking of Notch signalling may ameliorate acute DSS colitis by preventing reduction in the number of goblet cells. In these animals there is increased *Math1* and *Muc2* expression, and the severity of colitis is reduced. In IBD the Notch target gene *Hes1* is upregulated in epithelial cells [73]. This may suggest that the Notch pathway is upregulated in IBD and manipulating this would be of therapeutic benefit. Contradictingly though, *Notch1* expression was found to be significantly lower in mucosa of IBD patients [74].

1.4 Carcinogenesis

1.4.1 Stem cell dynamics

1.4.1.1 Neutral drift

Elegant work by the Winton and Clevers groups has shown that murine intestinal stem cells form an equipotent population that undergoes stochastic clone extinction, compensated by expansion and replacement by a neighbouring cell. This random enlargement and contraction of clones, known as neutral drift dynamics, can lead to stochastic clonal extinction or niche succession where one clone expands to fill the entire niche [75] [76]. Similar neutral drift dynamics are seen in human colon using mtDNA mutations as clonal markers [63].

1.4.1.2 A spectrum of stem cells

Recent groundbreaking work by Ritsma [77] used surgical implantation of abdominal imaging windows and continuous intravital imaging to temporally observe fluorescently labelled stem cell dynamics *in vivo*. Quantitative analysis of individual clonal lineages showed that "central cells" at the crypt base, optimally located near niche derived signals, had a survival advantage over "border cells" in the upper part of the niche. Compared with their centrally located counterparts, border cells were more likely to be displaced into the transit-amplifying compartment, lose stem cell properties and progress along the crypt-villus escalator. This indicates that there is a spectrum of stem cell function even within cells expressing the *Lgr5* marker and that these cells transit reversibly between states

of variable competence influenced by proximity to niche derived signals. Somatic events such as *APC* and *Kras* mutations that bestow a selective advantage can bias a stem cell towards clonal expansion within the niche, although Vermeulen et al [78] showed that this is not necessarily inevitable. Interestingly other mutations such as *p53* inactivation only resulted in a selective advantage and resultant niche succession in an inflammatory microenvironment, which highlights the critical interplay between genotype and environmental context in disrupted homeostasis and colorectal carcinogenesis.

1.4.2 The cell of origin debate

The ISC-driven models suggest a cell-autonomous induction of adenomas. However, in the Apc^{Min} mouse model (section 1.4.8.1.2), regulation by environmental factors is clearly observed. For example administration of DSS results in a strong increase in polyp formation in Apc^{Min} mice, indicating that extrinsic microenvironmental factors have an important role.

The work by Barker and others showed that loss of *APC* in *Lgr5*+ [79], *Lrig*+ [22] and *CD133/Prominin1* cells [80] can cause rapid adenoma development. This suggests that Wnt activation in stem cells is sufficient for adenoma formation. Further work though showed that in the context of microenvironmental dysregulation, non-stem cells could act as the cell of origin.

1.4.2.1 The "top-down versus bottom-up" debate

The cellular origin of colorectal neoplasia has been controversial, centred on the mechanism of clonal expansion in human colorectal precursor lesions. When the Vogelstein lab microdissected several early adenomas, they found that only cells at the luminal surface had mutations in *APC*, whereas the underlying crypts revealed no such mutations. This led to the "top-down" model, where tumour initiation starts at the top of the crypt and spreads laterally and downwards towards the normal crypt [81].

The "bottom-up" model was founded on the more conventional crypt base stem cell compartment and an assumed unidirectional tissue organisational hierarchy. This model proposed that dysplasia arose in the stem cells at the crypt base with subsequent spread of dysplastic progeny along the length of the crypt, as seen in monocryptal adenomas in Familial Adenomatous Polyposis (FAP) patients [82]. This model was strongly supported by the induction of progressive intestinal tumourigenesis as a result of the selective introduction of Wnt activating mutations into *Lgr5*+ crypt base columnar cells which was a stark contrast to the non-progressive phenotype provoked by introducing the same mutations into non-stem cells [79]. The bottom-up theory also received strong genetic support from Sangiorgi et al, as an activating beta-catenin mutation using *Bmi1-Cre* recombinase mice also led to the rapid development of full adenomas.

1.4.3 Non-stem cells as a potential cell of origin

1.4.3.1 Inflammation

Schwitalla et al used mouse models to demonstrate that activated nuclear factor-kappa B (NFKB) induced mucosal inflammation, in combination with constitutive epithelial Wnt signalling transgenically targeted to the non stem cell population, could induce dedifferentiation of *Lgr5*-ve cells situated outside the crypt base stem cell niche. Critically they also showed that it was these dedifferentiated villus cells that gave rise to the tumours that rapidly arose in these animals [83]. This highlights the dependence of both cell-intrinsic (genetic) and cell-extrinsic (microenvironmental) factors in promoting carcinogenic initiation. The same study showed that one of the consequences of a *KrasG12D* mutation in CRC was to activate NFKB signalling and hence *Kras* could also initiate tumourigenesis in differentiated cells when combined with Wnt pathway activation owing to loss of *Apc*.

Westphalen et al [61] showed that *Apc* loss in a non-stem cell population could initiate tumourigenesis after an extra event such as inflammation.

1.4.3.2 Morphogen disruption

A change in morphogen signalling can provoke a similar microenvironmental change in cell fate determination as inflammation. A working example of this is the human disease Hereditary Mixed polyposis syndrome (HMPS), an autosomal dominant condition named for the mixed morphology of polyps. Individual

lesions exhibit mixed adenomatous crypts, dilated cysts and epithelial serration. Characteristically these polyps develop small ectopic crypts that grow orthogonally to the crypt-villus axis (ectopic crypt foci, ECF). HMPS is caused by a 40kb duplication upstream of the BMP antagonist *GREM1* which results in a compartmental expression switch; from a restricted mesenchymal gradient to ectopic gene expression throughout the epithelium [84]. Patients develop CRC at a median age of 47 years. SOX9 is also positive in HMPS polyp ectopic crypts, as shown in figure 1.7.

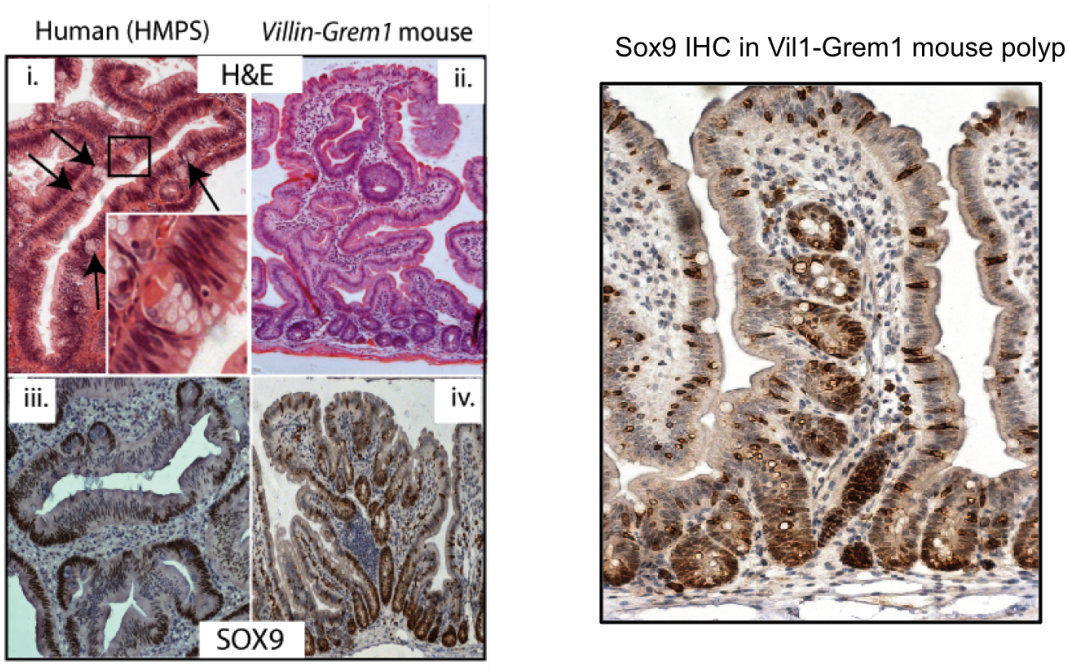

Figure 1.7: H&E stain and Sox9 staining in HMPS human polyps and in *Vil1-Grem1* mouse polyps. Adapted from [85]

A transgenic mouse was designed to model this condition, with a compartmental change in Grem1 expression (from mesenchymal to epithelial expression). It developed mixed morphology polyps arising from ectopic crypts. This led to the expansion of an *Lgr5-ve* progenitor cell population into ectopic crypts which pro-

liferate and accumulate somatic mutations resulting in intestinal neoplasia arising from outside the crypt base stem cell niche [85]. mRNA expression profiling confirmed no significant enrichment of *Lgr5*-based intestinal stem cell profiles on transgenic villi but there was enrichment of villus gene programmes characterising proliferating, early transit amplifying cells. There was marked expansion of a progenitor cell pool outside the intestinal stem cell niche that could be defined immunohistochemically as Sox9-positive EphB2-positive CK20-negative. Thus Sox9 was a specific marker of both crypt base and ectopic crypt progenitor cells. The role of *Sox9* in carcinogenesis is discussed below in section 1.4.9.

A sporadic equivalent of HMPS is the Traditional Serrated Adenoma (TSA). This is caused by ectopic epithelial GREM1 expression. Polyps occur in the distal colon in 2% of colonoscopies and can progress to an aggressive CRC type. They are much rarer than adenomatous or sessile serrated polyps, the other types of sporadic intestinal polyps. Interestingly TSAs also show ectopic crypt foci histologically.

1.4.4 Colorectal cancer as a clinical problem

Colorectal cancer (CRC) is the third most common cancer worldwide and is the fourth leading cause of cancer death. 95% of cases are adenocarcinoma and it is thought to be the product of sequential mutations in key genes. This is founded on the Fearon and Vogelstein model of mutations starting with *APC* and culminating in *p53* as the final step to cancer initiation. It is now known that not all CRC progresses in this way. The role of stem cells and morphogen pathway disruption

in carcinogenesis remains unclear.

1.4.5 A hierarchy of cells within cancer: The cancer stem cell theory

Colorectal cancer remains a paradigm for the cancer stem cell model, which proposes that tumours are maintained by a small population of tumourigenic, self-renewing cancer stem cells that are at the apex of a cellular hierarchy, not dissimilar to that seen in normal tissue. The bulk of the tumour is thus made up of non-clonogenic daughter cells that have initiated organ-specific differentiation programmes and have limited tumourigenic and metastatic potential. In contrast to the exquisitely controlled and balanced morphogen signalling seen in intestinal homeostasis, the cancer stem cell microenvironment is a disorganised and chaotic signalling mix, originating from cancer associated fibroblasts, infiltrating immunocytes and endothelial cells.

Tumours consist of heterogeneous populations of cells despite being monoclonal in origin due to genomic instability and differences in the tumour microenvironment. It is postulated that a cellular hierarchy also exists within tumours, with only cancer stem cells (CSCs) retaining the ability to self-renew to maintain tumour cell populations and drive metastasis. Tumours arising from CSCs demonstrate differentiation capacity *in vivo* with the majority of tumour cells contributing to tumour bulk but not maintaining the tumour. The acquisition of Epithelial-mesenchymal transition (EMT) may be important for CSCs.

By using spheroid cultures or freshly isolated tumour cells from CRC, there is

evidence to indicate that the capacity to propagate a tumour with all differentiated progeny resides in a single CSC. Single cell cloned CSCs can form an adenocarcinoma on xenotransplantation but do not generate the stroma within tumours. They can self-renew and are capable of multilineage differentiation [86]. Perhaps unsurprisingly human colorectal CSCs can be defined on the basis of high WNT signalling activity, and preferentially localise to myofibroblasts in xenotransplants.

In support of this model numerous researchers have used flow cytometry to identify specific populations of cells with variable tumour-initiating properties [87] [88]. Colon cancer stem cells have been sorted using FACS (fluorescence activated cell sorting) based on several factors including CD44, CD133, CD24 and ALDH1 [89]. Work on glioma identified GREM1 as a marker of CSCs [90] but there is no evidence of this in other organs. Stem cell functionality within cancers may in fact be defined spatiotemporally as cells at the tumour edge have been found to drive tumour expansion through proximity with cancer-associated fibroblasts [89].

1.4.6 Subtyping of colorectal cancer

There is recent evidence demonstrating the molecular heterogeneity of colorectal cancer. Several publications have sought to classify and subtype colorectal cancer based on (epi)genetic mutation and gene expression pattern [91] [92] [93]. These molecular profiles correlate with variable prognosis and response to therapy and appear to reflect considerable differences in tumour subtype biology that cannot be predicted from their acquired epithelial genetic mutation burden. The assess-

ment of the influence of other factors such as genetic predisposition, cell of origin and tumour environment on carcinogenic pathways, molecular phenotype and response to therapy will be an important future research prospect. The CCS and newer CMS systems of classification are illustrated in 1.8.

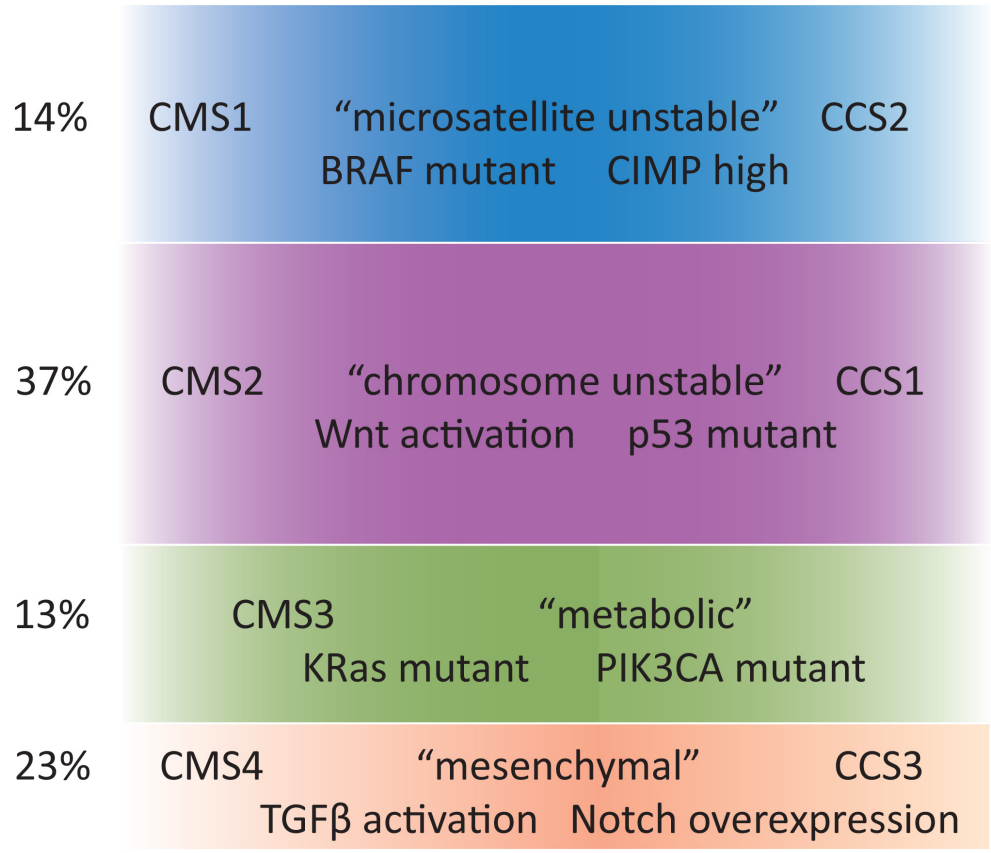

Figure 1.8: The four consensus molecular subtypes (CMS1-4) proposed by the colorectal cancer subtyping consortium [94], their frequency, and correspondence with the CCS subtypes [91].

The CMS1 subtype predominantly shows microsatellite instability and CMS2 shows chromosomal instability. The more recently described mesenchymal subtype CMS4 has an epithelial-mesenchymal transition (EMT) signature. A similar pattern was shown in the CCS3 subtype defined by De Sousa et al [91]. This

group has the worst outcome and is the least sensitive to EGFR targeted therapy. CMS4 tumours comprise 20% of tumours and are more likely to be from younger patients and those with higher stage disease. Two papers published in Nature Genetics show the importance of the tumour microenvironment on epithelial cell behaviour and response to treatment. They show that genes upregulated in CMS4 tumours are expressed by stromal elements (cancer associated fibroblasts, infiltrating lymphocytes and endothelial cells) [95] [96]. They are associated with a poorer prognosis and poor response to radiotherapy in rectal cancer. This mesenchymal signature can be linked to high *GREM1* expression, shown in tumour samples matched to the CCS3 signature using TCGA RNA-sequencing data [85]. Traditional serrated adenomas (TSAs), thought to be the precursor lesions to CCS3 subtype tumours, also show high *GREM1* expression.

1.4.7 Environmental factors in CRC

1.4.7.1 The inflammatory drive

In humans the strongest support for environmental control of CRC comes from the observation that chronic inflammation in IBD patients predisposes them to cancer. Patients with a long history of Ulcerative Colitis are known to be at higher risk of CRC; 2% after 10 years, 8% after 20 years and 18% after 30 years of disease [97]. Primary Sclerosing Cholangitis, an inflammatory condition of the bile ducts associated with IBD, increases the risk of CRC further. The risk of CRC development is 14% at 10 years and 31% at 20 years in PSC patients with concurrent IBD [98]. In CRC not associated with inflammation, there is also clear histopatho-

logical evidence for the function of immune cells in the stroma of malignancies. In addition, the administration of non-steroidal anti-inflammatory drugs lowers the risk of CRC-specific mortality, and specific cyclo-oxygenase 2 (COX-2) inhibitors cause reductions in intestinal polyps in Apc^{Min} mice. This effect is at least partially mediated by a decrease in prostaglandin E2 (PGE2) levels, leading to a reduction in myofibroblast secretion of tumour-supporting factors such as hepatocyte growth factor (HGF) and amphiregulin. In addition, lower PGE2 levels decrease the influx of tumour-associated macrophages and mast cells, which form an important tumourigenic component of the cellular stroma.

Population-based studies have shown that regular aspirin use reduces the incidence of colorectal cancer [99] [100]. Balancing the positive and negative effects of the inflammatory reaction has been key for the design of clinical treatments for a multitude of diseases. The advantage of healing tissue by recruitment of immune cells needs to be weighed against the disadvantage of chronic uncontrolled inflammation in which friendly inflammatory fire causes more harm than good. Dvorak et al proposed the theory that a tumor is a wound that never heals [101], which is still relevant as our understanding of microenvironmental control advances.

The inflammatory drive leads to differences in genetic mutations between colitis-associated cancer (CAC) and sporadic CRC. *p53* mutations in CAC occur during an early stage of neoplastic transformation [69]. This is in contrast to the Fearon and Vogelstein multistep genetic model in which *APC* mutation is the initiating event and *p53* loss is the final event [70] in the aberrant crypt foci-adenoma-carcinoma sequence. 50% of ulcerative colitis patients have *p53* mutations compared to approximately 10% of non-inflammatory adenomas. The presence of

p53 mutations in the adjacent, morphologically non-dysplastic epithelium in CAC suggests that chronic inflammation can induce genomic changes in the colonic mucosa and supports the theory of "field cancerisation". *APC* mutations are rare events in CAC, seen in 27.5% of adenomas with high grade dysplasia compared to 50% in non-CAC adenomas. Further acceleration of CAC tumourigenesis can be linked to inactivation of genes encoding DNA repair, such as mismatch repair (MMR) genes [102].

1.4.7.2 Myofibroblasts in cancer

Although myofibroblasts are essential components of both inflammatory and regenerative responses, their extensive proliferation without subsequent removal causes aberrant regeneration and excessive collagen deposition, leading to fibrosis. Cancer associated fibroblasts (CAFs) are a major component of the cancer stroma in providing cytokines and contributing to drug resistance. CAFs are similar in morphology to myofibroblasts, which are activated during wound healing, and a high proportion of stromal fibroblasts in cancer are thought to be activated. During wound healing activated fibroblasts would typically decrease but CAFs are perpetually activated and do not undergo apoptosis. Given the flexible dynamic of fibroblasts, CAFs can be considered a cell state rather than a cell type, and are an example of the importance of the microenvironment in controlling epithelial cell fate.

Normal activated fibroblast markers are Vimentin, αSMA, CD90, FSP1 and PDGFRα. Cancer associated fibroblast markers in addition to these are FAP, Desmin, PDGFRβ and VCAM1.

1.4.7.3 Genetic and environmental interaction

Hanahan and Weinberg proposed the theory of "hallmarks of cancer" [103] which are acquired both through accumulation of mutations and epigenetic/ microenvironmental changes: features are sustaining proliferative capacity; evading growth suppression; resisting apoptosis; enabling replicative immortality; inducing angiogenesis; activating invasion and metastasis; reprogramming energy metabolism; and evading immune destruction. With respect to intestinal tumourigenesis, predominantly thought to be driven by genetic mutation in epithelial stem cells, we must refer to the evolutionary maxim that phenotype is a consequence of the interaction of both genotype (which can be subdivided into germline and somatic mutation) and environment (subdivided into cell-intrinsic and cell-extrinsic environment) (1.9). The relative importance of these factors may vary within the increasing number of different tumour subtypes, but the cancer phenotype is determined by a variable and interacting contribution from all of these influences, not solely from acquired genetic mutation. For example FAP is driven almost wholly by a germline *APC* mutation without microenvironmental influence, whereas TSAs are driven by an aberrant morphogen environment.

1.4.8 Signalling pathways in carcinogesis

1.4.8.1 Wnt pathway in carcinogenesis

WNT hyperactivation is the key oncogenic driver in most CRCs. The Cancer Genome Atlas (TCGA) consortium estimated that up to 92% of sporadic CRCs contained at least one alteration in a known Wnt regulator [105]. Much of the

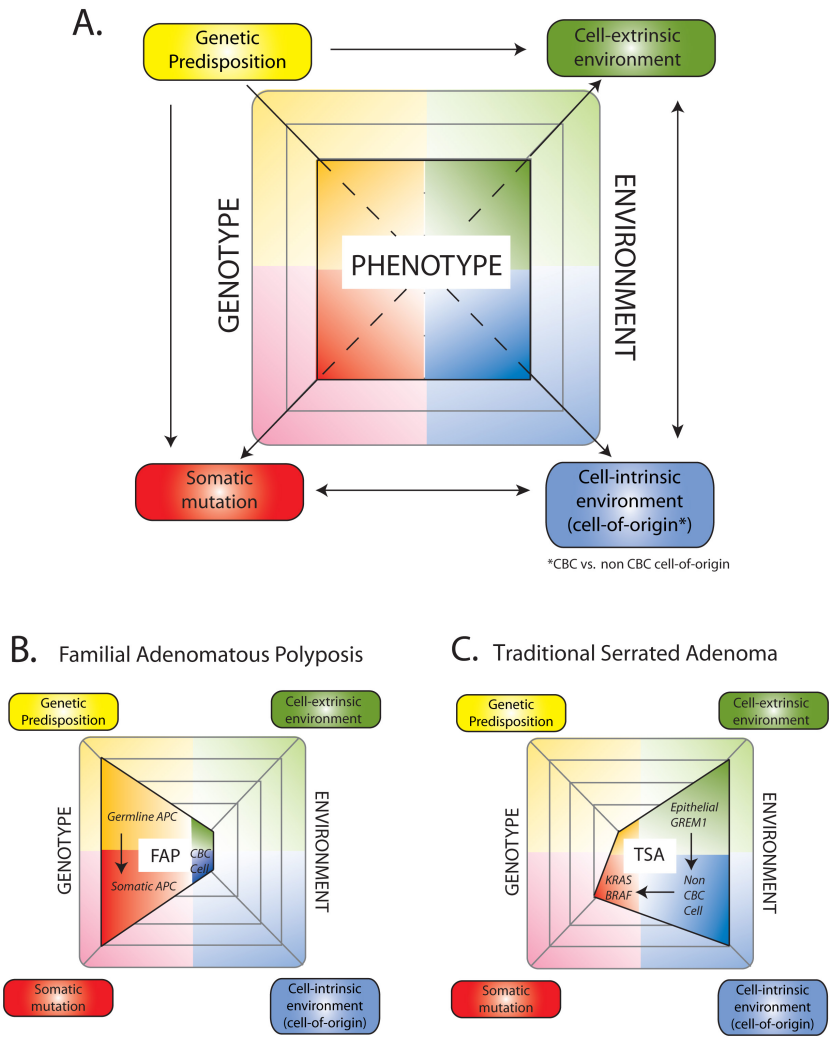

Figure 1.9: Genetic and environmental influences variably contribute to cancer phenotype in different colorectal cancer subtypes. A) Darwinian evolutionary theory is updated here by dividing genotype into genetic predisposition and somatic mutation, and environment into cell-intrinsic and cell-extrinsic environment. There is considerable interaction between these different influences e.g. the cell of origin selects for an optimal somatic mutation (arrows). The variety of cancer phenotypes can be related to the variable importance of these four different influences in tumour development. B) Familial Adenomatous Polyposis (FAP). In FAP, germline *APC* mutation in epithelial stem cells drives tumourigenesis without requirement for an altered cell-intrinsic or -extrinsic microenvironment. C) Traditional serrated adenomas (TSA). In contrast, in sporadic traditional serrated adenomas, the aberrant morphogen environment provoked by epithelial *GREM1* expression leads to cancer initiation from cells outside of the crypt base. Taken from [104].

current understanding of colorectal cancer stems from the study of rare, inherited colorectal cancer syndromes.

1.4.8.1.1 Wnt in inherited colorectal cancer syndromes Familial Adenomatous Polyposis (FAP) is an autosomal dominant disease causing colonic polyposis and CRC at a mean age of 39 years. It is caused by a germline mutation in *APC*, a tumour suppressor gene in Wnt signalling by binding β-catenin in the APC/Axin/GSK-3β-complex. Attenuated FAP is a distinct disease in which patients develop fewer polyps (less than 100), and CRC occurs 10-15 years later than in FAP. It is also autosomally dominantly inherited and 25% of patients have a mutation at the 3' or 5' ends of the *APC* gene.

1.4.8.1.2 Wnt disuption in transgenic mouse models The earliest genetic mouse model of CRC arose by chance from an ENU mutagenesis screen performed in the late 1980s in the laboratory of William Dove. The multiple intestinal neoplasia (Min) phenotype was subsequently mapped and identified as a single nonsense truncating mutation in *Apc* (Apc^{Min}) [106]. Polyps develop after loss of the second *Apc* allele and animals develop panintestinal polyposis after several months.

To model human CRC better, mouse strains containing different types of truncated Apc have been generated, representing the variety of human *APC* mutations, and these show subtle differences in the number and location of adenomas. This indicates that the dose of WNT signalling is crucial. Notably, Apc^{Min} mice with an extra mutation in the homeobox gene *Cdx2*, a regulator of colonic epithelial cell

differentiation, develop most polyps in the colon.

1.4.8.1.3 Wnt in sporadic colorectal cancer Despite the fact that the deletion of both *Apc* alleles results in rapid adenoma formation, WNT activity levels in human CRC seem to be strongly regulated during both initiation and progression. This is in part due to the genetic make-up of developing lesions and in part induced by the microenvironment. For instance, loss of the normal *APC* allele in individuals with FAP is a non-random event, because the nature of the germline *APC* mutation has been shown to influence the nature of the second *APC* hit [107]. In essence, it seems that the shorter the germline-truncated APC protein is, the longer the somatic-mutated APC protein will be, and vice versa. As the length of truncated APC is directly linked to the ability to prime β-catenin for degradation, this led to the "just right" signalling model, in which only a specific range of WNT signalling activity level is associated with transformation of intestinal epithelial cells.

1.4.8.2 BMP pathway in carcinogenesis

BMP drives differentiation and as such signalling can be presumed to be reduced in CRC. BMP signalling is downregulated in the majority of CRCs, but is conserved specifically in mesenchymal-subtype CMS4 tumours 1.4.6, where it interacts with Notch to induce an epithelial-mesenchymal transition (EMT) phenotype [108]. BMP disruption in HMPS has already been discussed above in 1.4.3.

1.4.8.2.1 BMP in inherited colorectal cancer syndromes Germline disruption of the BMP pathway by mutations in *SMAD4* and *BMPR1A* causes juvenile polyposis (JP) syndrome. Patients develop hamartomatous polyps with a 39% lifetime risk of CRC. The distinctive characteristic of hamartomas compared with adenomas is their abnormal mesenchymal component. Hamartomas in JP have an expanded mesenchymal stroma with a pronounced inflammatory infiltrate that consists primarily of lymphocytes and plasma cells.

PTEN is linked to the BMP and Wnt pathways and a mutation leads to overactivation of the mTOR pathway and causes Cowden syndrome, a rare autosomal dominant inherited disorder causing hamartomatous polyps from childhood.

Similarly, a germline mutation in *LKB1* (also known as *STK11*) causes Peutz-Jeghers syndrome. This causes hamartomatous polyps with a cumulative risk of 85% of developing GI or non-GI cancers by the age of 70. *LKB1* is a serine-threonine kinase implicated in *RAS*-induced cell metaplasia, *p53*-regulated apoptosis, and control of cell cycle arrest, and is coupled to both Wnt and TGF-β signalling.

1.4.8.2.2 BMP in sporadic colorectal cancer A number of recent studies have investigated a possible role for the BMP pathway in sporadic colorectal cancer. At the ligand level BMP2, BMP3 and BMP7 have been found to be growth-suppressive and expression of BMP3 is frequently lost through promoter methylation, compatible with a tumour suppressor role for BMPs in colorectal cancer. However, expression of BMP4 and BMP7 have been found to increase with passage through the adenoma-carcinoma sequence and to correlate with a

worse prognosis [109].

A study in which pSMAD1, pSMAD5 and pSMAD8 expression was examined in adenomas and colorectal carcinomas showed that loss of BMP signalling occurs at the transition from late adenoma to early cancer. Later in cancer progression intact BMP signalling is associated with more advanced tumour grade [109]. This suggests a role for the loss of BMP signalling in sporadic CRC, not as an initiator of carcinogenesis as in the hamartomas, but in tumour progression at the point of transition from adenoma to cancer.

In vitro BMP2 inhibits the proliferation and growth of human CRC cells [110]. Addition of Gremlin1 to CRC cell lines was found to inhibit differentiation and activate Wnt signalling [111].

An example of BMP inhibition specifically causing a type of progression to CRC is the Traditional Serrated Adenoma (TSA) (section 1.4.3).

1.4.8.2.3 BMP disuption in transgenic mouse models Mice with intestinal epithelial *Bmpr1a* knockout show impaired terminal differentiation of cells from the secretory lineage but no change in determination of cell fate [40]. Although there was increased proliferation and crypt fission, loss of Bmp signalling exclusively in the epithelial compartment was not sufficient for the initiation of the de novo crypt phenomenon seen in juvenile polyposis syndrome. Therefore loss of Bmp signalling in both mucosal components is required for hamartomatous polyp development in the mouse. Similarly *Smad4* epithelial knockout mice resulted in an obvious expansion of the Lgr5+ stem cells and significantly enlarged proliferative crypt compartment with increased numbers of Paneth cells [112].

Inhibition of BMP signalling by transgenic expression of *Noggin* results in the formation of numerous ectopic crypt units perpendicular to the crypt-villus axis which are Ki67-positive [113]. At 3 months mice develop polyps with dilated cysts and branched villi. No further work was done to characterise these ectopic crypts. A compartmental switch in *Gremlin1* from mesenchymal to epithelial expression can promote stem cell activity away from the crypt base [85] 1.4.3. Ectopic crypts accumulate mutations and can initiate neoplasia.

1.4.8.3 Hedgehog pathway in carcinogenesis

1.4.8.3.1 HH in sporadic colorectal cancer Stromal Hedgehog is downregulated in CRC. Diminished downstream Hh signalling enhances CRC development and stromal Hh activation can act as a colonic tumour suppressor [114]. However a specific Hh antagonist provided no benefit in a clinical trial [115]. It may be that stromal-specific Hh manipulation is required, as this markedly reduced tumour load in mice.

1.4.8.3.2 Hh disuption in transgenic mouse models Deletion of intestinal epithelial *Ihh* disrupted the intestinal mesenchymal architecture, with loss of the muscularis mucosae, breakdown of the extracellular matrix, and reduction in the number of crypt myofibroblasts. Concurrently, the epithelial compartment had increased Wnt signalling and disturbed crypt polarity with increased proliferation and increased numbers of ISCs. Hedgehog inhibition was found to deregulate BMP signalling and disrupt extracellular matrix proteins, fostering a proliferative environment for ISCs and progenitor cells, and mice developed patchy colitis

[116].

IHH is therefore required to maintain a stromal phenotype in which myofibroblasts and smooth muscle cells predominate. *Ihh* knockout in *APC* mutant mice almost abrogated adenoma development, and overexpression of *Shh* increased the number and size of adenomas that developed [117]. In adenomas that formed, the composition of the adenoma stroma changed, with no SMA or desmin-expressing cells and an increase in vimentin-positive cells.

Conditional deletion of *Patched1 (Ptch1)* receptor, a negative regulator of the pathway, led to constitutively active Hh signalling and resulted in accumulation of myofibroblasts and colonic crypt hypoplasia [118]. A reduction in the number of epithelial precursor cells was observed with premature development into the enterocyte lineage and inhibition of Wnt signalling. Activation of Hh signalling resulted in induction of the expression of bone morphogenetic proteins (Bmp) and increased Bmp signalling in the epithelium. When *Ptch1* was conditionally deleted in myeloid cells mice developed GIST (GI stromal tumour)-like tumours [119]. The Hh signalling pathway was activated in the tumour cells and Pdgfrα, known to be overexpressed in GIST, was overexpressed and activated.

By using the pan-Hh inhibitor Hhip under control of the *Villin* promoter, the Gumucio lab generated a murine model to study the effects of abrogating all Hh signals in the postnatal intestine [120]. The epithelium was flattened with lack of villus formation and epithelial remodelling. Changes in the mesenchyme occurred with expansion of smooth muscle progenitors and mislocalisation of intestinal subepithelial myofibroblasts (ISEMFs). There was resulting increased proliferation and enhanced β-catenin activity.

1.4.9 The role of *SOX9* in carcinogenesis

SOX9 (sex determining region Y box 9) is a gene at chromosome position 17q24 which encodes high mobility group box transcription factor *Sox9*. It is a Wnt target and is discussed separately here due to its relevance in this thesis as a key player in the HMPS model. *SOX9* is important in male sexual development and in skeletal development and a de novo mutation in *SOX9* causes Campomelic dysplasia, characterised by skeletal malformation and often autosomal sex reversal [121]. In early embryonic stages *SOX9* is expressed throughout the intestinal epithelium but later high expression is restricted to the crypt base columnar cells, enteroendocrine cells and Paneth cells.

1.4.9.1 *Sox9* as a marker of stem cells

Using transgenic mice expressing *GFP* under the control of a *Sox9* promoter, it was established that varying levels of Sox9 are expressed in the intestinal crypt [122]. Low levels are expressed in *LGR5*-positive crypt base stem cells and high levels in post-mitotic enteroendocrine cells and secretory progenitors. Sox9-low CBC cells were confirmed to have stem cell identity by their ability to generate multilineage intestinal organoids [123]. By contrast, Sox9-high cells were only able to proliferate and generate intestinal organoids *ex vivo* following irradiation, hence act as "reserve" +4 stem cells. Evidence for these quiescent cycling stem cells conferring resistance to radiation was also shown in [124] in which crypts from *Sox9*-knockout mice had increased sensitivity to radiation, compared with control mice, which could not be attributed to impaired cell-cycle arrest or DNA

repair.

Mice with either internal ribosome entry site (*IRES*)-enhanced *GFP* or *IRES-LacZ* knocked into the *Sox9* locus showed a similar Sox9 expression profile at the crypt base, but also reported endogenous Sox9 expression in Paneth cells [25]. *Sox9* is required for differentiation of Paneth cells as *Sox9* knockout mice have enlarged crypts in which Paneth cells are replaced by proliferating epithelial cells [125]. *Sox9* also acts cooperatively with transcription factor *Slug* to regulate stem cell fate in mammary cells [126].

The best evidence in support of Sox9-expressing cells being stem cells was provided by *in vivo* lineage tracing when typical stem cell-driven tracing clones were generated and maintained throughout the small intestine and colon [25]. Although the expression of Sox9 in various differentiated epithelial lineages reduces its value as a selective marker of endogenous intestinal stem cells, expression profiling of the *Sox9*-low population did reveal CD24 as a cell-surface marker that can be used to enrich for CBC stem cells through cell-sorting approaches [127].

1.4.9.2 *Sox9* as an oncogene or tumour suppressor gene

The oncogenic role of *SOX9* is unclear due to paradoxical evidence [128]. There is evidence for it acting as an oncogene as there is a gain of copy number in cancers and it promotes proliferation by activating *BMI1* [129] [130]. It is a direct Wnt signalling target of the TCF4 complex [130] and it activates S100P protein to promote invasion [131]. However the cancer genome atlas network found that *SOX9* is frequently mutated in non-hypermutated colon cancers [105] and other studies

have shown that overexpression of *Sox9* in a crypt cell line suppresses proliferation [122] by activation of insulin-like growth factor-binding protein 4 (*IGFBP-4*) [132]. *SOX9* is expressed in a heterogeneous way throughout cancers and there is no difference between expression in adenomas and cancers [130] [133], with no consistent correlation between *SOX9* expression and patient survival [134].

One explanation for the paradox of *SOX9* acting as an oncogene, is the presence of an alternative splicing variant, *MiniSOX9* [135] [136]. This is a truncated version of *SOX9* lacking a transactivation domain and leading to retention of the second intron. It acts as an inhibitor of *SOX9* and has been found to be overexpressed in human CRC samples. In a newer paper *SOX9* was mutated in 10.7% of CRC and overexpressed in most CRC cases. Recurrent truncating mutations in *SOX9*, leading to a structure similar to *MiniSOX9*, were common, suggesting this is oncogenic [137]. *SOX9* mutation in this paper was associated with better overall survival.

In medulloblastoma, a childhood brain tumour, *SOX9* has been shown to be a substrate of *FBW7*, a tumour suppressor [138]. *FBW7* recognises a conserved degron in *SOX9* that is phosphorylated by GSK3 kinase and consequently degraded. Failure to degrade *SOX9* promotes migration, metastasis, and treatment resistance in medulloblastoma. *FBW7* is either mutated or downregulated in medulloblastoma, and in cases where FBW7 mRNA levels are low, SOX9 protein is significantly elevated and this phenotype is associated with metastasis at diagnosis and poor patient outcome. Pharmacological inhibition of PI3K/AKT/mTOR pathway activity destabilises *SOX9* in a *GSK3/FBW7*-dependent manner, rendering medulloblastoma cells sensitive to cytostatic treatment. Therapy to alter *SOX9* activity has not yet been considered in CRC, perhaps due to conflicting evidence as to whether it

is an oncogene or tumour suppressor gene, and how to manipulate the truncated splicing variants.

1.4.10 Targets for therapy in CRC

Aside from CSCs, several important issues on the role of microenvironmental factors, the speed of tumour development and the true nature of human tumours need to be considered before translating this knowledge to human CRC. There is very good reason to understand the history of CRC as it may be crucial to understand whether different subtypes of CRC develop due to different genetic hits or from a distinct cell of origin. More importantly, with respect to prevention, knowing the cell of origin and understanding the signals that either maintain lesions as non-progressive or allow them to progress to carcinoma is of vital importance.

It is not entirely clear why exposure to chronic inflammation increases carcinogenesis but therapeutic targets are required. Currently in UC and PSC, regular colonoscopic surveillance is the only measure used to find pre-cancerous colorectal polyps and to resect them in advance of them becoming malignant. Targets for therapy in IBD which may reduce cancer risk include COX-2 inhibitors and anti-cytokine therapy such as TNFα inhibitors. Integrins activate the TGFβ pathway and integrin inhibitors have been used with success in reducing inflammation in IBD. Silencing of Smad7 with a specific antisense oligonucleotide downregulates inflammatory cytokine production and ameliorates experimental colitis in mice, and human trials are underway. Inhibition of NFKB activation may be a mechanism by which steroids exert an anti-inflammatory effect in IBD, and is another

potential target for therapy.

Organoid therapy and bone marrow-derived mesenchymal therapy are recent advances. Gene therapy for patients with a germline mutation predisposing them to CRC is yet to come to fruition, but with new techniques such as CRISPR gene editing and embryo experimentation, it may be an achievable goal.

1.5 Outline of thesis

My thesis explores the interaction between epithelium and mesenchyme with respect to different morphogen signalling pathways. The way that these change in epithelial restitution after ulceration or wounding is analysed. Manipulation of these pathways as contributors to carcinogenesis are explored. I have discussed the polarity of Wnt, BMP and HH pathways above and their importance in maintaining homeostasis in the rapidly proliferating epithelium of the intestine. I wish to further interrogate the compartments in which they are expressed and how this changes in disrupted homeostasis. The polarity of morphogens in homeostasis is analysed in chapter 3 (Epithelial-mesenchymal signalling pathways in homeostasis and inflammation). The dysregulation of polarity in inflammation is then discussed. The control by different components of mesenchyme on epithelial gradients is tested using sequencing.

Next the reciprocal interactions between morphogen pathways and between morphogens and their antagonists is explored. Hedgehog and BMP signalling are active in differentiated epithelial cells. The Hedgehog target genes are mesenchymally expressed but the way in which they control differentiation at the luminal

surface suggests they may be in the area of mesenchyme near the villi. The way BMP and Hedgehog interact is tested in *in vitro* and *in vivo* models in chapter 4 (*In vitro* and *in vivo* assessment of the role of *Grem1* in intestinal regeneration). The paracrine antagonism between BMP and Gremlin will be studied in organoid models, and evidence for *Grem1* as a promoter of organoid budding in a dose-dependent manner will be tested.

The concept of non-stem cells as a potential cell of origin is discussed above. Next, in a mouse model of BMP dysregulation, *Vil1-Grem1*, the ability of differentiated cells to acquire progenitor status will be discussed. Progenitor cells existing outside the crypt base stem cell niche may lead to mutation and "top-down" carcinogenesis. Using lineage tracing models and sequencing this will be explored further in chapter 5 (*Grem1* in cancer initiation: Form and function of ectopic crypts in the *Vil1-Grem1* mouse model).

Identification of stem cells and the fact that marker expression alone does not substitute for functional stem cell definition, is discussed above. *Sox9* is one of the few stem cell markers upregulated in ectopic crypts of HMPS polyps and *Vil1-Grem1* polyps. Whether this has functional importance in development of ectopic crypts and polyps will be questioned. It could be that this is a marker of ectopic crypts but not essential for their development. This will be tested by crossing *Vil1-Grem1* mice with an intestinal epithelial *Sox9* knockout model. The potential oncogenicity of *Sox9* will also be considered in chapter 6 (The functional effect of *Sox9* in inflammation and carcinogenesis). Crypts from the *Sox9* knockout model will be cultured as organoids and growth and phenotype compared to wild-type mouse crypts. Intestinal injury with DSS colitis and wounding will be contrasted

between *Sox9* knockout and wild-type mouse models to test whether *Sox9* is required in epithelial restitution.

My unifying hypothesis is that when the microenvironment of a tissue is altered, stringent control over cell fate is lost. Cells outside the stem cell niche may gain the ability to act as progenitors and give rise to daughter cells. This happens in a dysregulated manner away from the usually polarised morphogen gradients, and can give rise to mutation events leading to cancer. Re-instituting polarised morphogen gradients in the correct compartments may allow regain of cell fate and reduction in mutation events, and could be a target for a subtype of cancer therapy in the future.

Chapter 2

Materials and Methods

2.1 Human sample collection

2.1.1 Consent and ethics for human samples

All samples were collected at the Oxford University Hospitals NHS Foundation Trust. For endoscopic biopsies patients were consented using the GI illness biobank or IBD biobank. For surgical specimens the IBD biobank or Oxford Radcliffe Biobank (ORB) was used. Ethical approval for the collection and use of samples had been sought for these biobanks from independent ethical review committees: REC 11/YH/0020 for GI biobank, REC 09/H1204/30 for IBD biobank, REC 09/H0606/5+5 for Oxford Radcliffe Biobank.

2.1.2 Microdissection of fresh endoscopic biopsies

From healthy subjects attending for colonoscopy or flexible sigmoidoscopy, two pairs of 5mm forceps biopsies from each area of bowel were collected fresh in 5ml dissociation media (30 mM EDTA in DMEM without Ca2+ and Mg2+, 0.5 mM DTT, 2% RNAlater (Life Technologies)). The digested tissue was then transferred to PBS and shaken vigorously for 30 seconds to release individual crypts and villi. Single crypts were hemi-dissected within twenty minutes of collection under a dissection light microscope and transferred to RLT buffer containing beta-mercapto-ethanol. The remaining mesenchyme was shaken until no crypts were left. This was homogenised using a micropestle then a QIAshredder kit (Qiagen). For small bowel samples crypts and villi could be differentiated under the microscope without dissection. RNA was immediately extracted (see 2.5.1).

From patients with an active flare of ulcerative colitis (all previously proven to have UC based on histology and clinical reports) two pairs of biopsies were taken from an area adjacent to an ulcer. Two pairs of matched control biopsies were taken from healthy appearing colon at least 10cm away from the inflamed area. RNA was again immediately extracted (see 2.5.1).

2.1.3 Human surgical specimens

Fresh samples from IBD colectomy specimens were collected from the hospital Pathology Department. Areas of ulceration and adjacent normal areas were collected. They were fixed overnight in 10% neutral buffered formalin and then transferred to 70% ethanol. Samples were processed and embedded as per sec-

tions 2.3.2 and 2.3.3.

2.2 Mouse procedures

All mouse experiments were completed in accordance with UK Home Office regulations under the Animals (Scientific Procedures) Act 1986 (project license PPL30/3311). My personal license is I1C62A44F. All mice were housed in individually ventilated cages at the animal unit at Functional Genomics Facility, Wellcome Trust Centre for Human Genetics, University of Oxford. All strains used in this study were maintained on C57BL/6J background for at least 6 generations. *Vil1-Grem1* mice ([85]), *Rosa26*^{YFP} mice ([139]), *Villin Cre*^{ERT2} mice ([140]) and *Vill-Cre* mice ([140]) were already available in the lab.

2.2.1 Generation of *Sox9Cre*^{ERT2} *; Rosa26*^{YFP} mice

Sox9Cre-inducible mice were purchased from Riken BRC Japan (B6.129S7-Sox9 <tm1(cre/ERT2)Haak) [141] and were crossed with reporter YFP mice. YFP heterozygosity was sufficient for cells to show up using immunohistochemistry for YFP (see 2.6.1), as shown in Figure 2.1.

These were crossed with *Vil1-Grem1* mice. To induce recombination, mice were treated with one dose of 5 mg tamoxifen (dissolved in 90% corn oil:10% ethanol) by intraperitoneal injection. Sacrificing mice 30 days post injection allowed optimal time for lineage tracing to occur.

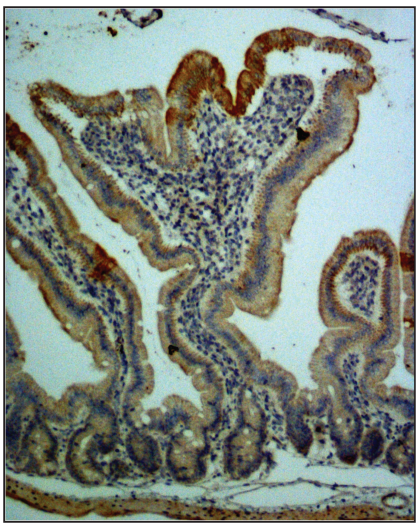

Figure 2.1: YFP heterozygosity is sufficient to show positive cells on IHC.

2.2.2 Generation of *Sox9*$^{fl/fl}$*/Vill-Cre* mice

Sox9 floxed mice were purchased from Jax labs, stock no# 013106 (B6.129S7-Sox9$^{tm2Crm/J}$) [142]. These floxed mutant mice possess a *loxP* site upstream of exon 2, a neomycin resistance (neo) cassette followed by another *loxP* site downstream of exon 3 of the *Sox9* gene. Mice that are homozygous for this allele are viable, fertile, normal in size and do not display any gross physical or behavioral abnormalities. When these mutant mice are bred to mice that express *Cre recombinase*, the resulting offspring have exons 2-3 deleted in the *Cre*-expressing tissue, resulting in inactivation of *Sox9* gene function.

These mice were bred with *Villin Cre ERT2* mice [140] and confirmed to be homozygous for *Sox9* and positive for *Villin Cre recombinase*. But mice lacked *Sox9* knockdown on qPCR and immunohistochemistry testing. It was decided to use a non-inducible model and *Sox9* floxed mice were bred with *Villin-Cre* mice. After validation as *Sox9*$^{fl/fl}$*/Vill-Cre* they were crossed with *Vill-Grem* mice.

2.2.3 *APC*^{Min} mice

These mice were already available in the lab and did not need to be bred.

2.2.4 Breeding

Breeding pairs were housed together from the age of sexual maturity (6 weeks) onwards. Trios of two females to one stud male were also used to enhance the number of required offspring per generation of breeding.

2.2.5 Ear snips

At three weeks of age, post-weaning, ear punches were taken from mice both for identification purposes and to provide material for genotyping. Different numbers of ear punches on one or both ears were used to ensure each mouse per cage had a different identification mark. DNA was extracted from these ear snips and used for genotyping using the HotSHOT method (2.4.1.1).

2.2.6 Gut preparation

The mice were sacrificed at either a pre-determined age or on showing symptoms of anaemia due to intestinal polyps (pale feet or hunching). Sacrifice was by cervical dislocation and gut preparation was performed immediately. The intestinal tract was divided into four segments, consisting of three equal lengths of small bowel (proximal SB1, middle SB2 and distal SB3) and the whole colon.

Intestines were opened longitudinally using a gut preparation apparatus described by Rudling et al [143], washed in PBS, fixed overnight in 10% neutral buffered formalin and then transferred to 70% ethanol for temporary storage prior to processing for embedding or adenoma scoring 2.3.1).

For frozen blocks used for laser capture of RNA, 2 cm sections of small bowel or colon were rolled in OCT compound (Optimal Cutting Temperature compound) within moulds. The mould was suspended in a beaker of isopentane in liquid nitrogen. Once fixed, this was stored in a -80°C freezer before sectioning on a cryostat 2.3.4.3).

2.2.7 Individual crypt isolation

After longitudinally opening the gut and washing with PBS, several 1 cm sections were sliced from the middle of SB1 and incubated in 5 ml dissociation media. The digested tissue was then transferred to PBS and individual crypts and villi along with mesenchyme were isolated as in section 2.1.2.

2.2.8 Mouse endoscopy

An adapted technique was used based on those published [144] [65]. First mice were encouraged to defaecate using a cotton bud to irritate the anus. Mice were anaesthetised using 4% isofluorane with oxygen in an induction chamber, then maintained at 2.5% isoflurane with oxygen by mask. They were laid supine and a miniature rigid endoscope (1.9mm outer diameter, KarlStorz) was inserted after lubrication. It contained a xenon light source, a high resolution camera, and a

channel for air insufflation. Endoscopic procedures were viewed with high resolution images on a flat panel colour monitor using DinoCapture imaging software. The scope was inserted to a maximum of 3 cm. If the endoscope could not be inserted easily, the scope was held still and mouse position manipulated by turning on its side. The degree of abdominal distension was monitored to prevent distress. Two 3-French biopsies were taken to induce wounding. Mice were monitored during recovery from anaesthesia, then checked after 4 hours and culled at specific timepoints. The colon was embedded and the whole block was cut, by taking 4 serial 4μm sections, with each set of 4 being 50μm apart. Every fourth section was processed with H+E in order to locate the biopsy sites. Adjacent sections were then stained for relevant markers by immunohistochemistry (2.6.1) and *in situ* hybridisation 2.5.6.

2.2.9 Dextran Sodium Sulphate (DSS) colitis

Two regimes of DSS colitis were used as described in [65].

A) 1.5% DSS (40kDa, Sigma Aldrich) dissolved in distilled water was given for three cycles of 5 days each, separated by a 2-week recovery period where normal drinking water was given. Weights were recorded weekly and mice were culled at 11 weeks.

B) One round of 2% DSS was given to mice for 5 days, then replaced with drinking water. Mice were weighed daily and culled after a maximum of two weeks. The threshold for sacrifice was $>$20% body weight loss.

2.3 Histology

2.3.1 Adenoma scoring

After fixation but before processing, gut preparations were stained with 0.2% methylene blue for 10 seconds and washed in PBS for 20 minutes. Tumours were counted with a dissection microscope at 3x magnification and categorised according to size.

2.3.2 Processing

Prior to processing, fixed gut sections were rolled into Swiss rolls, pinned together and placed in a histology cassette. Specimens were processed using a Histomaster machine (Bavimed) with the following protocol:

- 70% ethanol for 45 minutes
- 95% ethanol for 30 minutes
- 95% ethanol for 45 minutes
- 100% ethanol for 30 minutes
- 100% ethanol for 45 minutes
- 100% ethanol for 45 minutes
- Histoclear for 30 minutes
- Histoclear for 30 minutes

- Histoclear for 30 minutes
- Wax for 30 minutes
- Wax for 45 minutes
- Wax for 45 minutes

2.3.3 Embedding

Processed samples were embedded in paraffin wax using a paraffin embedding station (EG1150H, Leica).

2.3.4 Sectioning and staining

2.3.4.1 Sectioning

Paraffin blocks were sectioned in 4 μm slices using a microtome (RM2255, Leica) and placed on Superfrost slides. Slides were baked at 37°C overnight. For slides used for *In Situ* Hybridisation, sections were cut into DEPC (Diethyl pyrocarbonate)-treated water and slides were baked for one hour (see 2.5.6).

2.3.4.2 Serial sectioning for 3D processing

For serial sectioning and 3D IHC processing, blocks were sent to Barts Cancer Institute where 150 serial sections were cut and stained using an automated IHC system. Stained slides were sent to Leeds Digital Pathology services for scanning and 3D reconstruction using Aperio software scanner. 3D computerised models

were drawn using Free-D software (Institut Jean-Pierre Bourgin, INRA Versailles, France).

2.3.4.3 Laser capture microdissection and cresyl violet staining

For laser capture microdissection of RNA, MembraneSlide 1.0 PEN slides (Zeiss) required prior exposure to UV light for 30 minutes. 10 μm tissue slices were cut on the cryostat (Leica CM 3050 S) and placed on these slides. Slides were dried within the cryostat then incubated in ice-cold 70% ethanol. Next slides were stained with ice-cold cresyl violet (1% in 50% ethanol) for 30 seconds. Dehydration was completed by dipping in ice-cold 70% ethanol, and then ice-cold 100% ethanol before being air-dried at room temperature for 2 minutes. The laser capture PALM system (Zeiss) was used to dissect out areas of interest with at least three slides per sample. RNA was immediately extracted (see 2.5.1).

2.3.4.4 Haematoxylin and Eosin (H and E) staining

Paraffin sections were stained with Haematoxylin and Eosin for histological examination using the following protocol: Sections were dewaxed in xylene for 5 minutes, then rehydrated through graded ethanols (100%, 90%, 70%) for 5 minutes each, followed by 2 minutes in tap water. Sections were then stained in filtered Harris Haematoxylin for 30 seconds and washed in running water until the water ran clear. The slides were then briefly dipped into acid alcohol and left in water for 5 minutes. Sections were then stained in Eosin for 3 minutes, followed by a quick dip in water, and dehydrated through degraded alcohols for 2-5 minutes

each, before mounting a coverslip with DPX (Sigma).

2.3.4.5 Alcian Blue stain for goblet cells

Sections were dewaxed in xylene for 5 min, then rehydrated through graded ethanols (100%, 90%, 70%) for 5 minutes each followed by 2 minutes in tap water. Slides were then stained in Alcian Blue solution (Sigma) for 30 minutes, then washed in running tap water for 2 minutes, before being rinsed in distilled water. Slides were then stained in nuclear fast red solution (Sigma) for 5 minutes and washed in running tap water for 1 minute. Slides were then dehydrated through degraded alcohols for 2-5 minutes each, before mounting a coverslip with DPX.

2.4 DNA

2.4.1 DNA extraction

2.4.1.1 Isolation of DNA from mouse earsnips for genotyping

The hot sodium hydroxide and tris (HotSHOT) method was used to extract DNA for genotyping purposes following protocols described by Truett et al [145]. In brief, 50 μl of HotSHOT reagent (25 mM NaOH, 0.2 mM disodium EDTA, pH 12) was added to the ear snips in an eppendorf and incubated at 95°C for 30 minutes. 50 μl of neutralising buffer (40 mM Tris-HCL, pH 5) was then added and the mix cooled to room temperature. 2 μl of this mix was subsequently used in PCR analysis (2.4.1.2).

2.4.1.2 Polymerase Chain Reaction (PCR)

Genomic sequence and annotation data were downloaded from the Ensembl site (http://www.ensembl.org) and the University of California Santa Cruz genome site (http://genome.ucsc.edu). In all cases, PCR primers were designed using the Primer3 programme (http://frodo.wi.mit.edu/primer3/). Stock primers were diluted to 100 μM, with working stocks diluted at 1:10. A typical 25 μl PCR reaction contained 30-50 ng of template DNA, 0.4 pmoles of each primer, 1x Mg2+ free PCR buffer, 2mM $MgCl_2$, 0.2 mM of each dNTP and 1 unit of Taq DNA polymerase (all from Bioline). A standard PCR reaction consisted of an initial denaturation step at 95°C for 5 minutes, 35 cycles of 94°C for 1 minute, 55°C for 1 minute and 72°C for 1 minute and a final extension step at 72°C for 10 minutes.

PCR reactions were carried out on a PTC-225 thermocycler (MJ Research). Depending on the primer pair and target size, variations of several conditions (Mg2+ concentration, additives, annealing temperature) were necessary. PCR products were analysed using agarose gel electrophoresis and ethidium bromide staining. The gels were run alongside a 1 kb DNA ladder using Tris-Borate EDTA (TBE) running buffer. Table 2.1 shows primers used for genotyping.

PRIMER SET	PRIMER NAME	PRIMER SEQUENCE	PRODUCT SIZE
Cre genotyping	Cre F	CGGTCGATGCAACGAGTGATGAGG	600bp
	Cre R	CCAGAGACGGAAATCCATCGCTCG	
Villin Grem genotyping	Villin Grem F	GAGGTCGAGGCTAAAGAAGA	500bp
	Villin Grem R	ACCTAGTGTCGGGCATCTCC	
Sox9 genotyping	Sox9 geno F	AGACTCTGGGCAAGCTCTGG	Mut 300 bp
	Sox9 geno R	GTCATATTCACGCCCCCATT	Wt 250 bp
YFP genotyping	olMR 4982	AAGACCGCGAAGAGTTTGTC	Mut 320 bp
	olMR 8545	AAAGTCGCTCTGAGTTGTTAT	Wt 600 bp
	olMR 5546	GGAGCGGGAGAAATGGATATG	

Table 2.1: Genotyping primers.

2.5 RNA / cDNA

2.5.1 RNA extraction

RNA was isolated using the RNeasy minikit or microkit (Qiagen) according to manufacturer's instructions. Cells from culture were incubated in 75-350 μl RLT tissue lysis buffer and were disrupted by pipetting up and down. Ethanol was added to lysates creating conditions that promote selective binding of RNA to the membrane in the RNeasy column. Contaminants were washed away and purified RNA was eluted. This was treated with DNase I (Thermofisher Scientific) to degrade residual DNA, according to the manufacturer's protocol. RNA samples were quantified with the Nanodrop spectrophotometer (see 2.5.2.1).

2.5.2 Determination of nucleic acid concentration and quality

2.5.2.1 Nanodrop spectrophotometer

Determinaton of nucleic acid concentration and quality was performed using a microvolume UV-visible spectrophotometer (Nanodrop 2000, Thermofisher Scientific). In brief, 1 μl was loaded onto an optical pedestal and the absorbed light from the sample measured at a wavelength of 260 nm. The ratio of readings at 260 nm and 280 nm provided an estimate of the purity of DNA. The appropriate constant was selected to quantify double-stranded DNA, single-stranded DNA or RNA samples.

2.5.2.2 Qubit fluorometer

For quantification of smaller quantities of RNA, <100ng/μl, a Qubit 2.0 fluorometer (Thermofisher Scientific) was used. Firstly two standards were made up using 10μl standard and 190μl working solution. RNA samples were diluted by adding 2μl RNA to 198μl working solution. The working solution was made by diluting Qubit reagent in buffer, 1:200. The two standards were read first on the fluorometer, and then each sample measured.

2.5.3 Reverse transcription of RNA into cDNA

Complementary DNA (cDNA) was reverse transcribed from extracted RNA, using the High Capacity cDNA Reverse Transcription Kit (Applied Biosystems), according to the manufacturer's protocol. Sample concentration was determined using the NanoDrop (see 2.5.2.1).

2.5.4 Pre-amplification of cDNA

When using cDNA generated from individual crypts, pre-amplification was necessary prior to qPCR. A pooled mix of TaqMan probes was generated by adding 1 μl of each desired probe and adjusting to a final volume of 100 μl with TE. Pre-amplification reaction mixes were prepared as follows; 12.5 μl TaqMan PreAmp mastermix (2x) (ABI), 6.25 μl pooled assay mix (0.2x each assay), 6.25 μl cDNA sample (25 μl reaction). The pre-amplification reaction was run on a thermocycler with the following programme: initial step at 95°C for 10 minutes, followed by

14 cycles of 95°C for 15 s and 60°C for 4 minutes. Upon completion the reaction was immediately placed on ice. The pre-amplification product was diluted 1 in 20 in distilled water.

2.5.5 Quantitative Real Time-PCR (qPCR): TaqMan

Absolute quantification qPCR was performed on the ABI 7900HT cycler (Applied Biosystems) for each sample (at least in duplicate), and data were analysed using standard protocols to calculate relative expression as $2^{-}DDCT$, with GAPDH/Gapdh serving as an endogenous control [146]. TaqMan Gene Expression Assays were used for each gene of interest and are shown in the table below. These pre-prepared assays contain primer pairs and probes that have already been tested for optimal PCR efficiency by Applied Biosystems. A reporter dye (FAM dye in all cases in this thesis) is linked to the 5' end of the probe and a non-fluorescent quencher is at the 3' end of the probe.

A typical reaction contained 15ng of purified cDNA, 0.5μl of Gene Expression Assay for the gene of interest, 5μl of TaqMan FAST Universal Mastermix and dH_20 to a total volume of 10μl. The samples were run on the ABI PRISM 7900HT with the following conditions: 95°C for 20 seconds followed by 40 cycles of denaturation at 95°C for 1 second and simultaneous annealing and extension at 60°C for 20 seconds. Tables 2.2 and 2.3 show the probes used.

Probe	Code (Thermo Fisher Scientific)
BMP2	Hs00154192_m1
BMP4	Hs03676628_s1
BMPR1A	Hs01034913_g1
BMPR1B	Hs01010965_m1
BMPR2	Hs00176148_m1
GREM1	Hs01879841_s1
ID1	Hs03676575_s1
ID2	Hs00747379_m1
ID3	Hs00954037_g1
IHH	Hs00745531_s1
SHH	Hs00179843_m1
PTCH1	Hs00181117_m1
SMO	Hs01090242_m1
HHIP	Hs01011015_m1
GLI1	Hs01110766_m1
GLI2	Hs01119974_m1
GLI3	Hs00609233_m1

Table 2.2: Human Taqman probe list.

2.5.5.1 Fluidigm Biomark HD system

When numerous samples or numerous probes were required for qPCR testing, the Fluidigm Biomark HD system was used. This is a high-throughput qPCR assay based on the nanofluidic system that permits the analysis of up to 9216 qPCR reactions at once in a self-design open array chip.

2.5.6 *In situ* hybridisation

In situ hybridisation was carried out using the the RNAscope 2.5 HD Detection Kit (Advanced Cell Diagnostics) following manufacturer's instructions. GREM1 (312831), PPIB (313901), Grem1 (314741), Lgr5 (312171), Bmp4 (401301), Ppib

Probe	Code (Thermo Fisher Scientific)
Ihh	Mm00439613_m1
Shh	Mm00436528_m1
Ptch1	Mm00436026_ml
Smo	Mm01162710_m1
Hhip	Mm00469580_m1
Gli1	Mm00494654_ml
Grem1	Mm00488615_s1
Sox9	Mm00448840_m1
Wnt3	Mm00437336_m1
Wnt6	Mm00437353_m1
Wnt9b	Mm00457102_m1
Fzd2	Mm02524776_s1
Fzd5	Mm00445623_s1
Fzd7	Mm00433409_s1
Rspo1	Mm00507077_m1
Rspo2	Mm00555790_m1
Rspo3	Mm00661105_m1
Lrp5	Mm01227476_m1
Lrp6	Mm00999795_m1
Foxf1	Mm00487497_m1
Sfrp1	Mm00489161_m1
Wnt2b	Mm00437330_m1
Bmp4	Mm00432087_m1

Table 2.3: Mouse Taqman probe list.

(313911) and DapB (310043) (Advanced Cell Diagnostics) probes were used.

2.5.7 Microarrays of human biopsies

RNA was extracted using RNeasy micro spin column purification (Qiagen) and DNase treated (DNase I, Thermofisher Scientific). For mesenchyme the RNeasy mini system was used. It was quantified using Qubit fluorometric quantification (see 2.5.2.2). Nugen Ovation Pico WTA system V2 was used to amplify and Nugen Encore BiotinIL module used for labelling. Illumina HumanHT-12 v4 expression bead chip microarray was used and gene expression data downloaded in Genome Studio.

Raw data from Illumina gene expression arrays was processed using the VSN (variance-stabilisation and normalisation) algorithm. Initial quality control checks identified two outlier samples in the human colitis dataset ("colitis 1"), which were excluded from further analyses (see 3.7). All other samples were in a similar probe intensity range and there was hierarchical clustering. A filter was applied by only considering probes detected above background levels (detection score >0.95 for all samples) resulting in a total of 18,872 detectable probes for colitis samples, 24,228 for healthy colon samples and 5,594 for small bowel samples. Gene Set Enrichment Analysis (GSEA) was performed using Kolmogorov-Smirnov statistics and gene shuffling permutations as described by Subramanian et al [147]. Genes were ranked using moderated t-statistics from the 'limma' analysis for differential expression. Gene shuffling with 1,000 permutations was used to compute the P-value for the enrichment score.

2.5.8 RNA sequencing

RNA collected from laser capture dissection was sent for SMARTer RNA seq (Clontech) via HiSeq 4000. This did not require quantification or amplification of RNA as it can sequence as little as 2-100ng RNA. Sequencing depth was 8-12 million reads. GSEA was run as above.

2.6 Protein

2.6.1 Immunohistochemistry

Formalin-fixed, paraffin-embedded tissue sections (4 μm) were de-waxed in xylene and rehydrated through graded alcohols to water. Endogenous peroxidase was blocked using 1.6% H_2O_2 for 20 minutes. For antigen retrieval, sections were pressure cooked in 10 mmol/L citrate buffer (pH 6.0) for 5 minutes. Sections were blocked with 10% serum for 30 minutes. Slides were incubated with primary antibody for 2 hours. Sections were washed in PBS prior to applying secondary antibody for one hour at room temperature. Sections were then incubated in ABC (Vector labs, contains avidin and biotinylated horseradish peroxidase) for 30 minutes. DAB solution was applied for 2-5 minutes. Slides were washed in PBS, counterstained with haematoxylin, dehydrated, cleared and then mounted. Table 2.4 shows the antibodies used.

Primary antibody	Block	Primary antibody dilution
Sox9 (Abcam ab185230)	Goat	Rabbit 1:500
GFP (Life Technologies A-6455)	Goat	Rabbit 1:750
Lysozyme (Dako EC 3.2.1.17)	Goat	Rabbit 1:500
ALP (Abcam ab65834)	Goat	Rabbit 1:50
Chromogranin A (Abcam ab15160)	Goat	Rabbit 1:1250
Ki67 (DAKO, TEC-3)	Rabbit	Rat 1:125
pSmad1/5/8 (Cell Signaling, 9511L)	Goat	Rabbit 1:50
EphB2 (R & D, AF467)	Rabbit	Goat 1:125
Caspase 3 (R & D, AF835)	Goat	Rabbit 1:800

Table 2.4: Antibodies for mouse Immunohistochemistry.

2.6.1.1 Co-staining protocol

For co-staining, the first antibody was stained with Vector red stain (Vector laboratories) and the second with DAB. Vector serum was used for blocking, the first primary was incubated for 2 hours, and a ready-to-use Vector secondary was used. The Vector red stain (3.2μl reagent 1 and 2 for every 200μl of diluent) was applied for 2-5 minutes. After washing with PBS, the second antibody was applied overnight and the remaining protocol followed as above (2.6.1). If one antibody had a nuclear stain and the other a cytoplasmic stain, both primary antibodies could be raised in the same animal.

2.6.1.2 Immunohistochemistry quantification

To quantitate Ki67 immunohistochemistry of *Vill-Grem* and *Vill-Grem/Sox9*$^{fl/fl}$*/Vill-Cre*, images were captured at 20x magnification, followed by random selection of an equally-sized area and conducted blindly. The percentage of total cells which were Ki67 positive were calculated.

2.7 Cell culture

2.7.1 Counting cells

Cell numbers were counted using a Countess II Automated Cell Counter (Thermofisher Scientific). Cells were typically seeded at the following densities: 1 x 10^5 cells per well of a 6-well plate, 2.5 x 10^4 cells per well of a 24-well plate and 5 x 10^3 cells per well of a 96-well plate depending on the experiment.

2.7.2 CRC cell line culture

All cell culture protocols were carried out in a class II laminar flow hood. All cell lines were grown from frozen stocks, by thawing cells rapidly at 37°C, pelleting and re-suspending cells in appropriate tissue culture media. All cell lines used were maintained in DMEM medium plus L-Glutamine (PAA) supplemented with 10% foetal bovine serum (FBS) (PAA) and 1% penicillin-streptomycin (PAA). Cells were incubated at 37°C with 5% CO2 and were passaged before they reached confluence. In order to sub-culture cells, they were detached with trypsin-EDTA (Invitrogen). When not in use, cells were stored in liquid nitrogen. In preparation for storage, cells were harvested in the log phase of growth, then resuspended in freezing medium (90% FBS, 10% DMSO).

2.7.3 Lentiviral knockdown of Sox9

shRNA was purchased from Dharmacon (RHS4533-EG6662 glycerol set) and was transformed into E.coli plasmid. Ultracompetent XL10-Gold cells were transformed with bacterial plasmids as described by the manufacturer (Stratagene). Briefly, 70 μL of bacterial cells were incubated on ice for 10 minutes, mixed with approximately 400 ng plasmid DNA in the presence of β-mercaptoethanol, incubated on ice for 30 minutes, heat-shocked at 42°C for 30 seconds, incubated on ice for a further 30 seconds, and finally incubated at 37°C with shaking in 1ml SOC media for 1 hour. 1 μl of transformed bacterial cells was resuspended in 500 μl SOC media, spread onto LB plates and incubated overnight at 37°C. A colony was then picked and put in 1ml LB broth overnight at 37°C with shaking for 8 hours, then transferred to 200ml LB broth overnight. This was maxiprepped and aliquoted. A puromycin kill curve was done and 1μg/ml was the minimum concentration needed to kill 100% of cells. Lentivirus was then transduced into cell lines with polybrene. After 4 passages and puromycin treatment, RNA was extracted and qPCR run.

Lipofectamine transfection into SW480 cells resulted in 55% knockdown (TRCN0000020386) and 61% knockdown (TRCN0000020388) compared to scrambled shRNA lentivirus. These lines were then transformed into XL-10 gold ultracompetent cells (Stratagene), but from 50ng of lentivirus after 4 passages there was only 44% knockdown.

2.7.4 Mouse organoid culture

2.7.4.1 Crypt organoids

Mouse intestinal crypts were isolated and cultured as described by Sato et al [30]. After opening the gut longitudinally, it was pinned onto a plastic sheet on a polystyrene lid. A glass microscope coverslip was used to scrape off debris and villi. This was done repeatedly until little material came off. Next intestines were cut into 5mm slices and transferred to PBS. Coating pipettes in FBS, tissue was pipetted up and down to dislodge single cells, then washed five times with PBS. Tissue was resuspended in 25ml of 2.5mM EDTA/PBS and rotated at 4°C for 30 minutes. The pellet was resuspended in media: advanced Dulbeccos modified Eagle medium/F12 supplemented with penicillin/streptomycin, 10 mmol/L HEPES, Glutamax, 1 N2, 1 B27 (all from Invitrogen), and 1 mmol/L N-acetylcysteine (Sigma). Crypts were dislodged by pipetting up and down, and after the first fraction which was discarded, the subsequent three fractions were retained and spun down. They were passed through a 70 μM cell strainer and resuspended in Matrigel (BD Biosciences) and plated out in 24-well plates. The basal culture medium was overlaid containing the following growth factors; Epidermal Growth Factor at 50 ng/ml (Life Technologies), Noggin at 100 ng/ml (PeproTech) and R-spondin1 at 500 ng/ml (R and D) (ENS media). The medium was changed every 2 days. R-spondin1 conditioned media was used in most cases (2.7.4.3).

To collect organoids, cold PBS was used to melt the Matrigel, and individual organoids were selected under the dissection microscope. To collect material for embedding, multiple wells were combined. Samples were centrifuged, PBS and

Matrigel removed and after resuspension in PBS, spun down again. Next 4% PFA was added and left for 30 minutes at room temperature. After further washing, 150μl melted HistoGel (Thermo Scientific) was added and left to set on ice. The paraffin-embedded cell pellet was then processed and embedded using standard protocols (2.3.2, 2.3.3).

2.7.4.2 Villus organoids

Mouse intestines were opened longitudinally and the villi were scraped off with a coverslip. The first scrape of material was discarded and the subsequent scrapes were collected into sterile PBS. The material was gently washed with PBS and then centrifuged at 100g for 3 minutes. The villi were plated out in 24-well plates in Matrigel and were overlaid by standard media that was additionally supplemented with mWnt3a at 100 ng/ml (ENSW media) (R & D Systems). The media was changed every 2 days.

2.7.4.3 R-spondin1 conditioned media (CM)

To make 100% RSPO1-CM, HEK293T cells were transfected with an RSPO1 expression construct. Medium was replaced with basal medium 24 hours after transfection, and the CM was harvested after 7 days of incubation.

To generate the murine Rspo1 expression vector, Rspo1 cDNA was PCR amplified from a pLZRS expression vector using forward and reverse primers that included a Csp45I restriction site. The gel-extracted product and the pcDNA3.1(+)-Myc/HisB vector (Thermo Scientific) were digested with Csp45I restriction en-

zyme, ligated together and transformed into DH5 bacteria. Minipreps generated from transformed DH5 colonies were sequenced to check for correct integration and absence of novel DNA mutations ([148]).

2.7.5 Fibroblast culture

2.7.5.1 Purchased human colon fibroblasts

Purchased CCD-112CoN (ATCC) human colon fibroblasts were cultured in 24-well Primaria plates (Fisher Scientific) at a density of 2.5 x 10^4 cells per ml. The following media was used: DMEM with 10% FBS, 1% penicillin-streptomycin, 1% MEM non-essential amino acid, 1% fungizone, 0.5% neomycin, 0.08% gentamicin. Cells were serum starved for six hours after plating out and before addition of morphogens. All fibroblast cultures were kept in a low oxygen incubator (3% O_2, 5% CO_2) at 37°C.

2.7.5.2 Human colon fibroblasts

Two pairs of biopsies were collected from the sigmoid colon and rinsed in PBS several times, then minced using a scalpel. Tissue was digested in 40ml DMEM with 52.8mg of Collagenase type IV (225U/mg), and incubated at 37°C for 3 hours. The pellet was washed twice in DMEM and plated in Primaria plates in the medium above (2.7.5.1).

2.7.5.3 Mouse colon fibroblasts

3 cm of mouse colon was cut into 1-2mm pieces then rinsed at least 5 times in PBS. Tissue was digested as above in DMEM with Collagenase and incubated at 37°C for 1 hour. The pellet was washed 3 times in DMEM and passed through a 40μm cell strainer to remove crypts. Cells were plated in Primaria plates at 3 x 10^5 cells per ml.

Chapter 3

Epithelial-mesenchymal signalling pathways in homeostasis and inflammation

3.1 Aims

The key objectives were:

1. To assess intercompartmental signalling pathway contribution to homeostatic intestinal morphogen gradients.

2. To see how this balance is affected by mucosal inflammation and tissue regeneration.

3. To assess mesenchymal tissue functional heterogeneity

3.2 Introduction

Morphogens specify cell fate in a spatiotemporal pattern as described already in section 1.3.2. Interacting signalling pathways mean that cells are subject to very specific signals and these pathways are exquisitely controlled in homeostasis. In the intestine, polarised expression gradients of Wnt, BMP and Hedgehog have been described. It was traditionally thought that target gene expression was most intimately linked to the ultimate effect of the pathway. It is valuable to increase the granularity of our understanding of how these target gene gradients are generated, by exploring the spatiotemporal distribution of signalling pathway components (pathway ligands, receptors, signalling molecules and antagonists). The expression of these components also exert control on cells and have stimulatory or inhibitory effects. The analysis of these components of the pathways were described by Kosinski et al [111]. I was specifically interested in the degree of mesenchymal-epithelial interaction of these pathways as intercompartmental signalling mediated by secreted components is potentially amenable to therapeutic manipulation.

3.2.1 The polarised epithelial axis

In the paper by Kosinski [111] fresh human colectomy specimens were frozen and horizontal segments sliced to isolate crypt tops and crypt bases. They then isolated RNA and ran microarrays. In the crypt base they found two clusters of genes: one cluster was genes involved in cell proliferation and cell cycle regulation, and the other was genes that encode secretory proteins and those involved in matrix

modelling. At the crypt top they found genes inhibiting cell proliferation, cell adhesion molecules and genes encoding functional gut epithelial cells. The Wnt pathway was active at the crypt base with Wnt suppressors high at crypt tops. The BMP pathway was high at crypt tops and BMP antagonists were expressed at the base. The mesenchymal component of cell signalling could not be elucidated in this paper as samples included epithelium with attached mesenchyme. This was a limitation in the work and I wanted to re-explore this to examine the role of the mesenchyme, as well as to more accurately dissect individual crypt tops and bases. This is the basis for the rationale for this chapter.

The first aim was to separate the epithelium and mesenchyme to determine whether rigid morphogen gradients are driven by epithelial cell biology or are a function of intercompartmental signalling systems.

3.2.2 Changes in tissue regeneration

In tissue regeneration, important in human diseases such as IBD, the effect on morphogen signalling pathways has not been analysed by tissue compartment. An overall increase in Wnt ligands and Frizzled receptors has been reported, but no change in Wnt target genes [68]. BMP7 in animal models of colitis has been found to be reduced in the acute phase, and therapy with BMP7 improved the severity of colitis by upregulating BMP4 [149]. Hedgehog target genes as well as IHH have been reported to go down in IBD whole-biopsies [72]. I explored the effect of disruption of microenvironmental signalling on epithelial morphogen gradients by assessing regenerating crypts surrounding ulcers in active human Inflammatory

Bowel Disease.

3.2.3 The polarised mesenchymal axis

The mesenchyme provides important regulation of the Wnt, BMP and HH signalling pathways. The mesenchyme is heterogeneous though, comprising fibroblasts and myofibroblasts, blood and lymph vessels, and immune cells. Given the paracrine nature of morphogen signals, the mesenchyme surrounding the crypt base (subcrypt mesenchyme) must differ from the mesenchyme adjacent to the upper crypts (intercrypt mesenchyme). So my aim was to select spatially distinct areas of mesenchyme from human and mouse small bowel. I looked for components of the above pathways and for structural matrix markers that were differentially expressed across compartments to suggest polarised control over the crypt-villus axis.

3.3 Methods

The methods used in this chapter are described in chapter 2 and were as follows:

- Fresh human endoscopic biopsies were collected and microdissected into crypt halves and mesenchyme 2.1.2.
- Microarrays 2.5.7.
- Subcrypt mesenchyme and intercrypt mesenchyme were extracted using laser capture microdissection 2.3.4.3.

- RNA sequencing 2.5.8.
- Results were validated by qPCR 2.5.5 including use of Fluidigm 2.5.5.1.
- The findings were corroborated by immunohistochemistry 2.6.1 and *in situ* hybridisation 2.5.6.

3.4 Results

3.4.1 Microdissection of human intestinal biopsies in homeostasis

3.4.1.1 Colonic samples

Colonic biopsies from five control patients were microdissected into crypt tops, crypt bottoms and mesenchyme (see figure 3.1). This is described in 2.1.2. Two pairs of biopsies were collected from the sigmoid colon of patients at endoscopy, which were macroscopically and histologically normal in all cases. 20 crypts were dissected for each case. RNA was extracted and Illumina beadchip microarrays run. Analysis was performed using the R/BioConductor package limma to find genes differentially expressed between the three colonic compartments. Genes with log-fold change >2 and adjusted p-value <0.05 were considered significant. Further interpretation of the functional relevance was done using Gene Set Enrichment Analysis (GSEA) software from the Broad Institute. Bioinformatician

Helen Lockstone helped with this analysis.

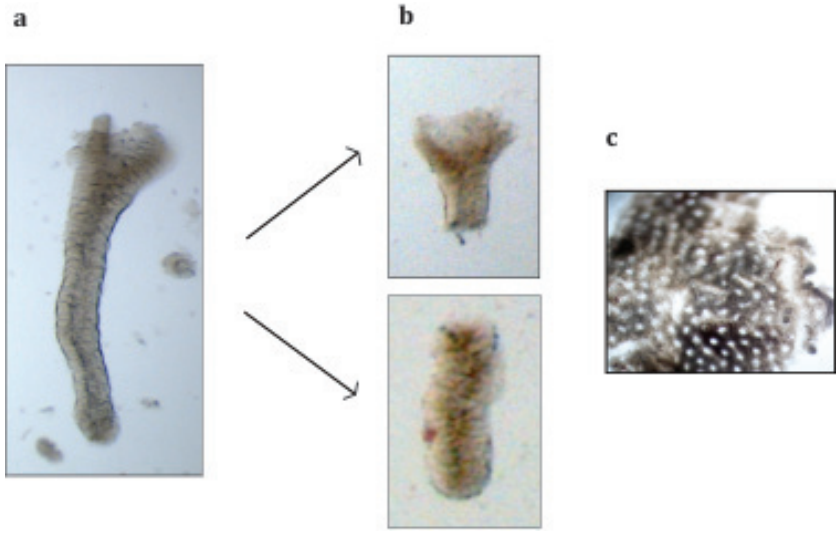

Figure 3.1: Microdissection of intestinal crypts. Light microscope photo at x20 resolution of a single human colonic crypt (a) microdissected into top and bottom halves (b). Following crypt extraction mesenchyme was separated (c).

3.4.1.2 Small bowel samples

Biopsies taken from five control patients from terminal ileum were microdissected into crypts, villi and mesenchyme. There was need to cut crypts in this case, as crypts and villi separated out and could be selected under the light microscope.

3.4.1.3 Microarray results

Samples clustered by tissue compartment on the Principal Component Analysis (PCA) plot (figure 3.2), suggesting similarity in patterns of gene expression. To illustrate whether this method had worked, differential expression of genes known to be associated with proliferation and differentiation was measured across com-

partments. Some characteristic genes are shown in figure 3.3. As shown several stem cell markers such as ASCL2 and OLFM4 were expressed at the crypt base. Markers of differentiation such as SGK1 were expressed at the crypt top. Given there is more than one probe for each gene in microarray design, mean expression was calculated for each gene. To confirm this pattern GSEA was run to custom signatures as described in [150]. Stem cells and transit amplifying cell markers were highly expressed at colon crypt bottoms with differentiation markers expressed at colon crypt tops (see figure 3.3). The gene set for markers of apoptosis did not yield a significant GSEA curve. GSEA to compartmental markers for small bowel were similar to that of colon and results are not shown.

Fibroblast markers smooth muscle actin (SMA) and Vimentin were very highly expressed in mesenchyme compared to epithelium. A filter was applied to the dataset that required genes to be expressed above background levels in at least 5 samples. Desmin was filtered out and so its expression must have been low overall.

These data showed that microdissection of single crypts is a viable way to assess gene expression across the crypt base and the crypt top. There is distinct gene expression between different epithelial compartments. As expected stem cell and transit amplifying genes are upregulated at the crypt base and differentiation marker genes are high at the crypt top. There is distinct gene expression between epithelium and mesenchyme, and structural fibroblast markers are expressed in the mesenchyme.

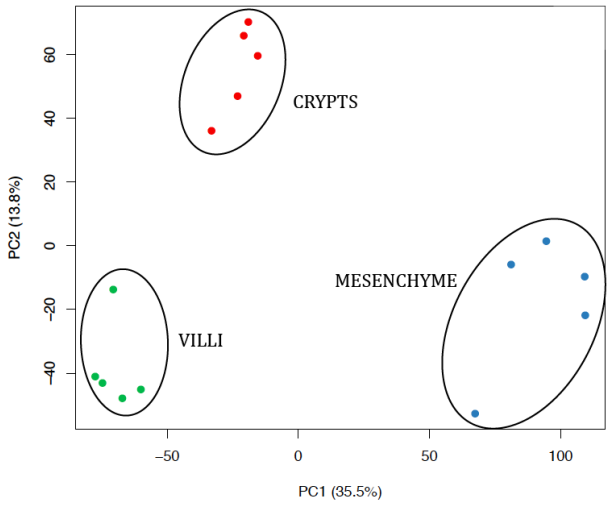

Figure 3.2: PCA plot showing clustering by tissue compartment in normal endoscopic biopsies from small bowel.

3.4.1.3.1 Morphogen pathways across compartments in homeostasis

The pathways of interest were Wnt, BMP and Hedgehog. It was noted from the differential expression that these pathways had several differences between genes expressed in different compartments, and this was analysed using heatmaps.

Heatmaps were generated with custom gene sets to Wnt, BMP and Hedgehog (figure 3.4). Firstly considering the Wnt receptors, there was variable expression of Frizzled receptors across the crypt-villus axis. FZD1, 3, 4 and 9 were expressed more highly at the base whereas FZD5 and FZD7 were expressed throughout the vertical axis. Wnt antagonists such DKK3 were higher in mesenchyme. Wnt target genes (CCND1/2, MYC, AXIN2) were higher at the crypt base, both in small bowel and colon.

For the BMP pathway, BMP2 ligand was higher at the crypt top and BMP4 was

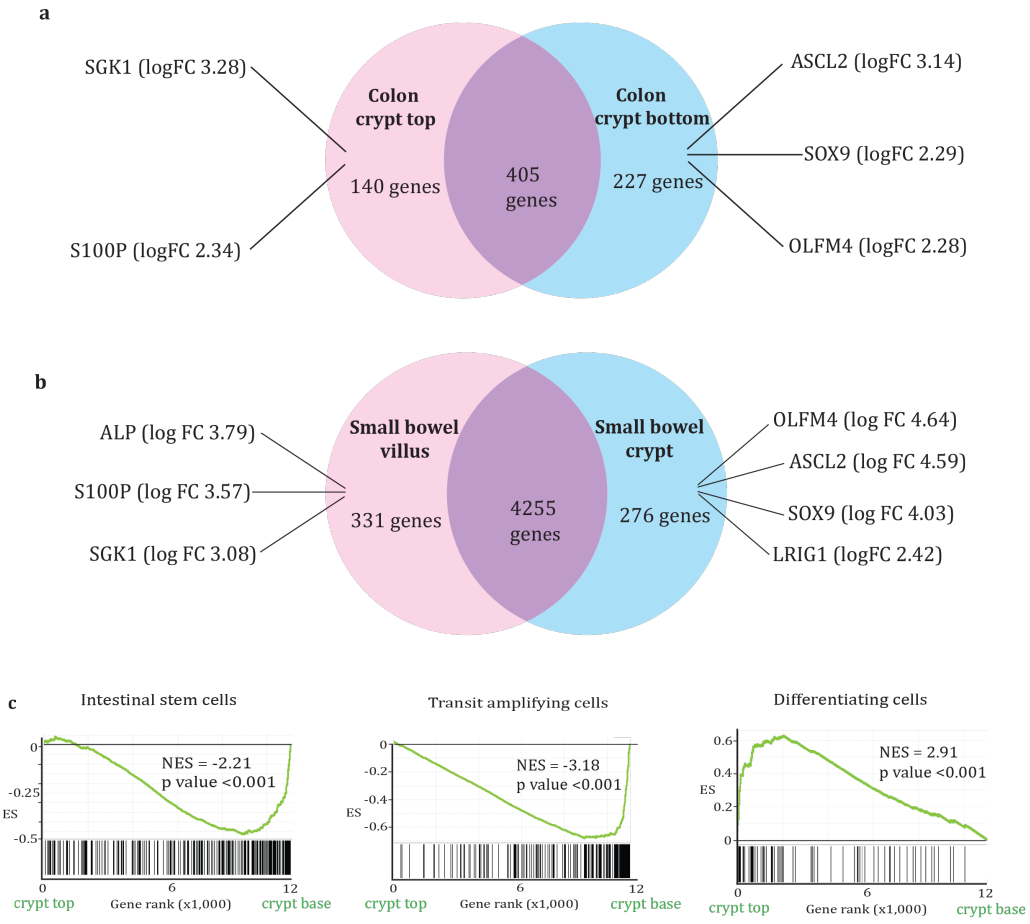

Figure 3.3: a) Differential gene expression in colon with known markers labelled with logFC (logfold change). b) Genes differentially expressed in small bowel. c) Enrichment plots for normal colon crypt top versus crypt base to custom gene sets for stem cells, transit amplifying cells and differentiating cells.

mesenchymal. It is known that BMP4 is secreted by intravillus and intercrypt mesenchymal cells. BMP receptors, especially BMPR1A, were expressed more highly at the base. Signalling molecule SMAD5 was expressed at the base and SMAD7 (inhibitory) at the top, in opposition to the pattern of BMP target genes. BMP antagonist GREM1 was expressed by mesenchyme. Target genes ID1 and ID2 were expressed, as expected, at the crypt top.

For the Hedgehog pathway there was more variable expression of ligands and target genes. Hedgehog receptors were broadly expressed at crypt tops and antagonist HHIP expression was more distinctly in the mesenchyme.

Validation by qPCR was done for the components of the BMP and Hedgehog pathways, as these were the pathways chosen for further investigation and for mouse models. cDNA from the colonic samples above were used in addition to five sets of fresh samples, so in total ten patients were sampled (see figure 3.5). The high-throughput Biomark HD system was used given the large number of samples (see 2.5.5.1). This confirmed that BMP is a mesenchymal-to-epithelial signalling pathway, with BMP4 ligand expressed in the mesenchyme, receptors expressed epithelially, and target genes in the upper crypt. BMP antagonist GREM1 is mesenchymal. The Hedgehog pathway is epithelial-to-mesenchymal, with IHH and SHH from the crypt top acting on PTCH1 and SMO receptors in the mesenchyme and allowing downstream transcription of GLI1 also in the mesenchyme. In the figure only GLI1 has been labelled a target gene, but in fact PTCH1 and HHIP expression can also be a readout of Hedgehog signalling. PTCH1 is a receptor and HHIP an antagonist so they have been labelled as such in the figure.

These data indicate that dissection of fresh intestinal biopsies is a novel way to ex-

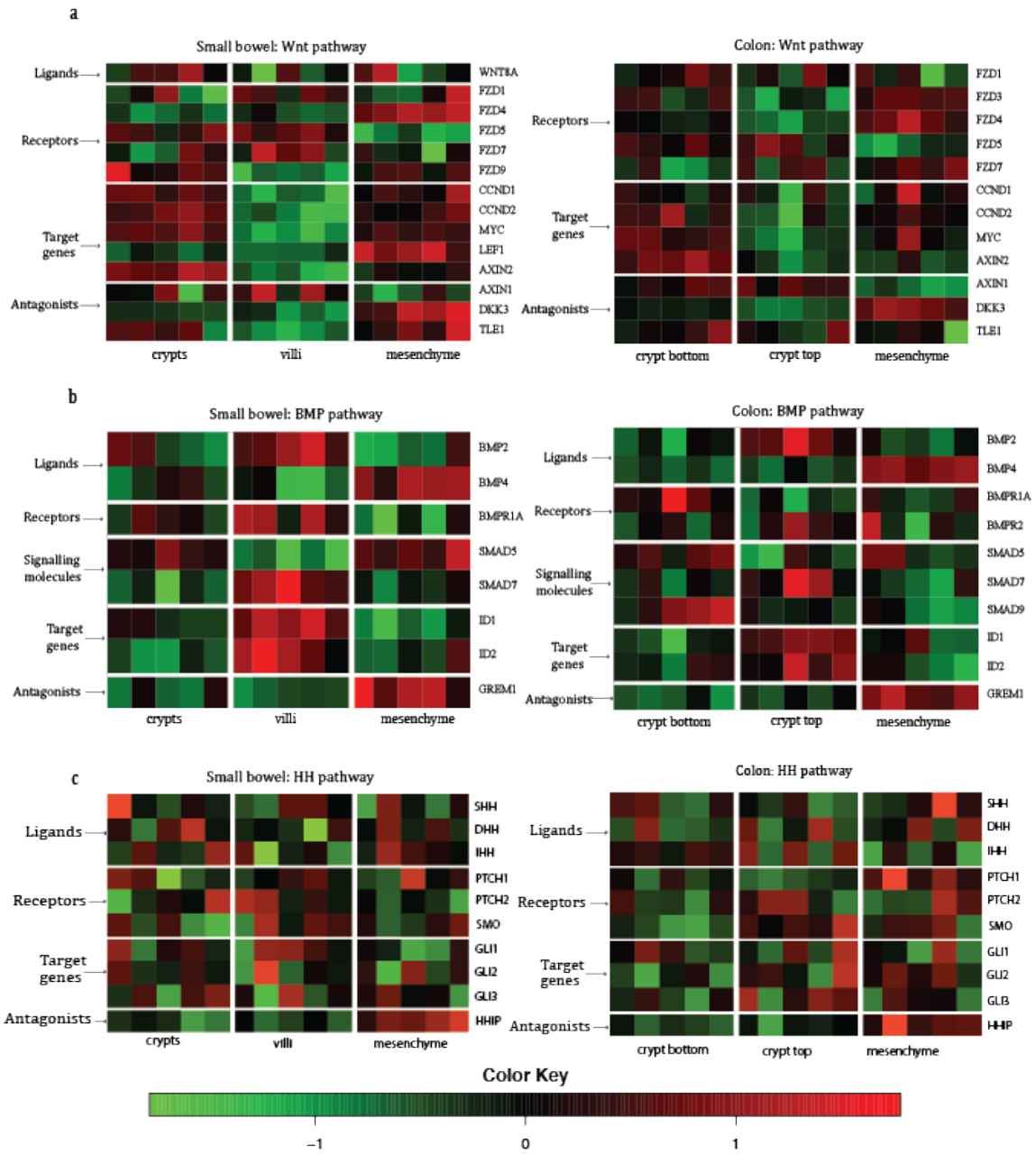

Figure 3.4: Comparison of signalling pathway components by compartment within small bowel and colon. Heatmaps of a) Wnt b) BMP and c) Hedgehog.

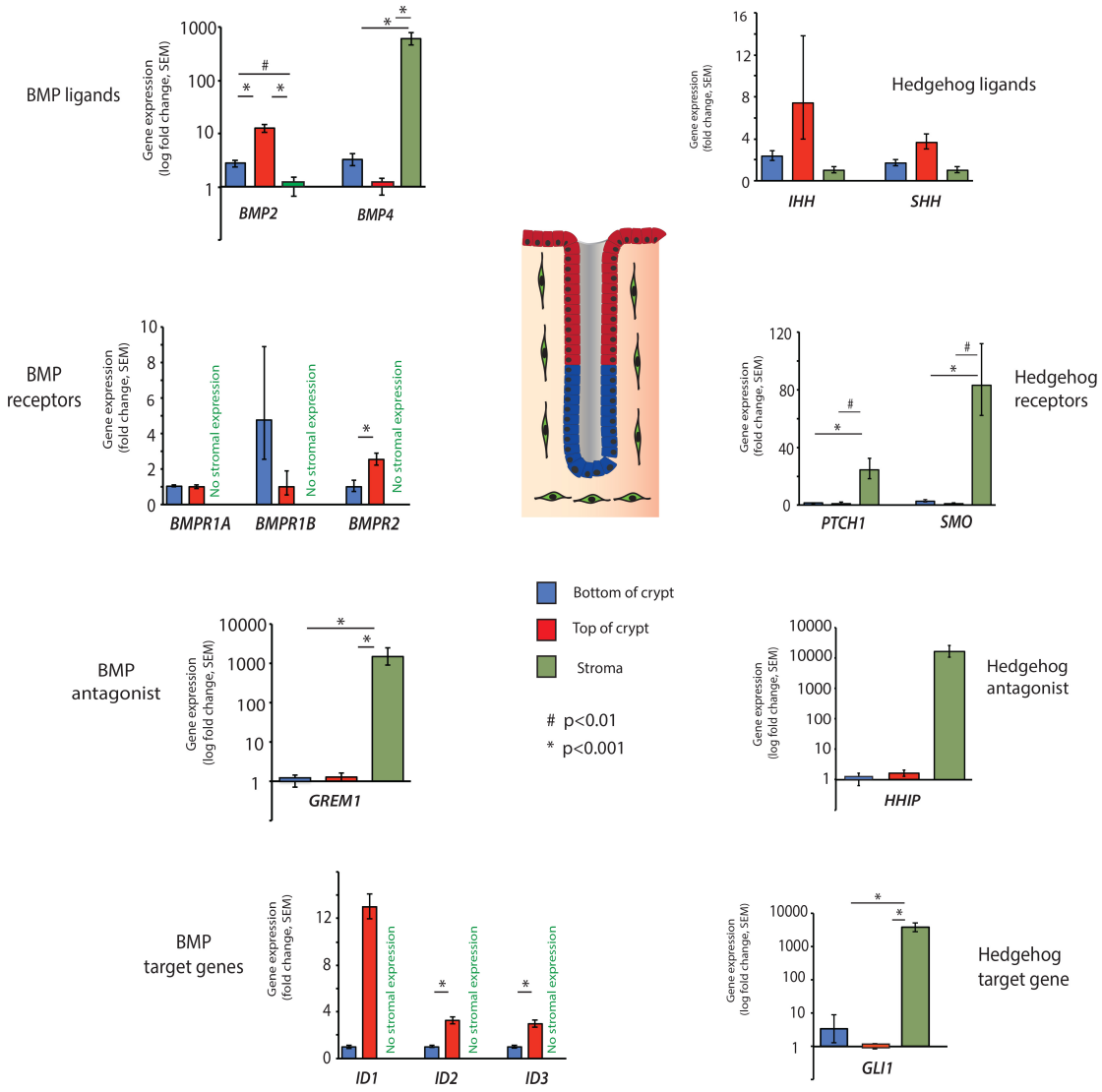

Figure 3.5: qPCR for BMP and HH pathways by colonic compartment in intestinal homeostasis. Ligands, receptors, antagonists and target genes for each pathway are highlighted. Values given are relative to housekeeping gene GAPDH.

plore differences in signalling pathway component expression. A disparity exists between target gene expression and ligand and receptor expression. It also shows that BMP is predominantly a mesenchymal-to-epithelial pathway and Hedgehog is an epithelial-to-mesenchymal pathway.

Next the changes in signalling were explored in disrupted homeostasis.

3.4.2 Human colonic biopsies in inflammation

In five patients with active Ulcerative Colitis, biopsies were taken adjacent to ulcers, with corresponding normal biopsies from the same patient for comparison. The ulcer itself was not sampled as it contains necrotic debris, whereas adjacent tissue was regenerative. Under the light microscope, crypt budding was noted in several crypts in inflamed samples, in contrast to normal samples where no budding was seen (figure 3.6). This suggests that crypts were actively undergoing fission. The crypts were again dissected in half and 20 crypts were used for each patient.

Differential gene expression was analysed across compartments. Again samples clustered by tissue compartment on the PCA plot (figure 3.7), more so than inflamed and non-inflamed tissue clustered, or individual patients clustered. There was one outlier patient, presumably due to technical failure of extraction, which was discarded for analysis.

More genes were expressed in inflamed tissue compared to normal tissue, in particular mucin encoding genes MUC17 and TFF1, stem cell marker OLFM4, and the islet-derived regenerating genes REG1A and REG1B known to be associated

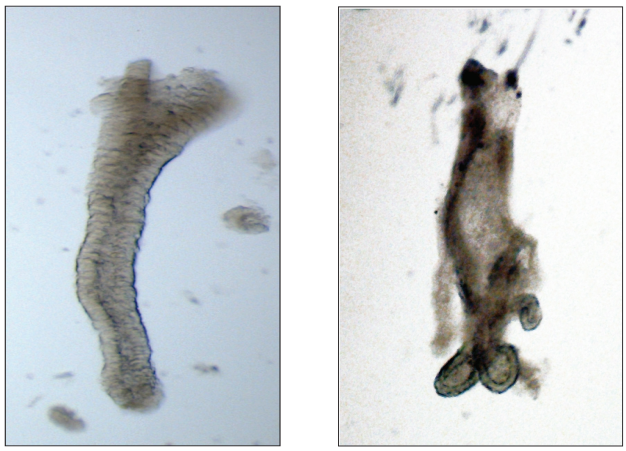

Figure 3.6: Light microscope photos of non-budding and budding cryts. Left: crypt from a histologically normal colonic sample. Right: crypt in fission from a sample with active Ulcerative Colitis.

with colitis [151] (figure 3.8). Mucin production is decreased in UC and the increase in mucin-encoding genes may represent a repair mechanism to compensate for damage to barrier function. There was upregulation of S100P in colitis mesenchyme. S100P codes for a calcium-binding protein and regulates cell cycle progression. It can act as an intestinal tumour biomarker as it is associated with invasion and metastasis [131].

GSEA for crypt top compared to crypt bottom for transit amplifying and differentiated cell gene sets were similar to control samples, suggesting normal cell fate determination is maintained in regenerating crypts (figure 3.9). GSEA for the stem cell gene set did not cluster, which could indicate an expansion of the stem cell zone. Comparison by compartment between colitis and control samples showed enrichment of transit amplifying progenitor cells in the crypt base in colitis (figure 3.8). Increased crypt fission has been reported in colitis [62] and it may be that expansion of the proliferating compartment contributes to this. Progenitor cells

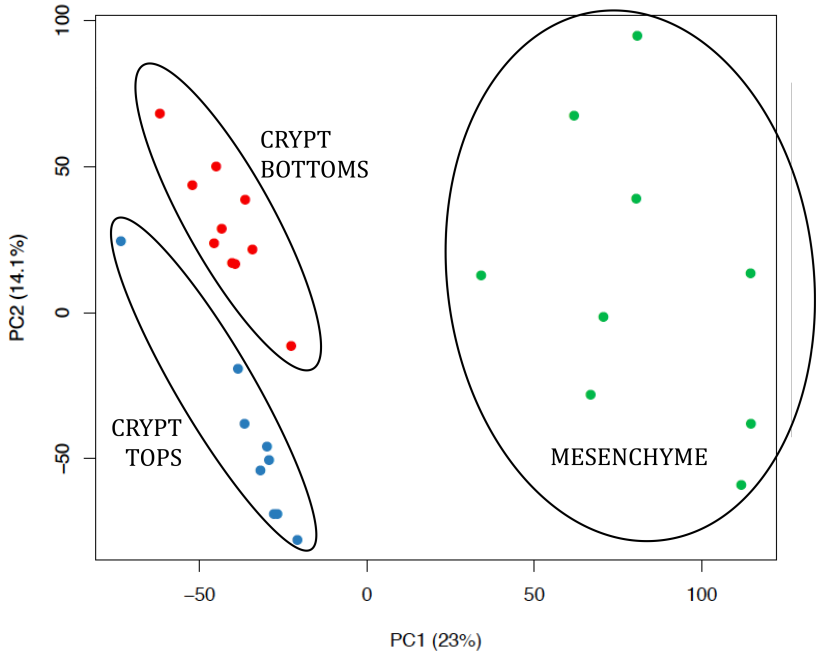

Figure 3.7: PCA plot showing clustering by tissue compartment in colitis. This includes both colitis samples and control healthy colon tissue.

contribute to stem cell function and this is discussed further in chapter 5.

The genes involved in negative regulation of apoptosis (such as CASP3, SOCS2/3) were upregulated in crypt tops in colitis (figure 3.8), showing impaired control of programmed cell death. DNA integrity and damage checkpoints (including ATR, CHEK1/2, RAD1/17), and DNA damage response were all negatively regulated in crypt tops in colitis also, suggesting altered response to DNA damage.

Together these data suggest that in Ulcerative Colitis there is flux in the usually tightly segregated tissue compartments. Crypt budding was observed, suggesting fission. Normal cell fate determination was maintained in regenerating crypts. There was enrichment of transit amplifying progenitor cells in the crypt base in colitis and possible expansion of the stem cell zone. In colitis DNA damage re-

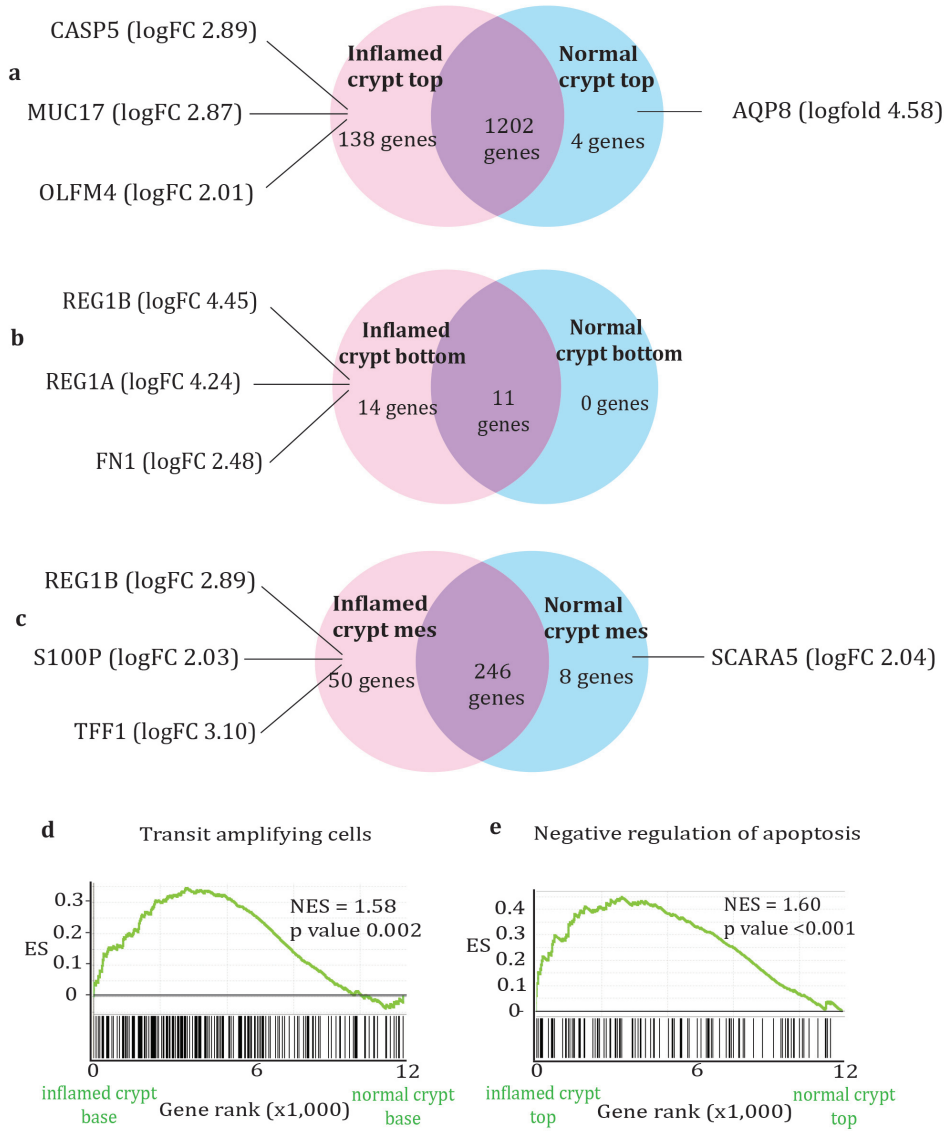

Figure 3.8: Comparison of inflamed and normal compartments. Differential gene expression of inflamed and normal crypt tops (a), crypt base (b) and mesenchyme (c) with highly expressed genes labelled. d) Enrichment plot of transit amplifying gene set in inflamed versus normal crypt base. e) Enrichment plot of gene set for negative regulation of apoptosis in inflamed versus normal crypt top.

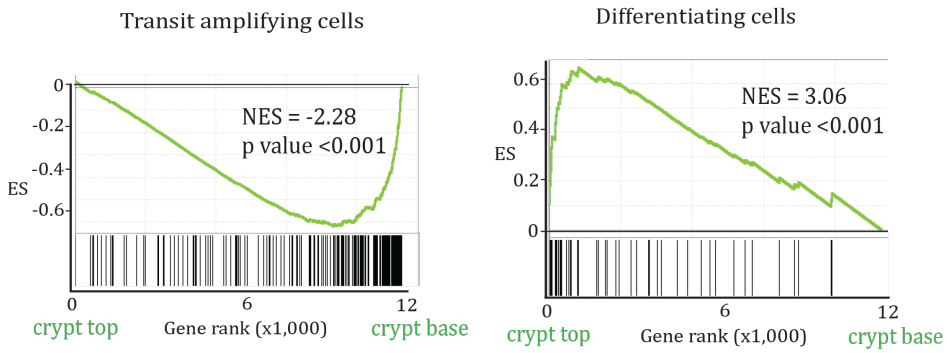

Figure 3.9: Enrichment plots for inflamed colon crypt top versus inflamed crypt bottom to custom gene sets for transit amplifying cells and differentiating cells.

sponse may be altered and there was reduced apoptosis at the luminal surface.

3.4.2.1 Morphogen pathways across compartments in inflammation

Heatmaps comparing colitis and normal samples for Wnt, BMP and Hedgehog gene sets were created. At the crypt base there was an increase in Wnt target genes MYC and CCND1 (figure 3.10), perhaps supporting the increase in transit amplifying cells and enhanced proliferation. At the crypt top there was an increase in Wnt target genes as well as antagonists. At the crypt top there was an increase in BMP ligands and ID1. Interestingly there was an increase in BMP receptors, SMAD5 and BMP target genes at the crypt base. This suggests that there is a flattening out of the usual polarised Wnt and BMP gradients in colitis.

In the mesenchyme the main difference was reduced BMP4 and increased GREM1 in colitis 3.10. Reduced BMP4 has been reported in colitis [149] but not localised to colonic compartment. There was a reduction in Hedgehog receptor signalling

and HHIP in the mesenchyme.

Validation by qPCR was done for the BMP and HH pathways, again the pathways of most interest. Expression was tested in the compartment in which the gene is expressed. In colitis there was a reduction in all components of the BMP and HH pathways, except BMP antagonist GREM1 which showed increased expression (see figure 3.11). This goes along with the concept that for repair there needs to be antagonistically more Wnt-driven proliferation to allow epithelial replacement and crypt budding. Wnt may antagonise these pathways or the reduction in signalling may be a direct response to injury.

These data indicate that in colitis there is a flattening out of the opposing Wnt and BMP/HH gradients, with an increase in Wnt at the crypt top and an increase in BMP at the crypt base. Overall BMP signalling reduced in colitis and antagonist GREM1 increased. All components of the Hedgehog signalling pathway were downregulated in colitis. Therefore loss of epithelial Hedgehog may lead to reduced BMP signalling in the mesenchyme and increased GREM1. This causes a net reduction in BMP activity and promotes the stem/progenitor phenotype.

3.4.3 Mouse intestinal compartments

To confirm parallels between human and mouse signalling pathways, small bowel segments were collected from a wild type mouse. In a similar way to above, crypts, villi and mesenchyme were collected by dissection under the light microscope. Only the Hedgehog pathway was tested due to time limitations. Hedgehog ligands Ihh and Shh were confirmed by qPCR to be epithelial and Hedgehog re-

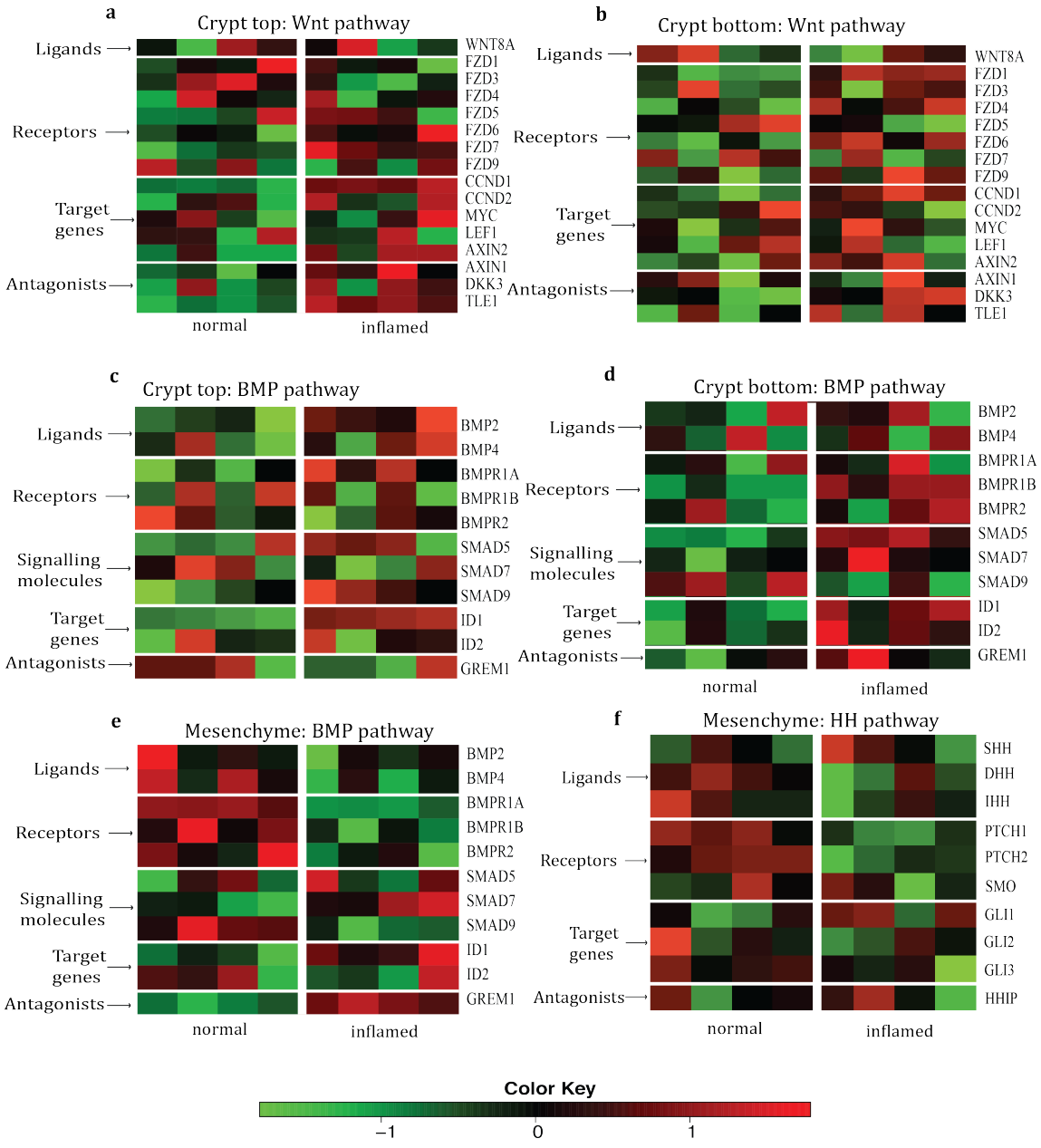

Figure 3.10: Comparison of signalling pathways by compartment in normal colon and colitis. a, b) Heatmap of Wnt pathway genes at crypt tops and bottoms. c, d) Heatmap of BMP pathway genes at crypt tops and bottoms. e) Heatmap of BMP pathway genes in mesenchyme. f) Heatmap of HH pathway genes in mesenchyme.

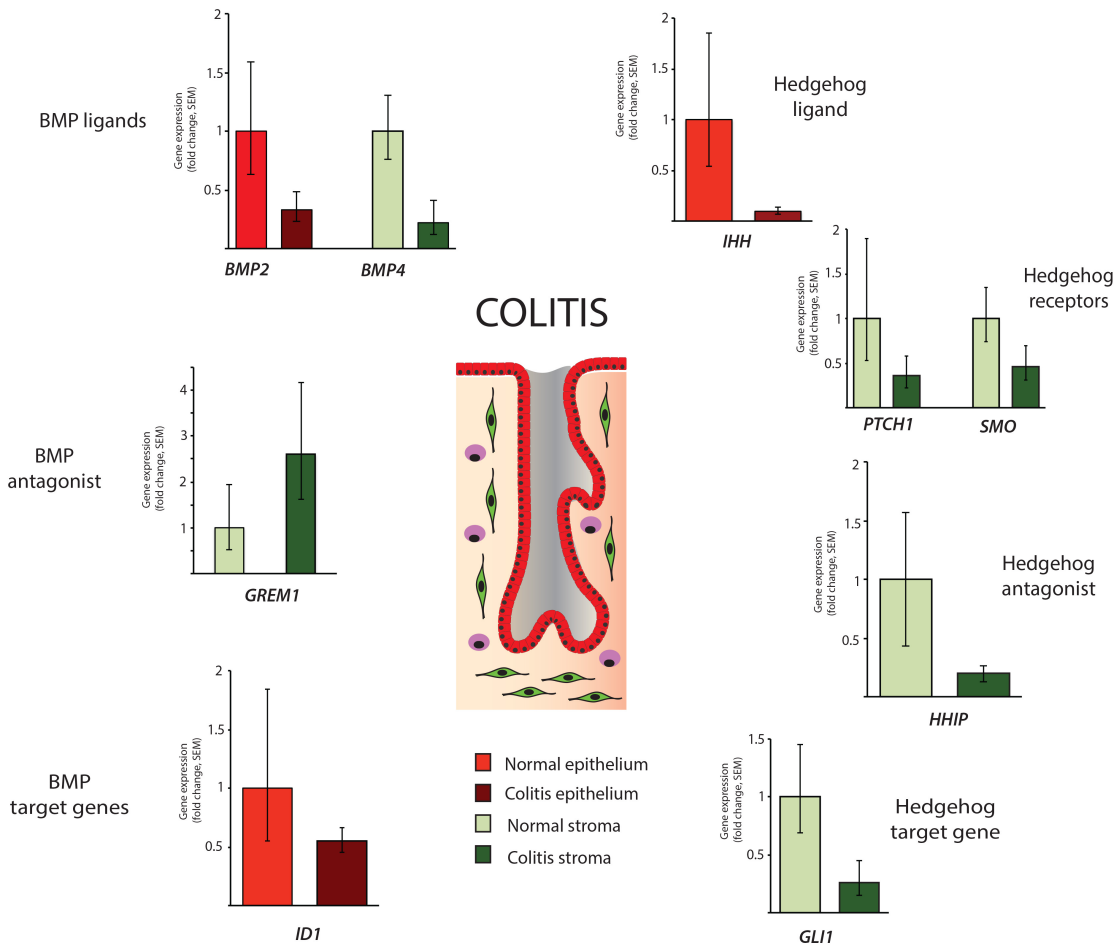

Figure 3.11: qPCR for BMP and HH pathway components in colitis and normal colon.

ceptors, target genes and antagonists were all mesenchymal (see figure 3.12).

Using qPCR for the Hedgehog signalling pathway, it was confirmed that there is correlation between the compartmental localisation of pathway components in human and mouse. This supported further experiments done in mice.

3.4.4 Downstream verification of signalling pathways in homeostasis and inflammation

Having confirmed parallels between human and mouse intercompartmental signalling gradients based on microdissected sample RNA extraction, immmunohistochemistry and *in situ* hybridisation were used to look for slide validation of the signalling components of interest. There is no reliable IHC antibody for BMP4 and several Grem1 IHC antibodies were optimised, but none gave specific staining, hence ISH probes were used for BMP4 and Grem1. BMP4 was expressed in homeostasis in the mesenchyme (figure 3.13). p-SMAD1/5/8 was expressed throughout villi by IHC. Grem1 ISH showed specific subcrypt mesenchymal expression. Wnt target genes EphB2 and Lgr5 were expressed exclusively at the crypt base, as shown by IHC.

This confirms the results from microarray and qPCR that there is discrete expression of different components of the signalling pathways in the intestine. Testing in mouse models of DSS colitis showed no difference in these staining patterns, except for Grem1 expression which is discussed further in chapter 4.

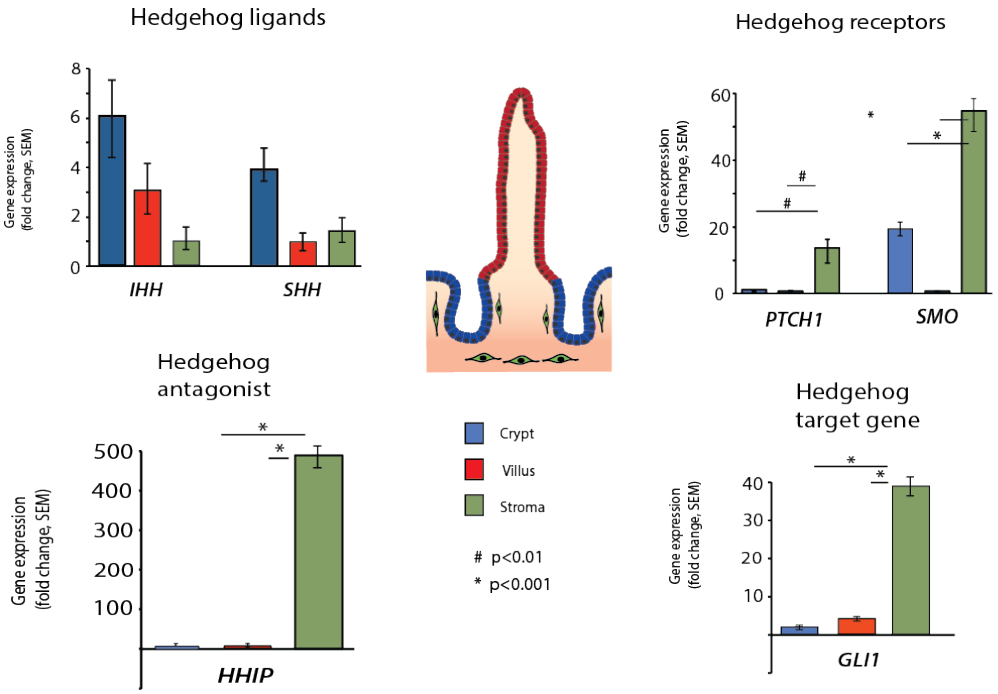

Figure 3.12: qPCR for HH ligands, receptors, antagonists and target genes in mouse small bowel compartments.

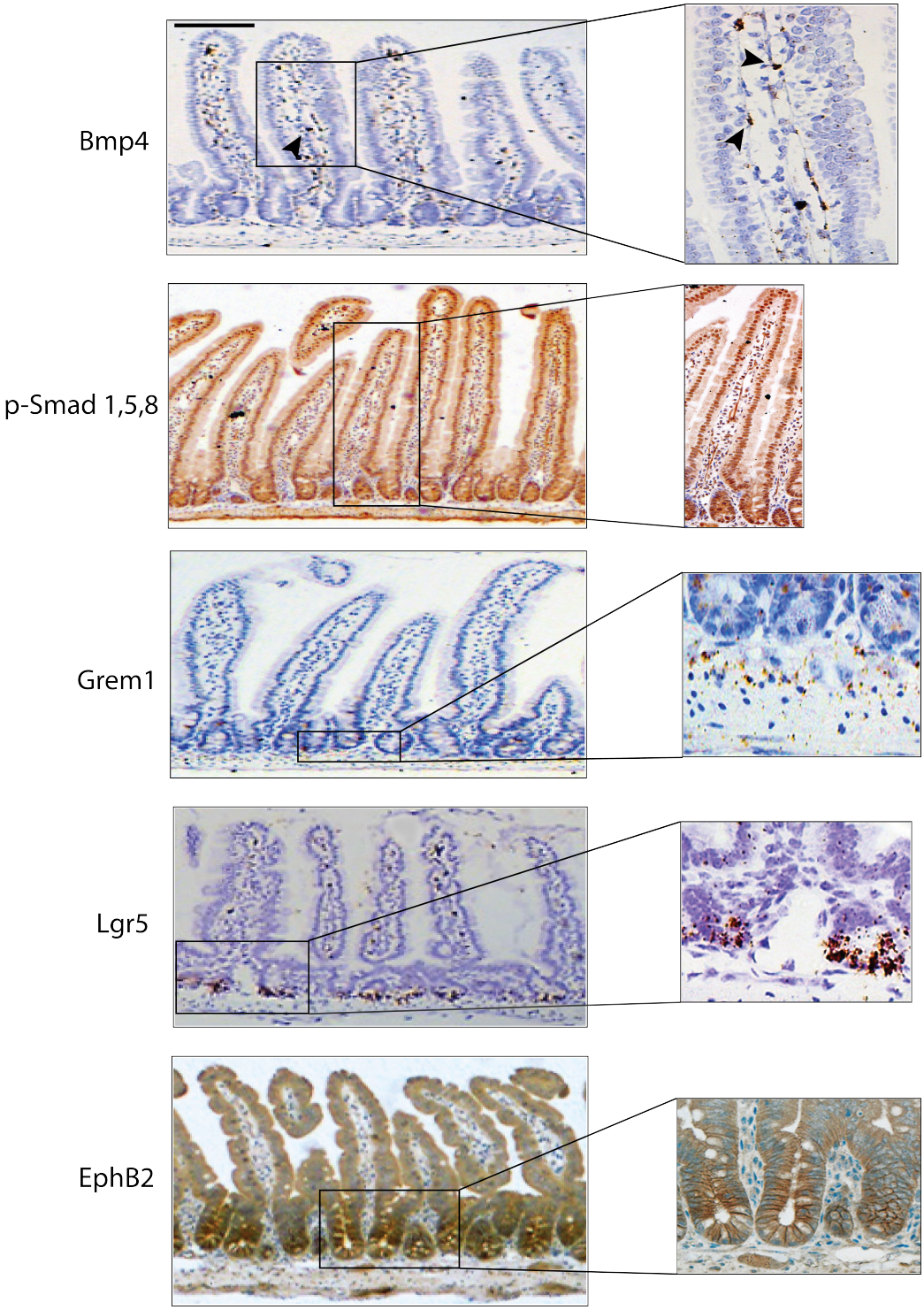

Figure 3.13: IHC and ISH stains in wild type mouse small bowel. ISH for BMP4, IHC for p-Smad-1,5,8, ISH for Grem1, ISH for Lgr5 and IHC for EphB2. Scale bars are 100μm.

3.4.5 Stromal heterogeneity in homeostasis

Having demonstrated an epithelial gradient of morphogen signalling target gene expression and identified a putative role for mesenchymal derived ligands and antagonists in maintaining these gradients, it was hypothesised that gradients along the crypt-villus axis might result from stromal functional heterogeneity. RNA sequencing was run for spatially distinct areas of mesenchyme. Wild type mouse frozen gut rolls were cut and sections stained for Cresyl violet (2.3.4.3). Laser capture microdissection was used to select areas of upper (intravillous) and lower (subcrypt) mesenchyme for small intestine. Normal human frozen surgical samples were cut in the same way. Small bowel was divided into upper (intravillous) and lower (subcrypt) mesenchyme, and colon was divided into upper (intercrypt) and lower (subcrypt) mesenchyme. For mouse colon only lower mesenchyme could be extracted as intercrypt areas were too small to be dissected. Three cases were used for mouse and human bowel. Approximately 10 slides were dissected for each tissue type. Figure 3.14 shows mouse small bowel before and after laser capture extraction of the upper mesenchyme.

Given the low yield of RNA, SMARTer RNA sequencing (Clontech) was used, which can analyse 2-100 ng of total RNA. The output gave 4-10 million reads for mouse and 2-5 million reads for human tissue. The PCA plot for mouse results is given in figure 3.15. Lower mesenchyme in both small bowel and colon clustered together, and separately from upper mesenchyme. There is an outlier for small bowel lower mesenchyme, likely due to issues with extraction, which was discarded during analysis.

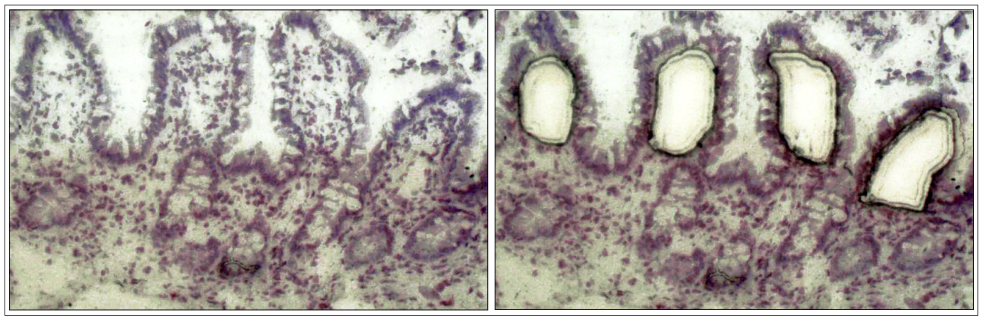

Figure 3.14: Mouse small bowel Cresyl violet stain before and after laser capture extraction of the upper mesenchyme.

Genes with log-fold change >2 and adjusted p-value <0.05 were considered significant. There were >1000 genes differentially expressed between upper and lower mesenchyme compartments: 1986 genes in mouse small bowel, 1312 for human small bowel and 1360 for human colon. Therefore there are significant differences between mesenchymal compartment expression. Figure 3.16 shows a schematic of genes expressed in each compartment in mouse small bowel with logfold change in expression. In all tissue types BMP antagonists *Grem1, Noggin* and *Chordl* were expressed highly in basal mesenchyme. Structural markers smooth muscle actin (SMA), desmin and vimentin were all expressed more highly at the base. Extracellular matrix proteins Lumican, Dystrophin and Decorin were also expressed at the base. Fibroblast activation protein (FAP), a marker of activated myofibroblasts, was present in subcrypt mesenchyme as expected.

Immune markers were mostly expressed in upper mesenchyme (figure 3.16). Hedgehog target genes Hhip, Gli1 and Ptch1 were also more highly expressed in upper mesenchyme. This suggests a polar gradient between Hedgehog expression and

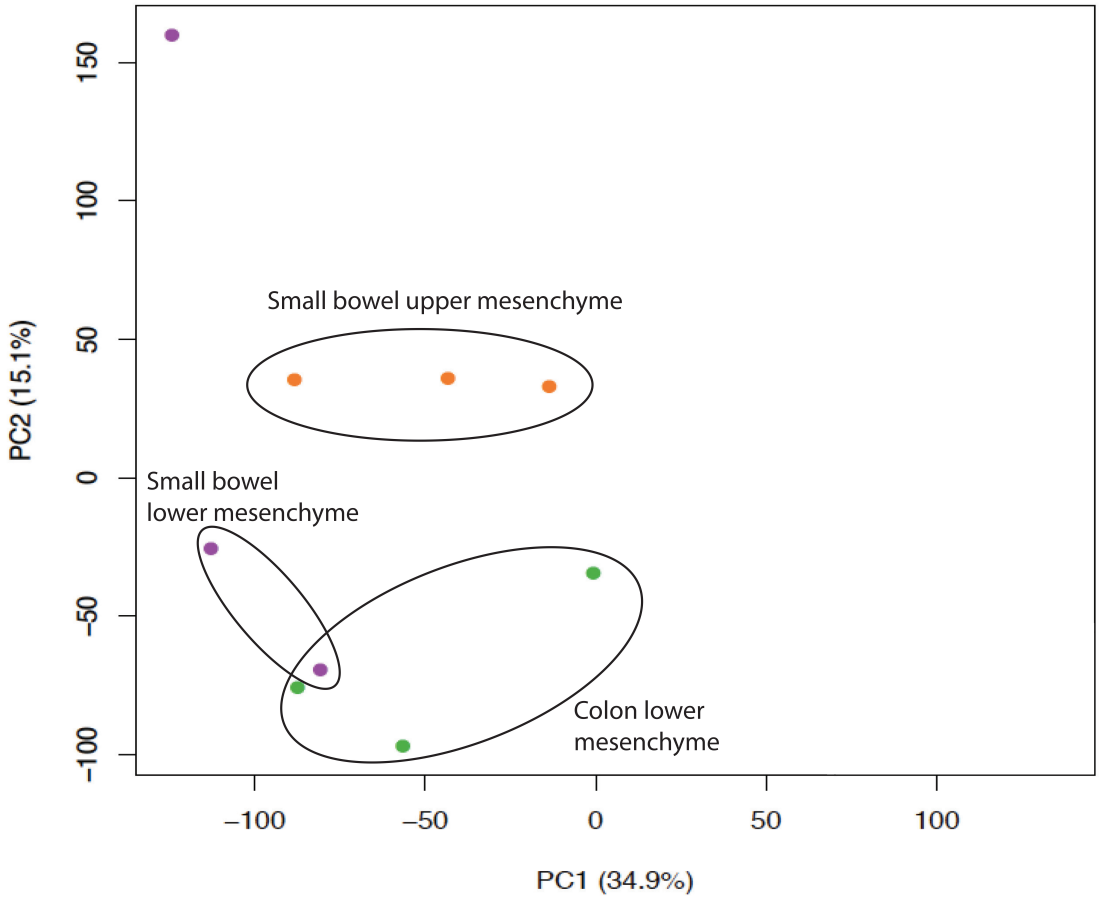

Figure 3.15: PCA plot showing clustering of mesenchyme compartments in mouse small bowel and colon.

Grem1 expression. Given the number of reads from sequencing was higher in mouse, these results have been shown here. There was similarity between human and mouse, and small bowel and colon in terms of genes expressed.

These data suggest that there is a difference in gene expression between areas of mesenchyme adjacent to the crypts and areas near the luminal surface. There was a difference in structural markers, immune markers and BMP and HH signalling components between mesenchyme compartments. This supports spatial functional heterogeneity between stromal cell populations and this might contribute to localised epithelial signalling pathway gradients.

3.4.5.1 Downstream verification of stromal markers

Grem1 was confirmed to be in basal mesenchyme by *in situ* hybridisation. Structural markers SMA, desmin and vimentin were stained for by IHC and found to be present in both upper and lower mesenchyme of mouse small bowel (see figure 3.16). It is difficult to quantify level of gene expression by IHC staining as it simply indicates presence or absence of expression.

3.5 Discussion

To answer the key objectives set out:

1. Intercompartmental signalling of BMP, HH and Wnt pathways is crucial in determining homeostatic intestinal morphogen gradients.

2. In mucosal inflammation and tissue regeneration these gradients are skewed.

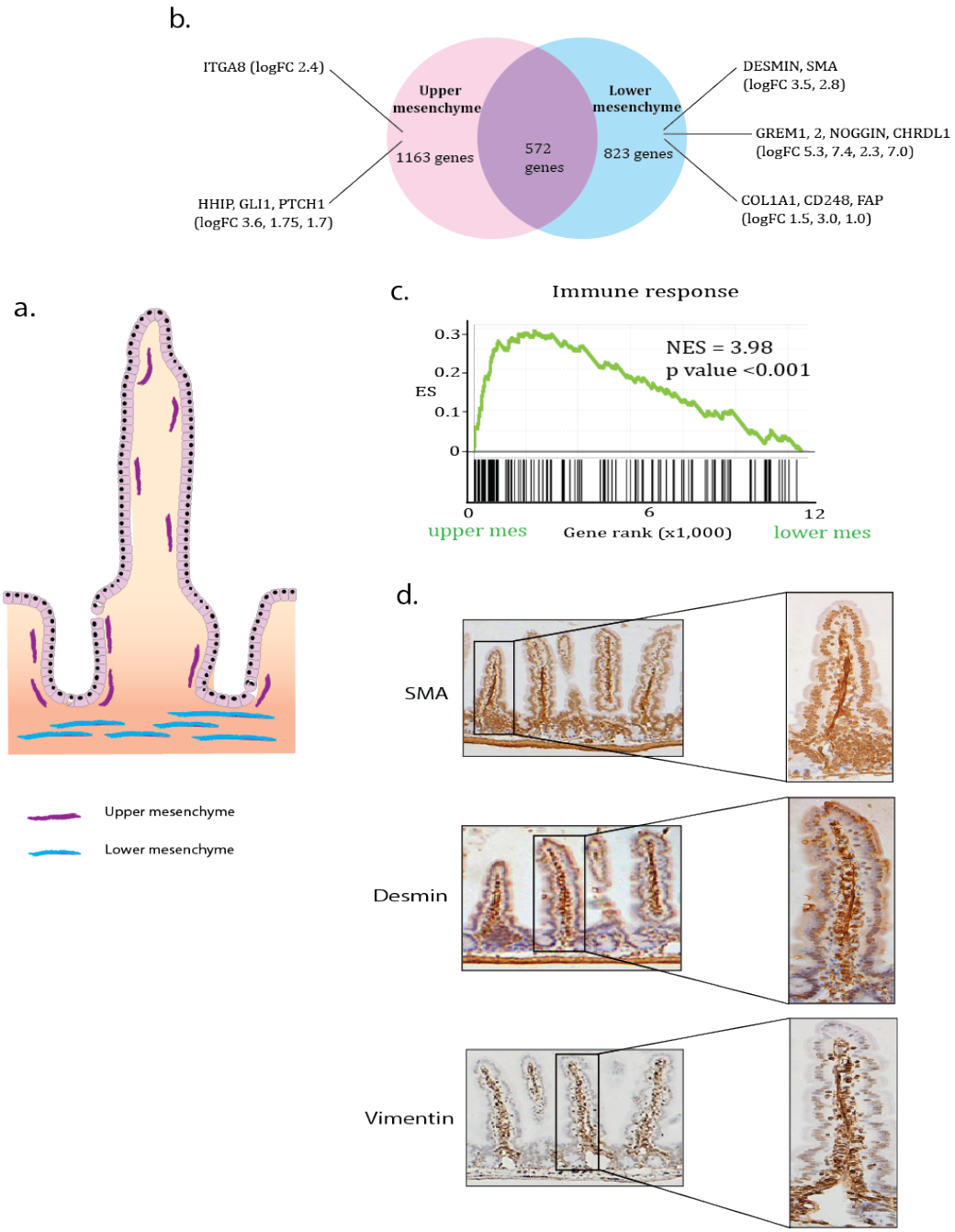

Figure 3.16: a) Schematic of mesenchyme sections in small bowel. b) Genes differentially expressed in mouse small bowel mesenchyme compartments. c) GSEA for immune response genes comparing upper and lower mesenchyme. d) IHC for mesenchymal markers SMA, desmin and vimentin in mouse small bowel.

3. There is functional heterogeneity between spatially distinct areas of mesenchyme.

3.5.1 Morphogen gradients

The first aim was to assess the importance of intercompartmental signalling in determining morphogen gradients. There is clear cross-talk between epithelial compartments and mesenchyme in all of the pathways assessed. BMP, Hedgehog and Wnt target gene assessment indicates crypt-villus morphogen expression gradients, but there is a disparity between target gene RNA expression and endogenous epithelial receptor and ligand expression. This could mean that there are post-transcriptional or translational modifications of genes expressed. It could also indicate that the apparent functional morphogen gradients are the result of receptor-independent control mechanisms from intercompartmentally expressed antagonists. The results provide new information to those from Kosinski et al [111] where strict Wnt and BMP pathways across the crypt-villus axis were demonstrated, but mesenchyme was included. This complexity of morphogen gradient control is vital for control of cell fate determination within the crypt-villus escalator. It provides positional information to organise cell fate as cells move up the crypt-villus escalator and proliferate, differentiate and apoptose.

3.5.2 Fibroblast heterogeneity

There is a difference in gene expression between subcrypt mesenchyme and intravillous mesenchyme. Immune markers constitute a part of this, and were mostly

expressed in upper mesenchyme, perhaps because this is closer to the toxic luminal contents. Structural markers SMA, desmin and vimentin were more highly expressed in lower mesenchyme from microarrays, as these mark activated myofibroblasts which reside under crypts. GREM1-expressing fibroblasts have been shown to express SMA and it may be that their expression is overlaid.

This fibroblast heterogeneity may account for some of the signalling gradient along the crypt-villus axis. This heterogeneity may be imposed by different cells of origin, a differentiation hierarchy or by varying environmental exposures. In skin, distinct fibroblast lineages give rise to upper and lower dermis mesenchyme [55]. This has relevance in repair and explains why skin wounding is linked to a specific type of fibroblast being upregulated in repair. In the intestine subepithelial myofibroblasts can also influence cell fate decisions in tissue regeneration.

Primary culture of fibroblasts is used experimentally to test morphogen production and to create a more physiological environment to grow epithelial cells. In fact there is a very heterogeneous population of cells in generic intestinal fibroblast culture and this would give a mixed picture of morphogen production, so results from such experiments need to be considered in context.

3.5.3 Organoid cultures

The importance of the homeostatic influence of the intestinal stroma may explain why organoid epithelium grows so rapidly in culture. As an example crypt fission in humans is a rare process occurring every 30 to 40 years [152]. In organoids derived from healthy human tissue, crypt fission occurs every 2 to 3 days [30].

In the absence of cultured stroma, mesenchymal homeostatic brakes are removed and the epithelium proliferates autonomously.

Crypt-villus polarisation occurs without mesenchymal presence, indicating epithelial cell-autonomous cell fate determination and that mesenchymal niche components are supplementary. Organoids are far from a realistic representation of cells in homeostasis. There is interaction and interdependence of the mesenchymal and epithelial compartments in homeostatic regulation which is missing in these artifical settings. Some cell autonomy in cell fate determination must be maintained but the whole system is dependent on uniform and high concentrations of critical stromally derived molecules. The uniformity of these concentrations may be responsible for the proliferative phenotype in organoids. This will be discussed further in chapter 4.

BMP expression is low in the crypts, in part due to adjacent Grem1 and Noggin expression. Wnt expression could be lower at the villi due to upper mesenchymal BMP4 expression - there is evidence that BMP directly suppresses Wnt genes [112]. There is also evidence that Wnt ligands secreted by Paneth cells can be transferred on membranes to stem cells by cell division [153]. This could account for the gradient in Wnt ligands seen across the crypt-villus escalator.

There was no differential expression of Wnt antagonists across mesenchymal compartments. Hedgehog genes were all higher in upper mesenchyme and account for high Hedgehog at the villus tip driving differentiation. This is purely an anatomical distinction and a functional separation of mesenchymal elements by FACS analysis by cell type may give more insight into the roles of mesenchymal function. Further work on fibroblast growth *in vitro* and the effect of HH

manipulation will be discussed in chapter 4.

3.5.4 Morphogens in wound repair

In wound repair the gradients are skewed and there is no longer controlled cross-talk and antagonism between Wnt and BMP/HH. Some compartments have increased signalling of both Wnt and BMP. In colitis there was increased Wnt target gene expression at the crypt top and BMP target gene expression at the crypt base, meaning a distortion and flattening out of the normally polarised gradients. This was again inconsistent with receptor and ligand expression. Disruption of microenvironmental control and signalling pathways in inflammation allows increased cell proliferation, altered apoptosis and impaired DNA damage response, suggesting an expansion of cells with potential stem cell function. This is likely to be physiologically relevant as the resultant induction of crypt fission will enhance re-epithelialisation and wound healing. However the expansion of a population of cells susceptible to somatic mutation and potential carcinogenic change has implications for the cell of origin in colitis-associated carcinogenesis (CAC). The mesenchyme in colitis shows upregulation of S100P, usually epithelially derived, which is associated with invasion and metastasis [131], and could potentially be evidence for EMT in inflammation. GREM1 is expressed more highly in inflamed mesenchyme and increased aberrant mesenchymal expression of GREM1 can lead to severe disruption in the homeostatic crypt-villus escalator process and give rise to neoplasia [85].

In keeping with the increase in Wnt signalling and proliferation in colitis, there

was a reduction in BMP and Hedgehog pathways. It may be that the increase in GREM1 antagonises the BMP pathway, and this in turn could have an effect on HH. IHH is known to promote BMP4 expression and vice versa. There is also reported to be a direct interaction between GREM1 and Hedgehog [114]. This interaction will be discussed further in chapter 4. The patterns in signalling shown in human are similar in mice, and thus the murine model is relevant to test the manipulation of morphogens and downstream effects on inflammation.

We have evolved such complex mechanisms to control these critical developmental and cell growth pathways. The implications for cancer are that this precise control is lost and cell fate is disrupted. Cell turnover changes and cells divide without brakes, leading to intestinal inflammation and potential mutagenesis.

3.5.5 Implications for therapy

If morphogens are important in controlling cell fate in homeostasis and repair, they could potentially be manipulated therapeutically. Returning morphogen gradients to a polarised controlled manner may prevent the above processes. Restoring a gradient would not be possible but increasing the level of a morphogen where it is deficient is feasible. The issue with administering any exogenous morphogen would be targeting this directly to the site of inflammation and ascertaining the amount required for repair. A proof of principle is the SMAD7 antisense oligonucleotide, Mongersen, used in IBD. SMAD7 is an inhibitory signalling molecule of the BMP pathway. This drug targets ileal and colonic SMAD7 and increases TGF-beta signalling. Early trials have shown this improves outcomes in IBD

but no long term data exist as to whether this reduces cancer risk. Another way would be to manipulate the Hedgehog pathway and this was tested in a mouse model of colitis-associated cancer with SHH inhibitors cerulenin and itraconazole [154]. This reduced tumour formation and was associated with inhibition of IL6 signalling.

This chapter has established a basis for the intercompartmental crosstalk of the Wnt, BMP and Hedgehog pathways. The next step will be to manipulate these pathways *in vitro* and *in vivo* and to look for downstream effects.

3.5.6 Limitations

- There was heterogeneity amongst patient samples in each group which may have led to error.
- The colitis samples would be even more heterogeneous, as although they had histologically proven Ulcerative Colitis, severity and degree of ulcer healing would have varied.
- Bisecting crypts is not an exact process.
- The low concentration of RNA from mesenchyme extraction meant that amplification was required, providing bias for error.

Chapter 4

In vitro and *in vivo* assessment of the role of *Grem1* in intestinal regeneration

4.1 Aims

The aims in this chapter were to explore the role of *GREM1* in disrupted homeostasis and its potential regulation by the HH pathway. The key objectives were:

1. To test whether Grem1 is a paracrine BMP antagonist.
2. To assess whether Hedgehog plays a part in Grem1 regulation and to assess for the paradoxical relationship between HH and Grem1 in intestinal fibroblasts.
3. To assess the expression and role of Grem1 in intestinal regeneration mod-

els.

4.2 Introduction

In chapter 3 I explored the BMP and HH pathways in colitis. I found an upregulation of the secreted BMP antagonist GREM1 in human IBD and a downregulation of all components of the Hedgehog pathway. In this chapter I explore the properties of Grem1 as a paracrine antagonist and examine the relationship between Hedgehog and Grem1.

4.2.1 Grem1 as a paracrine BMP antagonist

The fact that Grem1 is secreted by mesenchyme and exerts an effect on epithelial BMP ligands means that it must be a paracrine molecule, i.e. diffuses over a short distance to alter the behaviour of nearby cells. I wanted to test this cell-to-cell effect *in vitro* by adding recombinant Grem1 to matrix media and looking at the effect on organoid growth. To test whether Grem1 concentration has a positional effect on organoid growth, a modified version of the technique by Miyoshi et al was used [53]. This paper showed that when beads soaked in Wnt5a were placed next to spheroids, they caused clefting as if forming nascent crypts (figure 4.1). Grem1, in its role as a regenerative mediator, may have a similar effect. The effect of Grem1 on organoid survival and budding in the vicinity as compared to cells further away was tested.

Grem1 is also ligand-sequestering and binds preferentially to BMP2 and BMP4

[44]. This is a competitive inhibition and theoretically high levels of BMP2 and BMP4 in culture will prevent the regenerative effect of Grem1 on organoid growth. This was tested *in vitro*.

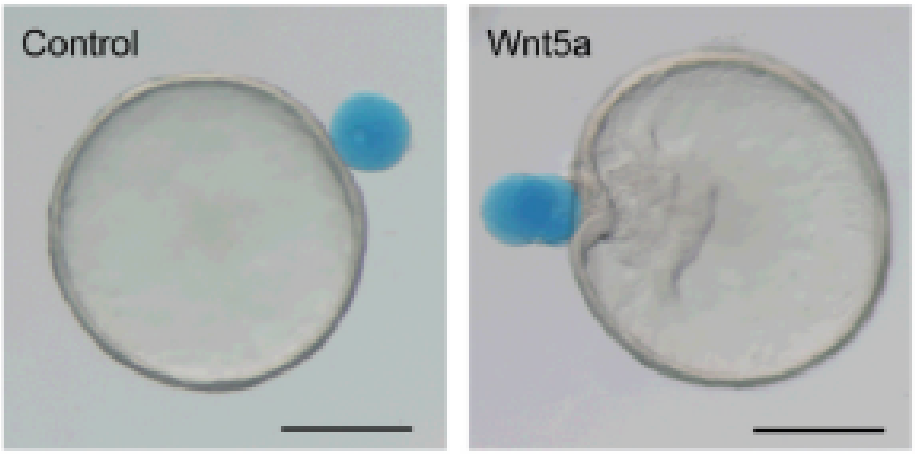

Figure 4.1: Focal Wnt5a-induced clefts in colonic epithelial organoids. A control (left panel) or a Wnt5a-soaked bead (right panel) was placed adjacent to different colonic organoids. Bars, 200 μm. Taken from [53].

4.2.2 Hedgehog may play a part in Grem1 regulation

It has been reported that Gli activators regulate the transcription of Grem1 in adult intestine and that Hedgehog indirectly upregulates mesenchymal BMP4 [155]. It has also been shown that stromal activation of Hedgehog reduces Grem1 expression [114]. In this paper, stromal-specific HH activation in mice reduced tumour load and was paralleled by a reduction in Grem1. I hypothesise that there is a paradoxical link between HH and Grem1, and this was tested *in vitro* first, using fibroblast cultures. It has been shown that treatment of human fibroblasts with recombinant IHH and SHH reduced GREM1 expression [114]. Hedgehog inhibitor

Cylopamine was used to manipulate Hedgehog signalling here.

A murine model of Ihh knockdown exhibited disruption of the mesenchymal architecture with loss of the αSMA-expressing muscularis mucosae. There was change to extracellular matrix proteins and reduction in numbers of crypt myofibroblasts [116]. Perhaps as a result of loss of control over the stem cell niche, crypts were wider and loosely organised with disruption of crypt epithelial fate and polarity as shown in published figure 4.2, in which there are differentiated cells in the crypt base. Grem1 expression was analysed in these animals.

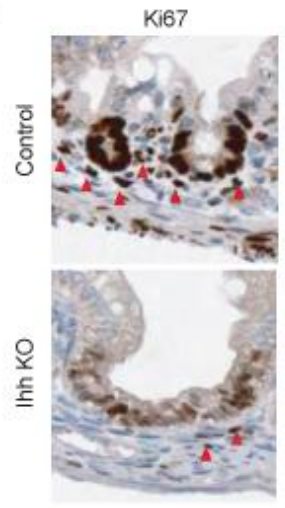

Figure 4.2: Ki67 staining in crypts from wild type and *Ah-Cre; IHH*$^{fl/fl}$ mice. Adapted from [116]. The red arrows highlight Ki67 positive cells and show that mesenchymal cell proliferation is present in control mice but is reduced in *Ah-Cre; IHH*$^{fl/fl}$ mice. The wide crypt in the knockout mouse contains fewer Ki67 positive cells and therefore these are non-proliferating differentiated cells.

4.2.3 Techniques to study wound regeneration

In IBD Hedgehog signalling is reported to be reduced [72]. Grem1 was found to be upregulated, so it can be postulated that in disrupted homeostasis, reduced Hedgehog signalling depresses Grem1 expression. Firstly Grem1 upregulation was confirmed by *in situ* hybridisation in human IBD and a mouse DSS model of colitis.

A more controlled way to disrupt homeostasis is to study wound healing and the timing of recruitment of morphogens after tissue injury. There are several methods to do this. I describe a more controlled way to induce mouse colonic injury by endoscopic biopsy, modified from recent publications. The timing of Grem1 expression at the site of wounding was studied and its role in repair considered.

When wounds are created in rat intestinal epithelial monolayers in culture, TGF-β is activated to promote healing and there is activation of NFKB. Lesions heal faster when the cells are co-cultured with myofibroblasts. The addition of fibronectin also accelerates recovery, showing that mesenchymal factors contribute to repair. The basic steps involve creating a "scratch" in a cell monolayer, capturing images at the beginning and at regular intervals during cell migration to close the scratch, and comparing the images to quantify the migration rate of the cells. The *in vitro* scratch assay is useful for studies on cellmatrix interactions and on cell migration [156].

A more physiological *in vivo* version of the scratch assay is the ability to wound the mouse epithelium and monitor it over time, as published in several studies [53] [157]. After biopsy injury, a layer of epithelial cell migrates from the adja-

cent uninjured crypts and envelops the wound surface by day 4 post-injury. These wound-associated epithelial (WAE) cells are post-mitotic and generate a temporary barrier that protects the injured sites. Beneath WAE cells, stromal cells proliferate and form an unstructured cell mass called wound bed mesenchyme. Cells in the wound bed appear histologically undifferentiated but include several lineages of stromal cells, such as fibroblasts, smooth muscle cells, endothelial cells and macrophages. After the wound bed is established, epithelial cells begin emanating from the adjacent crypts and migrate into the wound. Elongated crypts form a channel-like structure (the wound channel) by day 6 to 8 post-injury. At approximately day 6 post-injury, the proliferative zone in the wound channel is segmented by post-mitotic cells, which cause subdivision of elongated channels into de novo crypts. Finally the wound bed is replaced with regenerated crypts by day 8 to 14 post-injury. Unlike crypts after fission, regenerated crypts adopt irregular shapes that often have multiple branches with individual crypt openings, suggesting that wound healing prioritises rapid functional recovery rather than structural integrity.

To create wounds in mouse colon, endoscopic biopsies were taken and the specimens collected at varied timepoints. The histological repair was be considered and the timing of recruitment of Grem1 analysed. This was adapted from the technique described in [144] [65].

4.3 Methods

The methods used in this chapter are described in chapter 2 and were as follows:

- Organoid culture 2.7.4

- Fibroblast culture 2.7.5
- Mouse endoscopy and wounding 2.2.8
- Mouse gut preparation 2.2.6
- Histology preparation and staining 2.3

4.4 Results

4.4.1 Grem1 as a paracrine morphogen and proliferative mediator

To prove that Grem1 can act by cell-to-cell communication and alter the behaviour of nearby cells, wild type mouse intestinal organoids were cultured with media containing recombinant Grem1. Intestinal mouse crypt organoids are typically cultured in media containing Epidermal Growth Factor, Noggin and R-spondin1 which overlies the matrigel suspension [28]. Noggin is required to enable the maintenance and passage of organoids. It was postulated that Grem1 could act the same way through inhibition of BMP.

Here Noggin was omitted from the media from the first day of culture, and instead variable concentrations of recombinant mouse Gremlin (R&D) added from day 1. Organoids did grow and survive, and 100ng/ml of Gremlin was the optimum concentration required to cause maximal density and budding of organoids.

Concentrations below and above this caused fewer organoids to form and these did not survive. Hence Gremlin can cross the matrigel suspension to reach intestinal cells and cause budding.

Morphogens are defined as having a concentration-specific effect on cells. Next I wished to test this for Gremlin to find whether it has a different effect on cells nearby to those further away, in the absence of Noggin or Gremlin in the media. To do this microbeads were soaked in recombinant Gremlin and embedded within the matrigel suspension of normal mouse intestinal organoids to look for a proximity concentration effect. The beads were a way to introduce the morphogen in very close proximity to organoids and allow each organoid to be subject to different concentrations, instead of a uniform concentration of morphogen added to media. About 100 particles of Affi-Gel Blue Gel (Bio-Rad) were soaked in varying concentrations of Gremlin overnight at 4°C. Control beads were soaked in PBS containing 0.5% CHAPS (Fisher Scientific). Beads were masked with Advanced DMEM/F-12 medium supplemented with 20% FBS prior to use. Beads were mixed to the cell suspension from the first day of plating out, so there was a random bead distribution, in a method adapted from [53].

At a minimum concentration of 10μg/ml, there was organoid budding. Organoids adjacent to beads were larger and had a macroscopic budding phenotype compared to those further away. Some further away from beads showed no budding. Example pictures are shown (figure 4.3). Organoids placed near beads are seen to be larger and budding, where as small non-budding organoids are seen more distant from beads. The experiment was done without passaging the organoids to keep bead distance constant, so they were monitored up to 7 days from plating.

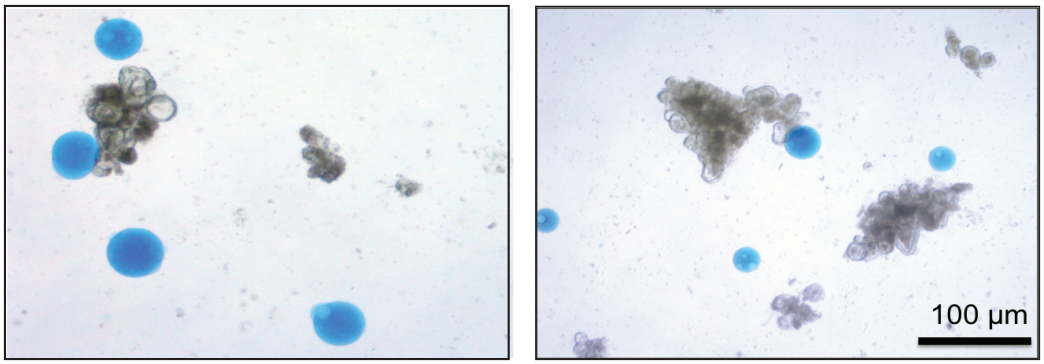

Figure 4.3: Gremlin-soaked microbeads in culture with mouse intestinal organoids.

Together these data indicate that Grem1 causes organoid budding, hence is a proliferative mediator. Grem1 has a concentration-specific effect and acts in a paracrine manner.

4.4.2 BMP as an inhibitor of Grem1-induced regeneration

BMP is known to promote differentiation [40] thus should prevent organoid budding. Grem1 preferentially sequesters BMP2 and BMP4, so it was hypothesised that as the concentration of these ligands rise, Grem1 should no longer be able to competitively inhibit BMP. This was tested by adding BMP ligands to media surrounding organoids, so diffusion could occur across the matrigel and affect organoids evenly, and by soaking beads in BMP ligands to affect organoids asymmetrically.

Gremlin was added to the media at a concentration of 100ng/ml. When beads were soaked in control CHAPS media and up to 1μg/ml BMP4, budding organoids grew. At concentrations above this, cells grew initially as spheroids and then died

(figure 4.4). Therefore when BMP4 exceeds a critical level of 1μg/ml, it prevents the organoid-promoting effect of Gremlin.

Given it was difficult to quantify the distance from organoid to bead, it was decided to add BMP ligands to media to look for the quantity required to prevent organoid growth. To find the concentration of BMP2 and BMP4 required to overcome the regenerative effect of Gremlin, these recombinant ligands were added to the media along with recombinant Gremlin from day 1. At a concentration of 5-20ng/ml, BMP4 had no effect on organoid growth. Above this, media supplemented with BMP ligand could inhibit budding organoid growth and cells died (figure 4.5). With BMP2, organoid growth was maintained at 50-100ng/ml but cells died at higher concentrations of BMP2 (figure 4.6). Cells were cultured up to day 8 and were not passaged.

This suggests that unopposed Grem1 promotes an *in vitro* stem/ progenitor phenotype, enabling the generation of intestinal organoids. Regeneration is an important part of epithelial repair, and this may lead to chronic inflammation. The delicate balance of Grem1 expression in the correct spatial and temporal manner is crucial for tissue restitution and the prevention of carcinogenesis.

4.4.3 *In vitro* interaction between Grem1 and HH

To examine the direct effect of HH manipulation on Grem1, *in vitro* work was done using intestinal fibroblasts. Fibroblasts are the physiologial source of Grem1 expression. Firstly human colon fibroblast line CCD-112 was cultured in surface-modified plates 2.7.5.1. Spindle shaped cells were seen (figure 4.7). Cells at

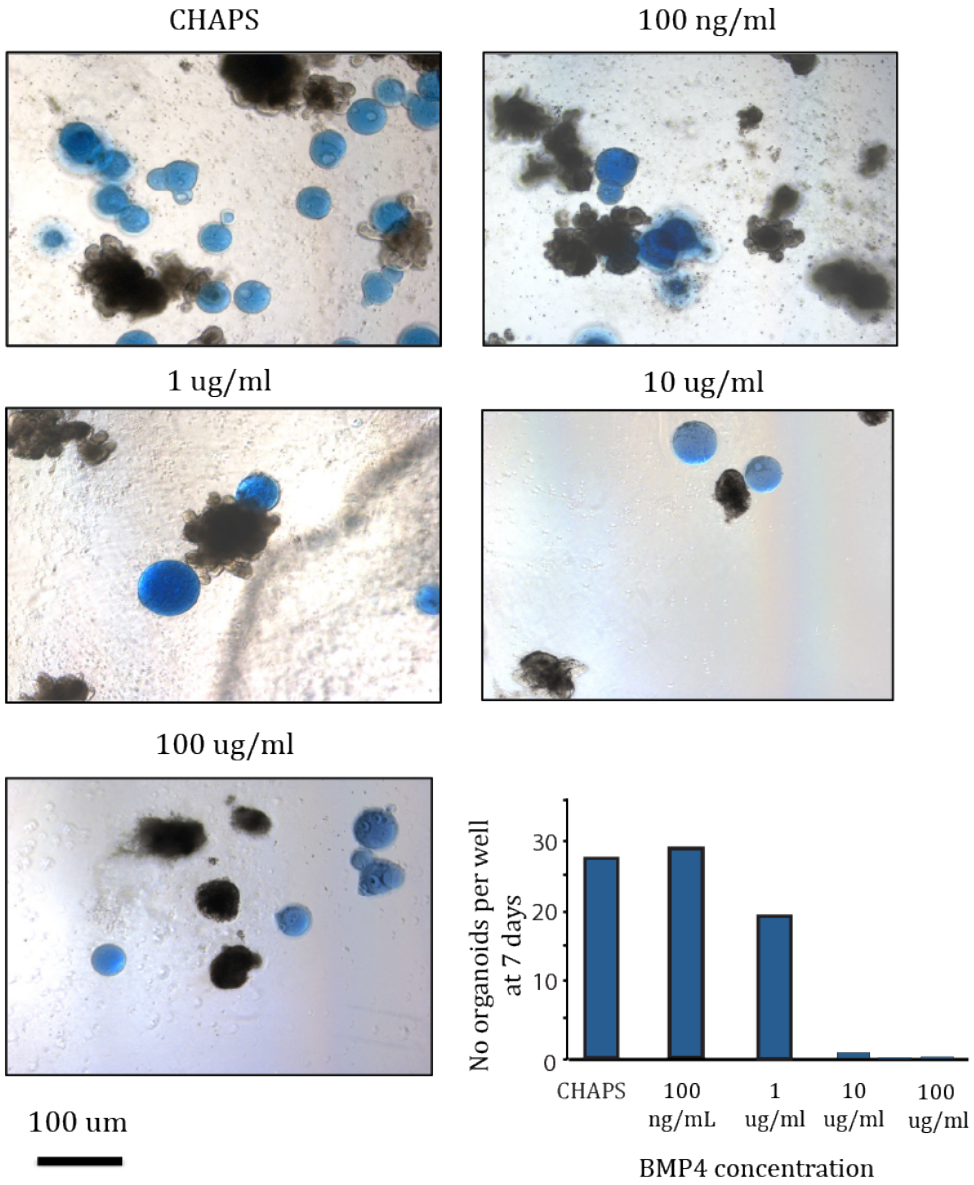

Figure 4.4: Microbeads soaked in varying concentrations of BMP4, in culture with mouse intestinal organoids with recombinant Gremlin in the media.

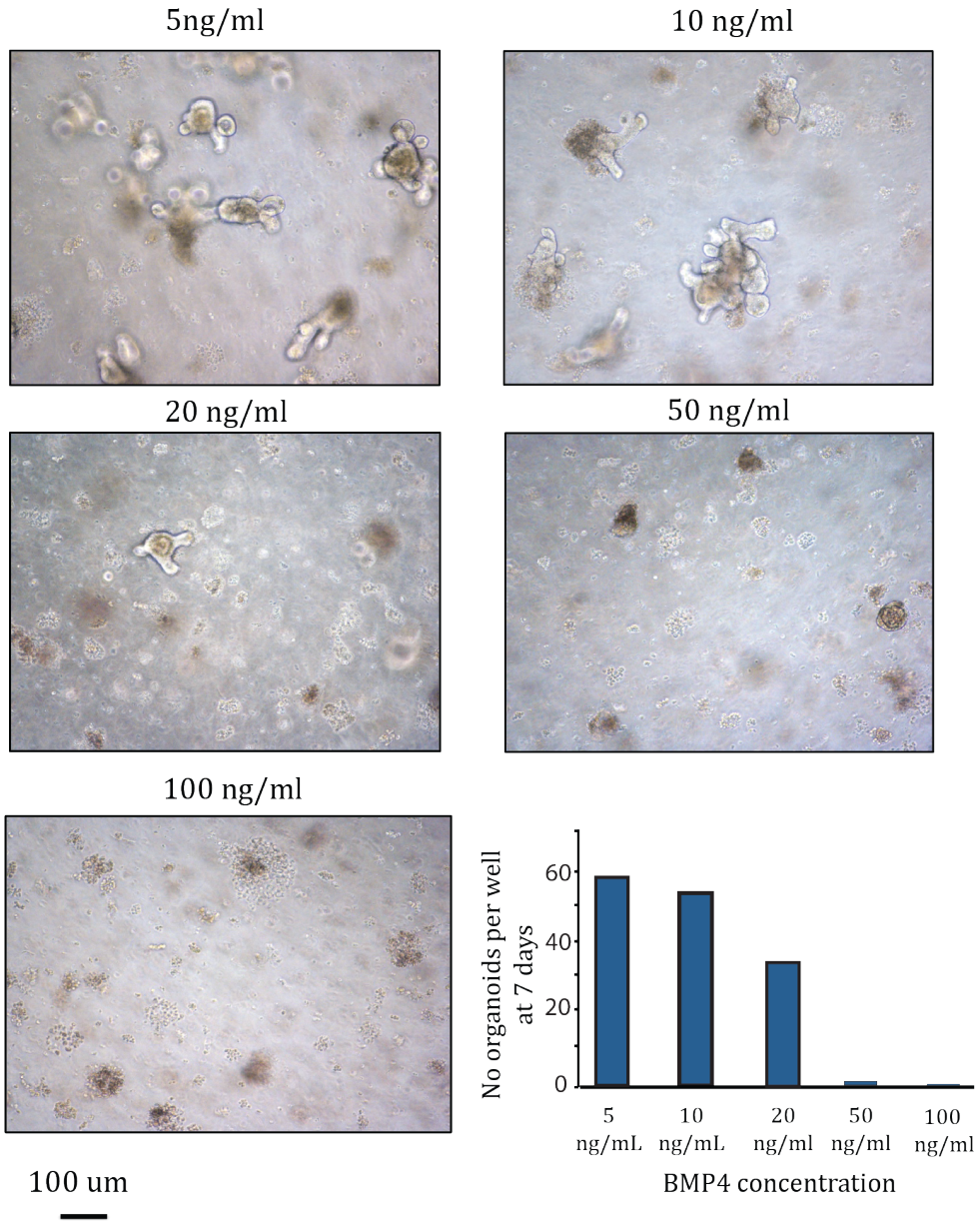

Figure 4.5: Varying concentrations of recombinant BMP4 in media with Gremlin. Number of organoids per well at each BMP4 concentration shown graphically.

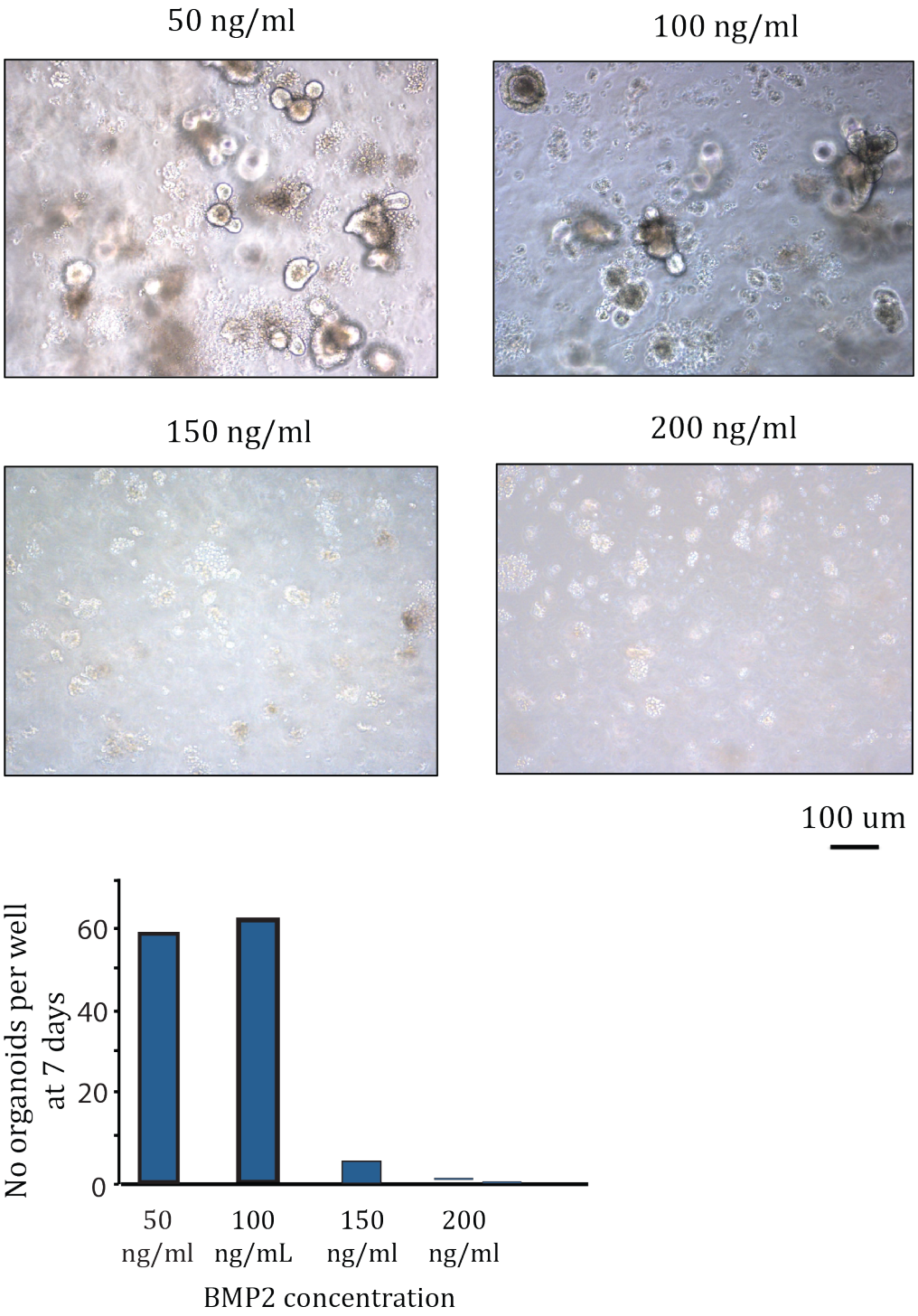

Figure 4.6: Varying concentrations of recombinant BMP2 in media with Gremlin. Number of organoids per well at each BMP2 concentration shown graphically.

passage 3 were plated at a density of 2.5 x 10^4 cells per ml. Hedgehog inhibitor Cyclopamine was used to manipulate the Hedgehog pathway and test downstream effects. Cyclopamine directly binds Smoothened and constitutively activates it, thereby inhibiting HH signalling in a dose-dependent manner. Varying concentrations of cyclopamine were added on the day of plating and then on alternate days. On day 7 cells were collected and RNA extracted for qPCR. Gli1 and Grem1 expression was measured (figure 4.7). There was a decrease in Gli1 and an increase in Grem1 expression as concentration of cyclopamine increased between 1 and 20μM.

Immortalised cell lines such as CCD-112 can evolve over time causing genotypic and phenotypic variation, and genetic drift can also cause heterogeneity in culture at a single point in time. For this reason primary cell culture was used to see if the findings above could be replicated. Human colonic fibroblasts were extracted from fresh endoscopic biopsies (see 2.7.5) and tested at passage 2. The same concentrations of cyclopamine were added in the same time period. Again GLI1 expression, measured as a readout of Hedgehog signalling, decreased, and there was an increase in GREM1 expression (figure 4.7).

Therefore inhibition of Hedgehog leads to an increase in Grem1 expression in fibroblasts in both human and mouse. I hypothesise that this is driven by a Gli1/Gli2 dependent mechanism [158]. This may mean that Gli1 directly inhibits Grem1 in fibroblasts. Fibroblasts away from the crypt base express Gli1 and perhaps that is why they do not express Grem1. When Gli1 is inhibited there is a reciprocal increase in Grem1. Gene regulation and interaction of Hedgehog and Grem in the mouse limb bud is extremely complex and the mechanistic interaction of this

a)

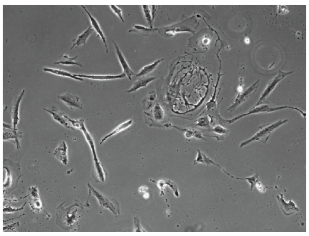

b)

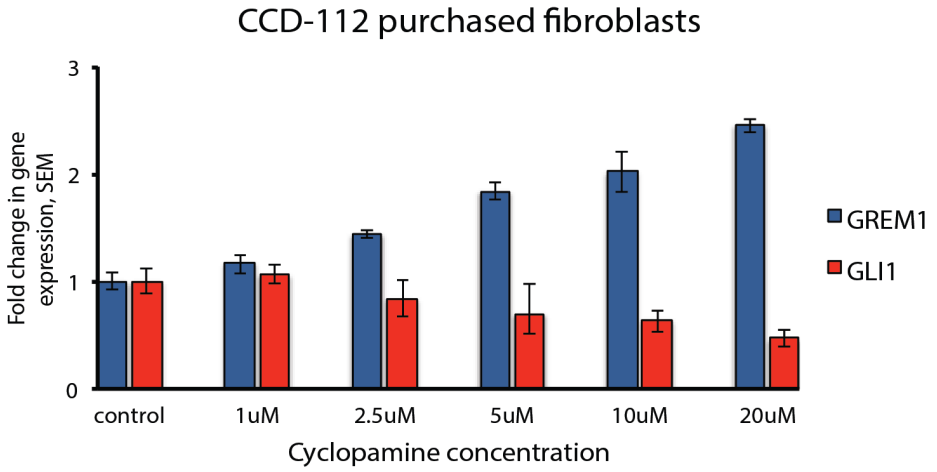

c)

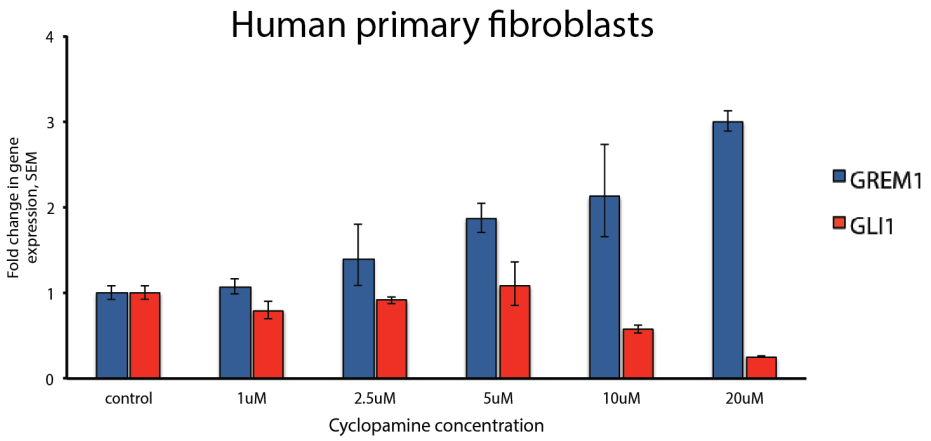

Figure 4.7: a) Human colon fibroblast CCD-112 cells in culture. b) Effect of cyclopamine on GLI1 and GREM1 expression in CCD-112 cells. c) Effect of cyclopamine on GLI1 and GREM1 expression in human colon fibroblast primary culture.

apparent paradoxical gene regulatory relationship in the intestinal fibroblast will require further extensive evaluation.

4.4.4 Grem1 in human IBD and mouse colitis

It was shown in chapter 3 that GREM1 is upregulated in human colitis. To demonstrate this on slide, human colitis surgical resection specimens were stained for GREM1 using *in situ* hybridisation. Samples were taken from three patients who underwent a subtotal colectomy for severe Ulcerative Colitis. Samples were promptly fixed in formalin. Normal colonic tissue was collected from the same patient specimen for comparison. Staining showed an expansion in GREM1 away from the subcrypt mesenchyme and into the intercrypt mesenchyme. This occurred in areas of discrete ulceration and an example is shown in 4.8.

To examine Grem1 expression in the murine model, a chemical model of DSS colitis was used. 2% DSS was given in the drinking water for five days to wild-type mice. Mice were weighed daily to ensure they did not lose more than 20% body weight, and were culled if this threshold was reached. On day 7 mice were culled and gut Swiss rolls made and stained for Grem1. This way the epithelium could be assessed in the acute phase of inflammation. Findings were analogous to human tissue. There were multiple ulcers throughout the colon and Grem1 expanded away from the subcrypt mesenchyme into intercrypt areas in regions of healing ulcers (figure 4.9). Again 3 biological replicates were used.

This change in Grem1 expression was seen at day 7 of DSS induction in mice, so crudely in the acute inflammatory period. To more closely model changes in a

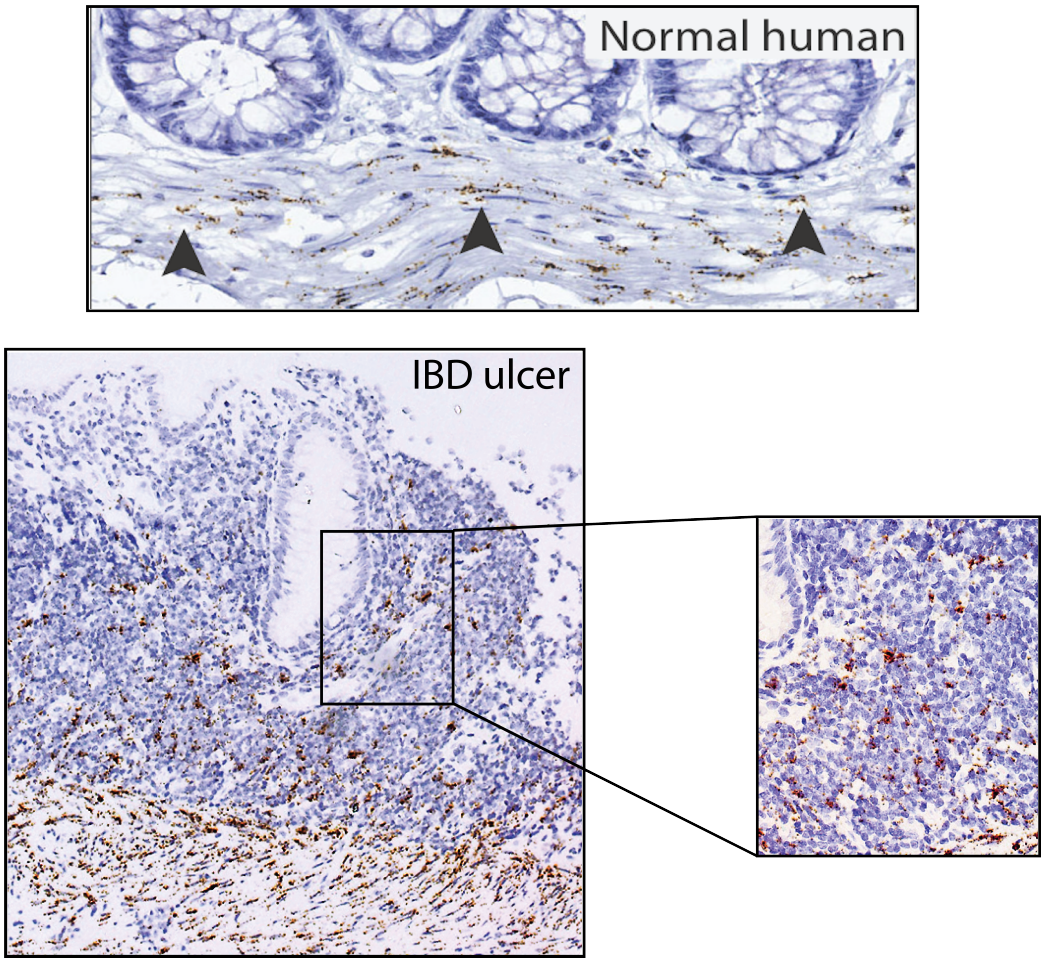

Figure 4.8: GREM1 ISH in human normal colon and IBD.

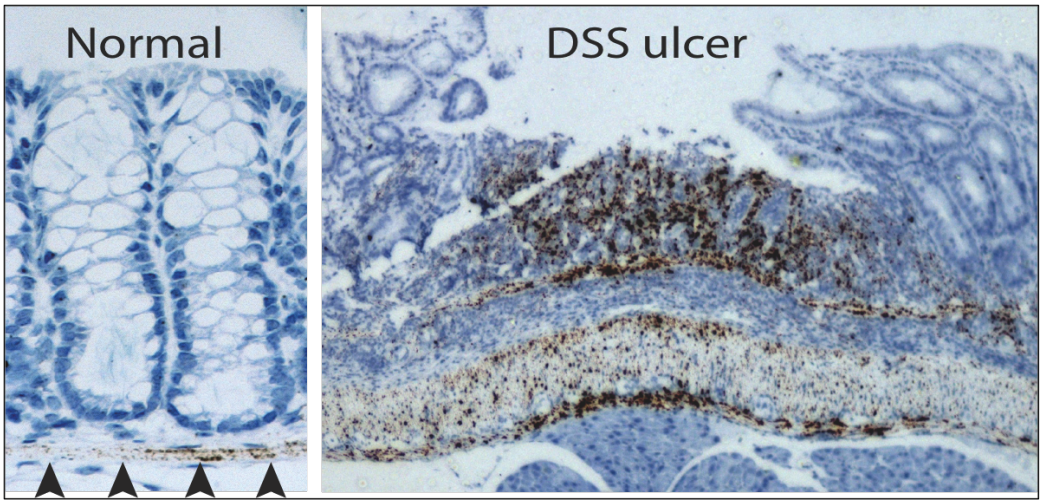

Figure 4.9: Grem1 ISH in mouse colon and in DSS colitis.

temporal manner, a precise way to induce ulceration was required.

Together this suggests that in inflammation fibroblasts away from the crypt base become activated and express GREM1.

4.4.5 Grem1 in murine endoscopic biopsy injury

The timing of Grem1 expansion could not be assessed in murine DSS colitis because ulcers develop and heal at different times after onset of DSS. To validate the temporal recruitment of Grem1 after injury, a technique was developed to induce colonic injury by biopsy via endoscopy. Endoscopy in mouse models has been reported [144] [65]. An adapted method was used (2.2.8) in which a rigid endoscope was inserted under general anaesthetic, and two 3-French biopsies (equivalent to 1mm diameter) taken under full visualisation. Figure 4.10 shows the endoscope in position and the monitor screen immediately post-biopsy. Animals were monitored during and after biopsy and culled at required timepoints. Finding the biopsy

within the colon Swiss roll required some optimisation. Several serial sections were cut every 50 microns throughout the whole paraffin block. H&E staining was used to find the location of the biopsies and adjacent slides then stained for markers of interest.

Figure 4.11 shows stages of wound repair from 5 hours to 6 days. There is loss of epithelial continuity and at 5 hours neutrophils are already infiltrating the wound to begin restitution. Re-epithelialisation of the damaged area can be seen from 24 hours, with a single cell layer forming over the wound which gradually expands.

At 24 hours Grem1 ISH is shown in figure 4.12. Adjacent to the ulcer, Grem1 expressing cells are present in the intercrypt as well as subcrypt areas. At the first timepoint at 5 hours, Grem1 was limited to the subcrypt mesenchyme. After 2 to 3 days Grem1 remained in fibroblasts surrounding the biopsy site, and at 6 days the wound had healed and fibroblast Grem1 expression was again limited to the subcrypt area. The size of the injury and presence of multiple adjacent wounds is likely to be related to the timing of repair, but this shows the timecourse of restitution in a single 1mm wound.

In this situation where acute inflammation completely resolved, Grem1 expression normalised within 7 days. This is in contrast to chronic inflammation in which Grem1 expression remains dysregulated, as seen in UC patient colectomy specimens, and contributes to the ongoing microenvironmental disarray.

In summary mouse biopsy wounding is a useful way to study temporal healing and recruitment of Grem1.



Figure 4.10: Mouse under general anaesthetic with endoscope in situ and view of monitor immediately after biopsy. Faecal matter is visible in the distance.

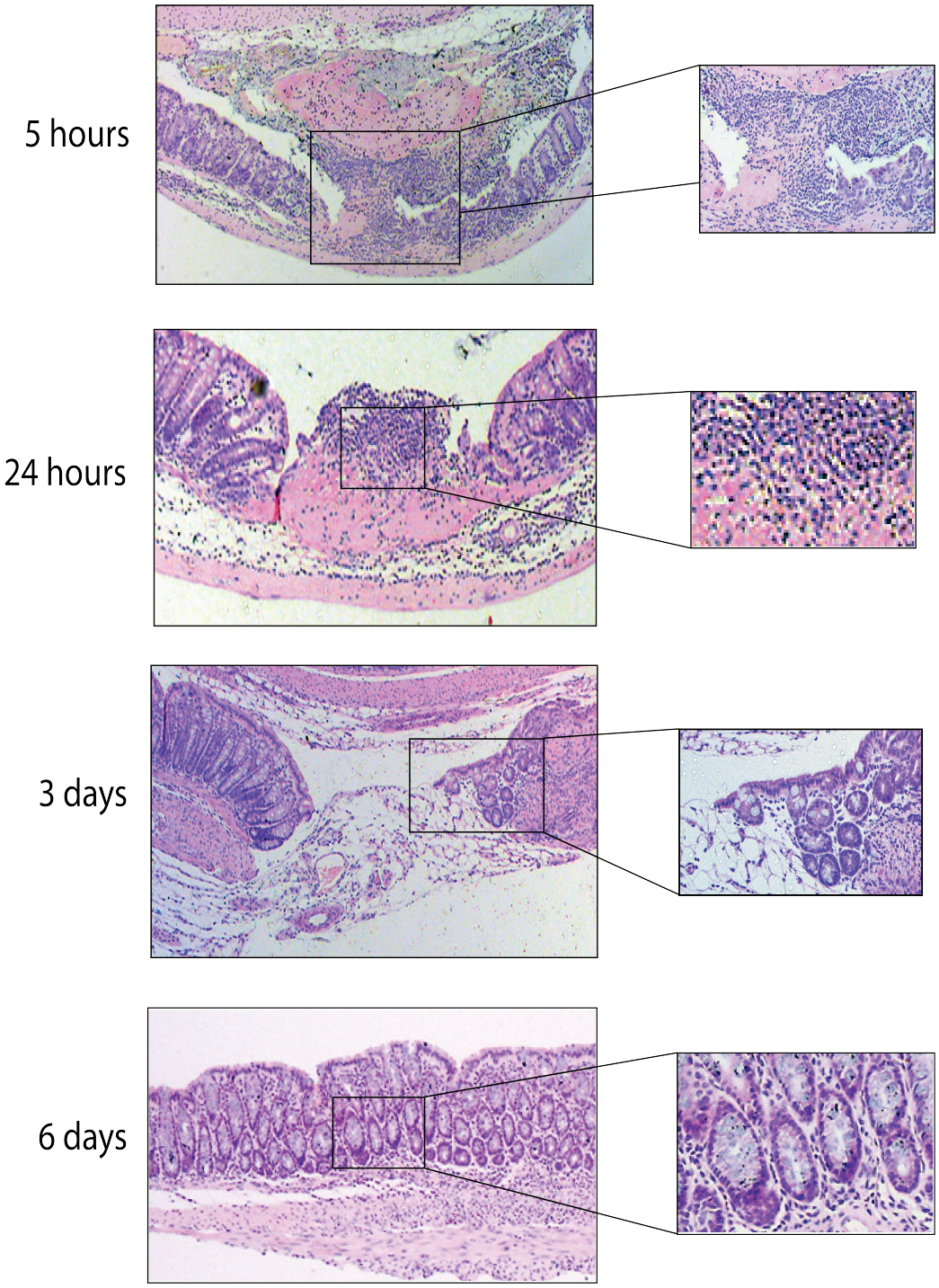

Figure 4.11: Mouse colonic biopsy after 5 hours, 24 hours, 3 days and 6 days: H&E stain.

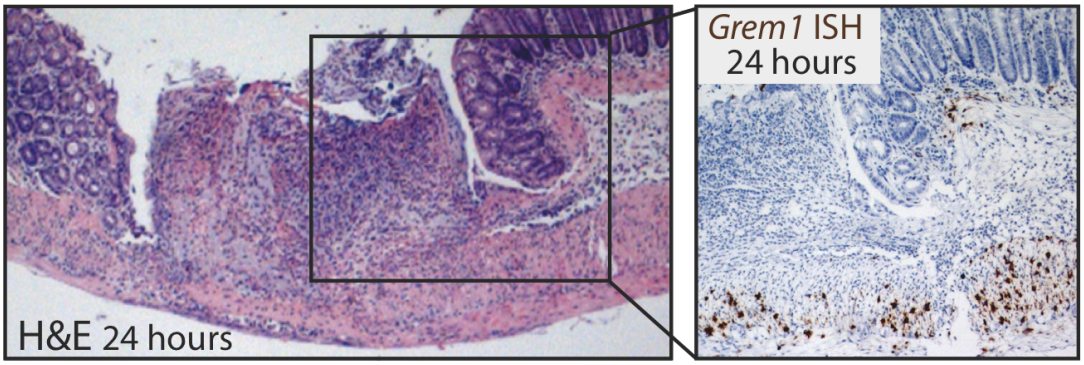

Figure 4.12: Mouse colonic biopsy after 24 hours: H&E stain and Grem1 ISH.

4.4.6 Grem1 in a model of Hedgehog knockdown

The association between Grem1 and HH has not been established, although there is a link between stromal Hh activation and reduced Grem1 expression [114]. To study this *in vivo*, a murine model of Hedgehog knockdown was used. *Ah-Cre; IHH*$^{fl/fl}$ mouse blocks were provided by the laboratory of Gijs van den Brink. Mice have a gut epithelial specific knockout of Ihh. Ah-Cre is expressed under a cytochrome P450 promoter, enabling inducible recombinase expression after administration of a lipophilic xenobiotic, conditional to the site of administration of the inducing chemical [159]. In this case beta-naphthoflavone in corn oil was mixed with standard murine food. Animals exhibited disruption of the mesenchymal architecture with loss of the αSMA-expressing muscularis mucosae. There was change to extracellular matrix proteins and reduction in numbers of crypt myofibroblasts [116]. Perhaps as a result of loss of control over the stem cell niche, crypts were wider and loosely organised with disruption of crypt epithelial fate and polarity as shown in published figure 4.2, in which there are differentiated cells in the crypt base. There was increased Wnt signalling: Cd44, Sox9 and

EphB2 expression was high throughout the crypt and along the villus in the small intestine as well as along the entire crypt length in the colon. Crypt fission incidence increased by 10%. Expression array analysis showed downregulation of BMP and increase in Grem1.

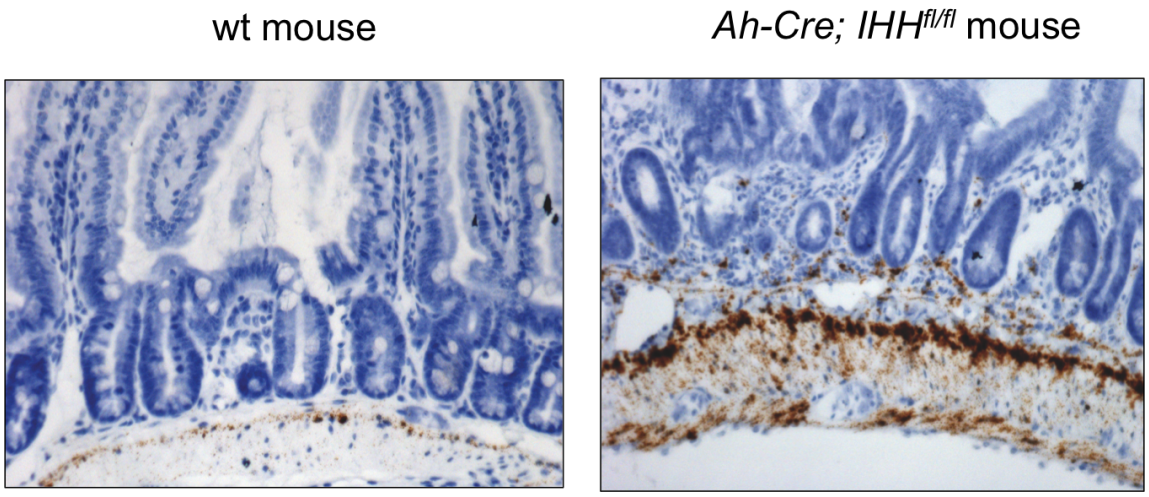

Figure 4.13: Grem1 ISH in wild-type mouse and *Ah-Cre; IHH*$^{fl/fl}$ mouse.

My aim was to look for spatial change in Grem1 in these mice. Blocks were cut and stained for Grem1 and this showed a similar response to mice with colitis. Grem1 expressing cells were not limited to subcrypt myofibroblasts but showed increased expression both in the subcrypt mesenchyme and in the intercrypt area 4.13. This was replicated in 3 animal blocks. This means that although muscularis mucosae cells expressing αSMA were lost, Grem1 must not be tightly confined to these cells, and other fibroblast cells can become activated and express Grem1 both at the crypt base and elsewhere. This could be by transdifferentiation of an existing non Grem1-expressing population. A way to test this would be to co-stain the cells for Grem1 with other fibroblast markers, and to time the onset of Grem1 expression. The similarity to the appearance of Grem1 in colitis could mean that

the downregulation of Hedgehog is associated with the increase in Grem1 expression in IBD.

4.5 Discussion

To answer the key objectives set out:

1. Grem1 is a paracrine antagonist of BMP2 and BMP4.
2. Hedgehog plays a part in the regulation of Grem1 and there is a paradoxical relationship between HH and Grem1 in intestinal fibroblasts.
3. Grem1 is upregulated in IBD and Grem1 expression is no longer limited to to the subcrypt mesenchyme. Temporally Grem1 expressing fibroblasts are seen adjacent to ulcers after 24 hours and Grem1 plays a role in intestinal restitution.

4.5.1 The paracrine proliferative effects of Grem1

The first aim was to determine whether Grem1 is a paracrine antagonist which promotes proliferation. I have shown that Grem1 does indeed act cell-to-cell and by inhibiting BMP promotes organoid budding. The way that Grem1 causes local budding may be analogous to Wnt5a in the paper by Miyoshi. Wnt5a-soaked beads caused clefting of spheroids when placed adjacent to them, as if forming nascent crypts. Proximity to Grem1-soaked beads, and even contact with beads, caused budding and survival of organoids. Grem1 was able to travel across matrigel to have this effect in a paracrine manner. This was overcome by high levels

of BMP2 and BMP4 in the media. There is a reciprocal cut off between Grem1 and BMP ligands at the point at which regenerative budding in organoids will not occur. Inflammation causes a physiological disruption of signalling with carefully coordinated mesenchymal epithelial signalling. There is disrupted morphogen balance which allows epithelial stem/ progenitor function and this then returns to normal.

4.5.2 Grem1 and HH in homeostasis

Work in this chapter has shown a direct link between Grem1 and HH expression. Suppressing HH *in vitro* with cyclopamine led to an increase in Grem1. In homeostasis I hypothesise that epithelial Hedgehog signalling maintains a BMP ligand active fibroblast population and restricts Grem1 expression to the subcrypt stroma. This interaction between Grem and HH seems to be in opposition to the developing mouse limb bud. Here Grem1 is a direct downstream target of Shh to maintain the AER (apical ectodermal ridge) [160]. Bmp2 and Gremlin are direct targets of Shh and in addition a distinct Gli activator-dependent enhancer independently regulates Gremlin.

The differences between the mouse limb bud and the intestinal fibroblast cannot be explained from the data. It may be the consequence of different gene regulatory regions, with the limb bud regulatory area downstream of Formin. The gene regulatory region for Grem1 in development is a Gli-binding region $>$100 kb downstream from the Grem1 gene. It is assumed that the intestinal gene regulatory region of Grem1 is *upstream* as there is a 40kb duplication upstream of

Grem1 in HMPS (see 1.4.3).

4.5.3 Grem1 in inflammation

Grem1 expression is increased in colitis in both humans and mice. There is aberrant expression by fibroblasts away from the crypt base. Mesenchymal expression increases 24 hours after endoscopic biopsy injury in mice. *In vivo* knockout of epithelial HH ligand showed similar changes. My theory is that in inflammation epithelial denudation leads to reduced IHH signalling, reducing BMP activity and promoting surrounding crypt fission to aid tissue restitution (figure 4.14). Fibroblasts away from the crypt base become activated like myofibroblasts and gain the potential to express GREM1. The morphology of these fibroblasts did not change on H&E staining. It is not clear where these Grem1-expressing stromal cells arise from. Possibilities include:

1. Transdifferentiation of an existing non Grem1-expressing stromal population

2. Clonal expansion of an endogenous Grem1-expressing population

3. The existence of a haematogenous source of mesenchymal stem cells with engraftment and differentiation

I hypothesise that the profound increase in Grem1 expression results in a net reduction of mucosal BMP signalling with subsequent impact on surrounding epithelial stem cell fate determination. This loss of polarisation of the axes was seen in microdissection of crypts in chapter 3.

There is functional heterogeneity between stromal elements with HH and BMP acting from polar ends. Chronic inflammation from repeated ulcers can lead to prolonged HH loss and hence a Grem1 increase. An acute rise in Grem1 is beneficial in wound healing but a chronic rise in turn keeps IHH low and turns on the inflammatory cascade that increases the risk of carcinogenesis.

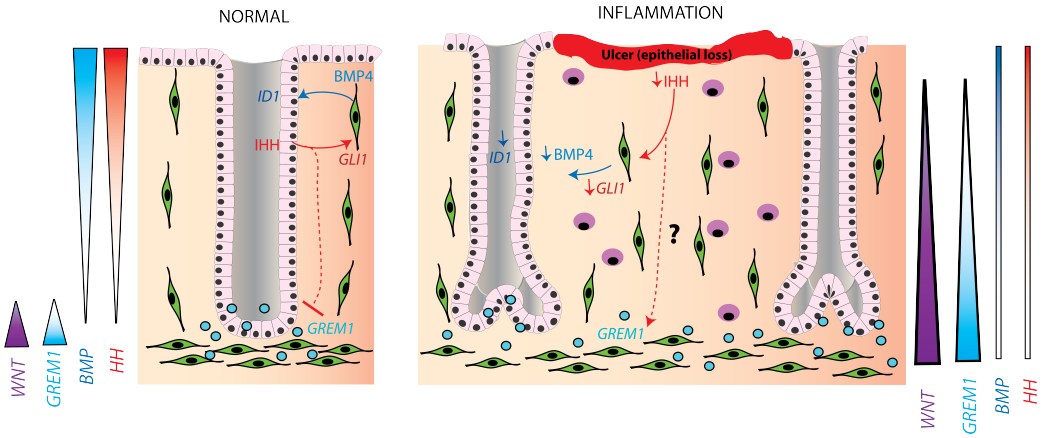

Figure 4.14: Interaction between BMP and HH in homeostasis and inflammation. In homeostasis the crypt top is rich in BMP and HH, and this inhibits Grem1 and restricts it to the crypt base. In inflammation epithelial denudation leads to reduced IHH signalling and therefore reduced BMP activity. This removes the negative feedback on Grem1 which is no longer restricted to the crypt base. Higher levels of Grem1 and Wnt promote crypt fission to aid tissue restitution.

This chapter has covered the role of Grem1 in intestinal restitution. The next chapter will go on to discuss how aberrant Grem1 expression leads to intestinal neoplasia.

4.5.4 Limitations

- Organoid culture is useful and gives information about morphogenic effect on 3D culture, but is not physiological. Epithelial cells growing in supra-

optimal levels of Wnt agonists and BMP antagonists, without adjacent mesenchymal brakes, are very likely to grow robustly in culture.

- It was difficult to quantify distance of organoids from microbeads and therefore assess exact spatial effects of morphogens on organoid growth.
- An issue with assessing repair of biopsy wounds is the lack of quantification. The size of the wound created is always slightly different and therefore the size alone should not technically be measured as a sign of recovery. The number of cells recruited to the wound bed will also therefore differ. The wounds are also not created in exactly the same position within mouse colon, and this could have an effect on rate of recovery. A digital pathological method to count cells per millimetre of wounding would be required.

Chapter 5

Grem1 in cancer initiation: Form and function of ectopic crypts in the *Vil1-Grem1* mouse model

5.1 Aims

The key objectives in this chapter were:

1. To assess whether ectopic cryts cells have a different transcriptional profile in contrast to crypt basal cells.
2. To assess whether ectopic crypts have clonogenic potential, proved by their ability to lineage trace.
3. To assess whether the villus stromal microenvironment around ectopic crypts and basal crypts differs.

5.2 Introduction

5.2.1 A model of compartmental disruption of *Grem1*

The human condition HMPS predisposes patients to colorectal cancer at a young age. Patients develop polyps of mixed histology with ectopic crypts that are positive for *Sox9* (section 1.4.3). This has given insight into how a compartmental switch in *GREM1* expression can lead to the formation of ectopic crypts, leading to mutagenesis and cancer. A mouse model has been developed for this condition in which *Grem1* is aberrantly expressed in epithelium. Mice develop polyps with ectopic crypts positive for stem cell/progenitor marker *Sox9* and the model gives further insight into stem cell dynamics in the intestine in this condition. In this chapter I explore this *Vil1-Grem1* mouse model.

As discussed in 1.4.3.2, traditional serrated adenomas can be thought of as a sporadic equivalent of HMPS polyps as they are also caused by ectopic epithelial *Grem1* expression and exhibit ectopic crypts.

Ectopic crypts are pockets of proliferative cells outside the context of the crypt base and result from an imbalance of morphogens. Usually stem cells and progenitor cells reside at the crypt base in the well controlled niche with Wnt, BMP and Hh in balance and with surrounding mesenchyme and Paneth cells providing essential signals. In ectopic crypts though there is no such control. They are away from the protected crypt base niche and within the different microenvironment of the villus. Given the high *Grem1* expression throughout the crypt-villus axis, Bmp and therefore Hh signalling may be downregulated. I wished to anal-

yse the effects on the Hh and Wnt pathways (figure 5.1). I hypothesise that the mesenchyme, which usually contains activated myofibroblasts at the crypt base and Hedgehog components at the luminal side, adjusts and provide proliferative signals to ectopic crypts.

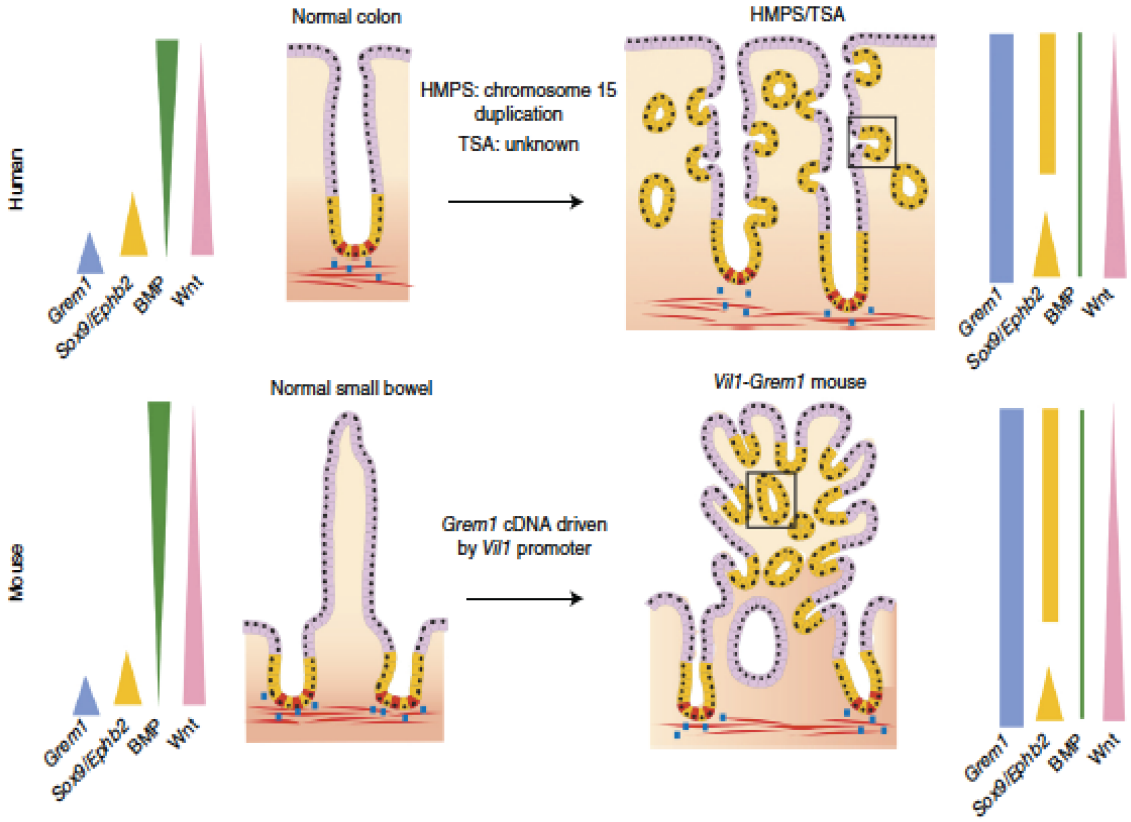

Figure 5.1: Model summarising the proposed mechanistic consequences of disrupted *GREM1* morphogen gradients. Aberrant ectopic epithelial expression of *GREM1* disrupts the coupling of cell fate determination to position along the crypt-villus axis and allows persistence and expansion of an Lgr5-negative progenitor cell pool (characterized by aberrant *SOX9* and *EPHB2* expression) that forms orthogonal ectopic crypt foci. Taken from [85].

5.2.2 Ectopic epithelial expression of *Grem1*; the *Vil1-Grem1* mouse model

It has previously been shown that aberrant BMP signalling can promote stem cell activity away from the crypt base by transgenic overexpression of *Grem1*. A transgenic mouse modelling HMPS with a compartmental switch in *Grem1* expression (from mesenchymal to epithelial expression) had already been developed in my lab, leading to low BMP levels throughout the crypt-villus axis. From 3 months animals have widened villi with ectopic crypt formation. Active proliferation is seen in ectopic intravillus crypts, and there is loss of p16 staining. By 7 months animals develop panintestinal polyposis with at least 150 polyps. They become anaemic with pale feet and hunching. The maximum age animals can live to before becoming unwell is 9 months. Figure 5.2 shows the intestine stained with methylene blue with polyps which decrease in number and size from proximal-to-distal intestine. There is a 28% increase in the length of intestine and width increases also. Colonic lesions also show mixed serrated/ adenomatous/cystic phenotype and have an enlarged stromal compartment.

mRNA expression profiling of *Vil1-Grem1* villi had shown no significant enrichment of Lgr5-based intestinal stem cell profiles but there was enrichment of gene signatures characterising proliferating, early transit amplifying cells. There was marked expansion of a progenitor cell pool outside the intestinal stem cell niche that was only positive for stem cell markers Sox9 and EphB2 (figure 5.3). Thus Sox9 was a specific marker of both crypt base and ectopic crypt progenitor cells.

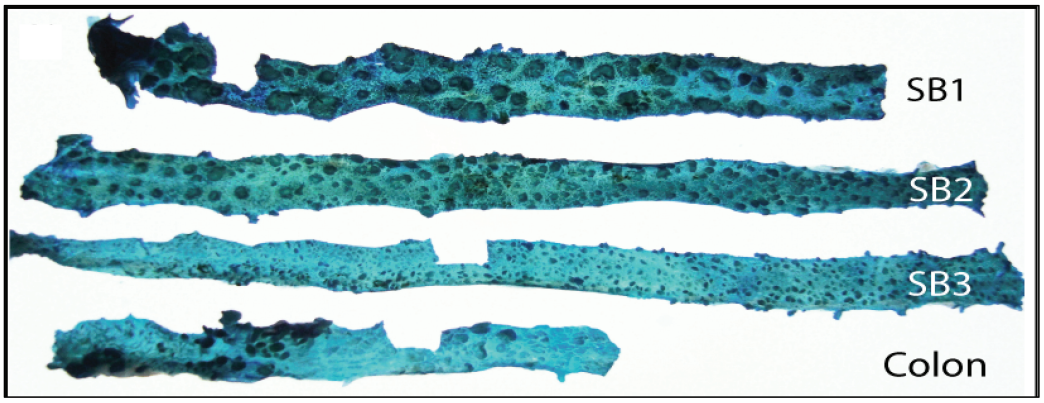

Figure 5.2: Methylene blue staining of *Vil1-Grem1* intestine. Small intestine is divided into 3 segments.

5.2.3 Hedgehog and Grem1 in colorectal cancer

Cancer can be thought of as a wound that never heals. An ongoing insult causes persistent disruption in immune and morphogen signalling which leads to desmoplasia, the growth of fibrous or connective tissue secondary to an insult. Desmoplasia is thought to be the first step in the chronic inflammatory process that can lead to risk of mutation and carcinogenesis. The role of Grem1 and Hedgehog was considered in tissue regeneration in chapter 4. Here the effect of a compartmental switch in Grem1 on HH expression was tested.

The implications for Hedgehog disruption in colorectal cancer are interesting. The Cancer Genome Atlas data in 155 CRC patients showed that compared to control tissue, there was a reduction in GLI1 and HHIP, BMP target genes ID1 and ID2, and a concomitant increase in GREM1. This was not classified according to CRC subtype. When association between GREM1 expression and survival in two publically available CRC data sets 5.4 was analysed in [85], individuals with above-median GREM1 expression had significantly shorter disease-free survival.

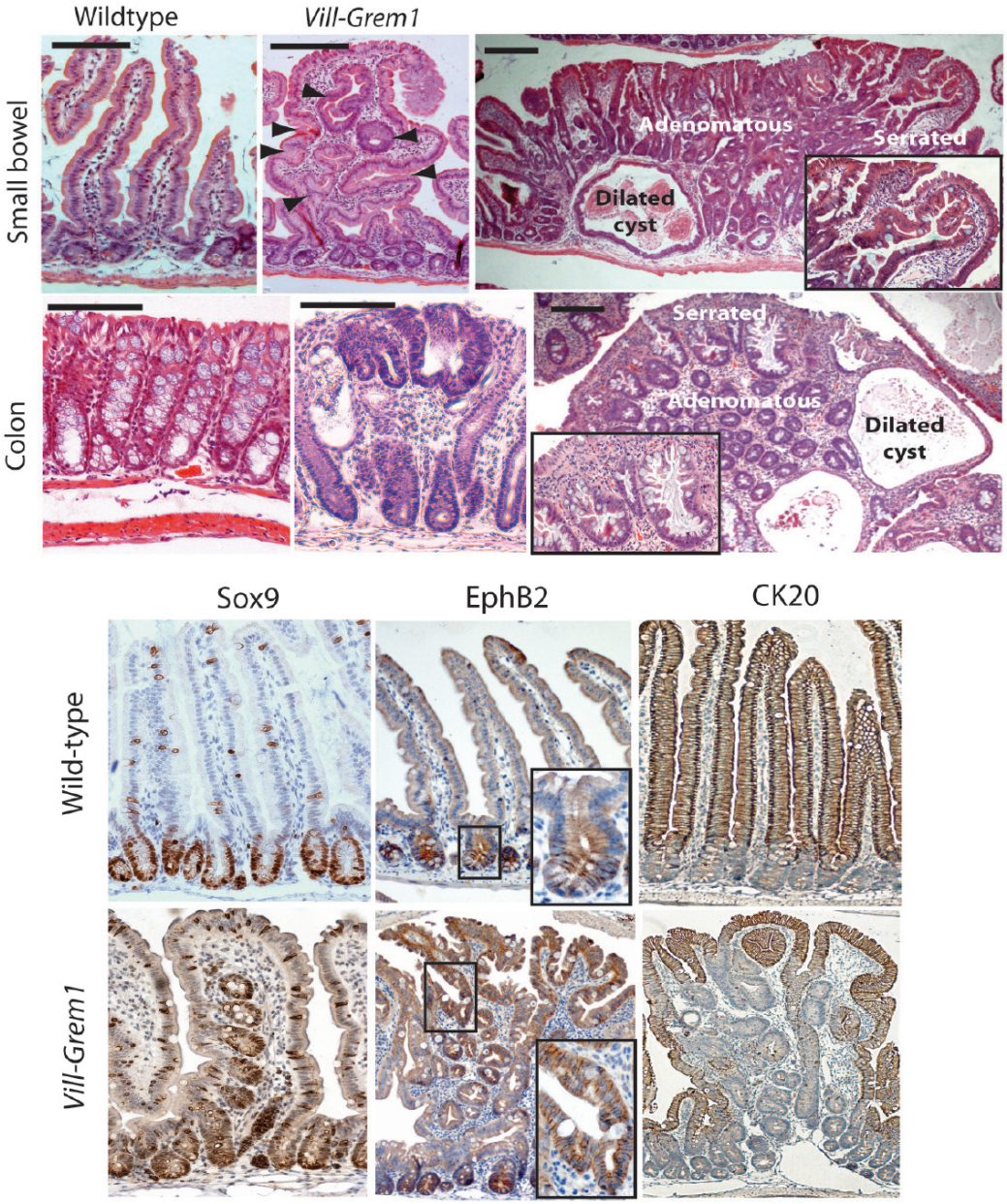

Figure 5.3: (a) Small intestinal lesions in *Vil1-Grem1* mice had widened villi with ectopic crypt foci (arrowheads). Top right, dysplastic polyp formation in a 7-month-old *Vil1-Grem1* animal showing mixed morphology with serrated features (inset). Bottom right, colonic polyp in a 7-month-old mouse with mixed crypt morphology (serrated crypts inset). (b) Immunohistochemical analysis of *Vil1-Grem1* versus wild-type small intestine shows Sox9 and EphB2 staining in the villus ectopic crypts. Ck20 differentiation marker staining was lost in villus ECFs. Taken from [85].

To see whether whole-tumour GREM1 expression correlated with the CCS classification, TCGA RNA-seq data was used and found a highly significant correlation between high GREM1 expression and CCS3-subtype tumours. Therefore there is evidence for increased GREM1 in colorectal cancer, particularly in the CCS3 subtype which is associated with a worse outcome. There is also evidence for reduced Hedgehog signalling in CRC although this has not been analysed by subtype. The background is therefore that in cancer, Hedgehog is downregulated and Grem1 is upregulated.

Complementing this, Gerling et al [114] showed that GLI1 mRNA levels correlated with TCGA stromal gene expression signatures, indicating that activation of downstream Hh signalling occurs in the stromal compartment. Mice with Ptch1 allele loss in the stroma, leading to upregulation of HH signalling, showed increased BMP and reduced Grem1 expression. After exposure to AOM/DSS mice developed fewer and smaller tumours, suggesting a protective effect of stromal Hh activation on colorectal carcinogenesis. In chapter 4 the opposite effect was tested in which an *in vivo* model of Hedgehog knockdown caused an increase in Grem1 expression away from the crypt base. Here the effect on Hh signalling in the *Vil1-Grem1* mouse model is tested.

5.2.4 "Top-down" cancer initiation

Ectopic stem/progenitor cells have been reported to be capable of "top-down" dysplasia initiation [85]. Ectopic crypts may be more prone to somatic mutation because of the following theories:

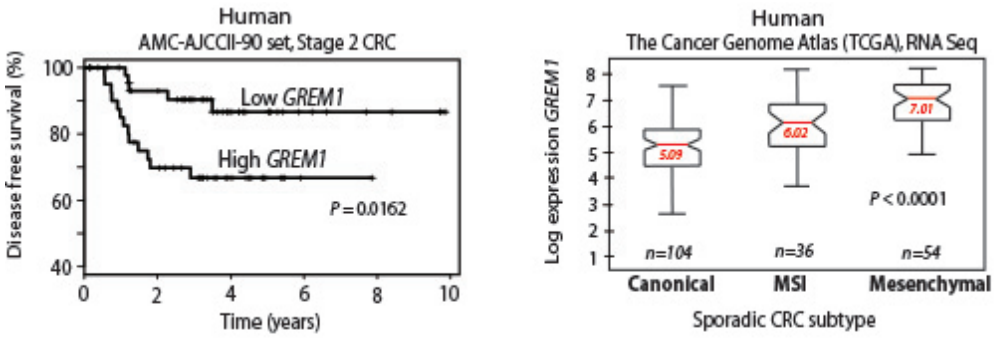

Figure 5.4: Left, expression of GREM1 in the AMC-AJCCII-90 human CRC set and correlation with disease-free survival. Right, classification of TCGA RNA-seq data into CCS subtypes (correlation between CCS3-subtype cancers and high whole-tumour GREM1 expression, P $<$ 0.0001, ANOVA). Figure adapted from [85].

1. Proximity to the luminal surface means they are exposed to intraluminal toxins.

2. They have altered DNA damage response. It was reported in chapter 3 that in chronic inflammation epithelial cells show reduced apoptosis and an altered response to DNA damage. This results from cellular stresses from inflammatory insult. BMP-Smad1 signalling is involved in the DNA damage response via the Atm-p53 pathway and BMP-Smad1 loss of function leads to tumourigenesis [161].

3. Ectopic cryt progenitor cells may proliferate at a faster rate than basal crypts, making them more prone to mutation.

4. They may be a different type of progenitor cell altogether, expressing different markers to the crypt base progenitors and carrying a different potential to mutate.

5. The ectopic niche may be different. Paneth cells have been noted within ectopic crypts but may act differently in terms of providing antimicrobial peptides and Wnt3a when outside the crypt base stem cell niche. Loss of organised polarised mesenchymal signals may lead to increased proliferative capacity.

Several of these theories will be tested in this chapter.

5.2.5 Stem cell potential in cells away from the crypt base

I hypthesise that there are differences between crypt base and ectopic crypt progenitor populations. To examine differential gene expression between crypt base stem cells and ECF stem/progenitor cells in terms of susceptibility to mutation, these two areas were compared in terms of transcriptomic signatures.

Next I hypothesise that stem cell potential exists in the ectopic crypt progenitors. Two out of three properties of stem cells were assessed:

- The ability to lineage trace and give rise to clones
- The potential to give rise to multiple cell lineages
- The capacity to generate organoids - this was not assessed

A *Vil1-Grem1; Sox9Cre^{ERT2}; Rosa26(-LoxP-STOP-LoxP-)^{YFP}* model allowed YFP recombination in Sox9-positive cells, to mark the progeny of Sox9 cells. Serial imaging with 3D reconstruction was done in order to find whether clones arise from ectopic progenitors in addition to those at the crypt base.

To explore whether these clones were multipotential, co-staining for YFP and

different cell type markers was done.

Next the microenvironment of the ectopic crypts was considered. The way in which ectopic crypts develop could be as a clone from crypt base stem cells, which retain proliferative capacity even after leaving the crypt base in the presence of aberrant *Grem1*. Alternatively the clone could acquire proliferative capacity only once it reaches the ectopic crypt due to the harsh microenvironment. Co-staining for YFP and Ki67 was done in the above mouse model to see if Ki67 was lost after the clone left the crypt base and then regained in the ectopic crypt, or whether Ki67 remained positive throughout.

The mesenchyme of *Vil1-Grem1* animals was compared with the mesenchyme of wild-type animals. Differences in the canonical and non-canonical Wnt pathways were analysed.

5.3 Methods

The methods used in this chapter are described in chapter 2 and were as follows:

- Laser capture 2.3.4.3
- RNA sequencing 2.5.8
- 3D processing of slides 2.3.4.2
- Immunohistochemistry and co-staining 2.6.1

5.4 Results

5.4.1 Contrasting crypt base and ectopic crypt progenitor cell populations

One hypothesis for the mutational potential of ectopic crypts is that they are a different population of cells to crypt base progenitors. Given ectopic cells are Lgr5-negative and are not within the confines of the crypt base stem cell niche, they are exposed to a different niche microenvironment. I wished to investigate whether these cell populations differed in terms of their transcriptional repertoire. In particular it is of interest whether the ectopic progenitors respond differently to DNA damage and are more or less susceptible to somatic mutation.

Laser capture microdissection was used to capture cells from each compartment. Frozen OCT-embedded *Vil1-Grem1* mouse gut rolls were cut into 10 μm sections and stained for Cresyl Violet. Three animals were used. Then crypt base and ectopic crypts were laser capture dissected and RNA extracted fresh and sent for SMARTer RNA sequencing (figure 5.5). There were 725 genes differentially expressed in the two compartments, with log-fold change >2 and adjusted p-value <0.05. Figure 5.6 shows some genes of interest expressed in each compartment. Stem cell markers Lgr5, Ascl2, Olfm4 and Cd24a were all more highly expressed at the crypt base. EphB2 and Sox9 were higher in ectopic crypts. Canonical Wnt ligand Wnt3 and receptor Fzd2 were higher at the crypt base. Pro-apoptotic protein Caspase3 was up in ectopic crypts but there was no significant difference in other pro- and anti-apoptotic proteins between compartments. Figure 5.6 shows

GSEA for a custom set of apoptosis genes which is more enriched in ectopic crypts but does not reach significance. DNA damage repair genes were enriched in basal crypts as shown in the figure. Tff1, a secretory protein involved in epithelial protection and repair and increased in IBD, was higher in ectopic crypts.

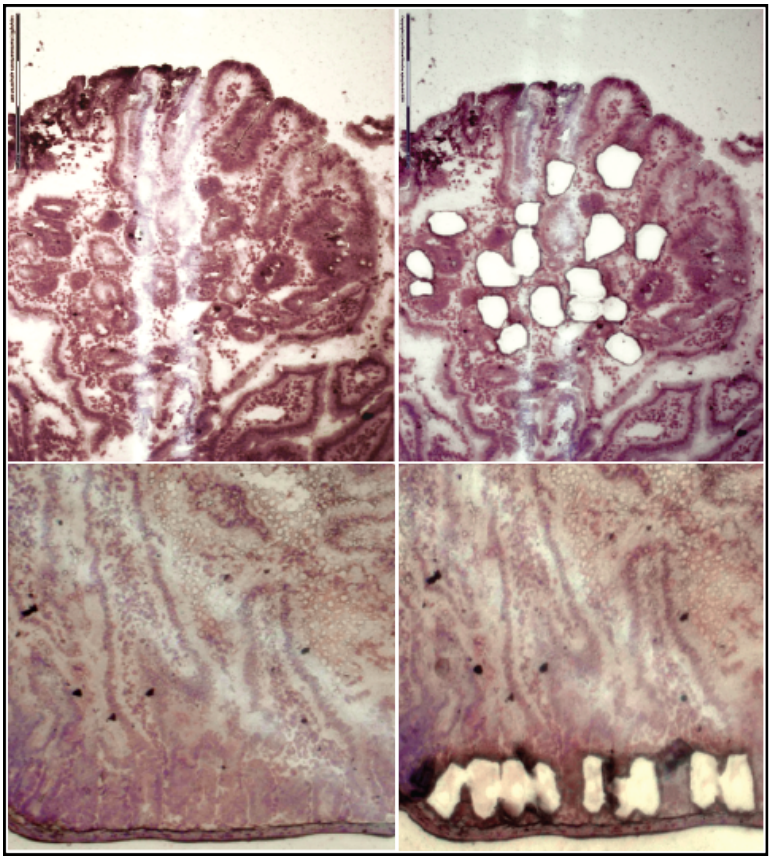

Figure 5.5: *Vil1-Grem1* mouse small intestine before and after laser dissection of ectopic and basal crypts.

To verify these findings at a protein level, IHC staining was done on *Vil1-Grem1* small intestine. It is already known that Sox9 and EphB2 are positive in ectopic crypts. Although Paneth cell markers Lysozyme 1 and 2 were found to be higher at the crypt base on RNA sequencing, Paneth cells were also present in ectopic crypts on Lysozyme staining (figure 5.7). Bag1, an anti-apoptotic protein, the expression

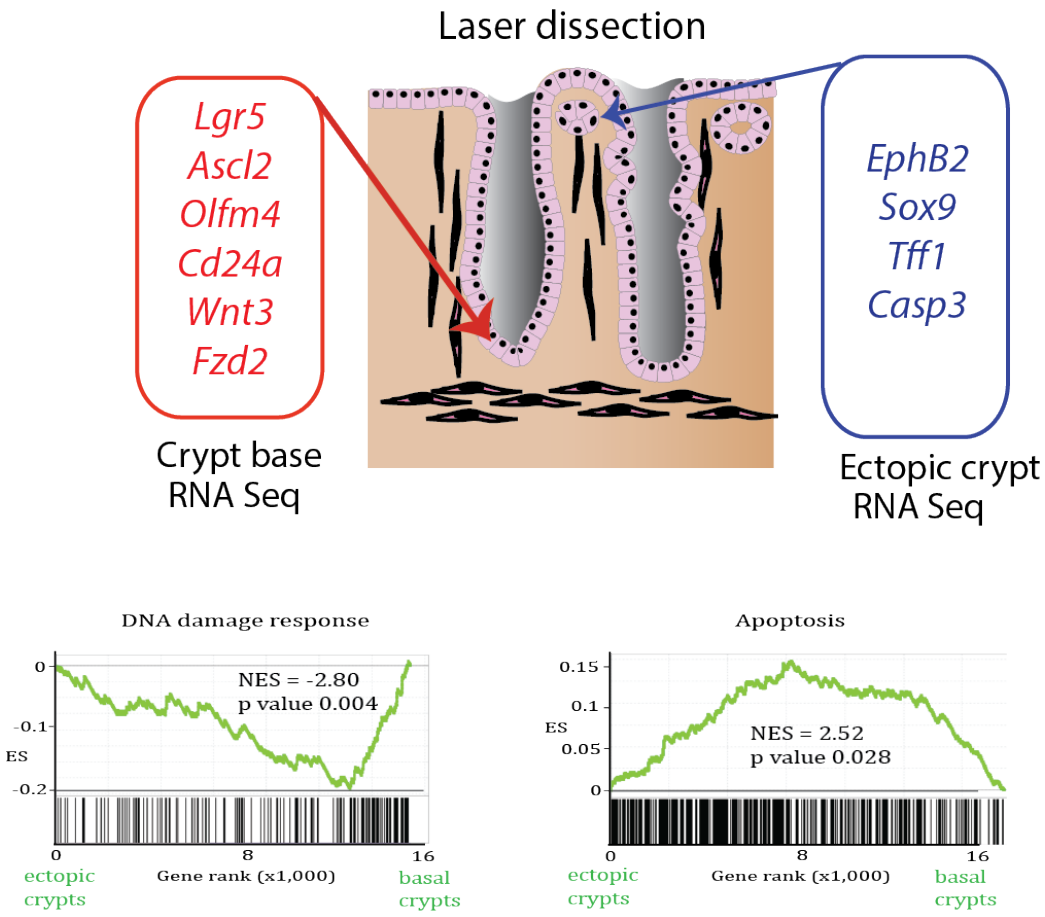

Figure 5.6: Genes differentially expressed in crypt base and ectopic crypts. GSEA for DNA damage repair and apoptosis across ectopic and basal crypts.

of which is enhanced by Sox9, was positive in ectopic crypts 5.7. Caspase 3, a mediator of apoptosis, was also present both at the crypt base and in ectopic crypts.

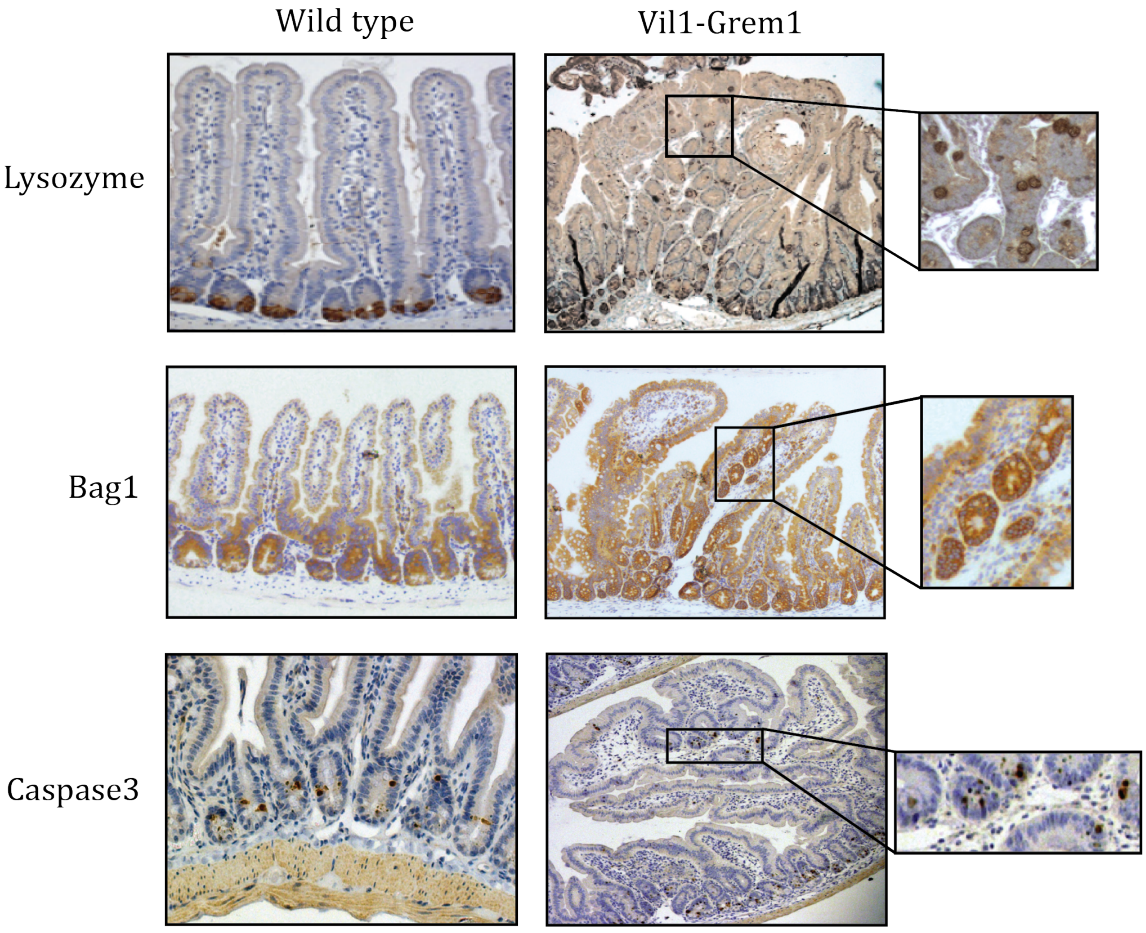

Figure 5.7: Lysozyme (a marker of Paneth cells), Bag1 (anti-apoptotic protein) and Caspase3 (mediator of apoptosis) IHC in wild-type and *Vil1-Grem1* mice. All three markers were positive in ectopic crypts.

In summary there were significant transcriptional differences between ectopic and basal crypts. Classical stem cell markers were expressed at the crypt base with only EphB2 and Sox9 expressed more highly in ectopic crypts. Paneth cells and apoptosis-related proteins were present in both ectopic and basal crypts.

GSEA did not yield differences in gene sets between the two populations of cells. There are limitations to transcriptomic work; it does not take into account post-translational modification and gene expression is used as a surrogate for gene function. I wished to explore the stem/progenitor capacity of the ectopic crypt cells in a more functional way.

5.4.2 Evidence for ectopic crypts as progenitor cells

5.4.2.1 Lineage tracing in the *Vil1-Grem1; Sox9CreERT2; Rosa26YFP* model

I wished to determine whether ectopic crypt cells were capable of cellular renewal and multilineage differentiation. Lineage tracing is the gold standard technique to define stem cell function thus my strategy was to induce permanent fluorescent marker tracing within Sox9 cells in the ECF and find out whether these cells are capable of generating lineage tracing ribbons.

Sox9 CreERT2 mice were purchased from Riken BRC Japan [141] and I crossed these with reporter YFP mice. YFP heterozygosity was sufficient for positivity on immunohistochemistry for YFP. I crossed these with *Vil1-Grem1* mice to allow tracing of Sox9 positive cells in ectopic crypts. I injected mice with one dose of 1mg of tamoxifen intraperitoneally, after optimisation showed that one dose was sufficient to cause Cre recombination. 8-week old mice were collected at 7 days and 32 days to compare the effect of lineage tracing at different timepoints. Those collected at 32 days displayed more lineage tracing ribbons apparently arising from ectopic crypts. Immunohistochemistry for YFP was carried out on serial slides to confirm no connection of the tracing ribbon to the crypt base (figure 5.8).

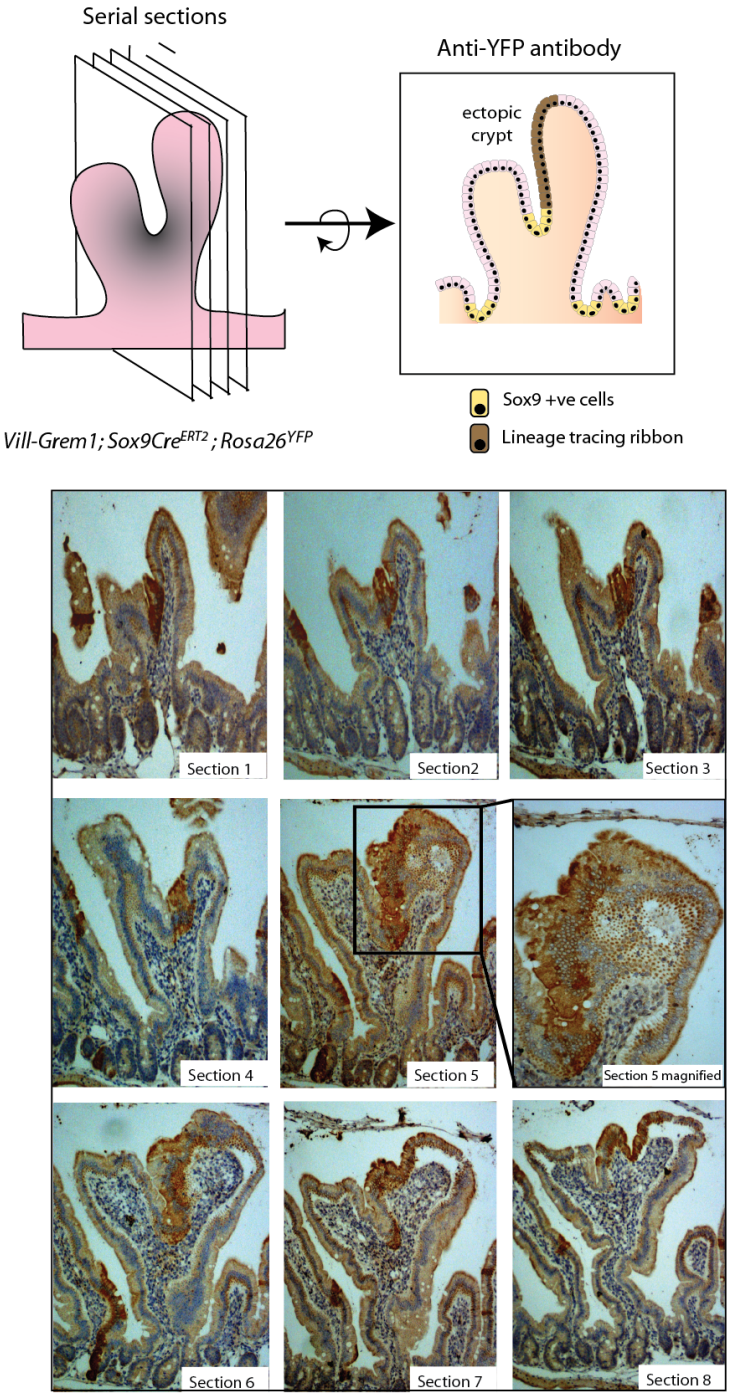

Figure 5.8: Serial sections from 8-week old *Vil1-Grem; Sox9CreERT2 ; Rosa26YFP* mouse intestinal polyp 32 days after tamoxifen induction, with immunohistochemical staining for YFP.

Although this method showed that tracing ribbons were likely to be arising from ectopic crypts, single sections are insufficient to exclude tracing ribbon origin from crypt base cells due to the complex 3D structure of polyps. Therefore a 3-dimensional IHC technique was developed. 3D imaging has advanced with the use of slide scanning and fluorescent quenching techniques to allow spatial and temporal imaging [162]. In collaboration with Barts Cancer Institute and the University of Leeds, 150 serial 4 μm sections were cut and stained for YFP from each mouse block. Slides were then digitally scanned to allow visualisation of tracing ribbons through entire polyps. The slides needed to be meticulously cut so that tissue segments were in the same position and serial scanning showed a smooth transition. Using 3D imaging software, serial images were combined to make videos of ribbons progressing through a block. Collaborators George Elia, Marnix Jansen and Darren Treanor helped with this work. To allow more polyps to form and for greater complexity of polyps, older mice aged 6 months were used with tamoxifen injection at 5 months of age.

Most tracing ribbons arose from Sox9 positive progenitors in the crypt base. After thorough examination of the whole set of sections, ribbons were found to be arising from ectopic crypts also. In the videos are two examples of ribbons arising from ectopic crypts without connection to the base. The entire ribbon can be seen using the 3D technology and it can be confirmed that there is no connection to the crypt base. Please see videos 1 and 2 on attached CD (or on RTDS online thesis submission website).

Next 3D reconstruction and modelling software (Free-D) was used to draw models around positive ribbons, as shown in figure 5.9. Then a mesh outline was drawn

around the surface of the polyp 5.9 and a video was created in which the polyp could be rotated (see videos 3 and 4). We developed the 3D model to carefully map tracing ribbons and ensure that ribbons apparently emerging from ectopic crypt cells that had no discrete connection to crypt basal cells. This schematic view allowed clearer visualisation of ribbons compared to histological images.

The schematics also highlighted the sheer complexity of polyp shape and tracing ribbons. Within each polyp there were several intertwining clones which traversed the polyp. While in normal colonic mucosa, clonal repopulation occurs along differentiation gradients from the crypt base towards the apex, the clonal architecture in polyps is less organised. Intestinal polyps are epigenetically diverse and the patchwork of competing clones makes the whole polyp even more intricate [163].

5.4.2.2 Multipotentiality of ectopic lineage tracing ribbons

In order to prove the existence of a stem/progenitor clone in the ectopic crypt compartment it was necessary to demonstrate evidence of cellular self renewal and multilineage potential. A double stain was done using Vector Red stain (Vector Labs) for YFP ribbons and DAB for individual cell types: Lysozyme (Paneth cells), Alkaline Phosphatase (enterocytes), Chromogranin A (enteroendocrine cells). For Alcian Blue stain (Goblet cells) DAB for YFP was done first, then the routine Alcian Blue protocol used. Figure 5.10 shows that within an ectopic crypt tracing ribbon there were Goblet cells and Paneth cells arising. This was proved to be an ectopic crypt ribbon by serial sectioning and YFP staining around the section. Enteroendocrine cells are rarer and do not appear in every villus, and within this trace none were seen. Alkaline phosphatase did not show

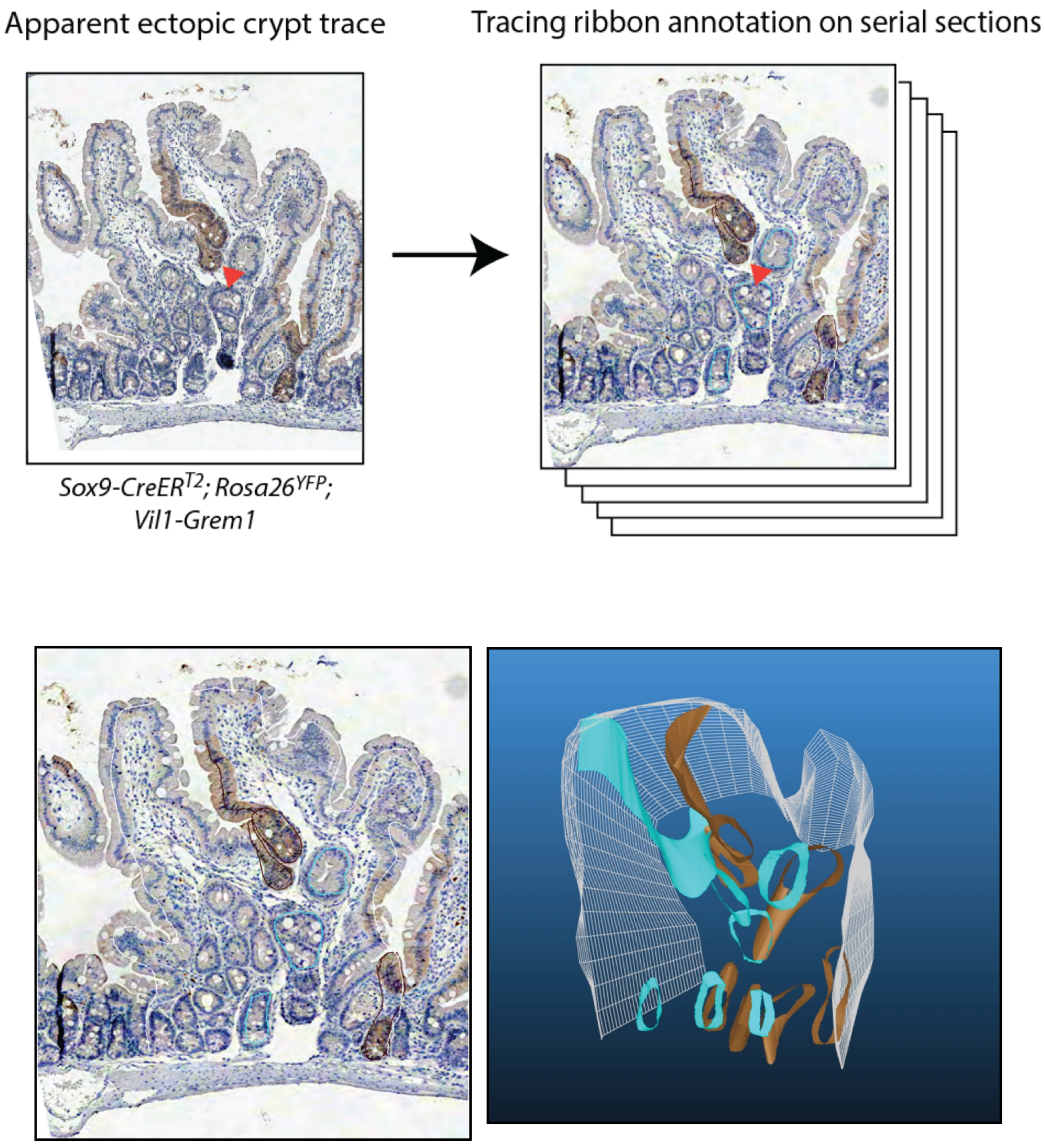

Figure 5.9: Schematic of tracing ribbon annotation for 3D software. Computerised image of polyp outline with tracing ribbons. The brown ribbons indicate cells originating from a Sox9 positive cell.

up on the co-stain as the primary antibodies for YFP and ALP were raised in the same animal, so the first stain washed out as the second primary antibody was applied.

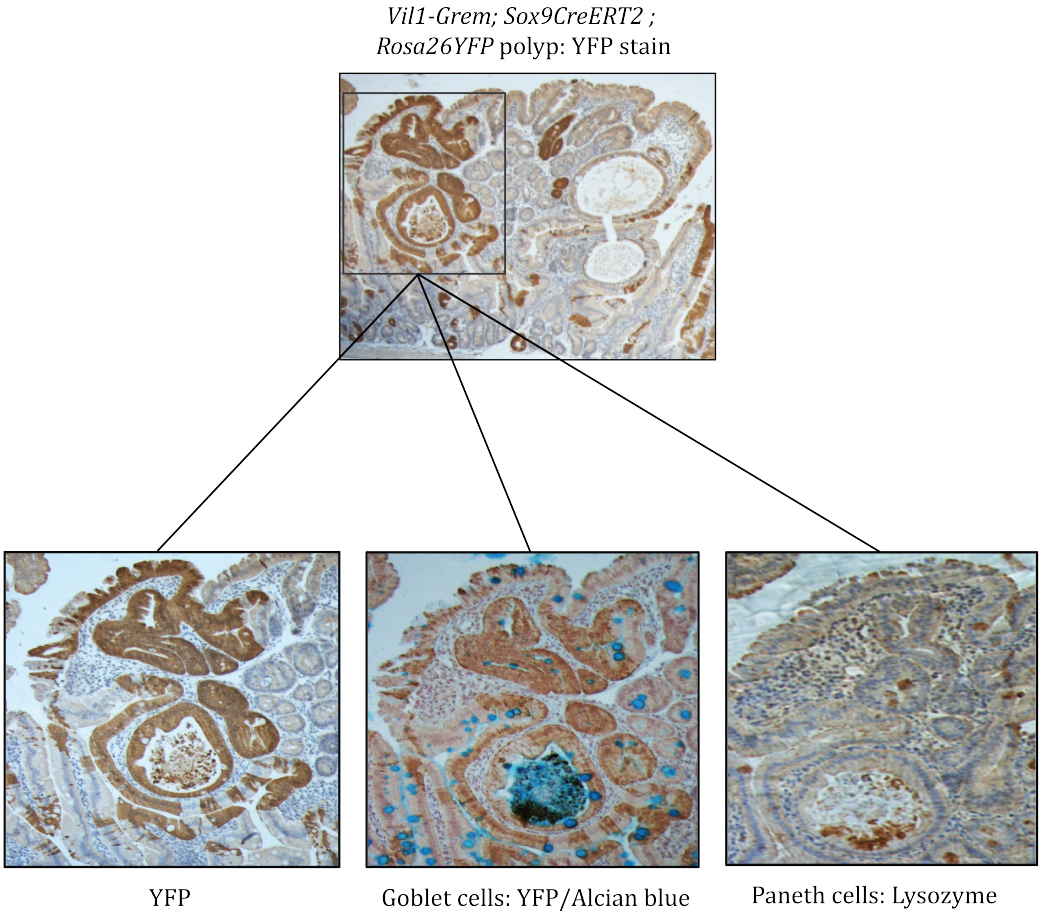

Figure 5.10: Co-staining for YFP and enteric cell types.

5.4.3 Proliferative capacity within ectopic crypts

It seems that ECF are highly proliferative compartments. I wanted to test this. Ki67 is a marker of proliferation so staining was used to reflect which cells are

actively cycling. A co-stain was done for YFP and Ki67. The aim was to find whether, within in a YFP positive tracing ribbon arising from the crypt base, cells stopped actively cycling on leaving the crypt base and then changed on entering the ectopic crypt to enter the cell cycle again. Figure 5.11 shows that this was the case. In a YFP positive tracing ribbon arising from the base, there were cells which co-stained for Ki67 both in the crypt base and in ectopic crypts.

Cells streaming in a ribbon from the crypt base retain their stem/progenitor potential and aberrantly re-enter the cell cycle only when in the ectopic crypt niche microenvironment.

5.4.4 Contrasting the microenvironment of the crypt base and ectopic crypts

Next the Wnt, BMP and Hh pathways were analysed in the stroma. It would have been difficult to extract sections of mesenchyme surrounding ectopic crypts by laser capture because they were so small, so ectopic crypt and basal crypt microenvironment could not be directly compared. Instead whole mesenchyme from wild-type mouse small intestine was compared with mesenchyme from *Vil1-Grem1* mouse small intestine. Mesenchyme was dissected using EDTA as in 2.1.2 then RNA was extracted and qPCR testing done.

qPCR for Hh markers in mesenchyme showed there was no significant difference between Gli1 and Ptch1 between wild-type and *Vil1-Grem1* mice, but there was a significant decrease in Hhip and Smo in *Vil1-Grem1* (figure 5.12). There was a reduction in Foxf1, which is a mediator of HH signalling. Sfrp1, a HH target, also

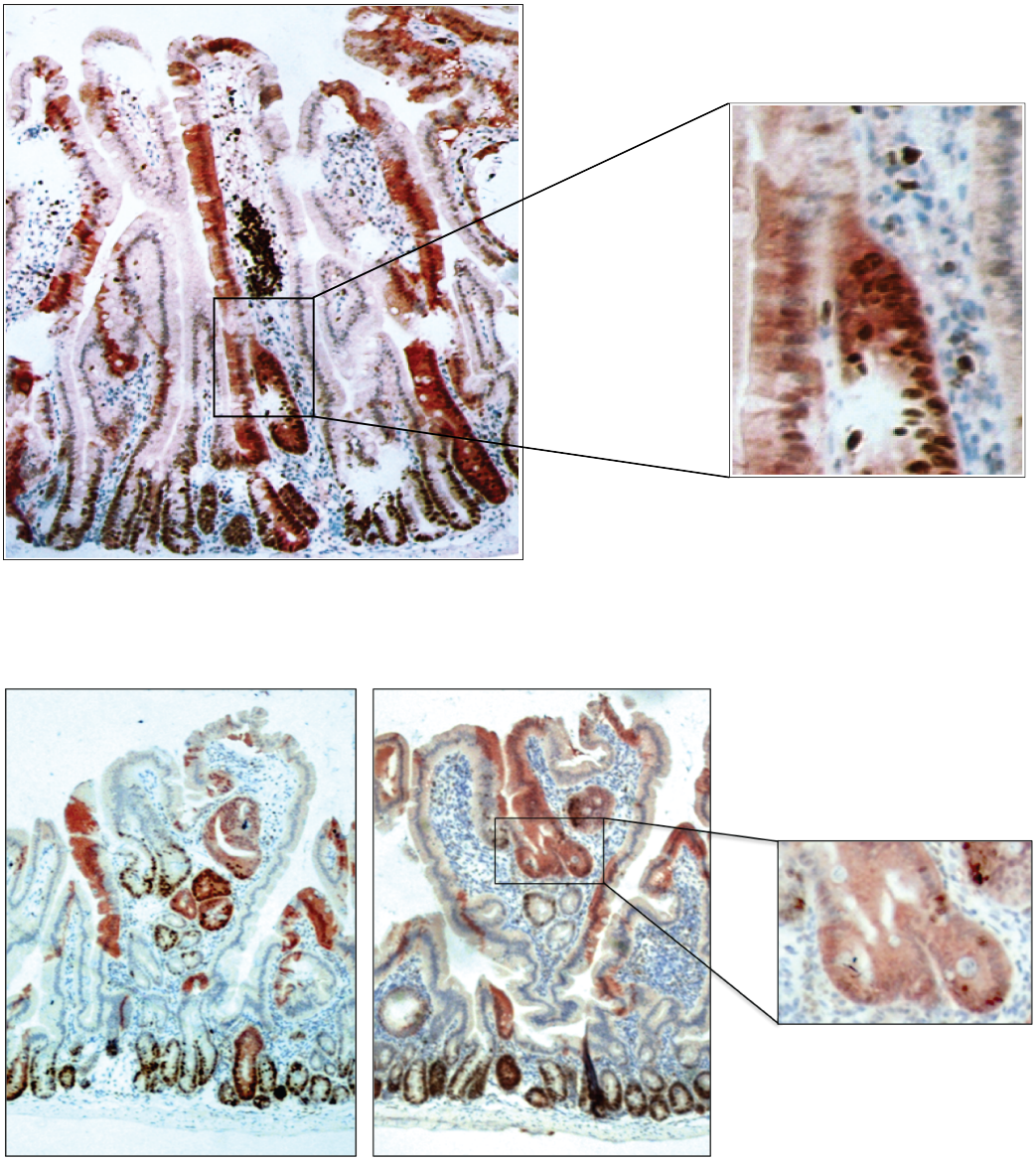

Figure 5.11: Two examples of co-stain for YFP and Ki67 in *Vil1-Grem; Sox9CreERT2 ; Rosa26YFP* mouse. YFP is stained with red and Ki67 with brown. In a YFP positive tracing ribbon arising from the crypt base, there were cells which co-stained for proliferation marker Ki67 both in the crypt base and in ectopic crypts. Cells therefore exit and re-enter the cell cycle as they move from crypt base to ectopic crypt.

went down. This is in parallel with a reduction in BMP in this model.

RNA sequencing data above showed that canonical Wnt ligands and receptors are higher in ectopic crypts, but that Rspondin target gene Lgr5 is only present at the base. It was postulated that the main difference between the two stem cells compartments is in non-canonical Rspondin-driven Wnt signalling. qPCR was done for Wnt pathway components. Canonical Wnt ligands Wnt3 and Wnt9b were higher in *Vil1-Grem1* mesenchyme compared to wild-type. Canonical Wnt receptors Fzd2,5,7 are also all higher in *Vil1-Grem1* mesenchyme. Rspondin1,2,3 are all lower as is Lgr5 (figure 5.12). Lrp5 and Lrp6 (co-receptors of Rspondin) do not significantly change.

5.4.4.1 Fibroblast markers

Fibroblasts surrounding villi are usually not activated and do not express Grem1. To find the types of fibroblasts present in *Vil1-Grem1* polyps, stains for mesenchymal markers SMA, desmin and vimentin were done (figure 5.13). Within polyps there was an increase in these markers surrounding ectopic crypts, in addition to expression in the subcrypt mesenchyme. These are all markers of activated myofibroblasts and suggest an activated stroma in the mesenchyme of *Vil1-Grem1* polyps. Desmin expression in CRC stroma has also been reported to be a marker of CRC invasiveness [164]. Therefore these markers may be linked to carcinogenesis and be a sign that the stroma in *Vil1-Grem1* is a cause of development of ECF and progenitor properties.

Therefore in *Vil1-Grem1* mesenchyme there is reduced BMP and HH, and an in-

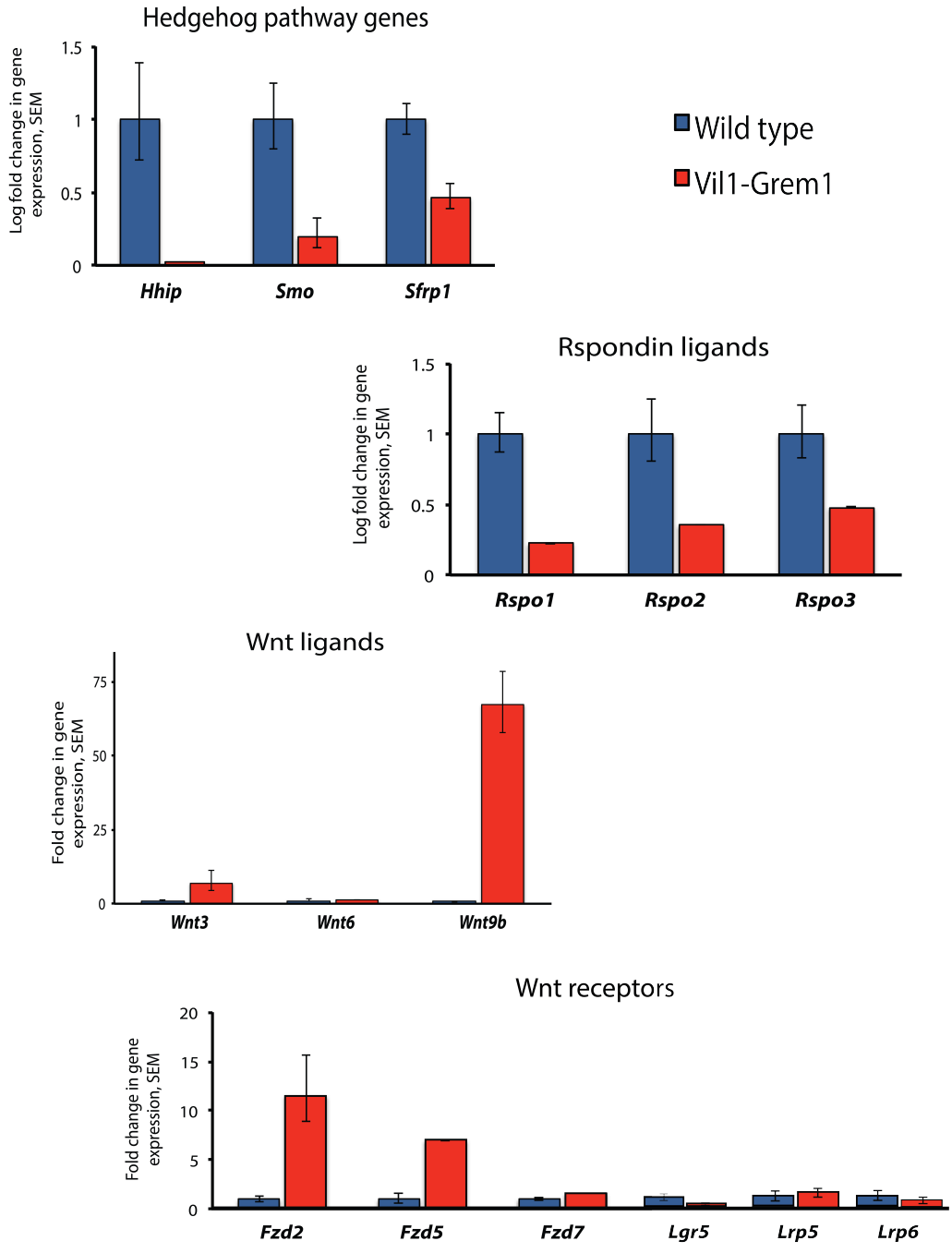

Figure 5.12: qPCR for Hedgehog and Wnt pathway genes in wild-type and *Vil1-Grem1* intestinal mesenchyme. There is an increase in canonical Wnt ligands and Frizzled receptors in *Vil1-Grem1*. There is a decrease in Hedgehog, non-canonical Wnt pathway Rspondin ligands and Lgr5 receptor in *Vil1-Grem1*.

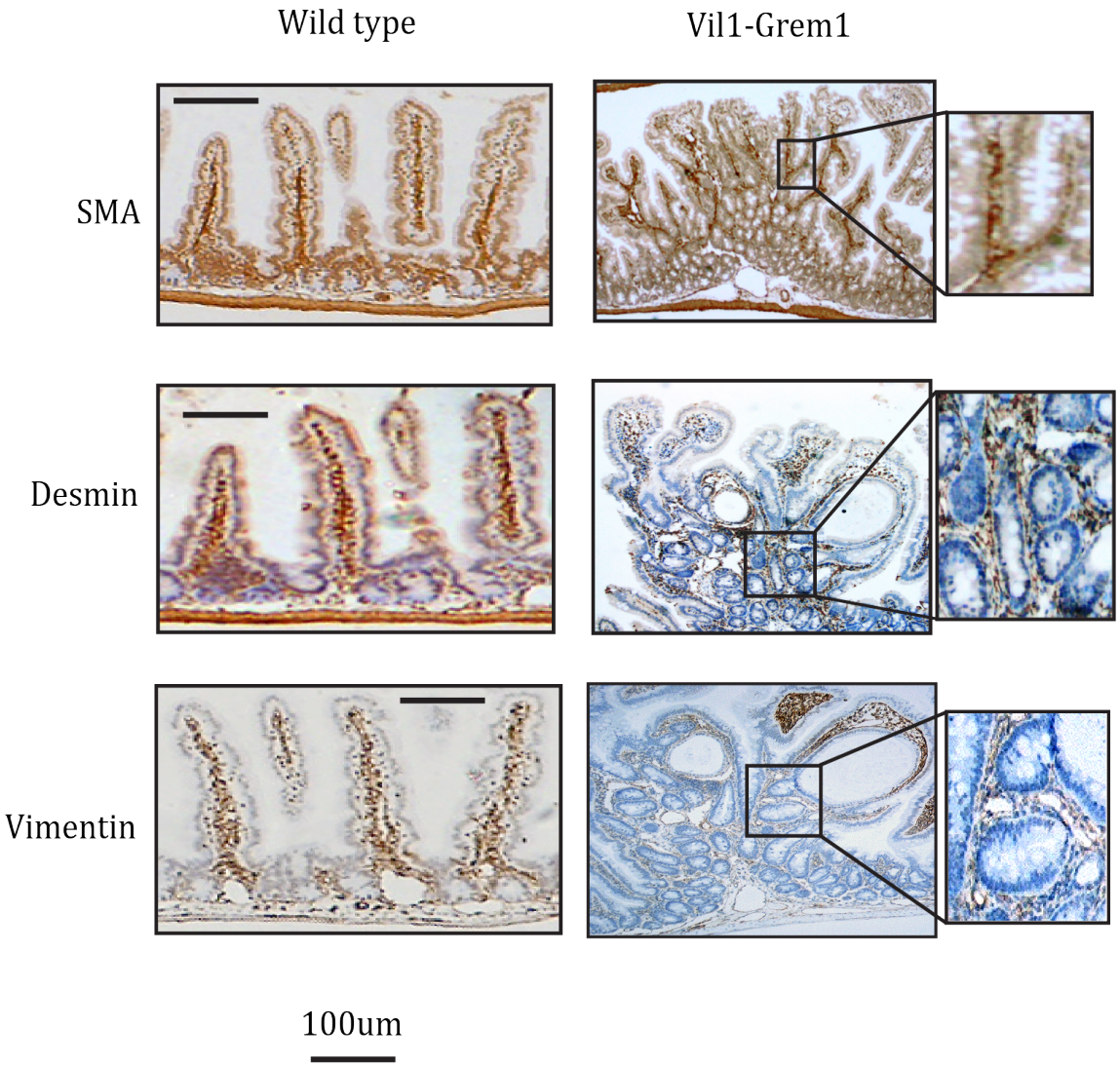

Figure 5.13: SMA, desmin and vimentin IHC in wild-type and *Vil1-Grem1* mouse small intestine. Within *Vil1-Grem1* polyps there was an increase in these markers of activated fibroblasts, both in the subcrypt mesenchyme and surrounding ectopic crypts.

crease in canonical Wnt pathway genes. There is a reduction in the Rspondin-driven Wnt axis. The canonical Wnt amplification may contribute to the proliferative activity within ECF. There is activation of fibroblasts as evidenced by increased SMA, desmin and vimentin in polyps.

5.5 Discussion

With reference to the key objectives, the findings in this chapter are:

1. Cells within ectopic cryts have a different transcriptional profile to cells within basal crypts.
2. Ectopic crypts have clonogenic potential, proved by their ability to lineage trace.
3. There is a difference between the stroma surrounding ectopic crypts and the stroma adjacent to basal crypts.

5.5.1 Ectopic crypts differ from crypt bases

Not all progenitor cells are equal and it seems that ectopic progenitor cells are more prone to carcinogenic change. This could be due to impaired DNA damage response, exposure to toxic luminal contents or lack of stem cell niche regulation due to altered microenvironment. It was shown by RNA sequencing that although there were transcriptional differences between the two compartments, the genes related to DNA damage response and apoptosis were similar. There was a difference in the mesenchyme surrounding crypts.

5.5.2 Stem cell potential in ectopic crypts

Overexpression of Gremlin1 throughout the epithelium instead of a restricted mesenchymal gradient causes cell fate disruption and ectopic crypts. Ectopic crypt progenitor cells on the villus are capable of self-renewal and tissue-specific differentiation. This chapter has given evidence for stem cell activity away from the crypt base in highly proliferative pockets. It is clear that the two stem cell compartments are different in terms of transcriptional signatures and may potentially respond differently to cellular stress. This may be a reason for increased somatic mutation events in ectopic crypts. It contributes to the theory of "top-down" carcinogenesis where some early adenomatous lesions develop on the luminal surface without any obvious contact to the crypt base.

Spheroids can be derived from *Vil1-Grem1* villi. When villus organoids are grown, Wnt3a needs to be added to the media. This is despite Wnt3 being upregulated in the mesenchyme of *Vil1-Grem1* mice. It could be that removing the epithelium without attached mesenchyme means that there is not enough exogenous Wnt as all the Wnt3 is provided from mesenchyme. Alternatively it could mean that although Wnt3 is higher, it is still not as high as the crypt base in supporting organoid growth. There is clearly a difference between the clonal capacity of ectopic crypts and basal crypts.

5.5.3 The microenvironmental difference between ECF and crypt base stem cells

The mesenchymal microenvironment was explored here. There was a reduction in mesenchymal BMP and Hedgehog, allowing proliferation within ECF. The canonical Wnt ligands and receptors were increased in the mesenchyme but not the non-canonical Wnt signals (Rspondins, Lrp5/6 and Lgr5). At the crypt base there was both Rspondin-driven Wnt setting stem cell tone, and canonical Wnt driving proliferation within the transit amplifying compartment [37]. It has been shown that these two pathways are not functionally equivalent but co-operate. Perhaps in the ectopic crypts the Rspondin axis is less active hence the lack of Lgr5-positive cells, but here canonical Wnt takes over and drives proliferation.

5.5.4 The development of ectopic crypts

The compartmental switch in gene expression in HMPS is a very unusual physiological phenomenon. There are no other disease models with a switch in gene expression like this to compare. The results are unexpected and as yet understood. Similar ectopic crypts form when Noggin is transgenically expressed in epithelium, so it is in keeping with this that the aberrant expression of BMP antagonists leads to ectopic crypts. The reason for ectopic crypts forming in this aberrant environment is unclear but theories are given below.

5.5.4.1 Theory 1: The crypt shape

The crypt gland shape is common in cancer, especially in well differentiated cancers. This could be because it is a remnant of the tissue architecture of origin, or the flask-like shape could somehow favour epithelial cell proliferation. The crypt shape may help the progression to cancer. Dysplasia is seen arising from ectopic crypts and not other cells because the shape may allow aberrant proliferation and mutagenesis. Perhaps only in the concave architecture of the ECF, within complex polyp shapes, is aberrant re-entry into the cell cycle permitted and is Wnt reactivated. The crypt-like shape may also favour the existence of stem/progenitor cells and not differentiating cells because of closer proximity to the mesenchyme which provides proliferative signals.

5.5.4.2 Theory 2: In-folding due to stoichiometric pressure

The increased proliferation of epithelial cells expressing Grem1 could mean that they are dividing so much that they buckle under the physical pressure within the villus. This could lead to in-folding to form pockets within villi. As pockets form, they could focus Wnt signalling within themselves, leading to an exponential rise in proliferation and a breakaway from the surrounding epithelium. This means that the pockets each contain their own microcosm of high Wnt, low BMP and HH with a high rate of proliferation and therefore risk of mutation.

In development it has been shown that this process occurs when villi form. Mouse epithelium buckles into small alcoves that could lead to local elevated concentrations of Shh protein prior to the onset of villus cluster gene expression. Stem cell

markers and Wnt-responsive genes are expressed uniformly throughout the gut epithelium prior to this point and are downregulated at the tips of the forming villi as the villus cluster genes are expressed [165]. Whereas there the net result of the Shh-Bmp signalling cascade is a restriction of proliferation and a decrease in expression of Wnt-dependent stem cell markers at the tips, the opposite occurs in the *Vil1-Grem1* model. In addition to this mechanism, forces could impact gene expression through mechanosensory signal transduction.

5.5.4.3 Theory 3: Control by aberrant mesenchyme

It has been shown that the mesenchyme of *Vil1-Grem1* animals has an increase in canonical Wnt ligands and receptors and a decrease in Hh. The Grem1 expressing epithelium could have this effect on surrounding mesenchyme. Grem1 acts with paracrine effect and in the same way that ISEMFs secrete Grem1 and keep BMP low in adjacent crypts, Grem1 in epithelium could be keeping BMP and HH low in adjacent fibroblasts. This in turn could enhance Wnt in mesenchyme and promote proliferation within ECF. As a consequence fibroblasts surrounding villi may become activated, as shown by increased SMA, desmin and vimentin expression. Interestingly although this is the case, Grem1 expression in mesenchyme of *Vil1-Grem1* animals has not been shown to move away from the crypt base, even in older animals. The mesenchymal axis pattern of Grem1 expression does not change in the presence of aberrant levels of epithelial Grem1.

5.5.4.4 Theory 4: Ectopic Paneth cells

Paneth cells in the crypt base secrete Wnt3a to promote stem cell growth and provide essential factors for maintenance of the stem cell niche. The presence of Paneth cells in ectopic crypts, using Lysozyme staining, suggests that these may contribute to ectopic progenitor maintenance. This occurs out of context without other elements of the niche such as ISEMFs, and may be the source of canonical Wnt signalling seen around ECF. Paneth cells also secrete antimicrobial peptides and may contrastingly have a protective effect on ectopic progenitors, particularly given proximity to the luminal surface and exposure to toxins.

Figure 5.14 shows a simplistic illustration of signalling within ECF.

5.5.5 Clinical implications

Cancer co-opts and corrupts physiologically relevant sigalling patwhays. It was shown in TCGA data that GREM1 is increased in CCS3-subtype colorectal cancers. Traditional serrated adenomas, a precursor to this cancer type, show an increase in GREM1 expression also as shown in figure 5.15.

Desmoplasia is the process of fibrosis and scarring in chronic inflammation. A desmoplastic tissue response has been thought to represent an important biological factor in cancer. A pronounced desmoplastic reaction is associated with a reduced immune response and has been shown to be an independent poor prognostic indicator in CRC and cancer recurrence [166]. A myofibroblast-driven desmoplastic stromal reaction rich in fibrillar collagens is reported to be a poor prognostic indicator in primary CRC. Understanding the role of the stromal cells

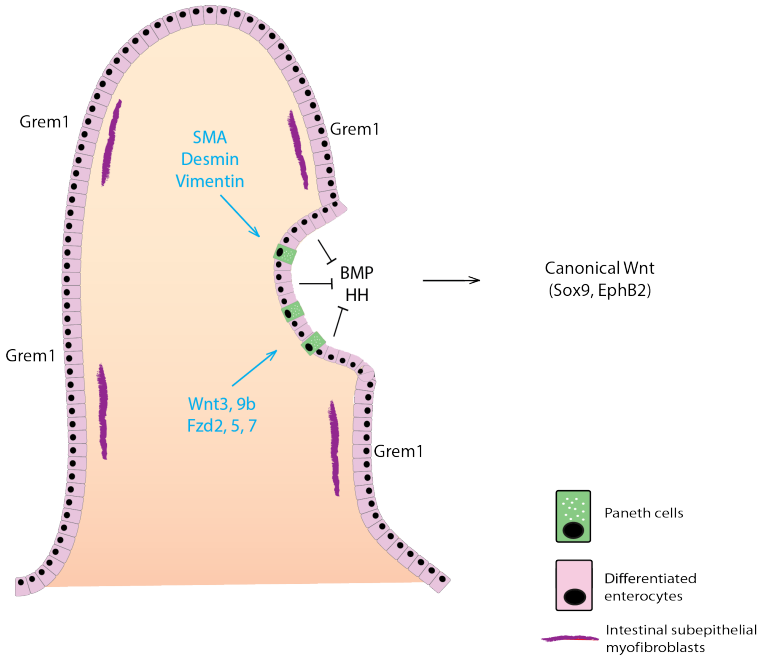

Figure 5.14: Schematic of signalling within an ectopic crypt. High epithelial Grem1 levels in a confined space lead to low BMP and HH. This may allow more canonical Wnt signalling. The mesenchyme plays a part and provides Wnt signals from activated fibroblasts.

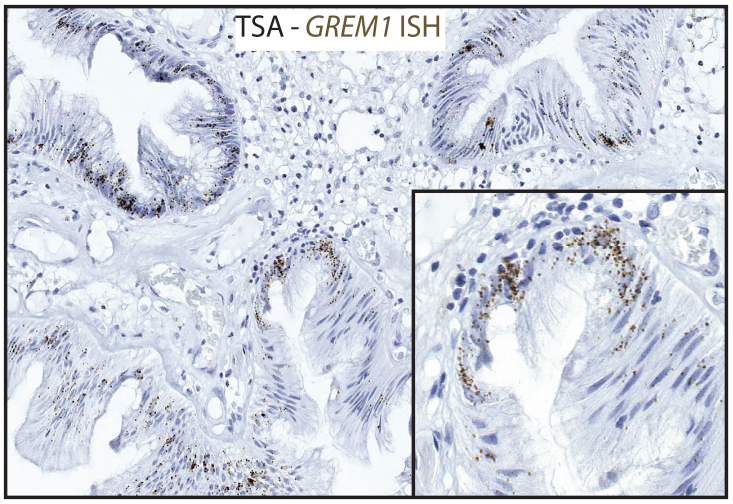

Figure 5.15: In situ hybridization for GREM1 in human TSA samples showing aberrant epithelial GREM1 mRNA expression in TSA epithelium. Taken from [85].

and extracellular matrix will allow us to identify more precise prognostic markers and potentially devise new therapeutic options.

A new prong in therapy could be to correct the imbalance in colitis and avoid colitis-associated cancer. Hedgehog pathway manipulation with small molecule agonists could in theory work but have not been tested. Basal cell carcinomas (BCC) and medulloblastomas are the two most common cancers identified with mutations in components of the Hedgehog pathway. The discovery of targeted Hedgehog pathway inhibitors has shown promising results in clinical trials, several of which are still undergoing clinical evaluation. Vismodegib (GDC-0449), an oral hedgehog signalling pathway inhibitor has reached the farthest in clinical development. Similarly BMP small molecule activators could target the HH pathway, and several have been identified [167].

This chapter has explored the form and function of ectopic crypts. It has been

noted that these ectopic progenitor cells are Sox9-positive. The next chapter will explore the functional significance of Sox9 in the crypts.

5.5.6 Limitations

- When laser capture dissection was done of crypt base and ectopic progenitors, if ectopic crypts appeared dysplastic, they were not collected as they were presumed to have undergone mutation. Therefore the population collected may be less proliferative and stem-like, i.e. a young population of progenitors. Differentiated cells surrounding ectopic crypts were also captured, as Alkaline Phosphatase, Villin1 and Krt20 was much higher here than in the crypt base.
- *Vil1* is used here as the promoter to target gene expression to the intestinal epithelium, but *Vil1* expression is in fact unevenly balanced towards villus expression. Microarrays from chapter 3 showed that *Vil1* is expressed 2-fold higher in villi than crypts. This means that models are skewed towards villus transgenic expression of genes and may not be an accurate reflection of downstream signalling.
- A frequent criticism of mouse models of polyposis is that mice develop small bowel polyps but not colonic polyps. This limits their ability to faithfully mimic colon-specific tumourigenesis.

Chapter 6

The functional effect of *Sox9* in inflammation and carcinogenesis

6.1 Aims

The key objectives in this chapter were:

1. To analyse whether *Sox9* mediates and is critical for the adaptive cell reprogramming response in WAE.

2. To assess the difference in reponse to tissue injury in a model of *Sox9* knockdown *in vivo*.

3. To characterise a mouse model with epithelial knockout of *Sox9* and look at functionality in terms of tissue restitution.

4. To find whether organoids could be derived from intestinal crypts from *Sox9*

knockout mice as an indication of stem/progenitor potential.

5. To assess any difference in phenotype when *Sox9* was knocked out in the *Vil1-Grem1* model.

6.2 Introduction

In this chapter *Sox9* is explored as a regulator in tissue restitution and in colorectal cancer. *Sox9* was chosen as it was one of the few stem cell markers which marked ectopic crypts when Grem1 is epithelially expressed in the *Vil1-Grem1* model. *Sox9* is a potential master transcription factor in Wnt and cell fate pathways (see 1.4.9). It is not clear whether it is a critical component of the ectopic crypt and gives progenitor properties to these cells, or is a bystander. I wanted to ascertain whether Sox9 expression is a cause or effect of the altered cell fate in ectopic crypt cells. In addition to its role in carcinogenesis, the role of Sox9 in inflammation was explored.

6.2.1 *Sox9* in inflammation

Sox9 is a Wnt target gene and is mutated more frequently in IBD-associated tumours than in sporadic tumours [168]. It has been shown to be strongly upregulated in recovering crypts, and is related to the regeneration of damaged tissue and the re-establishment of Lgr5+ stem cells after injury [169]. It was postulated that Sox9 would be a marker of wound associated epithelium (WAE). WAE was described by Miyoshi et al, where Cre recombinase was activated in the intesti-

nal epithelium to mark a subset of crypts prior to epithelial wounding injury [53]. Four days after injury, columns of LacZ-positive cells emanated from adjacent crypts from wound edges towards the wound centre (figure 6.1). This was postulated to be wound associated epithelium (WAE). Non-canonical Wnt signalling re-established the proximal-distal axis in the damaged tissue. Wnt5a-expressing cells attached to the bottom of the wound channels and Wnt5a was required for healing.

Sox9 is a canonical Wnt target gene and the increased canonical Wnt required in wound healing suggests that it would be upregulated in repair. Its role was considered in tissue injury by chemical colitis and biopsy wounding in mice. Staining for Sox9 was done in DSS colitis. To track the time course of injury, a model of endoscopic wounding was established and Sox9 staining was done at various timepoints.

To find whether *Sox9* knockout had an effect on wound healing, *Vill-Cre; Sox9fl/fl* mice [142] were compared with wild-type mice in terms of healing after colonic biopsy.

6.2.2 *Sox9* in carcinogenesis

There is evidence for *Sox9* as both an oncogene and a tumour suppressor gene and to investigate this, models of *Sox9* knockdown *in vivo* and *in vitro* were designed to look at effects on proliferation and carcinogenesis. This was discussed in 1.4.9, in which the conflicting roles as well as splicing variants of Sox9 where discussed.

There may be a critical dose of *SOX9* required in CRC. In the healthy intestinal

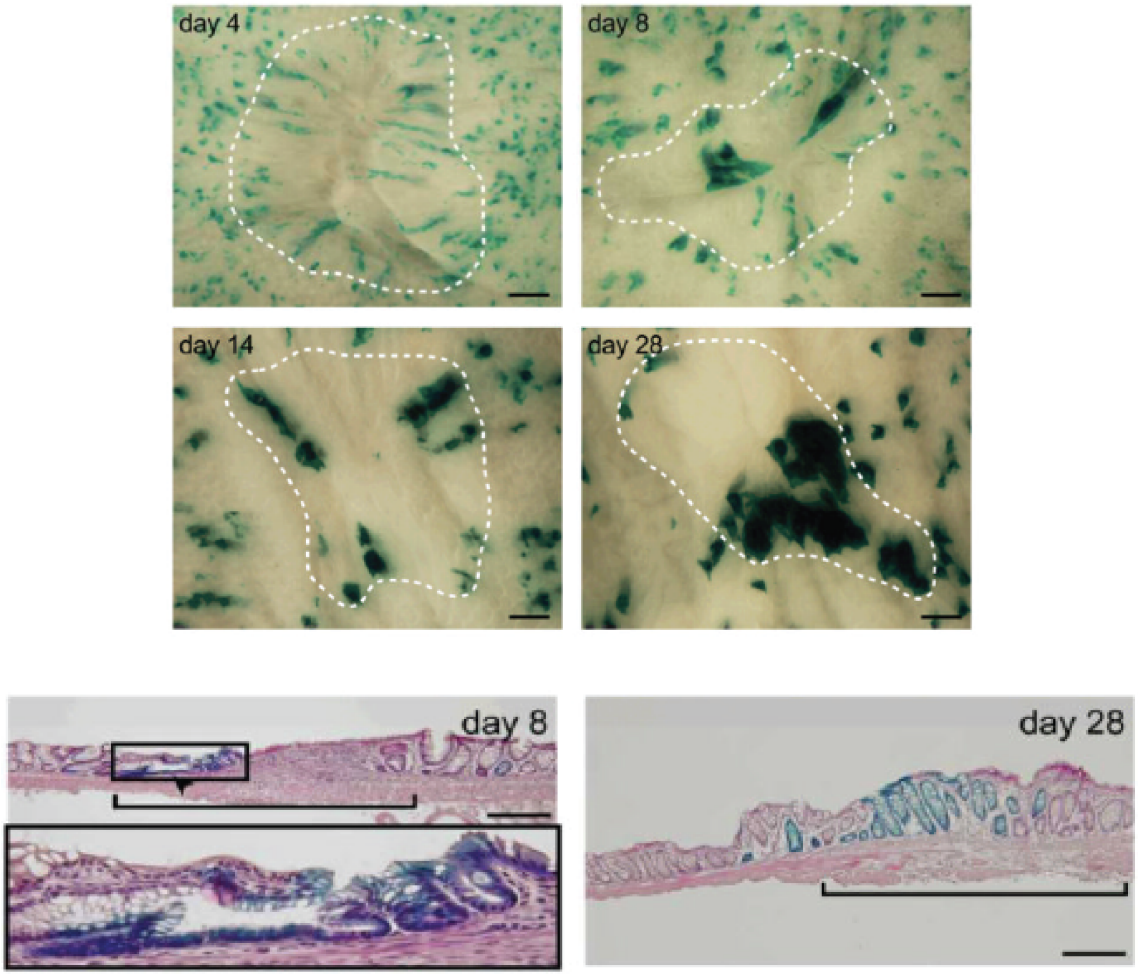

Figure 6.1: Migration of clonal cell populations from labelled crypts after wounding in *Vil-CreERT: Rosa26R* mice. Cells expressing LacZ were visualized by the staining with X-gal. Dotted lines outline original wound area. An HE section of a wound at day 8 post-injury in a *Vil-CreERT: Rosa26R* mouse. LacZpositive cells (blue) were present in the wound channel (arrowhead; see inset). An HEstained section of a wound at day 28 post-injury in a *Vil-CreERT: Rosa26R* mouse shows clusters of LacZ-positive crypts in the wound bed. Adapted from [169].

epithelium, Roche et al [124] postulated that *SOX9* dose modulates the balance between actively proliferating and reserve ISCs: an increase in *SOX9* causes actively proliferating ISCs (aISCs) to convert to reserve ISCs (rISCs). High doses of *SOX9* preserve the quiescence of rISCs that might differentiate into Paneth cells with time. In CRC cells, Prevostel et al [136] postulate that a critical dose of active *SOX9* is required for a maximum rate of proliferation and that increasing or decreasing this dose both result in a decrease in proliferative capacity (figure 6.2). This theory was considered in this chapter.

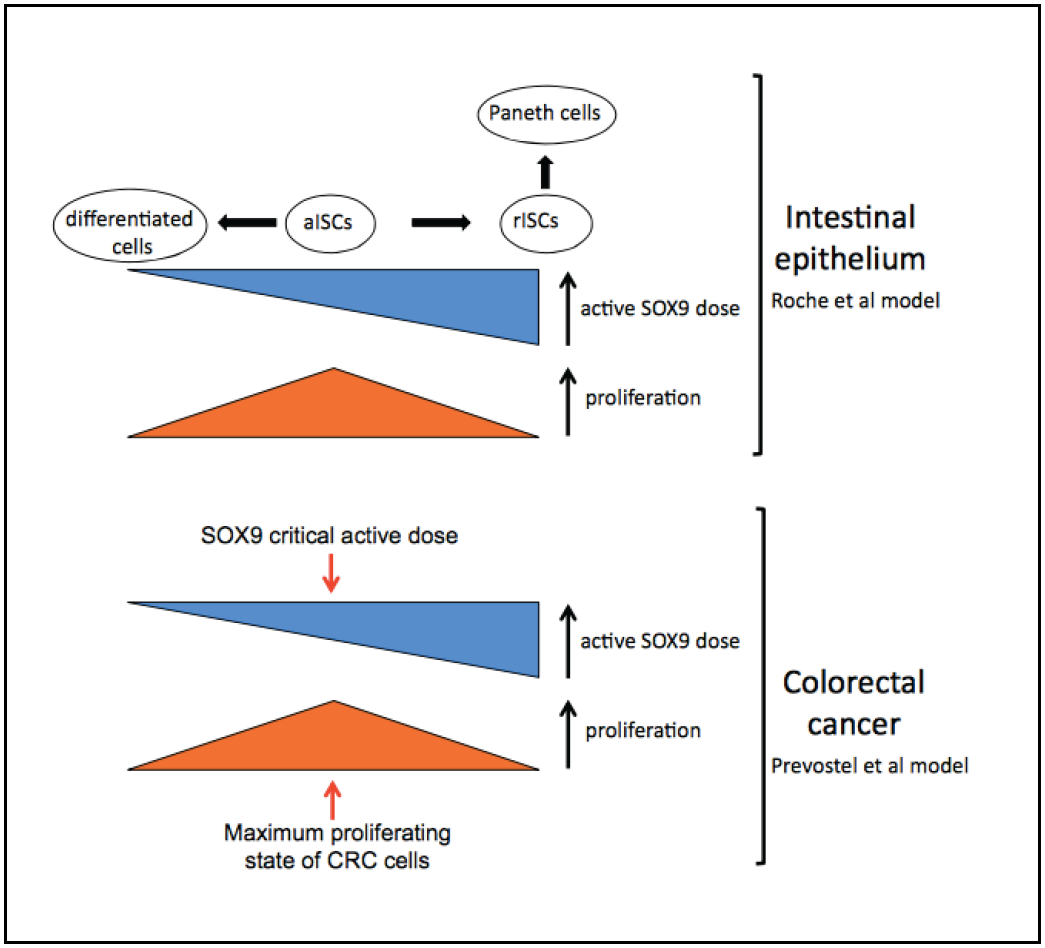

Figure 6.2: The dose-dependent effect of *SOX9* on cell proliferation in healthy intestine and in colorectal cancer. Taken from [170].

The phenotype of the *Vill-Cre; Sox9fl/fl* mice was studied. Data from this mouse has been published and showed enlarged crypts with an increase in Ki67 proliferating cells (figure 6.3). This apparent increase in proliferation could lead to mutation and initiation of carcinogenesis. Despite the increase in proliferation, cell fate was maintained with differentiated cells only present at the luminal surface. Interestingly Paneth cells were absent (figure 6.4), which could indicate lack of control over the stem cell niche.The functional characteristics were analysed in this chapter by culture of organoids from intestinal crypts from these mice compared to wild-type mice.

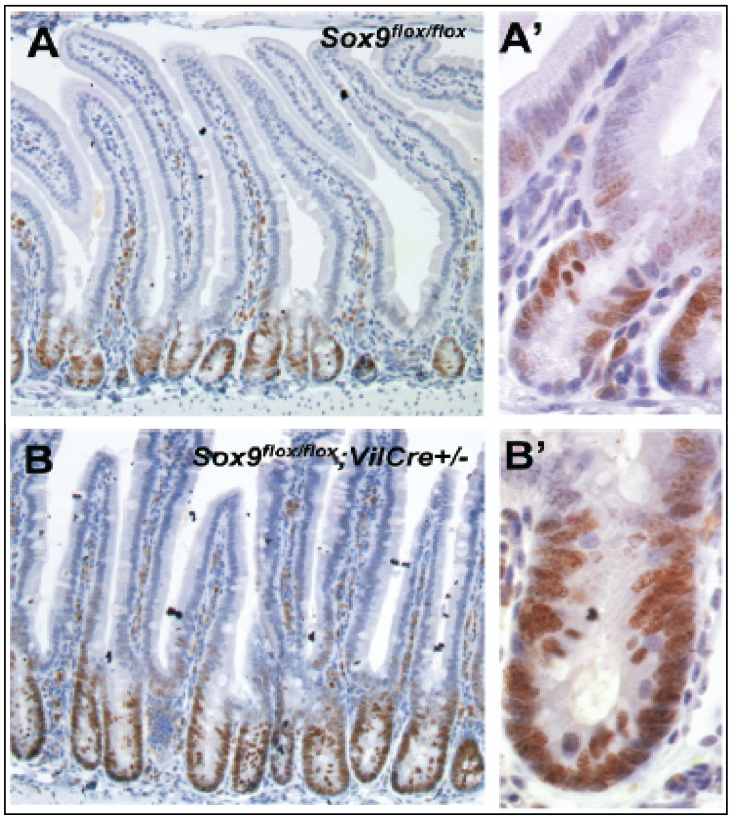

Figure 6.3: Ki67 IHC in wild-type and Sox9 floxed mice. Taken from [142].

It has been shown that in the *Vil1-Grem1* model, ectopic crypts are positive for

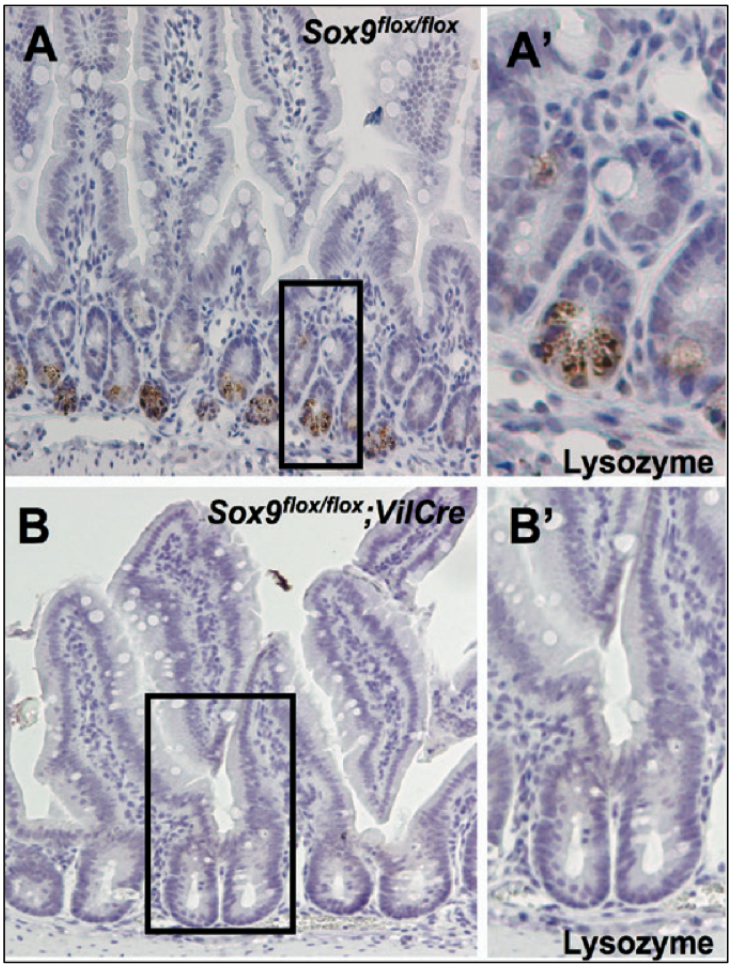

Figure 6.4: Lysozyme IHC for Paneth cells in wild-type and Sox9 floxed mice. Taken from [142].

Sox9. The functional effect of Sox9 in giving rise to ectopic crypts was tested by crossing the Sox9 floxed mouse with the Vil1-Grem1 model.

6.3 Methods

The methods used in this chapter are described in chapter 2 and were as follows:

- Mouse endoscopy and wounding 2.2.8
- DSS induction of colitis in mice 2.2.9
- Mouse gut preparation 2.2.6
- Histology preparation and staining 2.3
- Immunohistochemistry and co-staining 2.6.1
- Organoid culture 2.7.4

6.4 Results

6.4.1 Sox9 in tissue restitution

6.4.1.1 Presence of Sox9 expressing cells in wounds

Wild-type mice were given 2% DSS for 5 days to induce acute colitis. Mice were sacrificed immediately and staining for Sox9 done. Sox9 expression appeared over the surface of healing ulcers in an epithelial monolayer (figure 6.5). Sox9 was also seen at the base of de novo crypts forming adjacent to the wound bed in the so-called wound channel. There was an increase in Sox9 epithelial cells in crypts surrounding ulcers also. It was not clear at what stage in the ulcer healing process these Sox9-positive cells were recruited.

To study the timecourse of recruitment of Sox9-positive cells, biopsy wounding was carried out as described in 2.2.8. Sox9 expression over the wound was analysed at timepoints up to 10 days. Sox9 expression was highest over the surface of the injury on day 3 (see figure 6.6) and again seen in the wound channel. After this the monolayer expanded and crypts started to fill the wound bed, as seen at day 6.

Sox9 is actively expressed in wound associated epithelium. Sox9 may therefore be required for wound repair and clonal expansion of Sox9-positive cells adjacent to the wound may allow movement of these cells into the wound for healing. Next the requirement for Sox9 in wound healing from DSS colitis and biopsy was tested.

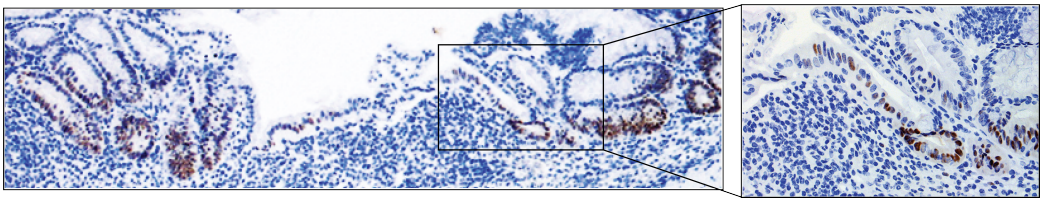

Figure 6.5: Sox9 IHC in DSS colitis.

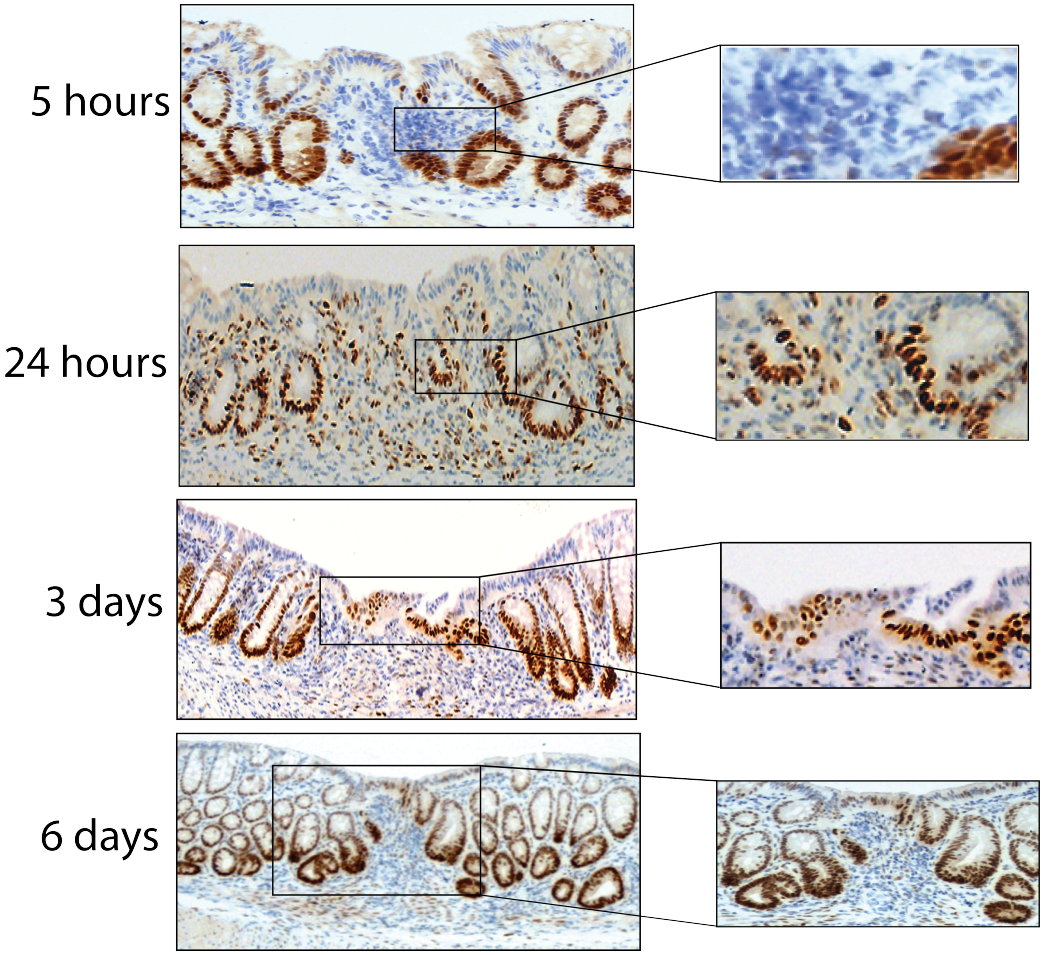

Figure 6.6: Mouse colonic biopsy after 5 hours, 24 hours, 3 days and 6 days: Sox9 IHC stain.

6.4.1.2 Functional requirement of Sox9 in healing: the Vill-Cre; Sox9fl/fl model

Phenotype of the *Vill-Cre; Sox9fl/fl* model

Sox9 floxed mice were purchased from Jax labs, stock no 013106 (B6.129S7-Sox9tm2Crm/J) [142]. They were bred with *Villin Cre ERT2* mice [140] for six generations and confirmed to be homozygous for Sox9 and positive for Villin Cre recombinase. Recombination was confirmed by PCR from mouse earsnips and gut DNA extraction, but *Sox9* was not significantly knocked down on qPCR. Immunohistochemistry did not show any reduction in Sox9 staining. The phenotype of mice was no different to wild-type.

Instead a non-inducible *Sox9* knockout model was used and *Sox9* floxed mice were bred with *Villin-Cre*. Again they were confirmed to be homozygous before testing. RNA extracted from small intestine and colon showed that *Sox9* was significantly reduced by qPCR (figure 6.7).

Mice showed no symptoms and the oldest mouse bred survived to 16 months of age. Histology showed enlarged crypts with an increase in Ki67 proliferating cells (figure 6.8). Cell fate was maintained with differentiated cells only present at the luminal surface. There were still some Paneth cells present, which is different to that reported in the paper in which there were none. Enteroendocrine cells were still present. Although the crypt base was larger with more proliferating cells, there was no change in Grem1 expression which was limited to the subcrypt mesenchyme (figure 6.8).

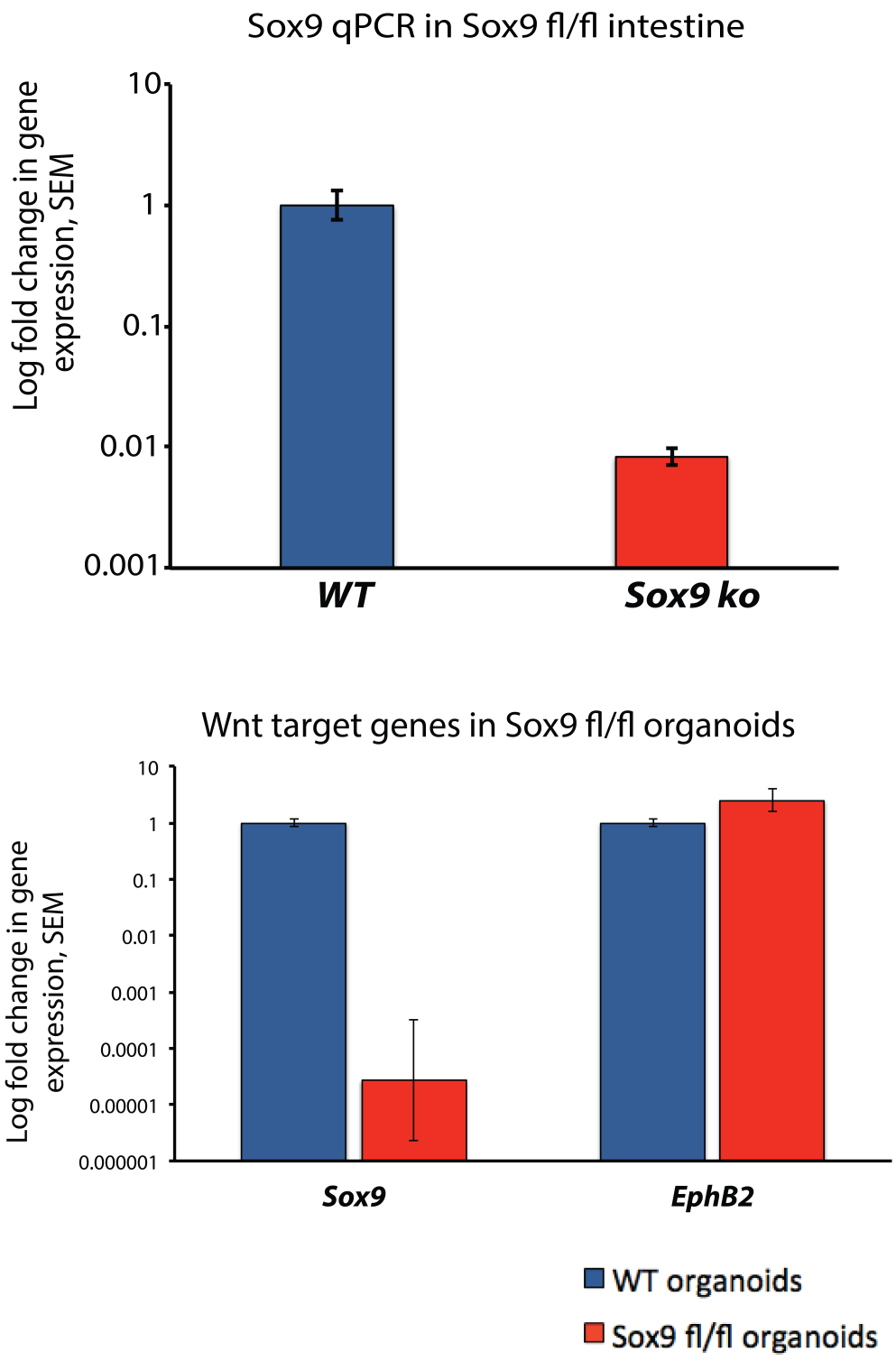

Figure 6.7: Sox9 qPCR of intestinal epithelium in wild-type and Sox9 fl/fl mice. Sox9 and EphB2 qPCR in wild-type and Sox9 floxed mouse organoids.

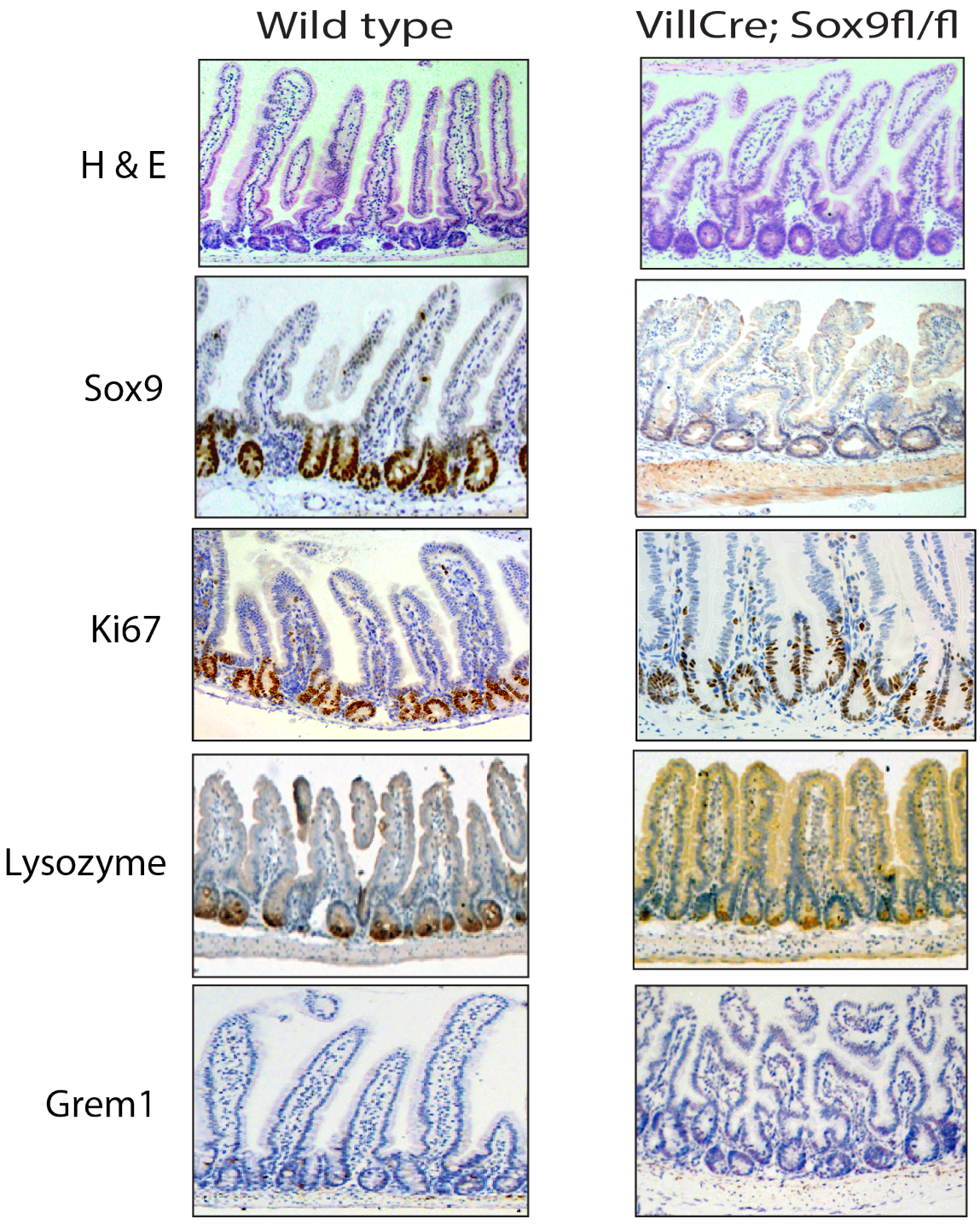

Figure 6.8: H+E, Sox9 IHC, Ki67 IHC, Lysozyme IHC and Grem1 ISH in wild-type and Sox9 floxed mice.

Vill-Cre; Sox9fl/fl intestinal crypt organoid growth

To compare stemness and proliferative capacity of the crypts in Sox9 floxed animals, crypt organoids were cultured. Small intestinal crypts were harvested and grown alongside age-matched control littermate mouse organoids (n=3 mice) in EGF, Noggin and Rspondin. Organoids grew from both mouse genotypes and there was no difference in number or budding of organoids up to 10 days (figure 6.9).

To confirm Sox9 knockdown, RNA extracted from individual organoids was tested by qPCR for Sox9. There was marked reduction in Sox9 expression as shown in figure 6.7. To look for any effect on other Wnt target genes, EphB2 was tested as an example Wnt target and did not significantly change. Therefore in the absence of Sox9, canonical Wnt must still be active as other Wnt target genes are present.

Intestinal crypts of Sox9 floxed mice therefore retain stemness and are capable of organoid growth.

Response to injury

Mice were exposed to 2% DSS for 5 days to induce acute colitis. Figure 6.10 shows the healing ulcers along with Sox9 IHC to confirm knockdown. It also shows the proportion of colon affected by ulcers in each animal group. As shown there was no significant difference in ulcer healing between wild-type and Sox9 knockout mice.

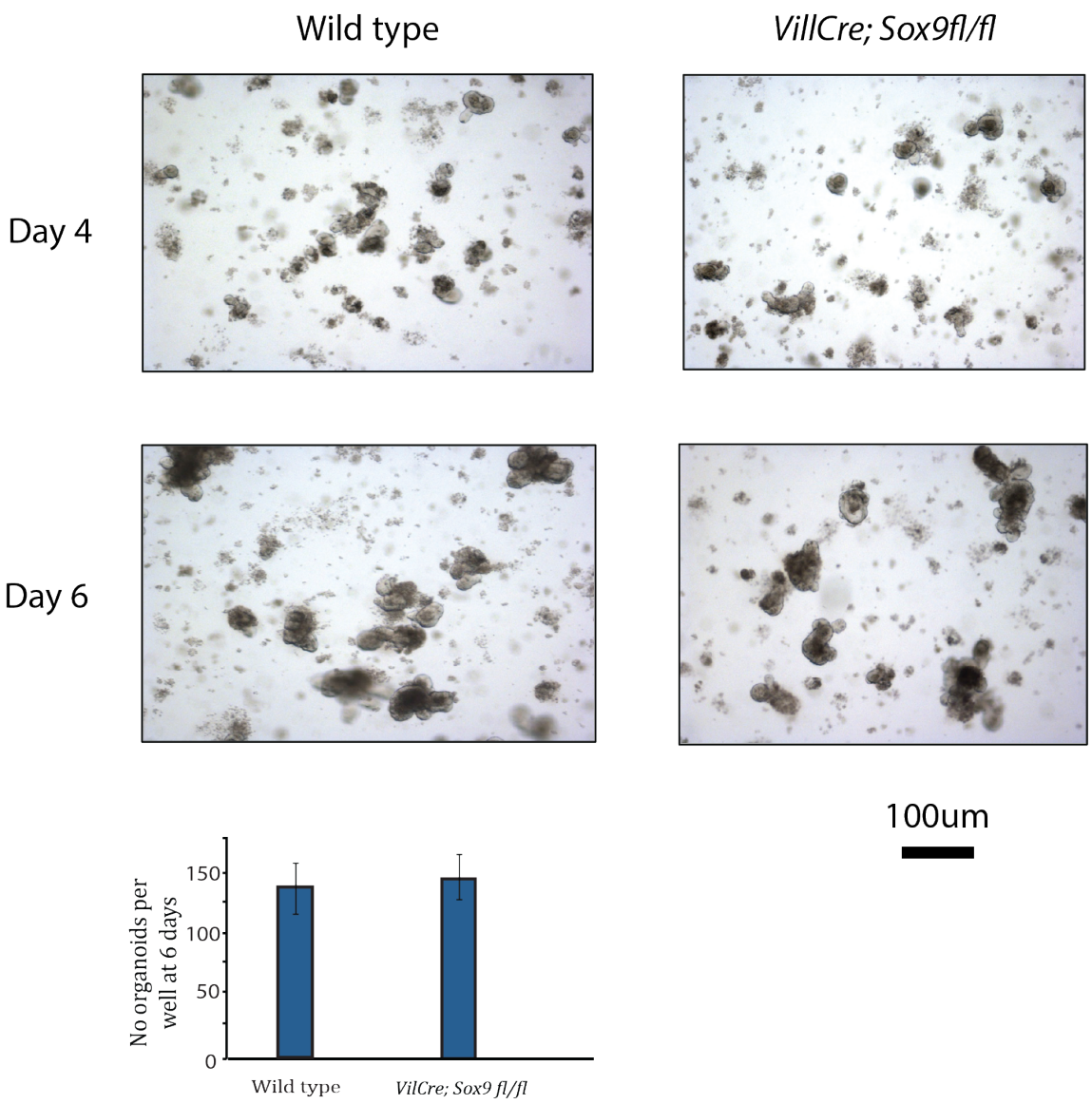

Figure 6.9: Small intestinal crypt organoids from wild-type and Sox9 floxed mice. Number of organoids per well at 6 days shown for each genotype.

Next test and littermate controls (n=3) were endoscoped and colonic biopsy injury induced. Wound healing was assessed at comparative timepoints. There was no difference in the time taken for wounds to heal. At 3 days the same process of WAE and de novo crypt formation was seen in both genotypes (figure 6.11). At 6 days wounds had mostly healed.

Therefore Sox9 knockout does not affect recovery from DSS-induced colitis or the timecourse of wound healing after biopsy injury.

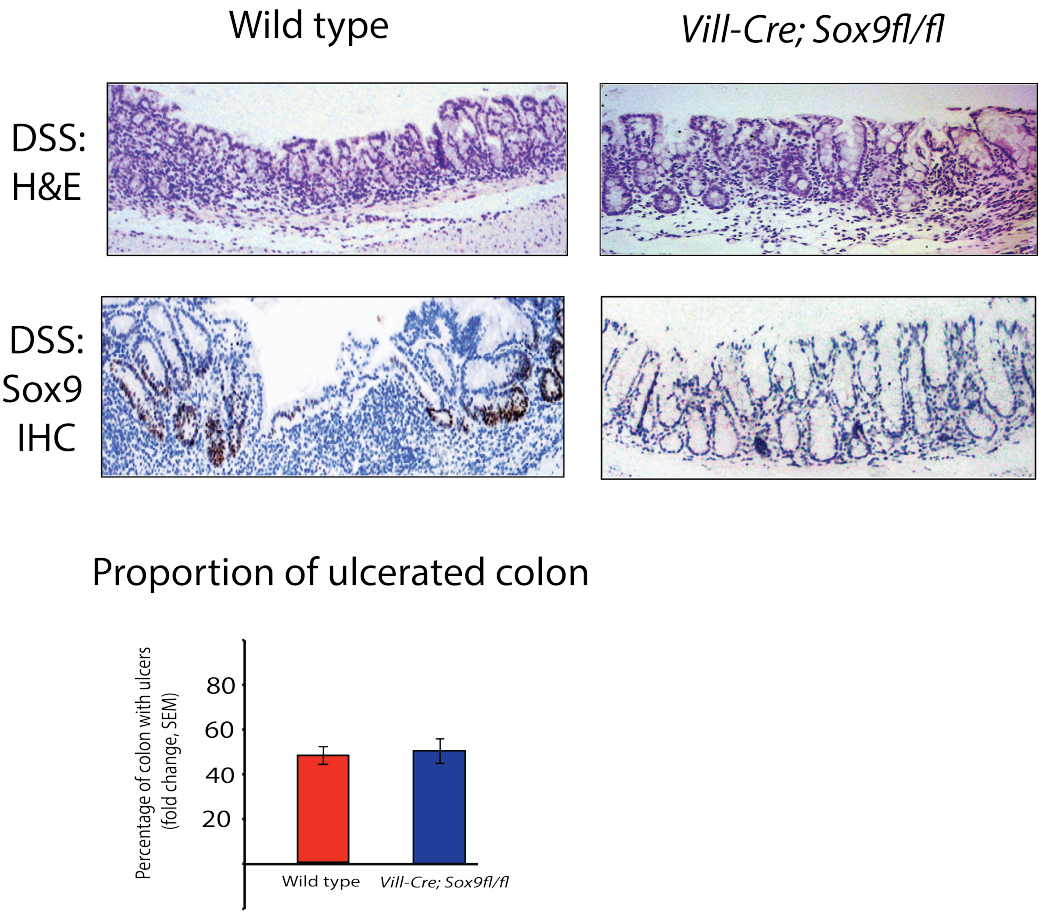

Figure 6.10: DSS in wild-type and Sox9 floxed mice: H+E stain and Sox9 IHC. Graph showing proportion of ulcerated colon in each group.

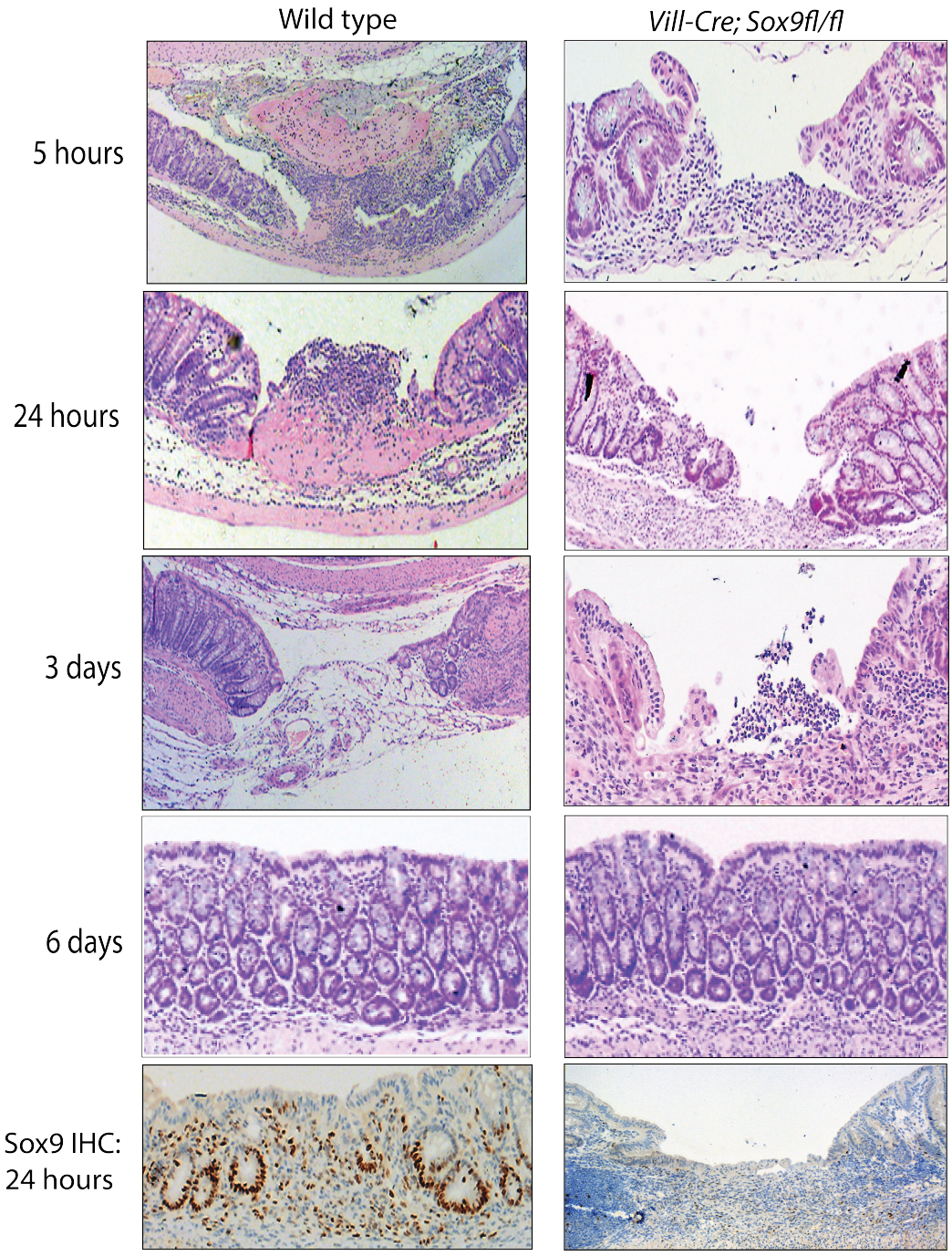

Figure 6.11: H+E stain at different timepoints after biopsy injury in wild-type and Sox9 floxed mice. Sox9 IHC at 24 hours.

6.4.2 Sox9 in carcinogenesis

6.4.2.1 Sox9 in CRC cell lines

Non-hypermutated colon cancers are known to have a higher frequency of SOX9 mutations. These are frameshift or nonsense mutations causing an increase in expression. Sox9 expression has been shown to be higher in cancer compared to wild-type epithelium [137], perhaps due to an oncogenic role of Sox9. Within cancers, expression is highest in SOX9-WT cancers and lowest in exon 1 or 2 SOX9-mutant cancers.

To test the degree of variability in SOX9 expression across CRC (colorectal cancer) cell lines, human CRC cell lines were tested for the presence of SOX9 (figure 6.12). Results were normalised by GAPDH level and are shown relative to CCD18C0, the line with the lowest expression of SOX9. The highest expression was in lines SW480 and VACO5.

This shows that Sox9 expression is highly variable across CRC cell lines. It may be that molecular CRC subtypes are linked to expression of Sox9. CRC subtyping by the CMS classification has not been tested for Sox9 and it may be that the CMS2 chromosome-unstable type with Wnt activation has increased Sox9 expression, because SOX9 is transcriptionally repressed by WNT signalling. In the paper classifying CRC cell lines by CCS type [91] there was no correlation between CCS type and Sox9 expression.

Sox9 splicing variant, truncated miniSox9, can inhibit Sox9 activity, so the level of Sox9 expression may also be less relevant that Sox9 function in tumours. The

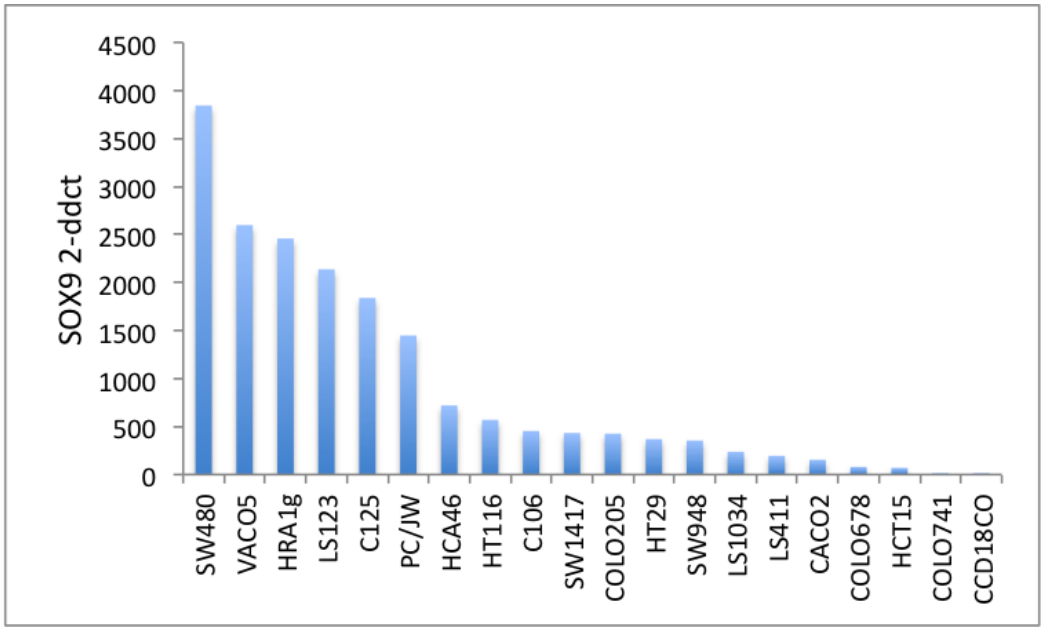

Figure 6.12: Sox9 expression in CRC cell lines.

paradox of Sox9's role in tumour formation was a reason for looking at this further.

6.4.2.2 The functional effect of *Sox9* in mediating the ECF phenotype: the *Vil1-Grem1; Vill-Cre; Sox9fl/fl* mouse model

After validation, I crossed *Vill-Cre;Sox9fl/fl* mice with *Vil1-Grem1* mice to look for any change in phenotype. It took time to breed these mice as they consistently produced small litters and fewer than expected by Mendelian inheritance were homozygous. This may have been due to homozygotes dying in utero. Table 6.1 shows the expected and actual numbers born which were *Vil1Grem1;Vill-Cre;Sox9fl/fl*. In a breeding pair a *Vil1-Grem1* positive mouse had to be crossed with a *Vil1-Grem1* negative mouse because previous work had shown that ho-

moygosity caused a severe phenotype at a younger age. In total out of 14 breeding pairs, 41 litters and 120 offspring, there were eight mice which were *Vil1Grem1;Vill-Cre;Sox9fl/fl.*

	Breeding pair	Expected rate	Actual rate	Total no off-spring
Pair 1	Vil1Grem1+;VillCre-;Sox9+/- X VillCre+;Sox9+/-	6.25%	4%	26
Pair 2	Vil1Grem1+;VillCre+;Sox9+/- X VillCre+;Sox9+/-	12.5%	8%	74
Pair 3	Vil1Grem1+;VillCre-;Sox9+/- X VillCre+;Sox9-/-	12.5%	0%	6
Pair 4	Vil1Grem1+;VillCre+;Sox9+/- X VillCre+;Sox9-/-	25%	10%	14

Table 6.1: Number of offspring with genotype *Vil1-Grem1+;VillCre+;Sox9-/-* born to different breeding pairs. Expected Mendelian rate and actual rate (p=0.19, χ^2 test).

Compared to age-matched *Vil1-Grem1* littermates, there was a reduction in polyp count and reduced size and dysplasia of polyps. Using methylene blue staining, polyps $>$1mm were counted in each section of small bowel and colon of each phenotype (figure 6.13). There were fewer dysplastic areas in polyps from Vil1Grem1;Vill-Cre;Sox9fl/fl mice, shown by H&E staining and reduced proliferative Ki67 cell staining.

Sox9 loss therefore reduces size and number of polyps in *Vil1-Grem1* mice and

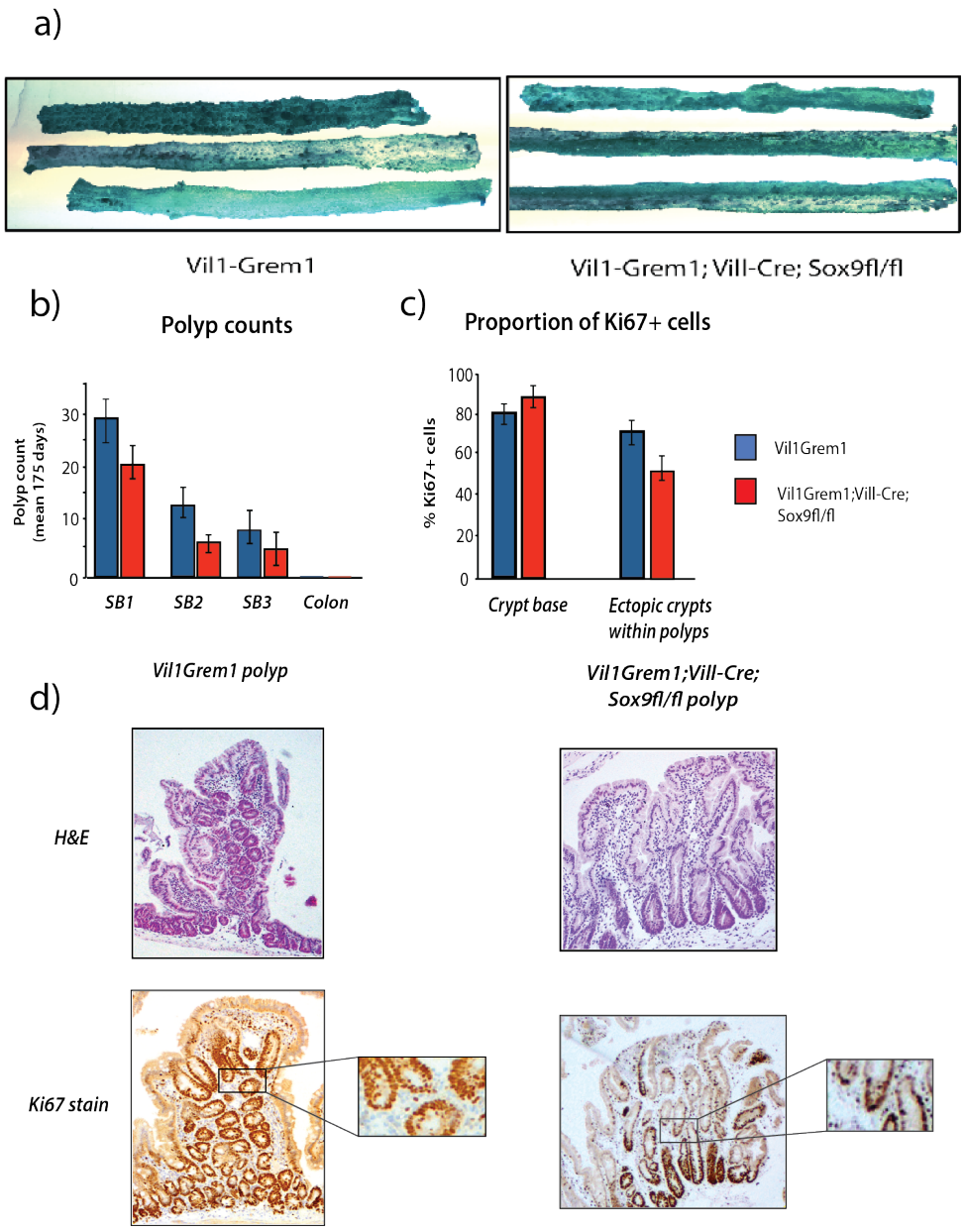

Figure 6.13: a) Methylene blue staining of small intestine in *Vil1-Grem1* and *Vil1-Grem1; Vill-Cre; Sox9fl/fl* mice. b) Number of polyps >1mm in *Vil1-Grem1* and *Vil1-Grem1; Vill-Cre; Sox9fl/fl* mice. c) Percentage of Ki67 positive cells in crypt base and polyp ectopic crypts. Mean age 175days. d) HE and Ki67 staining in polyps.

there is reduced proliferation in ectopic crypts, with no effect on crypt base proliferation. This is in contrast to the enlarged crypts with increased Ki67 cells at the crypt base of *Sox9* knockout mice. It is also in contrast to the unaffected organoid growth from *Sox9* floxed crypts. There must be a difference in the effect that *Sox9* has in the crypt base (where it regulates stemness) and ectopic crypts (where it promotes stemness). In ectopic crypts there is an increase in canonical Wnt as shown in chapter 5, which may be why *Sox9* plays more of a role in promoting proliferation. In the crypt base Rspondin is also active and the co-operative Wnt pathways may be less dependent on Sox9.

These data indicate that the role of *Sox9* may vary dependent on position along the crypt-villus axis. There is no apparent obligatory role for *Sox9* in crypt base transit amplifying cell proliferation where knockout has no effect on organoid growth or architecture. In contrast *Sox9* knockout does has an effect on ectopic crypt proliferating cells.

6.4.2.3 *Sox9* in the *Apc*^{Min} mouse model

Interestingly the *Apc*^{Min} mouse, with significantly enhanced canonical Wnt signalling, showed an increase in Sox9 expression in polyps (figure 6.14). Even in complex dysplastic polyps though there are no ectopic crypt foci positive for Sox9. Therefore canonical Wnt alone is not driving the Sox9 expression in ectopic crypts in *Vil1-Grem1* animals and it must result from the complex interacting model of Grem1 and Wnt.

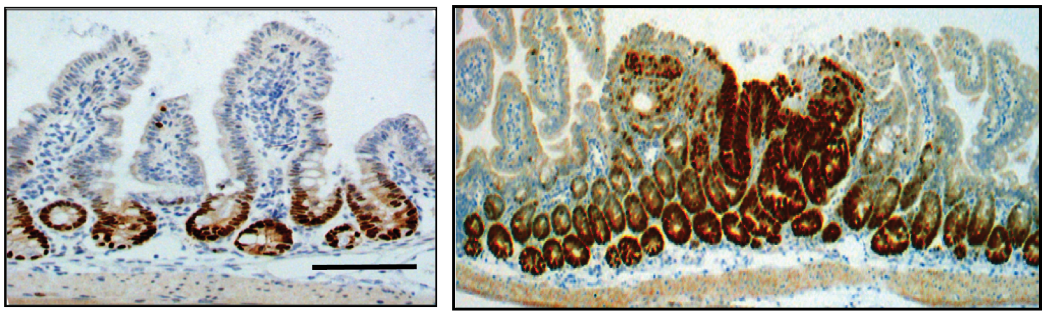

Figure 6.14: Sox9 IHC in wild-type and Apc^{Min} mouse small intestine.

6.5 Discussion

To answer the key objectives, the findings in this chapter are:

1. *Sox9* is upregulated in epithelial restitution.

2. The role of *Sox9* in wound healing is dispensable. *Sox9* knockout causes no change to organoid growth and does not affect healing post biopsy.

3. It is seen that in a model of BMP dysregulation, Sox9 is upregulated and localised to ectopic crypts although not excusively. In the *Vil1-Grem1* mouse, *Sox9* knockout does not prevent ectopic crypt formation, but knockout does reduce ectopic crypt cell proliferation and slows polyp progression.

6.5.1 Sox9 in inflammation

Sox9 is expressed by wound associated epithelium which develops from day 3 post injury. It could therefore be assumed to be part of the healing process. Epithelial knockout though does not prevent healing from biopsy injury, so other

genes in the Wnt cascade may take over. Alternatively it could mean that the wound associated epithelium expresses Sox9 but that this does not arise from a crypt base Sox9-positive stem cell. It may be that ulcer healing still takes place after Sox9 knockout but tissue architecture is altered.

In wound healing, increased and aberrant Grem1 expression has been described around ulcers. This is a sign of active stroma contributing to the recovery process. Sox9 is expressed by the wound associated epithelium and in de novo branching crypts of the wound bed, and may be an important part of restitution. Figure 6.15 highlights the changes that occur around day 4 post injury, including immune activation and temporary disruption of morphogen gradients.

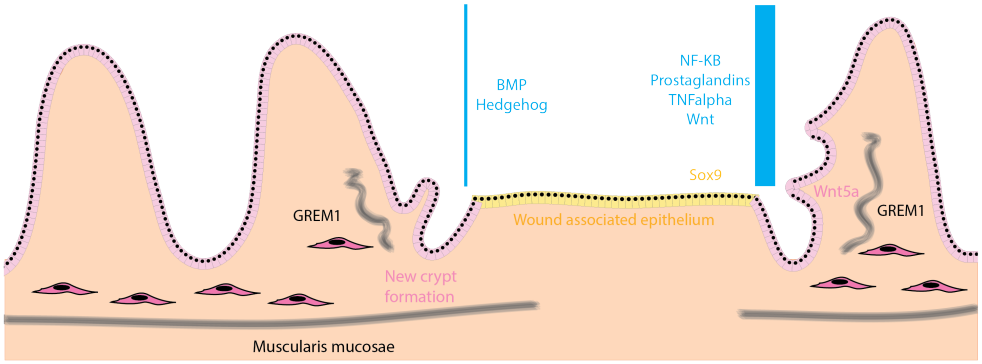

Figure 6.15: Acute phase post epithelial wounding. High levels of NFKB, prostglandins and TNFalpha drive regeneration. A monolayer of wound associated epithelium forms which is Sox9 positive. Fibroblasts are activated at the edge of the wound and express Grem1. New crypts form in the wound channel, driven by mesenchymally-derived Wnt5a. Levels of BMP and Hedgehog are low in the wound channel to allow proliferation and crypt budding.

The mechanistic implications are that levels of Wnt are increased in inflammation because damaged mucosa upregulates Wnt to allow increased cell turnover and repair. BMP and HH are conversely lower because they are not required by crypt base stem cells in turnover. In time BMP and HH are again upregulated when dif-

ferentiating cells reach the apical surface and require the balance of morphogens. Grem1 seems to be important in allowing the expansion of stem cells. Sox9, as a stem cell marker and a Wnt target, is seen in regenerating crypts.

6.5.2 Sox9 in carcinogenesis

The role of Sox9 in cancer is a paradox. There is increased expression in tumours but a relatively high frequency of inactivating mutations in human cancer. Conversely a number of studies indicate that high levels of Sox9 correlate with an inhibition of proliferation of both healthy intestine and cancer epithelial cells, while low levels of Sox9 promote sustained proliferation. Thus knocking down Sox9 would be expected to promote cell proliferation. However in the *Sox9* knockout model, mice showed no change in phenotype and there was no increase in capacity for organoid growth.

Sox9 is required for differentiation of Paneth cells which provide Wnt signals. Paneth cells can be thought of as the protective nursemaid cells of the crypt base which sustain and modulate epithelial stem and progenitor cells. The Sox9 knockout mouse model had fewer Paneth cells at the crypt base and it could be expected that there would be less Wnt signalling so reduced cell proliferation. In fact it did not affect growth of crypt organoids, so the Wnt signals may be provided by other epithelial cells or in organoids by exogenous Wnt.

The effect of Sox9 knockout appears to vary according to the position of the cell in the crypt-villus axis in this BMP disrupted model. Sox9 knockout in the *Vil1-Grem1* model reduced polyp burden and the number of proliferative cells in

polyps. This suggests that Sox9 acts as an oncogene in the ectopic crypts and contributes to polyp development. In a paper using the same Sox9 knockout model [132], the results suggested that Sox9 regulates cell proliferation via IGFBP-4, again suggesting that Sox9 has the opposite role as a tumour suppressor gene at the crypt base. Indeed Sox9 knockout mice had enlarged crypts with increased proliferating cells. When crossed with Apc^{Min}, mice showed increased tumour burden. Perhaps in the crypt base where both canonical and non-canonical Wnt act, Sox9 is dispensable and suppresses proliferation. In ectopic crypts where canonical Wnt is predominant, Sox9 takes over and promotes proliferation. Canonical Wnt may be higher in ectopic crypts because the mesenchyme is altered here and provides more canonical Wnt signals, as shown in chapter 5.

It has been reported that Sox9 knockout increases the polyp burden in Apc^{Min} mice, suggesting that Sox9 puts a hold on proliferation as it does at the crypt base. This raises the question of whether the extent to which the Wnt pathway is overactivated affects the role of Sox9. Perhaps in Grem1 activation Sox9 has a proliferative effect but when Wnt is hugely overactive as in Apc^{Min} mice, Sox9 is antiproliferative. There could be a cutoff point at which the effect of Sox9 changes. Sox9 may fine-tune and be fine-tuned by Wnt depending on the context.

A potential mechanism of buffering the effect of Sox9 is the presence of splice variants. *MiniSox9* is a truncated version of *Sox9* and acts as an inhibitor of *SOX9*. It has been found to be overexpressed in human CRC samples. It behaves as a dominant negative and stimulates the canonical Wnt pathway. The presence of *MiniSox9* in the ectopic and basal crypts of the *Vil1-Grem1* model would be a focus for further work.

Sox9 seems to have a bimodal role depending on the level expressed, and also depending on where in the crypt-villus escalator it is expressed. It is unique for a gene to bring about opposing effects in the same tissue in such close proximity. Given these conflicting roles, Sox9 is not a legitimate therapeutic target currently. The role of Sox9 in cancer and whether it is an oncogene or TSG is still not clear. It is clear though that the effect of Sox9 is intrinsically linked to the context of microenvironmental signalling.

6.5.3 Limitations

- Similarly to chapter 5, there is a quantification issue in determining wound healing in response to DSS and biopsy injury.
- Numbers of mice used in the biopsy wound healing experiment and *Vil1-Grem1; Vill-Cre; Sox9fl/fl* phenotyping was small (n=3), hence these are preliminary experiments.
- Polyp counting and determining which polyps are $>$1mm are subject to error.

Chapter 7

Discussion

7.1 Summary of results

The key findings of this thesis are:

- Epithelial-mesenchymal crosstalk is crucial in BMP, HH and Wnt pathways.
- In inflammation there is loss of crypt-luminal gradients across the axes and an overall reduction in BMP and HH signalling.
- Areas of mesenchyme surrounding crypts and surrounding villi have vastly different gene signatures.
- The reciprocal relationship between Grem1 and HH was confirmed. Grem1 is a regenerative mediator, antagonised in culture by BMP, and is important in epithelial restitution. In tissue regeneration Hedgehog is downregulated with an associated upregulation of Grem1.

- Next a mouse model of aberrant epithelial Grem1 expression was explored. Ectopic crypts formed within polyps and were positive for Sox9. These precursors away from the crypt base were capable of clonal expansion into multiple enteric cell types and could form organoids in culture. The presence of stemness outside the strict control of the crypt base niche led to altered DNA damage response and increased potential for somatic mutation. The microenvironment of ectopic crypts was found to be markedly altered, in particular with an amplification of canonical Wnt signalling.

- Finally Sox9 was demonstrated to be present in wound associated epithelium and hence important in wound healing, but Sox9 loss did not affect repair of biopsy injury. In the *Vil1-Grem1* model Sox9 loss reduced proliferation and number of polyps, but Sox9 loss alone led to increased proliferation at the crypt base. These differing effects of Sox9 are due to dependence of its action on the surrounding microenvironment and balance/imbalance of morphogens.

7.2 Morphogen gradients in homeostasis and inflammation

A shift in morphogen polarity has been shown in disrupted homeostasis. The usual opposition of Wnt and BMP/HH is maintained but Wnt is high and more constant throughout the crypt-luminal axis and BMP/HH are low throughout. The mechanistic implication is that Wnt is required for high cell turnover in repair before

re-establishing the polarised gradients for resolution of crypt-villus architecture. Figure 7.1 shows a schematic of these changes.

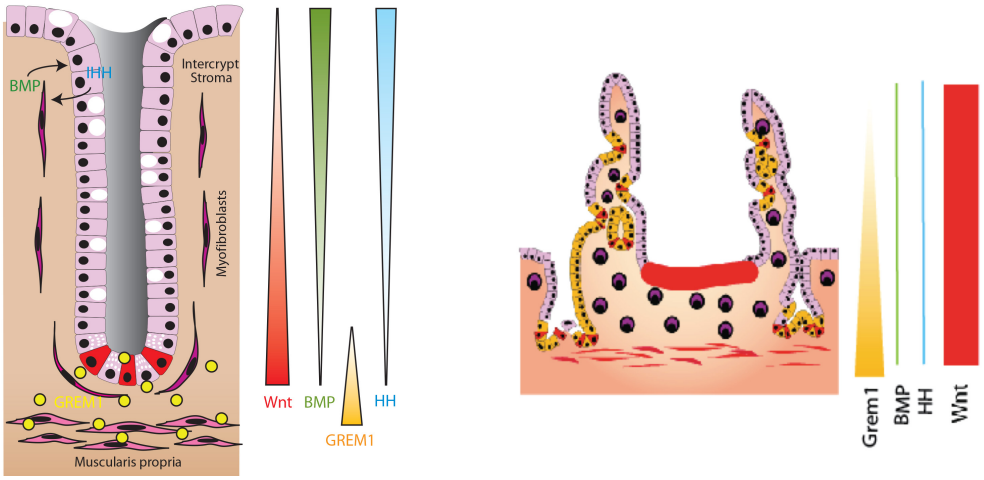

Figure 7.1: Morphogen gradients in inflammation. Wnt is expressed more highly to allow regeneration and crypt budding. The homeostatic gradients in which Wnt is higher at the base and BMP and HH are higher at the villus are lost. Instead Wnt is expressed at the villus and BMP/HH are found at the crypt base.

The translational implication is that after mucosal injury from chemical colitis or inflammatory bowel disease, allowing enhanced repair may restore morphogen signalling balance more promptly. After allowing high Wnt levels for the inital stage of repair, there may be a benefit in increasing the levels of BMP and HH to restore balance. This may prevent prolonged overproliferation contributing to mutation and tumorigenesis. Manipulating the BMP and HH pathway was discussed in chapters 3 and 4. This can be done through agonists and antagonists of the pathways to supply exogenous BMP and HH.

7.3 The *Vil1-Grem1* mouse model and formation of ectopic crypts

The work highlights that the stem cell pool should be thought of as a functional collective, comprising a dynamic and heterogeneous population of cells with variable stem cell competence imposed by position within the niche and microenvironmental morphogen context. As experimental techniques improve, our understanding of the position, fate and role of intestinal stem cells in homeostasis and carcinogenesis is evolving.

Perhaps it is of no surprise that Sox9 loss does not cause abrogation of ectopic crypt formation as the primary issue, Grem1 disruption, is unchanged. There is no known link between Grem1 and Sox9 and hence there is no reason why one should upregulate the other. Sox9 may be simply a marker of this unusual population of progenitors. The effect of Sox9 knockout in this model may also differ from Sox9 knockout alone because there is such a departure from homeostasis when Grem1 is disrupted in this way. The effect of uniform Grem1 on reducing BMP and Hh and increasing parts of the Wnt pathway is perhaps too crucial to be prevented by a downregulation in a Wnt target gene alone. It may be that BMP overexpression could antagonise the effect of Grem1, as it did in organoid culture, and together with Sox9 knockout could abrogate the phenotype.

7.4 New therapeutic targets in inflammation and colorectal cancer

The knowledge that different cells have altered responsiveness to signalling pathways leads us to the assumption that they will also respond differently to chemotherapy. Certain genes are more likely to be present within cancer stem cells and therefore targeting these specifically will remove the nidus of the cancer. Current chemotherapy targets differentiated cancer cells and does not take into account different replicative potentials within a tumour. Cancer cells mutate to avoid cell death by drugs and radiation, and finding and targeting these resistant clones will lead to enhanced clearance. Combined efforts with enhanced imaging and genetics prior to surgery will help with this.

Sox9 is complex in terms of its role in cancer and hence it is too early to target therapy towards this. The truncated anti-Sox9 variants and their role also complicate this.

Grem1 may be a target for therapy as it promotes proliferation and may be a marker of cancer stem cells. An inhibitor of *Grem1* combined with conventional chemotherapy may be of benefit in CMS4 tumours. In HMPS, reducing the level of *Grem1* with small molecule inhibitors or antibodies could reduce polyp burden and cancer risk.

The problem in IBD is that the temporary disruption in morphogens is a priority for tissue restitution, but ongoing imbalance leads to chronic inflammation and cancer risk. Thus trying to correct polarised Wnt and BMP gradients by restoring

SMAD levels may avoid continuing insult which leads to risk of carcinogenesis, but the timing of this is crucial to allow acute ulcer healing. Reducing Grem1 levels may be of benefit also, but it is likely that there is a spectrum of morphogen dysregulation within IBD in terms of disease duration, IBD subtype and genetic risk, so patient-tailored therapy would be more important than ever before considering this a biomarker.

Mongersen is a therapy for Crohn's currently in trial phase. It is an oligonucleotide which decreases Smad7 protein. It is on oral antisense oligonucleotide which targets colonic and ileal Smad7. Levels of SMAD7, which inhibits TGFB1, are high in Crohn's disease, and results of phase 2 trials were promising.

In the future molecular stratification, such as that done in breast cancer, will be done in colorectal cancer and in IBD. Mutational analysis and morphogen analysis will allow treatment according to one's personalised genetic and biochemical signature. This has been achieved in the FOCUS4 trial which divides patients into subgroups: BRAF mutant, PIK3CA mutant, KRAS mutant or eGFR dependent. Selective chemotherapy is given according to mutation status. In the future, a patient with IBD who has high levels of TGF1 or GREM1 or SOX9 could be stratified and given biological therapy alongside existing conventional therapy.

7.5 Further work

To further explore the effect of *Sox9* knockout, *in vitro* Sox9 knockdown in cancer cell lines would be a way to assess the effect on cell growth. As the lentiviral method was not successful, the CRISPR technique may be the best way to achieve

this. If this was thought to have an effect on cancer growth, Sox9-modified cancer cells could be xenotransplanted into immunocompromised mice as compared to unmodified cancer cells and tumour growth monitored. Growth would be monitored endoscopically or using a luciferase reporter in cells and fluorescent imaging.

The effect of Sox9 knockout in *Apc*^{Min} mouse polyps should be assessed. It has been reported that Sox9 knockout increases the polyp burden in *Apc*^{Min} mice.

MiniSox9 was not considered here, the truncated splicing variant which may act as a Sox9 inhibitor. There is no commercially available IHC antibody for this but primers could be designed to look for its presence in cancer and in *Vil1-Grem1* models using SYBR green.

The *Vil1-Grem1* model is not physiological, as Grem1 is expressed in epithelium instead of its usual position in mesenchyme. To overexpress Grem1 in mesenchyme, Cre mediated recombination can be limited to Gli1-positive cells. It would be interesting to know if ectopic crypts would still form without the burden of Grem1 overexpressing cells in the epithelium.

Villus organoids grow from *Vil1-Grem1* mouse models. Presumably the addition of BMP2 and BMP4 would prevent growth in the same way they prevent crypt organoid growth, but it would be important to know if the same process occurred when endogenous Grem1 is being secreted, as well as the level of BMP ligand required for inhibition.

The concept of GREM1 in cancer stem cells of glioblastoma has relevance for therapy to remove CSCs. This has not been studied in CRC, but FACS markers

could be used to assess the presence of Grem1 in the presumed CSCs. Different subtypes of CRC could also be tested, as presumably the CMS4 type would have an increase in GREM1 expressing cells compared to other subtypes.

The reason some experiments were not adequately finished and those above not carried out was due to time constraints of the funding received.

7.6 Closing summary

In conclusion, epithelial-stromal crosstalk is vital in maintaining homeostatic morphogen gradients. In intestinal injury epithelial denudation disrupts this crosstalk and breach of the mucosal barrier induces a localised innate immune response which transiently unsettles the intestinal cell-signalling balance. This induces a profound change in neighbouring intact epithelium, characterised phenotypically by crypt budding, fission and the generation of wound associated epithelium. The surrounding mesenchyme is also vital in this process and myofibroblasts are activated adjacent to the wound bed. At a cellular level this cell signalling perturbation alters epithelial cell fate determination. This is part of the physiological response to injury and is required to effect epithelial restitution, however these characteristics are also key attributes of malignant cells. Failure to restore homeostatic control in chronic inflammation or pathological disruption of signalling pathways can result in neoplasia initiation and progression. The *Vil1-Grem1* model is an example of this, where disrupted BMP signalling leads to a very abnormal microenvironment in which cells outside the stem cell niche become capable of clonal expansion and cancer initiation.

To target this, therapy in inflammation and cancer needs to be directed at restoring homeostatic morphogen gradients in a timely manner. Teasing apart how to manipulate disrupted signalling in tumours without affecting the role of that pathway in tissue homeostasis is the critical challenge for future drug design.

Bibliography

[1] J. P. Heath. Epithelial cell migration in the intestine. *Cell Biol Int*, 20(2):139–46, 1996.

[2] A. Humphries and N. A. Wright. Colonic crypt organization and tumorigenesis. *Nat Rev Cancer*, 8(6):415–24, 2008.

[3] S. J. Morrison and A. C. Spradling. Stem cells and niches: mechanisms that promote stem cell maintenance throughout life. *Cell*, 132(4):598–611, 2008.

[4] B. Degirmenci, T. Valenta, S. Dimitrieva, G. Hausmann, and K. Basler. Gli1-expressing mesenchymal cells form the essential wnt-secreting niche for colon stem cells. *Nature*, 558(7710):449–453, 2018.

[5] D. L. Worthley, A. S. Giraud, and T. C. Wang. Stromal fibroblasts in digestive cancer. *Cancer Microenviron*, 3(1):117–25, 2010.

[6] D. H. Scoville, T. Sato, X. C. He, and L. Li. Current view: intestinal stem cells and signaling. *Gastroenterology*, 134(3):849–64, 2008.

[7] J. P. Medema and L. Vermeulen. Microenvironmental regulation of stem

cells in intestinal homeostasis and cancer. *Nature*, 474(7351):318–26, 2011.

[8] H. Cheng and C. P. Leblond. Origin, differentiation and renewal of the four main epithelial cell types in the mouse small intestine. v. unitarian theory of the origin of the four epithelial cell types. *Am J Anat*, 141(4):537–61, 1974.

[9] C. S. Potten. Extreme sensitivity of some intestinal crypt cells to x and gamma irradiation. *Nature*, 269(5628):518–21, 1977.

[10] L. G. Van der Flier, J. Sabates-Bellver, I. Oving, A. Haegebarth, M. De Palo, M. Anti, M. E. Van Gijn, S. Suijkerbuijk, M. Van de Wetering, G. Marra, and H. Clevers. The intestinal wnt/tcf signature. *Gastroenterology*, 132(2):628–32, 2007.

[11] A. Gregorieff, D. Pinto, H. Begthel, O. Destree, M. Kielman, and H. Clevers. Expression pattern of wnt signaling components in the adult intestine. *Gastroenterology*, 129(2):626–38, 2005.

[12] N. Barker, J. H. van Es, J. Kuipers, P. Kujala, M. van den Born, M. Cozijnsen, A. Haegebarth, J. Korving, H. Begthel, P. J. Peters, and H. Clevers. Identification of stem cells in small intestine and colon by marker gene lgr5. *Nature*, 449(7165):1003–7, 2007.

[13] N. Barker and H. Clevers. Leucine-rich repeat-containing g-protein-coupled receptors as markers of adult stem cells. *Gastroenterology*, 138(5):1681–96, 2010.

[14] N. Barker, M. Huch, P. Kujala, M. van de Wetering, H. J. Snippert, J. H.

van Es, T. Sato, D. E. Stange, H. Begthel, M. van den Born, E. Danenberg, S. van den Brink, J. Korving, A. Abo, P. J. Peters, N. Wright, R. Poulsom, and H. Clevers. Lgr5(+ve) stem cells drive self-renewal in the stomach and build long-lived gastric units in vitro. *Cell Stem Cell*, 6(1):25–36, 2010.

[15] V. Jaks, N. Barker, M. Kasper, J. H. van Es, H. J. Snippert, H. Clevers, and R. Toftgard. Lgr5 marks cycling, yet long-lived, hair follicle stem cells. *Nat Genet*, 40(11):1291–9, 2008.

[16] E. Sangiorgi and M. R. Capecchi. Bmi1 is expressed in vivo in intestinal stem cells. *Nat Genet*, 40(7):915–20, 2008.

[17] N. Takeda, R. Jain, M. R. LeBoeuf, Q. Wang, M. M. Lu, and J. A. Epstein. Interconversion between intestinal stem cell populations in distinct niches. *Science*, 334(6061):1420–4, 2011.

[18] R. K. Montgomery, D. L. Carlone, C. A. Richmond, L. Farilla, M. E. Kranendonk, D. E. Henderson, N. Y. Baffour-Awuah, D. M. Ambruzs, L. K. Fogli, S. Algra, and D. T. Breault. Mouse telomerase reverse transcriptase (mtert) expression marks slowly cycling intestinal stem cells. *Proc Natl Acad Sci U S A*, 108(1):179–84, 2011.

[19] L. G. van der Flier, M. E. van Gijn, P. Hatzis, P. Kujala, A. Haegebarth, D. E. Stange, H. Begthel, M. van den Born, V. Guryev, I. Oving, J. H. van Es, N. Barker, P. J. Peters, M. van de Wetering, and H. Clevers. Transcription factor achaete scute-like 2 controls intestinal stem cell fate. *Cell*, 136(5):903–12, 2009.

[20] S. Itzkovitz, A. Lyubimova, I. C. Blat, M. Maynard, J. van Es, J. Lees,

T. Jacks, H. Clevers, and A. van Oudenaarden. Single-molecule transcript counting of stem-cell markers in the mouse intestine. *Nat Cell Biol*, 14(1):106–14, 2012.

[21] J. Munoz, D. E. Stange, A. G. Schepers, M. van de Wetering, B. K. Koo, S. Itzkovitz, R. Volckmann, K. S. Kung, J. Koster, S. Radulescu, K. Myant, R. Versteeg, O. J. Sansom, J. H. van Es, N. Barker, A. van Oudenaarden, S. Mohammed, A. J. Heck, and H. Clevers. The lgr5 intestinal stem cell signature: robust expression of proposed quiescent '+4' cell markers. *EMBO J*, 31(14):3079–91, 2012.

[22] A. E. Powell, Y. Wang, Y. Li, E. J. Poulin, A. L. Means, M. K. Washington, J. N. Higginbotham, A. Juchheim, N. Prasad, S. E. Levy, Y. Guo, Y. Shyr, B. J. Aronow, K. M. Haigis, J. L. Franklin, and R. J. Coffey. The pan-erbb negative regulator lrig1 is an intestinal stem cell marker that functions as a tumor suppressor. *Cell*, 149(1):146–58, 2012.

[23] L. G. van der Flier, A. Haegebarth, D. E. Stange, M. van de Wetering, and H. Clevers. Olfm4 is a robust marker for stem cells in human intestine and marks a subset of colorectal cancer cells. *Gastroenterology*, 137(1):15–7, 2009.

[24] B. K. Koo, M. Spit, I. Jordens, T. Y. Low, D. E. Stange, M. van de Wetering, J. H. van Es, S. Mohammed, A. J. Heck, M. M. Maurice, and H. Clevers. Tumour suppressor rnf43 is a stem-cell e3 ligase that induces endocytosis of wnt receptors. *Nature*, 488(7413):665–9, 2012.

[25] K. Furuyama, Y. Kawaguchi, H. Akiyama, M. Horiguchi, S. Kodama,

T. Kuhara, S. Hosokawa, A. Elbahrawy, T. Soeda, M. Koizumi, T. Masui, M. Kawaguchi, K. Takaori, R. Doi, E. Nishi, R. Kakinoki, J. M. Deng, R. R. Behringer, T. Nakamura, and S. Uemoto. Continuous cell supply from a sox9-expressing progenitor zone in adult liver, exocrine pancreas and intestine. *Nat Genet*, 43(1):34–41, 2011.

[26] H. Tian, B. Biehs, S. Warming, K. G. Leong, L. Rangell, O. D. Klein, and F. J. de Sauvage. A reserve stem cell population in small intestine renders lgr5-positive cells dispensable. *Nature*, 478(7368):255–9, 2011.

[27] S. J. Buczacki, H. I. Zecchini, A. M. Nicholson, R. Russell, L. Vermeulen, R. Kemp, and D. J. Winton. Intestinal label-retaining cells are secretory precursors expressing lgr5. *Nature*, 495(7439):65–9, 2013.

[28] T. Sato, R. G. Vries, H. J. Snippert, M. van de Wetering, N. Barker, D. E. Stange, J. H. van Es, A. Abo, P. Kujala, P. J. Peters, and H. Clevers. Single lgr5 stem cells build crypt-villus structures in vitro without a mesenchymal niche. *Nature*, 459(7244):262–5, 2009.

[29] T. Sato and H.l Clevers. Growing self-organizing mini-guts from a single intestinal stem cell: mechanism and applications. *Science*, 340(6137):1190–4, 2013.

[30] T. Sato, D. E. Stange, M. Ferrante, R. G. Vries, J. H. Van Es, S. Van den Brink, W. J. Van Houdt, A. Pronk, J. Van Gorp, P. D. Siersema, and H. Clevers. Long-term expansion of epithelial organoids from human colon, adenoma, adenocarcinoma, and barrett's epithelium. *Gastroenterology*, 141(5):1762–72, 2011.

[31] B. M. Kim, J. Mao, M. M. Taketo, and R. A. Shivdasani. Phases of canonical wnt signaling during the development of mouse intestinal epithelium. *Gastroenterology*, 133(2):529–38, 2007.

[32] R. N. Wang, J. Green, Z. Wang, Y. Deng, M. Qiao, M. Peabody, Q. Zhang, J. Ye, Z. Yan, S. Denduluri, O. Idowu, M. Li, C. Shen, A. Hu, R. C. Haydon, R. Kang, J. Mok, M. J. Lee, H. L. Luu, and L. L. Shi. Bone morphogenetic protein (bmp) signaling in development and human diseases. *Genes Dis*, 1(1):87–105, 2014.

[33] G. R. van den Brink. Hedgehog signaling in development and homeostasis of the gastrointestinal tract. *Physiol Rev*, 87(4):1343–75, 2007.

[34] S. C. Goetz and K. V. Anderson. The primary cilium: a signalling centre during vertebrate development. *Nat Rev Genet*, 11(5):331–44, 2010.

[35] M. Levin. Left-right asymmetry in embryonic development: a comprehensive review. *Mech Dev*, 122(1):3–25, 2005.

[36] M. Zebisch, Y. Xu, C. Krastev, B. T. MacDonald, M. Chen, R. J. Gilbert, X. He, and E. Y. Jones. Structural and molecular basis of znrf3/rnf43 transmembrane ubiquitin ligase inhibition by the wnt agonist r-spondin. *Nat Commun*, 4:2787, 2013.

[37] K. S. Yan, C. Y. Janda, J. Chang, G. X. Y. Zheng, K. A. Larkin, V. C. Luca, L. A. Chia, A. T. Mah, A. Han, J. M. Terry, A. Ootani, K. Roelf, M. Lee, J. Yuan, X. Li, C. R. Bolen, J. Wilhelmy, P. S. Davies, H. Ueno, R. J. von Furstenberg, P. Belgrader, S. B. Ziraldo, H. Ordonez, S. J. Henning, M. H. Wong, M. P. Snyder, I. L. Weissman, A. J. Hsueh, T. S. Mikkelsen,

K. C. Garcia, and C. J. Kuo. Non-equivalence of wnt and r-spondin ligands during lgr5+ intestinal stem-cell self-renewal. *Nature*, 545(7653):238–242, 2017.

[38] H. Miyoshi. Wnt-expressing cells in the intestines: guides for tissue remodeling. *J Biochem*, 161(1):19–25, 2017.

[39] J. Schuijers and H. Clevers. Adult mammalian stem cells: the role of wnt, lgr5 and r-spondins. *EMBO J*, 31(12):2685–96, 2012.

[40] B. A. Auclair, Y. D. Benoit, N. Rivard, Y. Mishina, and N. Perreault. Bone morphogenetic protein signaling is essential for terminal differentiation of the intestinal secretory cell lineage. *Gastroenterology*, 133(3):887–96, 2007.

[41] J. C. Hardwick, G. R. Van Den Brink, S. A. Bleuming, I. Ballester, J. M. Van Den Brande, J. J. Keller, G. J. Offerhaus, S. J. Van Deventer, and M. P. Peppelenbosch. Bone morphogenetic protein 2 is expressed by, and acts upon, mature epithelial cells in the colon. *Gastroenterology*, 126(1):111–21, 2004.

[42] X. C. He, J. Zhang, W. G. Tong, O. Tawfik, J. Ross, D. H. Scoville, Q. Tian, X. Zeng, X. He, L. M. Wiedemann, Y. Mishina, and L. Li. Bmp signaling inhibits intestinal stem cell self-renewal through suppression of wnt-beta-catenin signaling. *Nat Genet*, 36(10):1117–21, 2004.

[43] Q. Tian, X. C. He, L. Hood, and L. Li. Bridging the bmp and wnt pathways by pi3 kinase/akt and 14-3-3zeta. *Cell Cycle*, 4(2):215–6, 2005.

[44] R. H. Church, A. Krishnakumar, A. Urbanek, S. Geschwindner, J. Meneely,

A. Bianchi, B. Basta, S. Monaghan, C. Elliot, M. Stromstedt, N. Ferguson, F. Martin, and D. P. Brazil. Gremlin1 preferentially binds to bone morphogenetic protein-2 (bmp-2) and bmp-4 over bmp-7. *Biochem J*, 466(1):55–68, 2015.

[45] P. Jiramongkolchai, P. Owens, and C. C. Hong. Emerging roles of the bone morphogenetic protein pathway in cancer: potential therapeutic target for kinase inhibition. *Biochem Soc Trans*, 44(4):1117–34, 2016.

[46] N. V. Buller, S. L. Rosekrans, J. Westerlund, and G. R. van den Brink. Hedgehog signaling and maintenance of homeostasis in the intestinal epithelium. *Physiology (Bethesda)*, 27(3):148–55, 2012.

[47] T. K. Noah and N. F. Shroyer. Notch in the intestine: regulation of homeostasis and pathogenesis. *Annu Rev Physiol*, 75:263–88, 2013.

[48] S. Fre, M. Huyghe, P. Mourikis, S. Robine, D. Louvard, and S. Artavanis-Tsakonas. Notch signals control the fate of immature progenitor cells in the intestine. *Nature*, 435(7044):964–8, 2005.

[49] J. H. van Es, M. E. van Gijn, O. Riccio, M. van den Born, M. Vooijs, H. Begthel, M. Cozijnsen, S. Robine, D. J. Winton, F. Radtke, and H. Clevers. Notch/gamma-secretase inhibition turns proliferative cells in intestinal crypts and adenomas into goblet cells. *Nature*, 435(7044):959–63, 2005.

[50] C. S. Potten. A comprehensive study of the radiobiological response of the murine (bdf1) small intestine. *Int J Radiat Biol*, 58(6):925–73, 1990.

[51] R. Kalluri. The biology and function of fibroblasts in cancer. *Nat Rev Cancer*, 16(9):582–98, 2016.

[52] M. Brittan, V. Chance, G. Elia, R. Poulsom, M. R. Alison, T. T. MacDonald, and N. A. Wright. A regenerative role for bone marrow following experimental colitis: contribution to neovasculogenesis and myofibroblasts. *Gastroenterology*, 128(7):1984–95, 2005.

[53] H. Miyoshi, R. Ajima, C. T. Luo, T. P. Yamaguchi, and T. S. Stappenbeck. Wnt5a potentiates tgf-beta signaling to promote colonic crypt regeneration after tissue injury. *Science*, 338(6103):108–13, 2012.

[54] H. Horiguchi, M. Endo, K. Kawane, T. Kadomatsu, K. Terada, J. Morinaga, K. Araki, K. Miyata, and Y. Oike. Angptl2 expression in the intestinal stem cell niche controls epithelial regeneration and homeostasis. *EMBO J*, 36(4):409–424, 2017.

[55] R. R. Driskell, B. M. Lichtenberger, E. Hoste, K. Kretzschmar, B. D. Simons, M. Charalambous, S. R. Ferron, Y. Herault, G. Pavlovic, A. C. Ferguson-Smith, and F. M. Watt. Distinct fibroblast lineages determine dermal architecture in skin development and repair. *Nature*, 504(7479):277–81, 2013.

[56] K. R. Jessen, R. Mirsky, and P. Arthur-Farraj. The role of cell plasticity in tissue repair: Adaptive cellular reprogramming. *Dev Cell*, 34(6):613–20, 2015.

[57] C. Metcalfe, N. M. Kljavin, R. Ybarra, and F. J. de Sauvage. Lgr5+ stem

cells are indispensable for radiation-induced intestinal regeneration. *Cell Stem Cell*, 14(2):149–59, 2014.

[58] J. H. van Es, T. Sato, M. van de Wetering, A. Lyubimova, A. N. Nee, A. Gregorieff, N. Sasaki, L. Zeinstra, M. van den Born, J. Korving, A. C. Martens, N. Barker, A. van Oudenaarden, and H. Clevers. Dll1+ secretory progenitor cells revert to stem cells upon crypt damage. *Nat Cell Biol*, 14(10):1099–104, 2012.

[59] P. W. Tetteh, O. Basak, H. F. Farin, K. Wiebrands, K. Kretzschmar, H. Begthel, M. van den Born, J. Korving, F. de Sauvage, J. H. van Es, A. van Oudenaarden, and H. Clevers. Replacement of lost lgr5-positive stem cells through plasticity of their enterocyte-lineage daughters. *Cell Stem Cell*, 18(2):203–13, 2016.

[60] S. Yu, K. Tong, Y. Zhao, I. Balasubramanian, G. S. Yap, R. P. Ferraris, E. M. Bonder, M. P. Verzi, and N. Gao. Paneth cell multipotency induced by notch activation following injury. *Cell Stem Cell*, 23(1):46–59 e5, 2018.

[61] C. B. Westphalen, S. Asfaha, Y. Hayakawa, Y. Takemoto, D. J. Lukin, A. H. Nuber, A. Brandtner, W. Setlik, H. Remotti, A. Muley, X. Chen, R. May, C. W. Houchen, J. G. Fox, M. D. Gershon, M. Quante, and T. C. Wang. Long-lived intestinal tuft cells serve as colon cancer-initiating cells. *J Clin Invest*, 124(3):1283–95, 2014.

[62] R. Chen, P. S. Rabinovitch, D. A. Crispin, M. J. Emond, M. P. Bronner, and T. A. Brentnall. The initiation of colon cancer in a chronic inflammatory setting. *Carcinogenesis*, 26(9):1513–9, 2005.

[63] A. M. Baker, B. Cereser, S. Melton, A. G. Fletcher, M. Rodriguez-Justo, P. J. Tadrous, A. Humphries, G. Elia, S. A. McDonald, N. A. Wright, B. D. Simons, M. Jansen, and T. A. Graham. Quantification of crypt and stem cell evolution in the normal and neoplastic human colon. *Cell Rep*, 8(4):940–7, 2014.

[64] L. Bruens, S. I. J. Ellenbroek, J. van Rheenen, and H. J. Snippert. In vivo imaging reveals existence of crypt fission and fusion in adult mouse intestine. *Gastroenterology*, 2017.

[65] B. Chassaing, J. D. Aitken, M. Malleshappa, and M. Vijay-Kumar. Dextran sulfate sodium (dss)-induced colitis in mice. *Curr Protoc Immunol*, 104:Unit 15 25, 2014.

[66] T. Tanaka, H. Kohno, R. Suzuki, Y. Yamada, S. Sugie, and H. Mori. A novel inflammation-related mouse colon carcinogenesis model induced by azoxymethane and dextran sodium sulfate. *Cancer Sci*, 94(11):965–73, 2003.

[67] J. Cosin-Roger, D. Ortiz-Masia, S. Calatayud, C. Hernandez, J. V. Esplugues, and M. D. Barrachina. The activation of wnt signaling by a stat6-dependent macrophage phenotype promotes mucosal repair in murine ibd. *Mucosal Immunol*, 9(4):986–98, 2016.

[68] J. You, A. V. Nguyen, C. G. Albers, F. Lin, and R. F. Holcombe. Wnt pathway-related gene expression in inflammatory bowel disease. *Dig Dis Sci*, 53(4):1013–9, 2008.

[69] A. Serafino, N. Moroni, M. Zonfrillo, F. Andreola, L. Mercuri, G. Nicotera,

J. Nunziata, R. Ricci, A. Antinori, G. Rasi, and P. Pierimarchi. Wnt-pathway components as predictive markers useful for diagnosis, prevention and therapy in inflammatory bowel disease and sporadic colorectal cancer. *Oncotarget*, 5(4):978–92, 2014.

[70] J. M. Allaire, M. Darsigny, S. S. Marcoux, S. A. Roy, J. F. Schmouth, L. Umans, A. Zwijsen, F. Boudreau, and N. Perreault. Loss of smad5 leads to the disassembly of the apical junctional complex and increased susceptibility to experimental colitis. *Am J Physiol Gastrointest Liver Physiol*, 300(4):G586–97, 2011.

[71] J. J. Lee, M. E. Rothenberg, E. S. Seeley, B. Zimdahl, S. Kawano, W. J. Lu, K. Shin, T. Sakata-Kato, J. K. Chen, M. Diehn, M. F. Clarke, and P. A. Beachy. Control of inflammation by stromal hedgehog pathway activation restrains colitis. *Proc Natl Acad Sci U S A*, 113(47):E7545–E7553, 2016.

[72] C. W. Lees, W. J. Zacharias, M. Tremelling, C. L. Noble, E. R. Nimmo, A. Tenesa, J. Cornelius, L. Torkvist, J. Kao, S. Farrington, H. E. Drummond, G. T. Ho, I. D. Arnott, H. D. Appelman, L. Diehl, H. Campbell, M. G. Dunlop, M. Parkes, S. E. Howie, D. L. Gumucio, and J. Satsangi. Analysis of germline gli1 variation implicates hedgehog signalling in the regulation of intestinal inflammatory pathways. *PLoS Med*, 5(12):e239, 2008.

[73] M. Gersemann, S. Becker, I. Kubler, M. Koslowski, G. Wang, K. R. Herrlinger, J. Griger, P. Fritz, K. Fellermann, M. Schwab, J. Wehkamp, and E. F. Stange. Differences in goblet cell differentiation between crohn's dis-

ease and ulcerative colitis. *Differentiation*, 77(1):84–94, 2009.

[74] L. Werner, U. Berndt, D. Paclik, S. Danese, A. Schirbel, and A. Sturm. Tnfalpha inhibitors restrict t cell activation and cycling via notch-1 signalling in inflammatory bowel disease. *Gut*, 61(7):1016–27, 2012.

[75] C. Lopez-Garcia, A. M. Klein, B. D. Simons, and D. J. Winton. Intestinal stem cell replacement follows a pattern of neutral drift. *Science*, 330(6005):822–5, 2010.

[76] H. J. Snippert, L. G. van der Flier, T. Sato, J. H. van Es, M. van den Born, C. Kroon-Veenboer, N. Barker, A. M. Klein, J. van Rheenen, B. D. Simons, and H. Clevers. Intestinal crypt homeostasis results from neutral competition between symmetrically dividing lgr5 stem cells. *Cell*, 143(1):134–44, 2010.

[77] L. Ritsma, S. I. Ellenbroek, A. Zomer, H. J. Snippert, F. J. de Sauvage, B. D. Simons, H. Clevers, and J. van Rheenen. Intestinal crypt homeostasis revealed at single-stem-cell level by in vivo live imaging. *Nature*, 507(7492):362–5, 2014.

[78] L. Vermeulen, E. Morrissey, M. van der Heijden, A. M. Nicholson, A. Sottoriva, S. Buczacki, R. Kemp, S. Tavare, and D. J. Winton. Defining stem cell dynamics in models of intestinal tumor initiation. *Science*, 342(6161):995–8, 2013.

[79] N. Barker, R. A. Ridgway, J. H. van Es, M. van de Wetering, H. Begthel, M. van den Born, E. Danenberg, A. R. Clarke, O. J. Sansom, and

H. Clevers. Crypt stem cells as the cells-of-origin of intestinal cancer. *Nature*, 457(7229):608–11, 2009.

[80] L. Zhu, P. Gibson, D. S. Currle, Y. Tong, R. J. Richardson, I. T. Bayazitov, H. Poppleton, S. Zakharenko, D. W. Ellison, and R. J. Gilbertson. Prominin 1 marks intestinal stem cells that are susceptible to neoplastic transformation. *Nature*, 457(7229):603–7, 2009.

[81] I. M. Shih, T. L. Wang, G. Traverso, K. Romans, S. R. Hamilton, S. Ben-Sasson, K. W. Kinzler, and B. Vogelstein. Top-down morphogenesis of colorectal tumors. *Proc Natl Acad Sci U S A*, 98(5):2640–5, 2001.

[82] S. L. Preston, W. M. Wong, A. O. Chan, R. Poulsom, R. Jeffery, R. A. Goodlad, N. Mandir, G. Elia, M. Novelli, W. F. Bodmer, I. P. Tomlinson, and N. A. Wright. Bottom-up histogenesis of colorectal adenomas: origin in the monocryptal adenoma and initial expansion by crypt fission. *Cancer Res*, 63(13):3819–25, 2003.

[83] S. Schwitalla, A. A. Fingerle, P. Cammareri, T. Nebelsiek, S. I. Goktuna, P. K. Ziegler, O. Canli, J. Heijmans, D. J. Huels, G. Moreaux, R. A. Rupec, M. Gerhard, R. Schmid, N. Barker, H. Clevers, R. Lang, J. Neumann, T. Kirchner, M. M. Taketo, G. R. van den Brink, O. J. Sansom, M. C. Arkan, and F. R. Greten. Intestinal tumorigenesis initiated by dedifferentiation and acquisition of stem-cell-like properties. *Cell*, 152(1-2):25–38, 2013.

[84] E. Jaeger, S. Leedham, A. Lewis, S. Segditsas, M. Becker, P. R. Cuadrado, H. Davis, K. Kaur, K. Heinimann, K. Howarth, J. East, J. Taylor, H. Thomas, and I. Tomlinson. Hereditary mixed polyposis syndrome is

caused by a 40-kb upstream duplication that leads to increased and ectopic expression of the bmp antagonist grem1. *Nat Genet*, 44(6):699–703, 2012.

[85] H. Davis, S. Irshad, M. Bansal, H. Rafferty, T. Boitsova, C. Bardella, E. Jaeger, A. Lewis, L. Freeman-Mills, F. C. Giner, P. Rodenas-Cuadrado, S. Mallappa, S. Clark, H. Thomas, R. Jeffery, R. Poulsom, M. Rodriguez-Justo, M. Novelli, R. Chetty, A. Silver, O. J. Sansom, F. R. Greten, L. M. Wang, J. E. East, I. Tomlinson, and S. J. Leedham. Aberrant epithelial grem1 expression initiates colonic tumorigenesis from cells outside the stem cell niche. *Nat Med*, 2014.

[86] L. Vermeulen, M. Todaro, F. de Sousa Mello, M. R. Sprick, K. Kemper, M. Perez Alea, D. J. Richel, G. Stassi, and J. P. Medema. Single-cell cloning of colon cancer stem cells reveals a multi-lineage differentiation capacity. *Proc Natl Acad Sci U S A*, 105(36):13427–32, 2008.

[87] S. K. Singh, C. Hawkins, I. D. Clarke, J. A. Squire, J. Bayani, T. Hide, R. M. Henkelman, M. D. Cusimano, and P. B. Dirks. Identification of human brain tumour initiating cells. *Nature*, 432(7015):396–401, 2004.

[88] L. Ricci-Vitiani, D. G. Lombardi, E. Pilozzi, M. Biffoni, M. Todaro, C. Peschle, and R. De Maria. Identification and expansion of human colon-cancer-initiating cells. *Nature*, 445(7123):111–5, 2007.

[89] Z. Kozovska, V. Gabrisova, and L. Kucerova. Colon cancer: cancer stem cells markers, drug resistance and treatment. *Biomed Pharmacother*, 68(8):911–6, 2014.

[90] K. Yan, Q. Wu, D. H. Yan, C. H. Lee, N. Rahim, I. Tritschler, J. DeVecchio,

M. F. Kalady, A. B. Hjelmeland, and J. N. Rich. Glioma cancer stem cells secrete gremlin1 to promote their maintenance within the tumor hierarchy. *Genes Dev*, 28(10):1085–100, 2014.

[91] E. Melo F. De Sousa, X. Wang, M. Jansen, E. Fessler, A. Trinh, L. P. de Rooij, J. H. de Jong, O. J. de Boer, R. van Leersum, M. F. Bijlsma, H. Rodermond, M. van der Heijden, C. J. van Noesel, J. B. Tuynman, E. Dekker, F. Markowetz, J. P. Medema, and L. Vermeulen. Poor-prognosis colon cancer is defined by a molecularly distinct subtype and develops from serrated precursor lesions. *Nat Med*, 19(5):614–8, 2013.

[92] A. Sadanandam, X. Wang, F. De Sousa E Melo, J. W. Gray, L. Vermeulen, D. Hanahan, and J. P. Medema. Reconciliation of classification systems defining molecular subtypes of colorectal cancer: Interrelationships and clinical implications. *Cell Cycle*, 13(3):353–357, 2014.

[93] L. Marisa, A. de Reynies, A. Duval, J. Selves, M. P. Gaub, L. Vescovo, M. C. Etienne-Grimaldi, R. Schiappa, D. Guenot, M. Ayadi, S. Kirzin, M. Chazal, J. F. Flejou, D. Benchimol, A. Berger, A. Lagarde, E. Pencreach, F. Piard, D. Elias, Y. Parc, S. Olschwang, G. Milano, P. Laurent-Puig, and V. Boige. Gene expression classification of colon cancer into molecular subtypes: characterization, validation, and prognostic value. *PLoS Med*, 10(5):e1001453, 2013.

[94] J. Guinney, R. Dienstmann, X. Wang, A. de Reynies, A. Schlicker, C. Soneson, L. Marisa, P. Roepman, G. Nyamundanda, P. Angelino, B. M. Bot, J. S. Morris, I. M. Simon, S. Gerster, E. Fessler, E. Melo F. De Sousa,

E. Missiaglia, H. Ramay, D. Barras, K. Homicsko, D. Maru, G. C. Manyam, B. Broom, V. Boige, B. Perez-Villamil, T. Laderas, R. Salazar, J. W. Gray, D. Hanahan, J. Tabernero, R. Bernards, S. H. Friend, P. Laurent-Puig, J. P. Medema, A. Sadanandam, L. Wessels, M. Delorenzi, S. Kopetz, L. Vermeulen, and S. Tejpar. The consensus molecular subtypes of colorectal cancer. *Nat Med*, 2015.

[95] A. Calon, E. Lonardo, A. Berenguer-Llergo, E. Espinet, X. Hernando-Momblona, M. Iglesias, M. Sevillano, S. Palomo-Ponce, D. V. Tauriello, D. Byrom, C. Cortina, C. Morral, C. Barcelo, S. Tosi, A. Riera, C. S. Attolini, D. Rossell, E. Sancho, and E. Batlle. Stromal gene expression defines poor-prognosis subtypes in colorectal cancer. *Nat Genet*, 2015.

[96] C. Isella, A. Terrasi, S. E. Bellomo, C. Petti, G. Galatola, A. Muratore, A. Mellano, R. Senetta, A. Cassenti, C. Sonetto, G. Inghirami, L. Trusolino, Z. Fekete, M. De Ridder, P. Cassoni, G. Storme, A. Bertotti, and E. Medico. Stromal contribution to the colorectal cancer transcriptome. *Nat Genet*, 2015.

[97] J. A. Eaden, K. R. Abrams, and J. F. Mayberry. The risk of colorectal cancer in ulcerative colitis: a meta-analysis. *Gut*, 48(4):526–35, 2001.

[98] M. M. Claessen, F. P. Vleggaar, K. M. Tytgat, P. D. Siersema, and H. R. van Buuren. High lifetime risk of cancer in primary sclerosing cholangitis. *J Hepatol*, 50(1):158–64, 2009.

[99] M. J. Thun, M. M. Namboodiri, and Jr. Heath, C. W. Aspirin use and reduced risk of fatal colon cancer. *N Engl J Med*, 325(23):1593–6, 1991.

[100] Y. Cao, R. Nishihara, Z. R. Qian, M. Song, K. Mima, K. Inamura, J. A. Nowak, D. A. Drew, P. Lochhead, K. Nosho, T. Morikawa, X. Zhang, K. Wu, M. Wang, W. S. Garrett, E. L. Giovannucci, C. S. Fuchs, A. T. Chan, and S. Ogino. Regular aspirin use associates with lower risk of colorectal cancers with low numbers of tumor-infiltrating lymphocytes. *Gastroenterology*, 151(5):879–892 e4, 2016.

[101] H. F. Dvorak. Tumors: wounds that do not heal. similarities between tumor stroma generation and wound healing. *N Engl J Med*, 315(26):1650–9, 1986.

[102] A. M. Baker, W. Cross, K. Curtius, I. Al Bakir, C. R. Choi, H. L. Davis, D. Temko, S. Biswas, P. Martinez, M. J. Williams, J. O. Lindsay, R. Feakins, R. Vega, S. J. Hayes, I. P. M. Tomlinson, S. A. C. McDonald, M. Moorghen, A. Silver, J. E. East, N. A. Wright, L. M. Wang, M. Rodriguez-Justo, M. Jansen, A. L. Hart, S. J. Leedham, and T. A. Graham. Evolutionary history of human colitis-associated colorectal cancer. *Gut*, 2018.

[103] D. Hanahan and R. A. Weinberg. Hallmarks of cancer: the next generation. *Cell*, 144(5):646–74, 2011.

[104] S. Biswas, H. Davis, S. Irshad, T. Sandberg, D. Worthley, and S. Leedham. Microenvironmental control of stem cell fate in intestinal homeostasis and disease. *J Pathol*, 237(2):135–45, 2015.

[105] Network Cancer Genome Atlas. Comprehensive molecular characterization of human colon and rectal cancer. *Nature*, 487(7407):330–7, 2012.

[106] A. R. Moser, H. C. Pitot, and W. F. Dove. A dominant mutation that predisposes to multiple intestinal neoplasia in the mouse. *Science*, 247(4940):322–4, 1990.

[107] H. Lamlum, M. Ilyas, A. Rowan, S. Clark, V. Johnson, J. Bell, I. Frayling, J. Efstathiou, K. Pack, S. Payne, R. Roylance, P. Gorman, D. Sheer, K. Neale, R. Phillips, I. Talbot, W. Bodmer, and I. Tomlinson. The type of somatic mutation at apc in familial adenomatous polyposis is determined by the site of the germline mutation: a new facet to knudson's 'two-hit' hypothesis. *Nat Med*, 5(9):1071–5, 1999.

[108] S. Irshad, M. Bansal, P. Guarnieri, H. Davis, A. Al Haj Zen, B. Baran, C. M. A. Pinna, H. Rahman, S. Biswas, C. Bardella, R. Jeffery, L. M. Wang, J. E. East, I. Tomlinson, A. Lewis, and S. J. Leedham. Bone morphogenetic protein and notch signalling crosstalk in poor-prognosis, mesenchymal-subtype colorectal cancer. *J Pathol*, 242(2):178–192, 2017.

[109] J. C. Hardwick, L. L. Kodach, G. J. Offerhaus, and G. R. van den Brink. Bone morphogenetic protein signalling in colorectal cancer. *Nat Rev Cancer*, 8(10):806–12, 2008.

[110] Y. Zhang, X. Chen, M. Qiao, B. Q. Zhang, N. Wang, Z. Zhang, Z. Liao, L. Zeng, Y. Deng, F. Deng, J. Zhang, L. Yin, W. Liu, Q. Zhang, Z. Ya, J. Ye, Z. Wang, L. Zhou, H. H. Luu, R. C. Haydon, T. C. He, and H. Zhang. Bone morphogenetic protein 2 inhibits the proliferation and growth of human colorectal cancer cells. *Oncol Rep*, 32(3):1013–20, 2014.

[111] C. Kosinski, V. S. Li, A. S. Chan, J. Zhang, C. Ho, W. Y. Tsui, T. L. Chan,

R. C. Mifflin, D. W. Powell, S. T. Yuen, S. Y. Leung, and X. Chen. Gene expression patterns of human colon tops and basal crypts and bmp antagonists as intestinal stem cell niche factors. *Proc Natl Acad Sci U S A*, 104(39):15418–23, 2007.

[112] Z. Qi, Y. Li, B. Zhao, C. Xu, Y. Liu, H. Li, B. Zhang, X. Wang, X. Yang, W. Xie, B. Li, J. J. Han, and Y. G. Chen. Bmp restricts stemness of intestinal lgr5+ stem cells by directly suppressing their signature genes. *Nat Commun*, 8:13824, 2017.

[113] A. P. Haramis, H. Begthel, M. van den Born, J. van Es, S. Jonkheer, G. J. Offerhaus, and H. Clevers. De novo crypt formation and juvenile polyposis on bmp inhibition in mouse intestine. *Science*, 303(5664):1684–6, 2004.

[114] M. Gerling, N. V. Buller, L. M. Kirn, S. Joost, O. Frings, B. Englert, A. Bergstrom, R. V. Kuiper, L. Blaas, M. C. Wielenga, S. Almer, A. A. Kuhl, E. Fredlund, G. R. van den Brink, and R. Toftgard. Stromal hedgehog signalling is downregulated in colon cancer and its restoration restrains tumour growth. *Nat Commun*, 7:12321, 2016.

[115] J. Berlin, J. C. Bendell, L. L. Hart, I. Firdaus, I. Gore, R. C. Hermann, M. F. Mulcahy, M. M. Zalupski, H. M. Mackey, R. L. Yauch, R. A. Graham, G. L. Bray, and J. A. Low. A randomized phase ii trial of vismodegib versus placebo with folfox or folfiri and bevacizumab in patients with previously untreated metastatic colorectal cancer. *Clin Cancer Res*, 19(1):258–67, 2013.

[116] C. Kosinski, D. E. Stange, C. Xu, A. S. Chan, C. Ho, S. T. Yuen, R. C. Mif-

flin, D. W. Powell, H. Clevers, S. Y. Leung, and X. Chen. Indian hedgehog regulates intestinal stem cell fate through epithelial-mesenchymal interactions during development. *Gastroenterology*, 139(3):893–903, 2010.

[117] N. V. Buller, S. L. Rosekrans, C. Metcalfe, J. Heijmans, W. A. van Dop, E. Fessler, M. Jansen, C. Ahn, J. L. Vermeulen, B. F. Westendorp, E. C. Robanus-Maandag, G. J. Offerhaus, J. P. Medema, G. R. D'Haens, M. E. Wildenberg, F. J. de Sauvage, V. Muncan, and G. R. van den Brink. Stromal indian hedgehog signaling is required for intestinal adenoma formation in mice. *Gastroenterology*, 148(1):170–180 e6, 2015.

[118] W. A. van Dop, A. Uhmann, M. Wijgerde, E. Sleddens-Linkels, J. Heijmans, G. J. Offerhaus, M. A. van den Bergh Weerman, G. E. Boeckxstaens, D. W. Hommes, J. C. Hardwick, H. Hahn, and G. R. van den Brink. Depletion of the colonic epithelial precursor cell compartment upon conditional activation of the hedgehog pathway. *Gastroenterology*, 136(7):2195–2203 e1–7, 2009.

[119] P. Pelczar, A. Zibat, W. A. van Dop, J. Heijmans, A. Bleckmann, W. Gruber, F. Nitzki, A. Uhmann, M. V. Guijarro, E. Hernando, K. Dittmann, J. Wienands, R. Dressel, L. Wojnowski, C. Binder, T. Taguchi, T. Beissbarth, P. C. Hogendoorn, C. R. Antonescu, B. P. Rubin, W. Schulz-Schaeffer, F. Aberger, G. R. van den Brink, and H. Hahn. Inactivation of patched1 in mice leads to development of gastrointestinal stromal-like tumors that express pdgfralpha but not kit. *Gastroenterology*, 144(1):134–144 e6, 2013.

[120] B. B. Madison, K. Braunstein, E. Kuizon, K. Portman, X. T. Qiao, and

D. L. Gumucio. Epithelial hedgehog signals pattern the intestinal crypt-villus axis. *Development*, 132(2):279–89, 2005.

[121] J. W. Foster, M. A. Dominguez-Steglich, S. Guioli, C. Kwok, P. A. Weller, M. Stevanovic, J. Weissenbach, S. Mansour, I. D. Young, P. N. Goodfellow, and et al. Campomelic dysplasia and autosomal sex reversal caused by mutations in an sry-related gene. *Nature*, 372(6506):525–30, 1994.

[122] E. J. Formeister, A. L. Sionas, D. K. Lorance, C. L. Barkley, G. H. Lee, and S. T. Magness. Distinct sox9 levels differentially mark stem/progenitor populations and enteroendocrine cells of the small intestine epithelium. *Am J Physiol Gastrointest Liver Physiol*, 296(5):G1108–18, 2009.

[123] L. Van Landeghem, M. A. Santoro, A. E. Krebs, A. T. Mah, J. J. Dehmer, A. D. Gracz, B. P. Scull, K. McNaughton, S. T. Magness, and P. K. Lund. Activation of two distinct sox9-egfp-expressing intestinal stem cell populations during crypt regeneration after irradiation. *Am J Physiol Gastrointest Liver Physiol*, 302(10):G1111–32, 2012.

[124] K. C. Roche, A. D. Gracz, X. F. Liu, V. Newton, H. Akiyama, and S. T. Magness. Sox9 maintains reserve stem cells and preserves radioresistance in mouse small intestine. *Gastroenterology*, 2015.

[125] P. Bastide, C. Darido, J. Pannequin, R. Kist, S. Robine, C. Marty-Double, F. Bibeau, G. Scherer, D. Joubert, F. Hollande, P. Blache, and P. Jay. Sox9 regulates cell proliferation and is required for paneth cell differentiation in the intestinal epithelium. *J Cell Biol*, 178(4):635–48, 2007.

[126] W. Guo, Z. Keckesova, J. L. Donaher, T. Shibue, V. Tischler, F. Reinhardt,

S. Itzkovitz, A. Noske, U. Zurrer-Hardi, G. Bell, W. L. Tam, S. A. Mani, A. van Oudenaarden, and R. A. Weinberg. Slug and sox9 cooperatively determine the mammary stem cell state. *Cell*, 148(5):1015–28, 2012.

[127] A. D. Gracz, S. Ramalingam, and S. T. Magness. Sox9 expression marks a subset of cd24-expressing small intestine epithelial stem cells that form organoids in vitro. *Am J Physiol Gastrointest Liver Physiol*, 298(5):G590–600, 2010.

[128] M. L. Espersen, J. Olsen, D. Linnemann, E. Hogdall, and J. T. Troelsen. Clinical implications of intestinal stem cell markers in colorectal cancer. *Clin Colorectal Cancer*, 14(2):63–71, 2015.

[129] A. Matheu, M. Collado, C. Wise, L. Manterola, L. Cekaite, A. J. Tye, M. Canamero, L. Bujanda, A. Schedl, K. S. Cheah, R. I. Skotheim, R. A. Lothe, A. Lopez de Munain, J. Briscoe, M. Serrano, and R. Lovell-Badge. Oncogenicity of the developmental transcription factor sox9. *Cancer Res*, 72(5):1301–15, 2012.

[130] B. Lu, Y. Fang, J. Xu, L. Wang, F. Xu, E. Xu, Q. Huang, and M. Lai. Analysis of sox9 expression in colorectal cancer. *Am J Clin Pathol*, 130(6):897–904, 2008.

[131] Z. Shen, H. Deng, Y. Fang, X. Zhu, G. T. Ye, L. Yan, H. Liu, and G. Li. Identification of the interplay between sox9 and s100p in the metastasis and invasion of colon carcinoma. *Oncotarget*, 6(24):20672–84, 2015.

[132] Z. Shi, C. I. Chiang, T. A. Mistretta, A. Major, and Y. Mori-Akiyama. Sox9

directly regulates igfbp-4 in the intestinal epithelium. *Am J Physiol Gastrointest Liver Physiol*, 305(1):G74–83, 2013.

[133] S. Ramalingam, G. W. Daughtridge, M. J. Johnston, A. D. Gracz, and S. T. Magness. Distinct levels of sox9 expression mark colon epithelial stem cells that form colonoids in culture. *Am J Physiol Gastrointest Liver Physiol*, 302(1):G10–20, 2012.

[134] A. Panza, V. Pazienza, M. Ripoli, G. Benegiamo, A. Gentile, M. R. Valvano, B. Augello, G. Merla, C. Prattichizzo, F. Tavano, E. Ranieri, P. di Sebastiano, M. Vinciguerra, A. Andriulli, G. Mazzoccoli, and A. Piepoli. Interplay between sox9, beta-catenin and ppargamma activation in colorectal cancer. *Biochim Biophys Acta*, 1833(8):1853–65, 2013.

[135] R. Abdel-Samad, H. Zalzali, C. Rammah, J. Giraud, C. Naudin, S. Dupasquier, F. Poulat, B. Boizet-Bonhoure, S. Lumbroso, K. Mouzat, C. Bonnans, C. Pignodel, P. Raynaud, P. Fort, C. Quittau-Prevostel, and P. Blache. Minisox9, a dominant-negative variant in colon cancer cells. *Oncogene*, 30(22):2493–503, 2011.

[136] C. Prevostel, C. Rammah-Bouazza, H. Trauchessec, L. Canterel-Thouennon, M. Busson, M. Ychou, and P. Blache. Sox9 is an atypical intestinal tumor suppressor controlling the oncogenic wnt/ss-catenin signaling. *Oncotarget*, 7(50):82228–82243, 2016.

[137] B. M. Javier, R. Yaeger, L. Wang, F. Sanchez-Vega, A. Zehir, S. Middha, J. Sadowska, E. Vakiani, J. Shia, D. Klimstra, M. Ladanyi, C. A. Iacobuzio-Donahue, and J. F. Hechtman. Recurrent, truncating sox9 mutations are

associated with sox9 overexpression, kras mutation, and tp53 wild type status in colorectal carcinoma. *Oncotarget*, 7(32):50875–50882, 2016.

[138] A. Suryo Rahmanto, V. Savov, A. Brunner, S. Bolin, H. Weishaupt, A. Malyukova, G. Rosen, M. Cancer, S. Hutter, A. Sundstrom, D. Kawauchi, D. T. Jones, C. Spruck, M. D. Taylor, Y. J. Cho, S. M. Pfister, M. Kool, A. Korshunov, F. J. Swartling, and O. Sangfelt. Fbw7 suppression leads to sox9 stabilization and increased malignancy in medulloblastoma. *EMBO J*, 35(20):2192–2212, 2016.

[139] S. Srinivas, T. Watanabe, C. S. Lin, C. M. William, Y. Tanabe, T. M. Jessell, and F. Costantini. Cre reporter strains produced by targeted insertion of eyfp and ecfp into the rosa26 locus. *BMC Dev Biol*, 1:4, 2001.

[140] F. el Marjou, K. P. Janssen, B. H. Chang, M. Li, V. Hindie, L. Chan, D. Louvard, P. Chambon, D. Metzger, and S. Robine. Tissue-specific and inducible cre-mediated recombination in the gut epithelium. *Genesis*, 39(3):186–93, 2004.

[141] T. Soeda, J. M. Deng, B. de Crombrugghe, R. R. Behringer, T. Nakamura, and H. Akiyama. Sox9-expressing precursors are the cellular origin of the cruciate ligament of the knee joint and the limb tendons. *Genesis*, 48(11):635–44, 2010.

[142] Y. Mori-Akiyama, M. van den Born, J. H. van Es, S. R. Hamilton, H. P. Adams, J. Zhang, H. Clevers, and B. de Crombrugghe. Sox9 is required for the differentiation of paneth cells in the intestinal epithelium. *Gastroenterology*, 133(2):539–46, 2007.

[143] R. Rudling, A. B. Hassan, J. Kitau, N. Mandir, and R. A. Goodlad. A simple device to rapidly prepare whole mounts of murine intestine. *Cell Prolif*, 39(5):415–20, 2006.

[144] C. Becker, M. C. Fantini, and M. F. Neurath. High resolution colonoscopy in live mice. *Nat Protoc*, 1(6):2900–4, 2006.

[145] G. E. Truett, P. Heeger, R. L. Mynatt, A. A. Truett, J. A. Walker, and M. L. Warman. Preparation of pcr-quality mouse genomic dna with hot sodium hydroxide and tris (hotshot). *Biotechniques*, 29(1):52, 54, 2000.

[146] K. J. Livak and T. D. Schmittgen. Analysis of relative gene expression data using real-time quantitative pcr and the 2(-delta delta c(t)) method. *Methods*, 25(4):402–8, 2001.

[147] A. Subramanian, P. Tamayo, V. K. Mootha, S. Mukherjee, B. L. Ebert, M. A. Gillette, A. Paulovich, S. L. Pomeroy, T. R. Golub, E. S. Lander, and J. P. Mesirov. Gene set enrichment analysis: a knowledge-based approach for interpreting genome-wide expression profiles. *Proc Natl Acad Sci U S A*, 102(43):15545–50, 2005.

[148] M. A. Koppens, G. Bounova, G. Gargiulo, E. Tanger, H. Janssen, P. Cornelissen-Steijger, M. Blom, J. Y. Song, L. F. Wessels, and M. van Lohuizen. Deletion of polycomb repressive complex 2 from mouse intestine causes loss of stem cells. *Gastroenterology*, 151(4):684–697 e12, 2016.

[149] I. Maric, N. Kucic, T. Turk Wensveen, I. Smoljan, B. Grahovac, S. Zoricic Cvek, T. Celic, D. Bobinac, and S. Vukicevic. Bmp signaling in rats

with tnbs-induced colitis following bmp7 therapy. *Am J Physiol Gastrointest Liver Physiol*, 302(10):G1151–62, 2012.

[150] A. Merlos-Suarez, F. M. Barriga, P. Jung, M. Iglesias, M. V. Cespedes, D. Rossell, M. Sevillano, X. Hernando-Momblona, V. da Silva-Diz, P. Munoz, H. Clevers, E. Sancho, R. Mangues, and E. Batlle. The intestinal stem cell signature identifies colorectal cancer stem cells and predicts disease relapse. *Cell Stem Cell*, 8(5):511–24, 2011.

[151] P. M. Clark, N. Dawany, W. Dampier, S. W. Byers, R. G. Pestell, and A. Tozeren. Bioinformatics analysis reveals transcriptome and microrna signatures and drug repositioning targets for ibd and other autoimmune diseases. *Inflamm Bowel Dis*, 18(12):2315–33, 2012.

[152] H. S. Park, R. A. Goodlad, and N. A. Wright. Crypt fission in the small intestine and colon. a mechanism for the emergence of g6pd locus-mutated crypts after treatment with mutagens. *Am J Pathol*, 147(5):1416–27, 1995.

[153] H. F. Farin, I. Jordens, M. H. Mosa, O. Basak, J. Korving, D. V. Tauriello, K. de Punder, S. Angers, P. J. Peters, M. M. Maurice, and H. Clevers. Visualization of a short-range wnt gradient in the intestinal stem-cell niche. *Nature*, 530(7590):340–3, 2016.

[154] N. Kangwan, Y. J. Kim, Y. M. Han, M. Jeong, J. M. Park, and K. B. Hahm. Concerted actions of ameliorated colitis, aberrant crypt foci inhibition and 15-hydroxyprostaglandin dehydrogenase induction by sonic hedgehog inhibitor led to prevention of colitis-associated cancer. *Int J Cancer*, 138(6):1482–93, 2016.

[155] Y. Katoh and M. Katoh. Hedgehog target genes: mechanisms of carcinogenesis induced by aberrant hedgehog signaling activation. *Curr Mol Med*, 9(7):873–86, 2009.

[156] G. J. Todaro, G. K. Lazar, and H. Green. The initiation of cell division in a contact-inhibited mammalian cell line. *J Cell Physiol*, 66(3):325–33, 1965.

[157] H. Seno, H. Miyoshi, S. L. Brown, M. J. Geske, M. Colonna, and T. S. Stappenbeck. Efficient colonic mucosal wound repair requires trem2 signaling. *Proc Natl Acad Sci U S A*, 106(1):256–61, 2009.

[158] Q. Li, J. P. Lewandowski, M. B. Powell, J. L. Norrie, S. H. Cho, and S. A. Vokes. A gli silencer is required for robust repression of gremlin in the vertebrate limb bud. *Development*, 141(9):1906–14, 2014.

[159] H. Ireland, R. Kemp, C. Houghton, L. Howard, A. R. Clarke, O. J. Sansom, and D. J. Winton. Inducible cre-mediated control of gene expression in the murine gastrointestinal tract: effect of loss of beta-catenin. *Gastroenterology*, 126(5):1236–46, 2004.

[160] S. A. Vokes, H. Ji, W. H. Wong, and A. P. McMahon. A genome-scale analysis of the cis-regulatory circuitry underlying sonic hedgehog-mediated patterning of the mammalian limb. *Genes Dev*, 22(19):2651–63, 2008.

[161] J. F. Chau, D. Jia, Z. Wang, Z. Liu, Y. Hu, X. Zhang, H. Jia, K. P. Lai, W. F. Leong, B. J. Au, Y. Mishina, Y. G. Chen, C. Biondi, E. Robertson, D. Xie, H. Liu, L. He, X. Wang, Q. Yu, and B. Li. A crucial role for bone morphogenetic protein-smad1 signalling in the dna damage response. *Nat Commun*, 3:836, 2012.

[162] J. Fink, A. Andersson-Rolf, and B. K. Koo. Adult stem cell lineage tracing and deep tissue imaging. *BMB Rep*, 48(12):655–67, 2015.

[163] A. Humphries, B. Cereser, L. J. Gay, D. S. Miller, B. Das, A. Gutteridge, G. Elia, E. Nye, R. Jeffery, R. Poulsom, M. R. Novelli, M. Rodriguez-Justo, S. A. McDonald, N. A. Wright, and T. A. Graham. Lineage tracing reveals multipotent stem cells maintain human adenomas and the pattern of clonal expansion in tumor evolution. *Proc Natl Acad Sci U S A*, 110(27):E2490–9, 2013.

[164] G. Arentz, T. Chataway, T. J. Price, Z. Izwan, G. Hardi, A. G. Cummins, and J. E. Hardingham. Desmin expression in colorectal cancer stroma correlates with advanced stage disease and marks angiogenic microvessels. *Clin Proteomics*, 8(1):16, 2011.

[165] A. E. Shyer, T. R. Huycke, C. Lee, L. Mahadevan, and C. J. Tabin. Bending gradients: how the intestinal stem cell gets its home. *Cell*, 161(3):569–80, 2015.

[166] J. Conti and G. Thomas. The role of tumour stroma in colorectal cancer invasion and metastasis. *Cancers (Basel)*, 3(2):2160–8, 2011.

[167] K. Vrijens, W. Lin, J. Cui, D. Farmer, J. Low, E. Pronier, F. Y. Zeng, A. A. Shelat, K. Guy, M. R. Taylor, T. Chen, and M. F. Roussel. Identification of small molecule activators of bmp signaling. *PLoS One*, 8(3):e59045, 2013.

[168] A. I. Robles, G. Traverso, M. Zhang, N. J. Roberts, M. A. Khan, C. Joseph, G. Y. Lauwers, F. M. Selaru, M. Popoli, M. E. Pittman, X. Ke, R. H. Hruban, S. J. Meltzer, K. W. Kinzler, B. Vogelstein, C. C. Harris, and N. Pa-

padopoulos. Whole-exome sequencing analyses of inflammatory bowel disease-associated colorectal cancers. *Gastroenterology*, 150(4):931–43, 2016.

[169] L. A. Davidson, J. S. Goldsby, E. S. Callaway, M. S. Shah, N. Barker, and R. S. Chapkin. Alteration of colonic stem cell gene signatures during the regenerative response to injury. *Biochim Biophys Acta*, 1822(10):1600–7, 2012.

[170] C. Prevostel and P. Blache. The dose-dependent effect of sox9 and its incidence in colorectal cancer. *Eur J Cancer*, 86:150–157, 2017.